



# **Environmental Exposure Effects on DOT-CFFC Cylinders with Modal Acoustic Emission Examination**

**JUNE 2015**

Prepared for:

US DOT/PHMSA  
Mark Toughiry, PE  
1200 New Jersey Ave, SE  
Washington, DC 20590  
+1 (202) 366 – 4545

Prepared by:

Digital Wave Corporation  
Dr. Brian Burks, Dr. Steven Ziola, Dr. Michael Gorman  
13760 E Arapahoe Road  
Centennial, CO 80112  
+1 (303) 790-7559 x13

## Table of Contents

Table of Contents.....	1
1. Executive Summary .....	2
2. Introduction.....	4
3. Technical Approach .....	6
3.1 Hard Water Exposure .....	6
3.2 Chemical Exposure.....	7
3.3 Salt Water Immersion .....	8
3.4 Fire Exposure .....	9
4. Modal Acoustic Emission Examination.....	11
4.1 Modal Acoustic Emission Instrumentation and Hardware.....	11
4.2 Modal Acoustic Emission Spectral Analysis .....	12
4.3 Sensor Calibrations.....	13
4.4 Stability .....	14
4.5 Background Energy .....	15
4.6 Fiber bundle Fracture Energy .....	15
4.7 Single MAE Event Energy.....	16
5. Visual Inspection.....	16
5.1 Hard Water Exposure .....	16
5.2 Chemical Exposure.....	17
5.3 Salt Water Immersion .....	18
5.4 Fire Exposure .....	18
6. Mechanical Testing Results .....	21
6.1 Fatigue Analysis .....	21
6.2 Hard Water Exposure .....	22
6.3 Chemical Exposure.....	25
6.4 Salt Water Immersion .....	29
6.5 Fire Exposure .....	31
7. Modal Acoustic Emission Results .....	35
7.1 Hard Water Exposure .....	35
7.2 Chemical Exposure.....	36
7.3 Salt Water Immersion .....	39
7.4 Fire Exposure .....	40
7.5 Predictive Capability of MAE .....	44
8. Conclusions .....	46
9. References .....	48
APPENDIX A .....	50
APPENDIX B .....	59
APPENDIX C.....	80
APPENDIX D .....	99
APPENDIX E .....	119

## 1. Executive Summary

The present work addresses aggressive environmental exposure effects on DOT-CFFC composite cylinders, and the use of Modal Acoustic Emission (MAE) examination of the cylinders to identify cylinders with compromised strength due to the aggressive environmental exposure. In this study the effects of hard water exposure on the aluminum liner, chemical exposure to the composite overwrap, salt water immersion of the composite cylinder, and structural fire exposure of the composite cylinder were evaluated. This study was a follow up to an in-depth study on the use of MAE examination during physical testing of one hundred (100) DOT-CFFC composite cylinders in which it was shown that expired service life cylinders still possessed the required at manufacture strength, impact and notch tolerance, and the ability to withstand an additional 20 years of service life (through fatigue pressure cycling).

In this work, it was confirmed that prolonged contiguous hard water exposure (10 days) had a detrimental effect on the fatigue performance of the 6061 T6 Al liner incorporated in DOT-CFFC cylinder designs. Water with high mineral content etches the grain boundaries of the 6061 T6 Al liner, introducing a flaw initiation site. Upon pressure cycling, the flaw grows and eventually grows through the liner wall incapacitating the cylinder's ability to hold pressure (it is noted that the failure is not catastrophic, the cylinder fails in a fail-safe manner). Through a coupled laminated plate theory, fracture mechanics, and fatigue life estimation analysis, Digital Wave Corporation developed a re-autofrettage process that mitigated the corrosion induced flaw initiation site problem and drastically improved the fatigue performance of DOT-CFFC composite pressure cylinders. The re-autofrettage process was utilized on all fatigue cycled DOT-CFFC cylinders considered in the present study with overwhelming success; all cylinders (which were not exposed to a structure burning fire) were able to achieve an additional twenty (20) years of simulated service life through fatigue cycle testing to the maximum developed pressure during fast fill.

Further, it was found that neither sulfuric acid nor sodium hypochlorite exposure to DOT-CFFC cylinders held at service pressure diminished the burst strength or fatigue life of the cylinders. It was also found that salt water immersion testing of DOT-CFFC cylinders cycled up to service pressure did not diminish the burst strength or fatigue performance of the cylinders.

Fire exposure of DOT-CFFC pressure cylinders was found to be potentially damaging to the composite cylinder's strength and fatigue performance. Any cylinder which exhibits Level 3 fire damage should not be put back in to service. It is pointed out that all fire exposed cylinders would have been visually rejected, as all cylinders exhibited Level 3 fire exposure damage as defined by CGA C6.2. While this report focused on expired service life cylinders, the potential for material property degradation had nothing to do with the cylinder's age, but rather the extremely damaging nature of fire exposure on carbon fiber reinforced epoxy composite pressure cylinders.

In light of the findings of this study, it is concluded that the DOT-CFFC cylinder design requirements provide for an extremely robust cylinder. Expired service life cylinders were still found to be resilient to chemical exposure and salt water immersion. Prolonged hard water exposure of the 6061 T6 Al liner was found to be potentially damaging; however, Digital Wave Corporation has developed a re-autofrettage process which greatly enhances the liner's fatigue performance even if prolonged hard water exposure of the aluminum liner has occurred. Furthermore, it was found that direct exposure to a structural burning fire of DOT-CFFC

cylinders can potentially degrade the burst strength and fatigue performance of the cylinder. The effect was not due to the cylinder's age, but rather the extremely damaging nature of the direct fire exposure to the epoxy resin system of the carbon fiber reinforced composite overwrap.

Finally, it was found that previously developed MAE accept/reject criteria successfully identified all DOT-CFFC composite pressure cylinders which had compromised strength due to an aggressive environmental exposure. Because MAE relies on fracture mechanics and wave propagation theories as opposed to the occult accept/reject criteria of traditional Acoustic Emission testing, it was able to successfully sort compromised cylinders from cylinders which still possessed adequate strength. With the ability of MAE to identify cylinders with compromised strength, a method exists for expired service life cylinders to be examined, and if the required strength is still possessed by the cylinder to be requalified for extended life service. The work done using the MAE method in this and previous works provides a greater level of safety to the public than special permits which currently provide for cylinder life extension, which have previously been granted by DOT/PHMSA.

## 2. Introduction

For roughly eighteen years carbon fiber reinforced composite cylinders have been utilized in Self-Contained Breathing Apparatus (SCBA) service due to the attractiveness of their comparatively light weight while still being operated at relatively high pressures. In the United States of America (USA), such cylinders are designed to the “DOT-CFFC basic requirements for fully wrapped carbon-fiber reinforced aluminum lined cylinders,” [1] and manufactured and operated under various DOT special permits. In the DOT-CFFC, a provision is set forth in paragraph CFFC-3 that the Associate Administrator of the Pipeline and Hazardous Materials Safety Administration (PHMSA) may approve cylinder service life’s up to 30 years. In the early 2000’s several large manufacturers attempted to have their cylinder designs granted the extended service life [2], with no success. From the OEM manufacturer’s submissions, clearly the manufacturers felt thirty (30) years of service life was not an issue for DOT-CFFC cylinders. However, no means for properly identifying compromised cylinders had been identified.

Recently, a new means of composite cylinder inspection and requalification, known as Modal Acoustic Emission (MAE), has been introduced that shows the ability to adequately identify cylinders which have been damaged or possess compromised strength [3, 4, 5]. In a recent study on a population of 100 expired service life DOT-CFFC cylinders collected from some of the busiest fire departments in the USA (e.g., FDNY, Fairfax, VA, Houston, TX, etc.), it was found that the burst pressure distribution of expired service life DOT-CFFC cylinders was in agreement with virgin DOT-CFFC cylinders [5]. Furthermore, cylinders which experienced a simulated additional 20 years of service life via fatigue cycling to maximum developed pressure during fast fill exhibited a statistically identical burst strength distribution to expired service life (and therefore virgin) cylinders [5].

Modal Acoustic Emission was utilized on every burst test performed in [5], and was found to properly identify and reject every cylinder which burst below the minimum required burst pressure as set forth by the DOT-CFFC [1]. It was found that MAE far outperformed the currently used approach of elastic expansion measurements for identifying compromised cylinders at the time of requalification [5]. Such findings show that extended service life of DOT-CFFC cylinders is possible through the use of MAE testing to identify and reject compromised cylinders; this approach to requalification provides a greater level of safety than what is currently allowed via elastic expansion measurements.

In [5], it was found that a small percentage of the tested population of expired service life cylinders exhibited heavy corrosion indications in the aluminum liner due to prolonged hard water exposure causing approximately 8% of the initial fatigue cycle tested population to leak before achieving an additional 15 years of simulated service life. To address this issue, Digital Wave Corporation developed a re-autofrettage procedure which results in a fatigue resistant liner. An experimental study on a particular population of cylinders which exhibited a propensity to leak was performed, in which half of the cylinders were re-autofrettaged and half of the cylinders were not re-autofrettaged and then all cylinders were subjected to fatigue cycles to maximum developed pressure during fast fill; results were extremely promising, showing that

the re-autofrettage process significantly enhanced the 6061 T6 Al liners fatigue life performance [5]. A coupled laminated plate theory, fracture mechanics, and fatigue life estimation analysis provided a theoretical confirmation that the re-autofrettage process should extend the aluminum liner's fatigue life [5].

While the study of 100 DOT-CFFC cylinders was quite in-depth, questions relative to environmental exposure effects remained. Thus the aim of this work was to investigate the effects of certain environmental exposures on expired service life DOT-CFFC cylinders used in SCBA service. It was felt that the effects of prolonged hard water exposure on the 6061 T6 Al liner, chemical exposure of the composite overwrap, cylinder salt water immersion, and cylinder fire exposure should be investigated.

The deleterious effect of hard water exposure on the fatigue performance of 6061 aluminum lined composite pressure cylinders has been highlighted by the Compressed Gas Association in CGA C-22 2012 [6]. From CGA C-22 it was found that tap water exposure of the aluminum liner in composite overwrap 6061 aluminum lined cylinders consistently reduced the fatigue life of cylinders by up to 75%. In C-22, metallographic images identify that the 6061 Al alloy is susceptible to intercrystalline corrosion allowing for a crack initiation site to develop, which when subsequently mechanically cycled leads to crack growth and the potential for the crack to grow through wall [6]. These observations were independently confirmed in a study performed by the Digital Wave Corporation (DWC) in 2014 on expired service life DOT-CFFC cylinders which exhibited signs of corrosion due to water exposure; calcium carbonate deposits were noted during the internal visual inspection of several of the cylinders [5]. During fatigue cycling a few of the corroded cylinders leaked, while a majority of the cylinders were able to obtain the desired simulated twenty (20) years of additional service life. As previously mentioned, in the DWC study it was found that a re-autofrettage process allowed cylinders to achieve the desired additional twenty (20) years of fatigue life [5]. With the leakage of the 6061 T6 Al liners being a potential issue, a greater statistical set of data on the effects of hard water initiated flaw sites and the efficacy of the DWC developed re-autofrettage process were desired.

The detrimental effect of chemical exposure on fiber overwrapped composite pressure cylinders was investigated by Failure Analysis Associates due to an in-service failure of a DOT-FRP1 (fiberglass) cylinder caused by stress corrosion cracking [7]. The investigation concluded that the glass fiber composite cylinder most probably failed due to stress corrosion cracking caused by exposure of the composite overwrap to an aluminum cleaner known as Alume™ [7]. A more recent investigation of sulfuric acid exposure on five (5) DOT-CFFC designed cylinders was performed by DWC [5]. The cylinders were subjected to a 40% sulfuric acid mixture while being held at service pressure for 100 hours, and then subjected to an EOL burst test. The test procedure followed the procedures of Section 8.5.17 of ISO 11515 [8]. It was found that the DOT-CFFC cylinder designs were highly resistant to chemical exposure due to the inability of the chemical to diffuse through the gel coat layer and have the chance to attack the load bearing carbon fibers [1]. To provide greater assurance that chemical exposure of expired service life DOT-CFFC cylinders is not an issue, both sulfuric acid and sodium hypochlorite (bleach) exposure were investigated.

Little information is known about the salt water immersion performance of DOT-CFFC cylinders as such cylinders are typically only used in Self Contained Breathing Apparatus (SCBA) service and not Self Contained Underwater Breathing Apparatus (SCUBA) service. Upon DOT/PHMSA's request, Digital Wave Corporation has investigated such an environmental exposure, to see if any adverse effects on the mechanical performance of DOT-CFFC cylinders were caused by salt water exposure.

DOT-CFFC cylinders are commonly used in civilian Self Contained Breathing Apparatus (SCBA) service applications which are often associated with firefighting services. Previous performance and Modal Acoustic Emission (MAE) examinations of cylinders from some of the busiest fire departments in the United States of America (e.g., FDNY, Fairfax, VA, Houston, TX) has revealed that a full fifteen (15) years of service had no negative effects on cylinder strength or fatigue performance [5]. Presumably the aforementioned cylinders were subjected to in service fire exposure during their service life; such speculation is easily verified by simply smelling some of the cylinders, in which a "camp fire" smell is readily observed.

While no deleterious effects of typical in service fire exposure have been observed from some of the most heavily used DOT-CFFC SCBA pressure cylinders, an accelerated fire test methodology was requested by DOT/PHMSA to understand the potential implications of extreme fire exposure of DOT-CFFC cylinders. Further, the application of MAE for the examination of fire exposed cylinders provided valuable information about the ability to identify fire exposed cylinders by means less subjective than visual inspection, and safely remove them from service.

In light of the preceding discussion on the potentially adverse effects of certain environmental exposure conditions on the strength and fatigue performance of DOT-CFFC cylinders, a comprehensive study of fifty (50) expired service life DOT-CFFC cylinders was performed in this work. In the following section, each environmental exposure procedure, subsequent mechanical test protocol(s), and acquired data will be described.

### **3. Technical Approach**

#### **3.1 Hard Water Exposure**

An accelerated study was performed to evaluate the efficacy of the proposed re-autofrettage process in a worst case scenario (i.e., hard water sat in the Al liner for multiple contiguous days). The aluminum liner of ten (10) expired service life DOT-CFFC cylinders was intentionally exposed to water with high calcium carbonate ( $\text{CaCO}_3$ ; Centennial, CO tap water was used) content for ten (10) contiguous days. Pre and post hard water exposure, the aluminum liner of all ten (10) cylinders was inspected using RF Systems Lab VJ borescope. Using the borescope, which is capable of capturing images, the effects of corrosion due to prolonged hard water exposure were quantified.

After the hard water exposure, five of the cylinders were re-autofrettaged following the procedure of Section 5.6 in [5], while the remaining five (5) cylinders were not. All ten (10) cylinders were then subjected to the fatigue cycling test procedure of Section 8.5.5 of ISO

11119-2:2002 [9], for up to a maximum of 10,000 cycles. Cylinders were hydraulically cycled from 400 – 5192 psi (5192 psi being the maximum developed pressure during fast fill of a 4500 psi service pressure cylinder). The pressurizing media was water with a corrosion inhibitor.

During the re-autofrettage process a hoop strain gage was mounted to the side wall of the cylinder to measure the amount of permanent deformation imparted onto the 6061 T6 Al liner. Also, a single broadband MAE transducer was coupled to the cylinder to insure that the re-autofrettage process was not resulting in significant fiber tow fracture, delamination emission, or that background energy had not begun to oscillate.

Identical to the fatigue test procedure of [5], the hoop stiffness of cylinders was monitored during fatigue cycling to ensure that no degradation of the composite overwrap was occurring. Further, three (3) broadband MAE transducers were coupled to each cylinder during fatigue cycling to monitor for any damage accumulation within the composite overwrap during fatigue cycling. If a cylinder was capable of achieving 10,000 fatigue cycles, it was subject to an End-of-Life (EOL) burst test following the approach in [5]. One axial and one hoop oriented strain gage was mounted to the cylinder side wall to measure the axial and hoop modulus of the cylinder, respectively. Also, a single MAE transducer was coupled to the cylinder side wall to monitor the propagating stress waves that were released due to the microstructural deformation processes that occur during the failure of the cylinder. Matching the procedure in [5], prior to the burst pressurization ramp the cylinder was subjected to two (2) test pressure holds where the MAE life extension criteria of DOT-SP 15720 and 16343, and the requalification criteria of NB10-0601 were evaluated [4, 10, 11].

### 3.2 Chemical Exposure

The chemical exposure of the cylinders was performed in accordance with Section 8.5.17 of ISO 11515 [8], with the following modifications:

1. For the sulfuric acid exposure, the concentration of the acid was 40% (as opposed to the 30% called for in Section 8.5.17 of ISO 11515 [8]).
2. The cylinders were held at service pressure (4500 psig) for 100 h, as opposed to the 260 bar (3770 psig) required by ISO 11515 [8].
3. Ten (10) of the fifteen (15) cylinders were exposed to sodium hypochlorite (Clorox™ bleach), as opposed to the sulfuric acid exposure.

The first two modifications that were made to the chemical exposure portion of the test resulted in a more aggressive testing environment, resulting in a more conservative examination of the cylinders performance. The ten (10) cylinders that were subjected to sodium hypochlorite were done so to address DOT/PHMSA's question regarding the effects of bleach exposure on DOT-CFFC cylinders. Two MAE transducers were used to monitor each cylinder during the entire 100 hour chemical exposure. Figure 3.1 shows a cylinder connected to the pressurization equipment with the 6.5 inch exposure area outlined, and the MAE transducers mounted to the cylinder to monitor the cylinder.

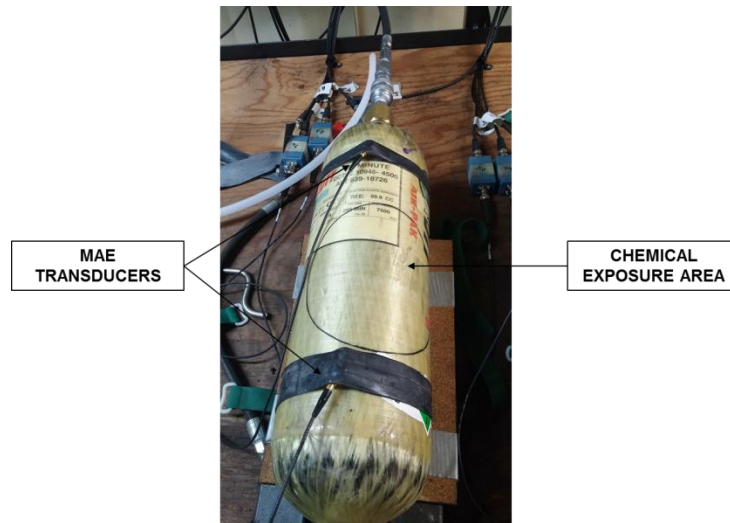


**Figure 3.1 – DOT-CFFC cylinder connected to pressurization equipment with chemical exposure area outlined, and two MAE transducers mounted to the cylinder to monitor the cylinder during the entire 100 hours of chemical exposure.**

Of the fifteen chemical exposure cylinders, five (5) cylinders were re-autofrettaged and subjected to 10,000 fatigue cycles to maximum developed pressure during fast fill, while the remaining ten (10) cylinders were subjected directly to an EOL burst test. The testing, and data collection procedures for the re-autofrettage process, fatigue cycling, and EOL burst test procedure were detailed in Section 3.1.

### 3.3 Salt Water Immersion

The salt water immersion of the cylinders was performed in accordance with Section 8.5.11 of ISO 11119.2:2002 [9]. For each cycle, the following steps were performed:

1. Unpressurized cylinders were immersed for 2 hours in a 3.5% sodium chloride/water solution which was continuously aerated.
2. Cylinders remained in the solution, were pressurized to their service pressure (4500 psig) and held for 22 hours.
3. Cylinders were de-pressurized, removed from the salt water solution, and allowed to dry for 22 hours.
4. After the 22 hour drying period cylinders remained out of the solution and were pressurized to service pressure (4500 psig) and held for 2 hours.
5. Pressure was released.

The preceding five steps constituted one salt water immersion cycle, while a total of fifteen cycles were completed for each cylinder. Note, the pressurizing media was Colorado tap water, which was not removed from the Al liner during the entire 30 days of salt water immersion testing.

One MAE transducer was used to monitor each cylinder during the entire salt water immersion process. The left image in Figure 3.2 shows ten (10) cylinders connected to the pressurization

equipment with the cylinders in the raised position, while the right image in Figure 3.2 shows all ten cylinders submerged in the 3.5% salt water solution. A total of ten (10) cylinders were subjected to salt water immersion testing; five (5) of the cylinders were subjected directly to an EOL burst test, while the remaining five (5) cylinders were re-autofrettaged and then subjected to 10,000 fatigue cycles to maximum developed pressure during fast fill, followed by an EOL burst test.



**Figure 3.2 – Ten (10) DOT-CFFC cylinders connected to pressurization equipment, with one MAE transducer mounted to each cylinder to monitor the cylinder during the entire salt water immersion process. The left image shows the cylinders in the drying position, while the right image shows the cylinders in the submersed position.**

### 3.4 Fire Exposure

A total of fifteen (15) DOT-CFFC cylinders were subjected to a wood (cedar) burning fire for seven (7) contiguous minutes. Prior to the fire exposure all cylinders were subjected to an internal and external visual inspection per CGA C.6.2 [12]. Figure 3.3 shows the fire pit arrangement, while Figure 3.4 shows three cylinders during the seven minute fire exposure. All cylinders were not pressurized, meaning only the effect of fire exposure on the aluminum lined carbon fiber composite overwrapped cylinder was considered in this work.



**Figure 3.3 – Fire pit with stacked cedar used for fire exposure of DOT-CFFC cylinders.**



**Figure 3.4 – Three DOT-CFFC cylinders during the seven minute fire test exposure.**

During the entire seven minute fire exposure, the temperature of each cylinder was measured at one minute intervals. To measure the temperature of the cylinders a laser guided infrared thermometer was used (Electronic Specialties Inc. Model Number EST-65). To better match the fixed thermal emissivity of the infrared thermometer (0.95) a black swatch was painted on each cylinder (Figure 3.5), and used as the location to make the thermal measurements. After the seven minute fire exposure, cylinders were removed from the fire pit and sprayed off with a hose to extinguish any portion of the cylinder which had caught on fire.

Post fire test, the severity of the fire exposure on each cylinder was assessed visually and then ten (10) cylinders were subjected to the EOL burst test procedure with MAE examination, which is fully described in Section 3.1. The remaining five (5) cylinders were assessed visually for the extent of fire damage and then re-autofrettaged and subjected to a maximum of 10,000 fatigue cycles to maximum developed pressure during fast fill (5192 psig for a 4500 psig service pressure cylinder), and then subjected to an EOL burst test.



**Figure 3.5 – Black swatch painted on DOT-CFFC cylinder to more closely match the 0.95 thermal emissivity used by the infrared thermometer.**

Figure 3.6 provides the temperature of all fifteen (15) cylinders which were subjected to fire exposure. From Figure 3.6, it is observed that in general the temperature of the cylinders increased exponentially. Also observed in Figure 3.6 was that cylinders ALT639-9769, ALT639-17831, and ALT604-3764 experienced the highest temperatures during the fire exposure test. As will be shown in the Visual Inspection Results, and the EOL Burst Results sections the aforementioned cylinders were the cylinders most severely impacted by the fire exposure.

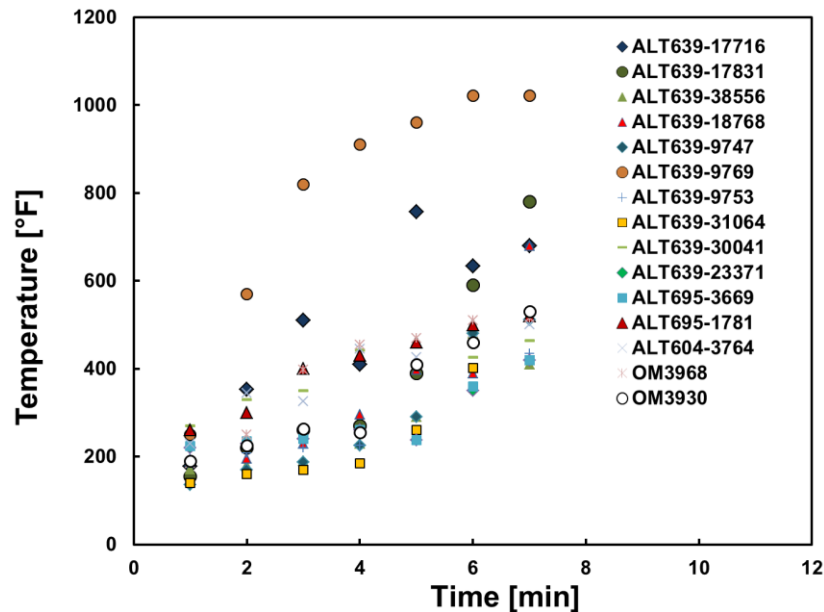


Figure 3.6 – Temperature as a function of exposure time for all fifteen fire exposed cylinders.

#### 4. Modal Acoustic Emission Examination

Modal acoustic emission (MAE) is a branch of Acoustic Emission (AE) that utilizes the capture of the high fidelity stress waves which propagate through a structure as strain energy releases occur due to highly localized damage mechanisms occurring. It has been shown through the use of four accept/reject criteria derived from MAE metrics that composite overwrapped pressure cylinders which have diminished strength may be identified [5]. The four criteria used in this report to evaluate the integrity of the SCBA cylinders are defined and explained in sections 4.4 - 4.7. All four criteria were evaluated during the end-of-life (EOL) burst test procedure (during the cycles up to and holding at test pressure, refer to [5] for details), while Background Energy Oscillation (BEO) was also evaluated on the burst ramp to develop a predictive capability on the burst pressure of the cylinder. The pressurization schedule described in [10, 11] was used to evaluate the cylinders prior to the burst test, and is described in greater detail in [5].

##### 4.1 Modal Acoustic Emission Instrumentation and Hardware

A key component to the Modal Acoustic Emission testing technique is the instrumentation used for high fidelity waveform transduction and recording. These two requirements were met using Digital Wave Corporations in-house MAE equipment. All equipment used in this study for MAE

waveform recording and analysis met the requirements of ASME Section X and NB10-0601 [3, 4]. The hardware, software, and data acquisition system settings used during testing were as follows:

### Hardware

Sensors: Digital Wave Corporation B1025  
Preamplifiers: Digital Wave Corporation PA0  
Signal Conditioning Unit: Digital Wave Corporation FM-1

### Software

Data Acquisition and Analysis: Digital Wave Corporation WaveExplorer™

### Data Acquisition System Trigger Settings

A/D Rate: 5 MHz  
Total Trigger Gain: 48 dB  
Total Waveform Gain: 42 dB  
Bandpass trigger filter: 50 - 2300 kHz  
Point per waveform: 8192  
Pre-trigger points: 2048

An important aspect of detecting modal acoustic emissions is properly acoustically coupling the broadband transducer to the surface in which the stress waves are propagating. To this end, sensors were coupled to the outer surface of the SCBA pressure cylinders using medium viscosity vacuum grease with a small amount of normal force, provided by rubber inner-tubes, used to insure consistency of acoustic coupling (Figure 4.1).

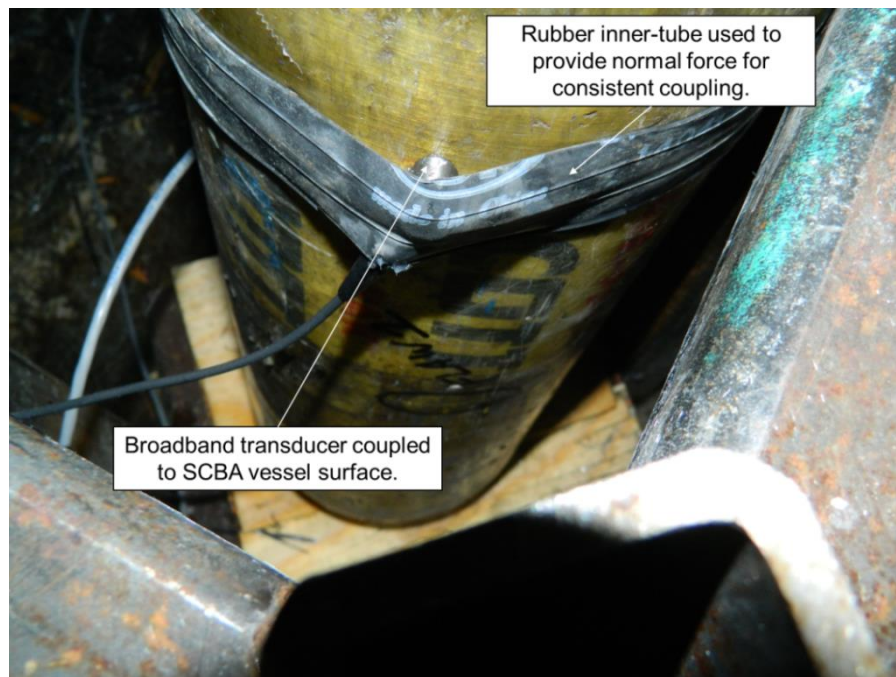


Figure 4.1 – Broadband MAE transducer acoustically coupled to an SCBA pressure cylinder.

## 4.2 Modal Acoustic Emission Spectral Analysis

Due to the large number of events that may be captured during MAE testing, a few metrics were used to identify the natural clustering in the frequency domain of source mechanisms. Specifically, the Modal Acoustic Emission Frequency ( $MF$ ), and spectral standard deviation ( $\sigma_F$ ) was used to identify natural clustering of the various damage mechanisms which occur within composite materials as they are subjected to a stress state. The weighted peak frequency is calculated by

$$WPF = \sqrt{\frac{f_{max} \int f \cdot \hat{U}(f) df}{\int \hat{U}(f) df}}, \quad (1)$$

while the spectral standard deviation was defined as

$$\sigma_F = \sqrt{\frac{\int f^2 \cdot \hat{U}(f) df}{\int \hat{U}(f) df}}. \quad (2)$$

In equations (1) and (2),  $\hat{U}(f)$  is the fast Fourier transform (FFT) of a given waveform  $U(t)$ ,  $f$  is the frequency vector associated with the FFT of a waveform, and  $f_{MAX}$  is the frequency at which the maximum amplitude of the FFT was observed. The  $MF$  may be thought of as a scaled centroidal frequency, while the spectral standard deviation can be thought of as the second moment (standard deviation or spread) of a given waveform's FFT. Through these two metrics the natural clustering of MAE waveforms which are related to the various types of damage mechanisms can be observed in the frequency domain.

#### 4.3 Sensor Calibrations

Two primary sensor calibrations are required in [3, 4, 10, 11], which were also used in this study. First, to insure that a given transducer has an appropriate level of sensitivity to sense the out-of-plane surface motions that are generated by the propagating stress waves, an absolute calibration of the sensor is required. The absolute calibration of the B1025 transducers was accomplished using a heterodyne Michelson interferometer, following the approach of Wagner [13]. An example of the magnitude response of a B1025 (S/N R1464) is shown in Figure 4.2, from which it is clear that the response of the sensor is flat (within  $\pm 6$  dB) over a broad frequency range (50 – 500 kHz). The flatness of a sensor is a key component in the ability to identify the propagating plate wave modes, and thus perform MAE analyses.

The second calibration which is required in [3, 4, 10, 11] is referred to as a Rolling Ball Impact (RBI) calibration. The essence of the RBI calibration is to determine the conversion factor from mechanical energy to transduced electrical energy for a given sensor-system configuration. In the calibration a hardened steel ball rolls down an inclined plane and impacts the mid-plane of a 7075-T6 Aluminum plate having large lateral dimensions with the transducer under test mounted to the plate. The impact of the ball generates the fundamental extensional and flexural plate modes, as shown in Figure 4.3. The recorded energy of the first cycle of the transduced extensional mode is then compared to the known mechanical energy of the rolling ball [4], and a conversion factor for a given transducer is determined.

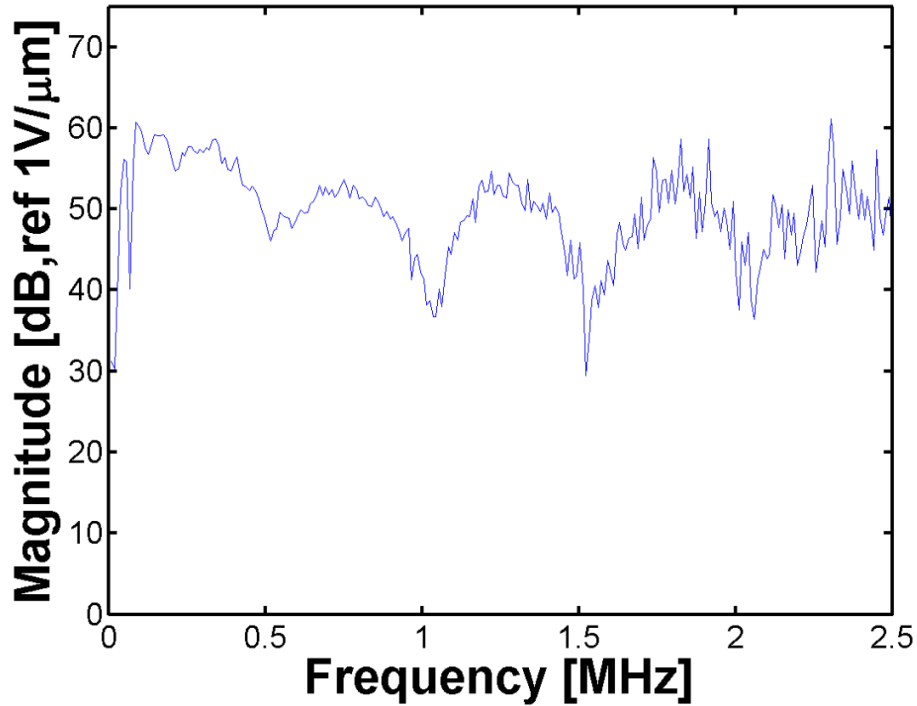


Figure 4.2 – Absolute magnitude response of a B1025 sensor (S/N: R1464)

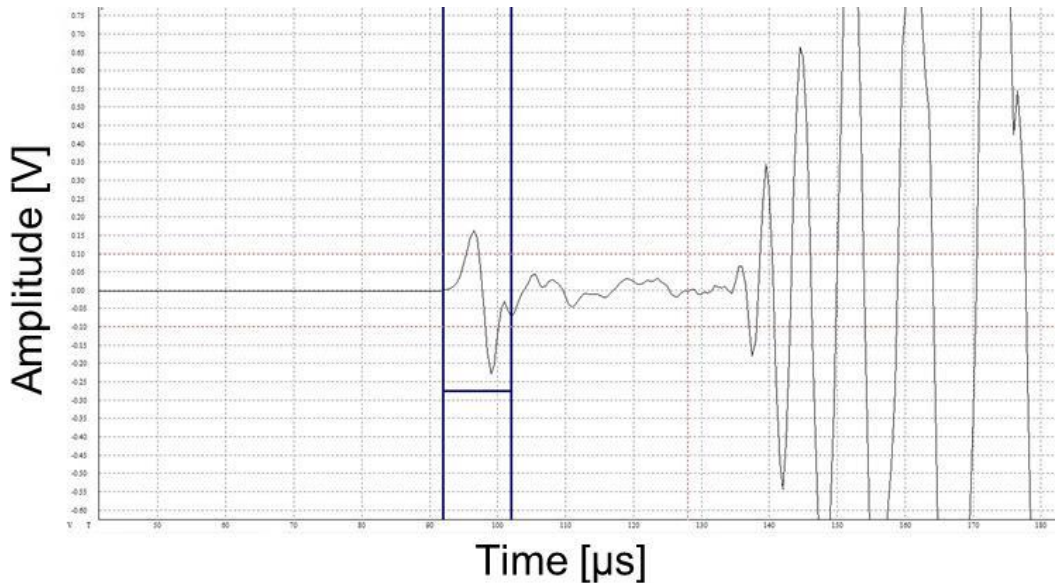


Figure 4.3 – Example of the waveform captured from a rolling ball impact calibration.

#### 4.4 Stability

During the two holds at the test pressure of the cylinder, both the number of events and the cumulative energy from the events are partitioned into equally spaced bins for the entire hold time. Both metrics must be found to be exponentially decaying, with the requirements for the exponential decay rate parameter ( $B$ ) and the goodness of fit ( $R^2$ ) summarized in Table 4.1.

**Table 4.1 – Summary of the requirements for stability curve fitting parameters.**

Metric	Exponential Decay Parameter (B) Requirements	R <sup>2</sup> Requirement
Events	-0.1 < B < -0.0001	R <sup>2</sup> ≥ 0.80
Energy	-0.2 < B < -0.0001	R <sup>2</sup> ≥ 0.80

Typically, stability is a metric that is more applicable to cylinders that have just been manufactured, and is less applicable to cylinders that have experienced several cycles to operating and test pressure. Due to several cycles to operating and test pressure during the in-service life of the current SCBA cylinders, minimal new matrix cracking is taking place resulting in very few events occurring during the holds at test pressure; such observations are in good agreement with the Kaiser Effect. If not enough events occur during the holds at test pressure the composite is deemed to be stable due to a lack of emission, and is considered to meet the stability criteria.

#### 4.5 Background Energy

The background energy is defined as the minimum value of energy of a windowed contiguous portion of a given waveform.

A rise in the background energy level above the quiescent level greater than a multiplicative factor, call it  $M_R$ , indicates that a large amount of localized damage is occurring.

An oscillation in an N point moving average of the background energy values on a given channel greater than a multiplicative factor, call it  $M_O$ , between the adjacent maximum background energy level to the minimum background energy level indicates that the composite pressure cylinder has begun progressing towards failure, and that the internal pressure within the cylinder should be reduced immediately.

It has been shown in [5], and will be shown in this report, that an oscillation of the background energy of greater than two occurs on average at 60% of the burst strength of the SCBA pressure cylinder. Hence, by using the background energy oscillation metric, cylinders with burst strengths below a minimum value may be identified and removed from service.

Thus, any rise in the background energy level greater than  $M_R$ , or any oscillation in the background energy greater than  $M_O$  at or below the test pressure of a DOT-CFFC cylinder shall fail the cylinder under test.

#### 4.6 Fiber bundle Fracture Energy

Fiber bundle fracture energy during the second pressurization cycle to test pressure shall be less than  $2.7 \times 10^{-16}$  J for carbon fiber composite cylinders. The burst strength of composite overwrapped pressure cylinders is known to be a fiber dominated property, thus by setting a criteria of only allowing ~6,000 filaments to fracture on a single event, a conservative restriction has been put in place to extend the life of a cylinder. Note that the energy conversion for wave transduction by the specific sensor must be accounted for using the Rolling Ball Impact calibration described in National Board Inspection Code NB10-0601 Supplement S9 [4]. An

example calculation of the mechanical energy released from a single fiber fracture is provided in [4]. Further, NB10-0601 and DOT-SP 15720 provide the energy ratios in particular frequency bands used to determine if a fiber fracture has occurred.

#### 4.7 Single MAE Event Energy

The energy of any single MAE event on the second test pressurization cycle shall be less than  $2.7 \times 10^{-14}$  J. Extremely large energy events are indicative that a significant stress concentrator exists in the structure that could compromise the cylinders structural integrity. See Section 4.6 regarding energy scaling for a given transducer and the necessity for the Rolling Ball Impact calibration.

### 5. Visual Inspection

#### 5.1 Hard Water Exposure

Prior to the hard water exposure an external and internal visual inspection of the cylinder was performed per CGA C6-2 [12], the results of which are summarized in Table 5.1. For the internal visual inspection a RF System Lab 6.9 mm VJ-Advanced borescope camera was used to provide enhanced internal visual inspection capabilities. It is highlighted that of the ten (10) cylinders, nine (9) cylinders showed some form of corrosion during the internal visual inspection. Figure 5.1a shows the 6061 T6 Al liner of ALT639 - 9573 prior to hard water exposure. As shown in Table 5.1, cylinder ALT639 - 9573 did not exhibit any significant signs of a corrosion process occurring to the 6061 Al liner prior to hard water exposure, and only showed signs of mild water staining. Figure 5.1b shows an image from the internal visual inspection of ALT639 - 9573 after the hard water exposure, where a significant amount of calcium carbonate build up (white spotting) was readily observed. The calcium carbonate build up observed in ALT639-9573 was representative for all ten cylinders subjected to the hard water exposure, and was consistent with the crack initiation sites observed in [5].

**Table 5.1 – Summary of the ten (10) DOT-CFFC cylinders subjected to hard water exposure, a re-autofrettage process, fatigue cycling, and then an EOL burst test.**

Test	Location	Manufacturer	DOT-SP	Time	SN	Mfg Date	Pressure	Internal Visual Inspection	External Visual Inspection	Visually Condemned [Y/N]
Re-autofrettage, Fatigue, and EOL	Walker Township	SCI	10945	30	ALT639-18114	12-98	4500	Water stained throughout; Mineral Build up throughout; Good threads	L1 abrasions BD	N
Re-autofrettage, Fatigue, and EOL	Mid-Atlantic Fire and Air	SCI	10945	30	ALT639-9573	02-98	4500	Good liner; Good Threads	L1 cuts and abrasions throughout	N
Re-autofrettage, Fatigue, and EOL	Riverside	SCI	10945	30	ALT639-34075	08-99	4500	Water stains bottom dome; scratches visible; Good threads	L1 cuts throughout; L2 cut on bottom dome	N
Re-autofrettage, Fatigue, and EOL	FDNY	SCI	10945	45	ALT695-5916	09-98	4500	Water stained throughout; Worn threads	L1 abrasions throughout; L2 cuts on bottom dome	N
Re-autofrettage, Fatigue, and EOL	FDNY	SCI	10945	60	ALT604-6148	10-98	4500	Water stained throughout; observable pitting; Good threads	L1 abrasions throughout; L2 cuts on bottom dome	N
Re-autofrettage, Fatigue, and EOL	Fairfax, VA	Luxfer	10915	45	OM3924	08-98	4500	Water stained throughout; minor pitting; Good threads	L1/2 abrasions throughout	N
Re-autofrettage, Fatigue, and EOL	Fairfax, VA	Luxfer	10915	45	OM3972	08-98	4500	Water stained throughout; minor pitting; Good threads	L1/2 abrasions throughout	N
Re-autofrettage, Fatigue, and EOL	Fairfax, VA	Luxfer	10915	45	OM3943	08-98	4500	Water stained throughout; minor pitting; Good threads	L1/2 abrasions throughout	N
Re-autofrettage, Fatigue, and EOL	Fairfax, VA	Luxfer	10915	45	OM3992	08-98	4500	Minor water stains throughout; good threads	L1/2 abrasions throughout	N
Re-autofrettage, Fatigue, and EOL	Fairfax, VA	Luxfer	10915	45	OM3936	08-98	4500	Water stained throughout; minor pitting; Good threads	L1/2 abrasions throughout	N

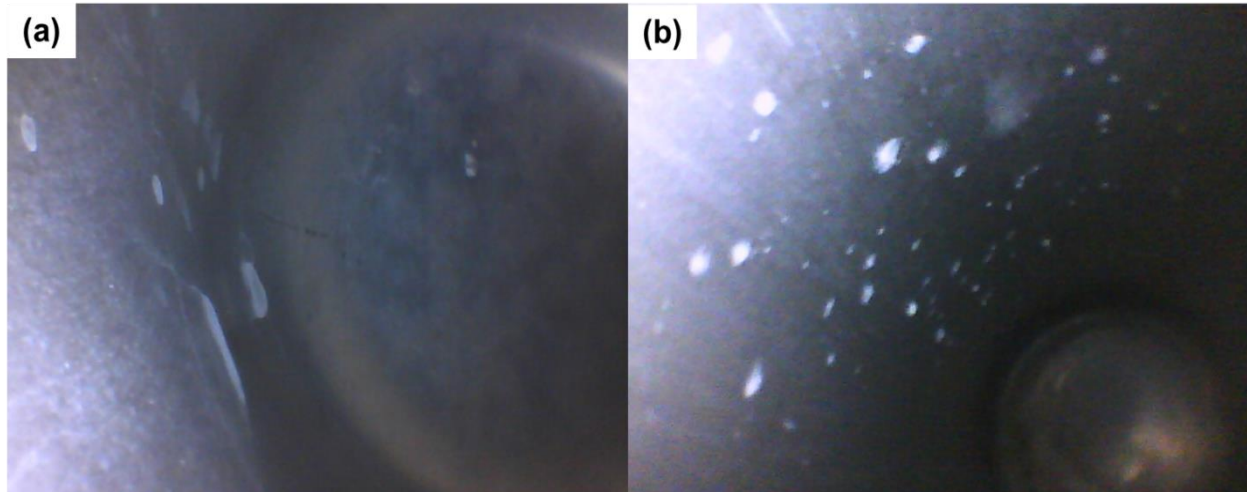


**Figure 5.1 – Internal visual inspection image from borescope imaging (a) prior to, and (b) post hard water exposure.**

## 5.2 Chemical Exposure

Prior to any physical testing (i.e., chemical exposure while under pressure, re-autofrettage, fatigue cycling, and/or EOL burst testing) an external and internal visual inspection of the cylinder was performed per CGA C6-2 [12], the results of which are summarized in Table 5.2. For the internal visual inspection a RF System Lab 6.9 mm VJ-Advanced borescope camera was used to provide enhanced internal visual inspection capabilities. It is highlighted that of the fifteen (15) cylinders examined, fourteen (14) cylinders showed some form of corrosion or internal discontinuity during the internal visual inspection. In addition, fourteen (14) of the fifteen (15) cylinders passed the external visual inspection; ALT639-33989 was found to have a level 3 chip on the bottom dome which would have condemned the cylinder.

**Table 5.2 – Summary of the fifteen (15) DOT-CFFC cylinders subjected to chemical exposure while under pressure.**

Location	Chemical	DOT-SP	Time	SN	Mfg Date	Pressure	Internal Visual Inspection	External Visual Inspection	Visually Condemned [Y/N]
Walker Township	Sulfuric Acid	10945	30	ALT639-70015	11/00	4500	Corrosion throughout	Good	N
FDNY	Sulfuric Acid	10945	45	ALT695-5660	09/98	4500	Corrosion throughout	L2 abrasion on bottom dome	N
FDNY	Sulfuric Acid	10945	45	ALT695-1665	03/98	4500	Minor corrosion throughout	L2 abrasion on bottom dome	N
Riverside	Sulfuric Acid	10945	30	ALT639-29405	06/99	4500	Scratches on bottom dome	L2 abrasions on port dome and bottom dome	N
Mid-Atlantic Fire and Air	Sulfuric Acid	10945	30	ALT639-9765	02/98	4500	Minor corrosion throughout	L1 abrasions throughout	N
Riverside	Bleach	10945	30	ALT639-33989	08/99	4500	Water stains throughout	L3 chip on bottom dome	Y
Walker Township	Bleach	10945	30	ALT639-18726	01/99	4500	Stained, mineral deposits throughout	L1 abrasions on bottom dome	N
Riverside	Bleach	10945	30	ALT639-34079	08/99	4500	Water stains throughout	L1 abrasions throughout	N
Fairfax	Bleach	10915	45	OM3909	08/98	4500	Corrosion on bottom dome	L1 abrasions on bottom dome	N
Riverside	Bleach	10945	30	ALT639-34011	08/99	4500	Scratches on bottom dome	L1 abrasions throughout	N
Walker Township	Bleach	10945	30	ALT639-19026	01/99	4500	Good liner and threads	L1 abrasions on bottom and port domes	N
Mid-Atlantic Fire and Air	Bleach	10945	30	ALT639-9605	02/98	4500	Minor corrosion throughout	Good	N
FDNY	Bleach	10945	45	ALT695-5483	09/98	4500	Minor corrosion throughout	L2 chips throughout	N
Mid-Atlantic Fire and Air	Bleach	10945	30	ALT639-9948	02/98	4500	Minor corrosion throughout	L1 abrasions throughout	N
Walker Township	Bleach	10945	30	ALT639-17946	12/98	4500	Minor corrosion throughout	Good	N

### 5.3 Salt Water Immersion

Prior to any physical testing (i.e., salt water immersion while under pressure, or EOL burst testing) an external and internal visual inspection of the cylinder was performed per CGA C6-2 [12], the results of which are summarized in Table 5.3. For the internal visual inspection a RF System Lab 6.9 mm VJ-Advanced borescope camera was used to provide enhanced internal visual inspection capabilities. Eight (8) of the ten (10) cylinders passed the external visual inspection; ALT639-95898 was found to have a Level 3 chip on the bottom dome which condemned the cylinder two years before its allotted fifteen year life and OM3966 had an L3 chip on its port dome. Eight (8) of the ten (10) cylinders inspected exhibited corrosion indications during their internal visual inspection.

**Table 5.3 – Summary of the ten (10) DOT-CFFC cylinders subjected to salt water immersion testing.**

Location	Manufacturer	DOT-SP	Time	SN	Mfg Date	Pressure	Internal Visual Inspection	External Visual Inspection	Visually Condemned [Y/N]
Walker Township	SCI	10945	30	ALT639-18030	12-98	4500	Water stains throughout	L1 abrasion on port dome	N
Walker Township	SCI	10945	30	ALT639-18454	01-99	4500	Mineral deposits throughout	L2 abrasion on bottom dome, L1 abrasions throughout	N
Mid-Atlantic Fire and Air	SCI	10945	30	ALT639-9987	02-98	4500	Good liner, good threads	L1 abrasions throughout	N
Mid-Atlantic Fire and Air	SCI	10945	30	ALT639-9959	02-98	4500	Good liner, good threads	L1 abrasions on port dome	N
Mid-Atlantic Fire and Air	SCI	10945	30	ALT639-9465	02-98	4500	Minor corrosion throughout	L2 chips on port dome;	N
Riverside	SCI	10945	30	ALT639-95898	09-01	4500	Machine marks on bottom dome and cylinder wall	L3 chip on bottom dome	Y
Riverside	SCI	10945	30	ALT639-34061	08-99	4500	Water stains throughout; axial oriented scratch on cylinder wall	L2 cut on bottom dome	N
FDNY	SCI	10945	45	ALT695-5031	08-98	4500	Corrosion on bottom dome	L2 chips on bottom dome	N
FDNY	SCI	10945	45	ALT695-5020	08-98	4500	Corrosion throughout	L1 abrasions throughout	N
Fairfax, VA	Luxfer	10915	45	OM3966	08-98	4500	Minor corrosion throughout	L3 chip on port dome; L1 abrasions throughout	Y

### 5.4 Fire Exposure

Table 5.4 summarizes the results of the visual examination of the fifteen fire exposed DOT-CFFC cylinders which were subjected to the EOL burst test procedure. Prior to the fire exposure, two of the fifteen cylinders had Level 3 damage which would have condemned the cylinders per CGA C.6.2. Post fire exposure, all fifteen cylinders would have met the Level 3 definition of fire damage provided in Section 10.6.3 of CGA C.6.2 [12]. To provide a more in depth analysis, Digital Wave developed a ranking scheme of the severity of fire damage ranging from minor to moderate to severe, shown representatively in Figure 5.2 - Figure 5.4, respectively. Minor Level 3 fire exposure resulted in a light oxidation layer of the sacrificial layer (Figure 5.2). Moderate Level 3 fire exposure resulted in a significant oxidation layer of the sacrificial layer (Figure 5.3). Severe Level 3 fire exposure resulted in resin decomposition that exposed dry fiber (Figure 5.4). It is highlighted that three cylinders experienced severe Level 3 fire exposure, and this was due to the cylinders actually catching on fire for over two minutes during the fire exposure.

**Table 5.4 – Summary of the visual inspection results, pre and post fire exposure for all fifteen EOL burst tested cylinders.**

Location	SN	DOT-SP	Time	Mfg Date	Pressure	Internal Visual Inspection	External Visual Inspection	Visually Condemned [Y/N]	Fire Exposure Level
Walker Township	ALT639-17716	10945	30	12-98	4500	Minor corrosion Throughout	L2 abrasions on bottom dome	N	Moderate
Walker Township	ALT639-17831	10945	30	12-98	4500	Minor corrosion on Bottom Dome	L1 scratches on bottom dome	N	Severe
Walker Township	ALT639-38556	10945	30	11-99	4500	Corrosion and water stains throughout	L2 cut on bottom dome	N	Minor
Walker Township	ALT639-18768	10945	30	01-99	4500	Good	Good	N	Moderate
Mid-Atlantic Fire and Air	ALT639-9747	10945	30	02-98	4500	Good	L1 abrasions on port dome	N	Moderate
Mid-Atlantic Fire and Air	ALT639-9769	10945	30	02-98	4500	Good	L1 abrasions/cuts throughout	N	Severe
Mid-Atlantic Fire and Air	ALT639-9753	10945	30	02-98	4500	Good	L2 abrasions on bottom dome	N	Moderate
Riverside	ALT639-31064	10945	30	07-99	4500	Axial and circumferential scratches throughout; corrosion indications throughout	L2 abrasions on port dome	N	Moderate
Riverside	ALT639-30041	10945	30	06-99	4500	Axial and circumferential scratches throughout; corrosion indications throughout	L3 abrasion on port dome, L2 abrasions throughout	N	Moderate
Riverside	ALT639-23371	10945	30	03-99	4500	Axial and circumferential scratches throughout; corrosion indications throughout	L3 cut on bottom dome	Y	Minor
FDNY	ALT695-3669	10945	45	06-98	4500	Corrosion and water stains on cylinder side wall	L3 cut on bottom dome	Y	Moderate
FDNY	ALT604-3764	10945	45	09-98	4500	Corrosion and water stains throughout	L2 abrasions throughout	N	Severe
FDNY	ALT695-1781	10945	45	03-98	4500	Good	L2 abrasions on bottom dome and cylinder side wall	N	Moderate
Fairfax, VA	OM3968	10915	45	08-98	4500	Good	L2 cuts on bottom dome and cylinder wall	N	Moderate
Fairfax, VA	OM3930	10915	45	08-98	4500	Good	L2 abrasions on cylinder side wall and bottom dome	N	Moderate



**Figure 5.2 – Cylinder exhibiting minor fire exposure damage.**



Figure 5.3 – Cylinder exhibiting moderate fire exposure damage.



Figure 5.4 – Cylinder exhibiting severe fire damage.

## 6. Mechanical Testing Results

### 6.1 Fatigue Analysis

Throughout this work, the thin-walled pressure cylinder equations were used to calculate the hoop ( $\sigma_H$ ) and axial ( $\sigma_A$ ) stress

$$\sigma_H = \frac{pr}{t} \quad (3)$$

$$\sigma_A = \frac{pr}{2t} \quad (4)$$

where  $p$  is the pressure,  $r$  is the radius of the cylinder, and  $t$  is the complete cylinder wall thickness. The hoop stiffness of cylinders was monitored via strain and pressure measurement throughout the entire fatigue cycle testing. As an example, Figure 6.1 shows the hoop modulus fit during a single fatigue cycle of ALT639 – 34075, while Figure 6.2 shows the hoop modulus as a function of the number of cycles applied to ALT639 – 34075. The hoop modulus as a function of number of fatigue cycles for all monitored cylinders is provided in Appendix A. Observations relative to cylinder performance during fatigue cycle testing will be provided in the respective sections.

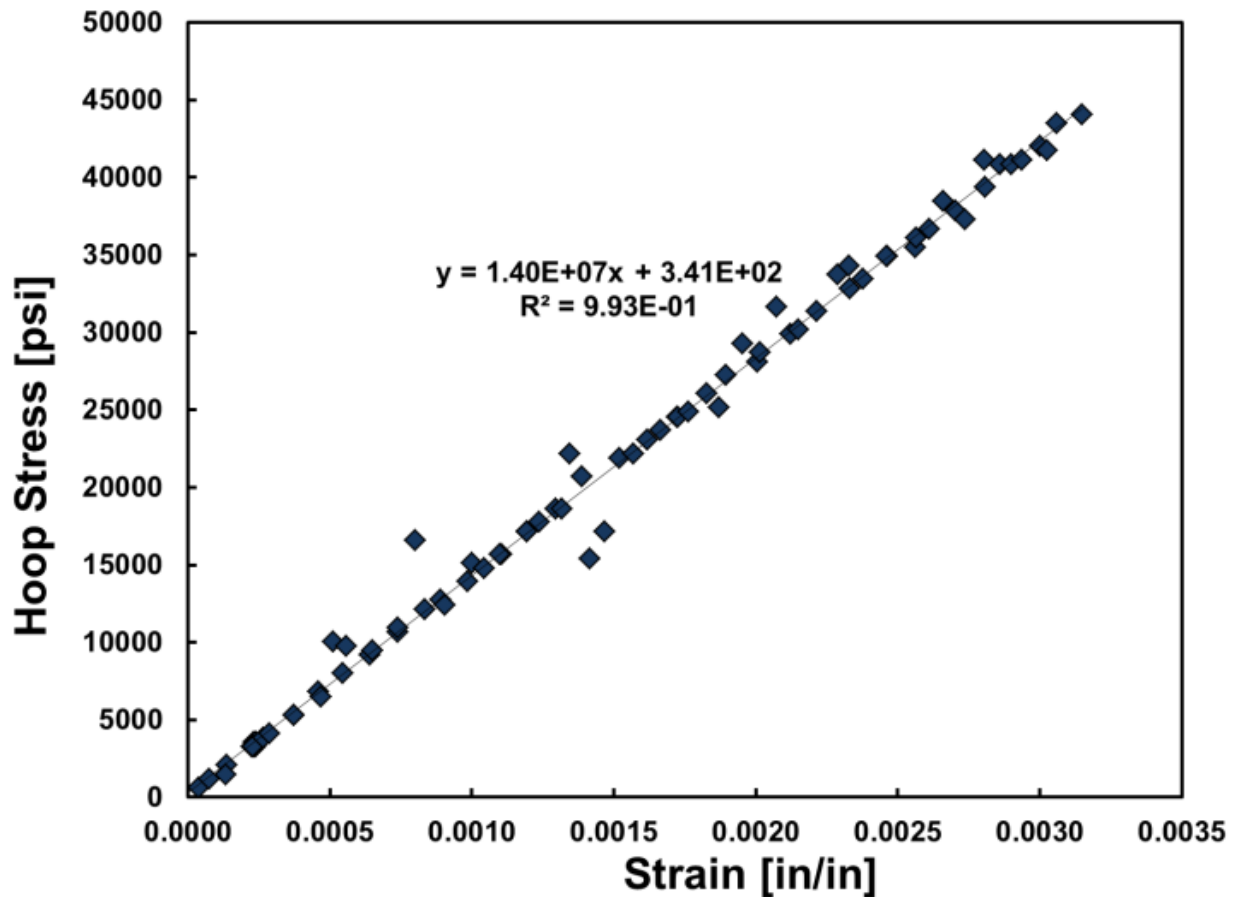


Figure 6.1 – Hoop modulus fit from a single cycle for ALT639 – 34075.

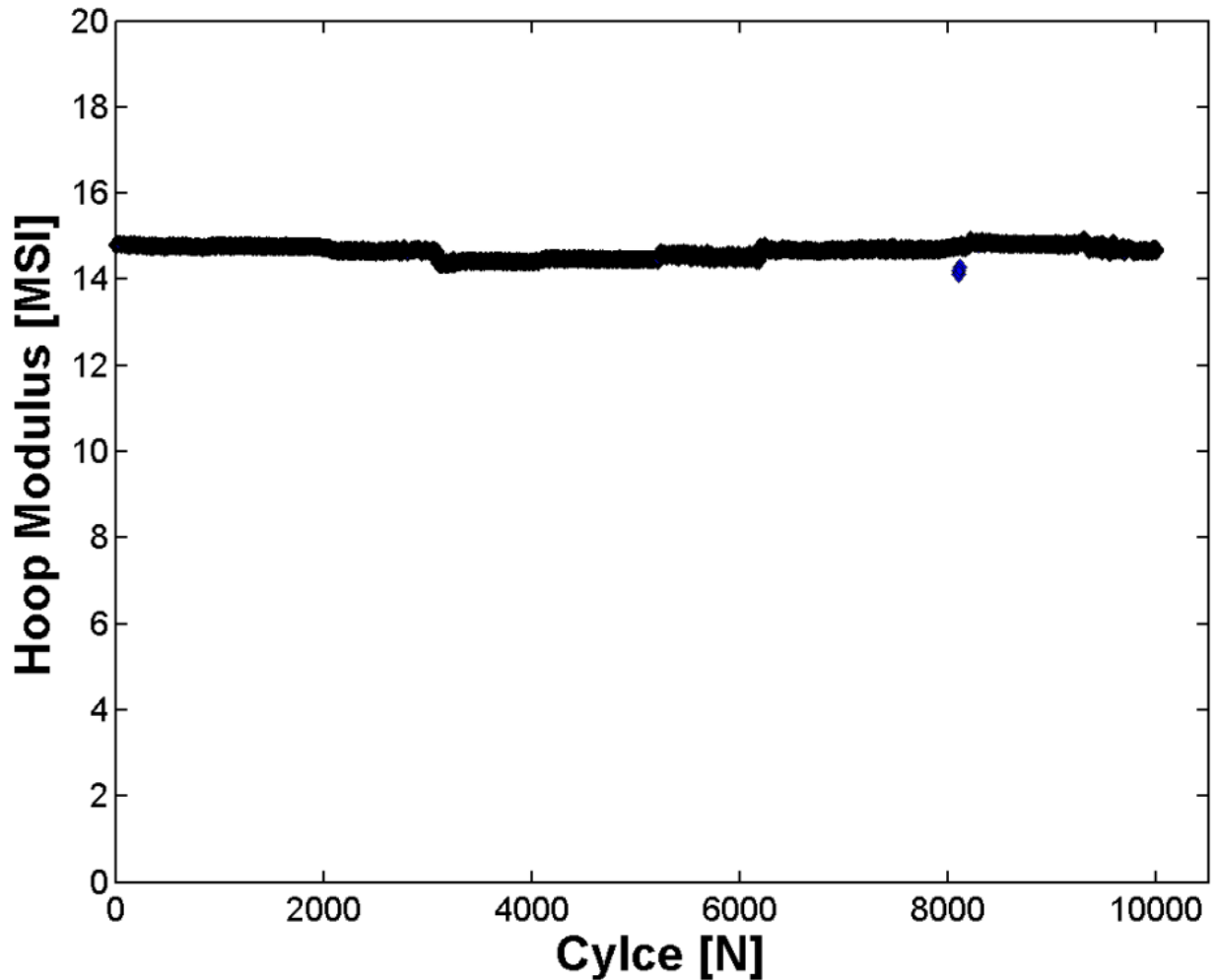


Figure 6.2 – Hoop modulus as a function of the number of applied fatigue cycles for ALT639 – 34075.

### 6.2 Hard Water Exposure

Figure 6.3 provides the stress-strain response during the re-autofrettage process of OM3924. From Figure 6.3 it was observed that upon unloading the cylinder from 8500 psi, roughly 350  $\mu\epsilon$  of permanent deformation had been imparted upon the composite cylinder. Because DOT-CFFC cylinders have been shown to respond in an elastic bi-modulus fashion [5], the permanent deformation ( $\epsilon_p$ ) is attributed to plastic deformation of the aluminum liner. Table 6.1 summarizes the amount of permanent deformation imparted upon each cylinder that was re-autofrettaged. At any location where a crack initiation site exists the local state of stress will be magnified due to the stress concentrator creating a significant plastic zone around the crack tip. Upon removal of the re-autofrettage pressure the material surrounding the crack tip will be put into residual compression, which has been shown to retard the crack growth rate [5].

Modal AE waveforms were captured during the entire re-autofrettage process of all five cylinders identified in Table 6.1. No cylinder failed the MAE acceptance criteria defined in [10], thus all cylinders were subjected to fatigue cycling.

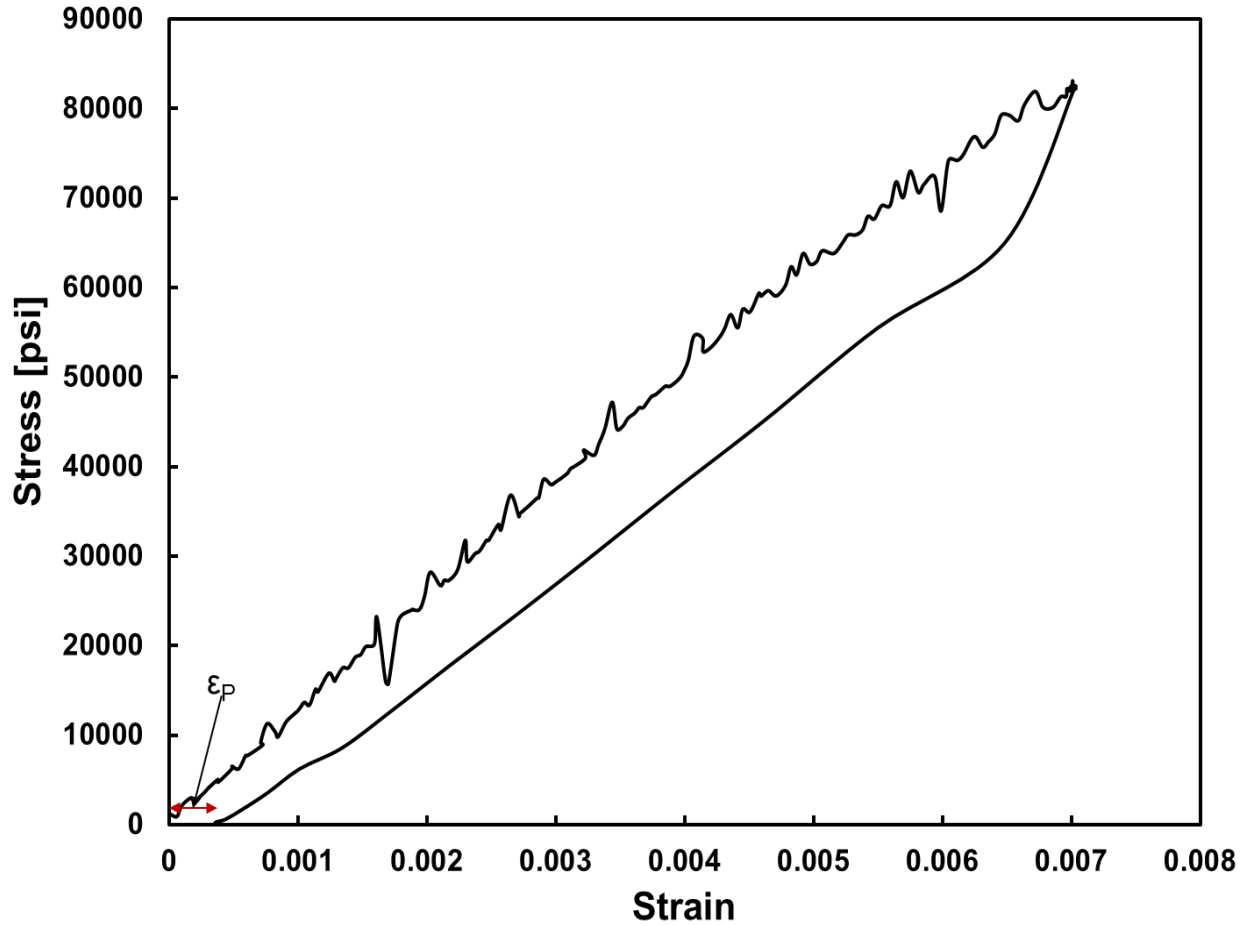


Figure 6.3 – Hoop stress-strain response of OM3924 during the re-autofrettage process.

Table 6.1 – Summary of the permanent deformation imparted upon all cylinders subjected to the re-autofrettage process.

Location	Manufacturer	DOT-SP	Time	SN	Mfg Date	Pressure	Re-autofrettaged [Y/N]	Plastic Deformation [ $\mu\epsilon$ ]
Walker Township	SCI	10945	30	ALT639-18114	12-98	4500	Y	99
Mid-Atlantic Fire and Air	SCI	10945	30	ALT639-9573	02-98	4500	Y	225
Riverside	SCI	10945	30	ALT639-34075	08-99	4500	Y	250
FDNY	SCI	10945	45	ALT695-5916	09-98	4500	N	-
FDNY	SCI	10945	60	ALT604-6148	10-98	4500	N	-
Fairfax, VA	Luxfer	10915	45	OM3924	08-98	4500	Y	349
Fairfax, VA	Luxfer	10915	45	OM3972	08-98	4500	N	-
Fairfax, VA	Luxfer	10915	45	OM3943	08-98	4500	Y	313
Fairfax, VA	Luxfer	10915	45	OM3992	08-98	4500	N	-
Fairfax, VA	Luxfer	10915	45	OM3936	08-98	4500	N	-

Figure 6.1 shows the hoop modulus fit during a single fatigue cycle of ALT639 – 34075, while Figure 6.2 shows the hoop modulus as a function of the number of cycles applied to ALT639 – 34075. The hoop modulus as a function of number of fatigue cycles for all monitored cylinders is provided in Appendix A. From Figure 6.2 it is clear that the stiffness of the cylinder was not deteriorating during fatigue cycling. Further, in Appendix A it is shown that no cylinder which was subjected to hard water exposure and subsequently fatigue cycled exhibited any

degradation in stiffness. Additional confirmation of the lack of any composite degradation during fatigue cycling was found via analysis of the MAE waveforms. During cycling to maximum developed pressure no events related to composite material failure were detected, with all detected waveforms being very low frequency and attributed to mechanical rubbing against the containment saddles.

What was observed during the cyclic fatigue testing of the ten cylinders was the detrimental effect that hard water exposure had on the fatigue performance of the cylinders which were not re-autofrettaged. All five cylinders which were not re-autofrettaged leaked well before the target 10,000 cycles, and well before the number of cycles at which cylinders from [5] leaked (when the liners were not subjected to hard water exposure). Further confirmation of the efficacy of the re-autofrettage process proposed in [5] was established in this work, as all five cylinders which were subjected to the re-autofrettage process obtained 10,000 fatigue cycles and all burst well above the minimum required burst pressure of DOT-CFFC 5<sup>th</sup> Revision [1]. Table 6.2 summarizes the total number of cycles achieved by each cylinder subjected to hard water exposure.

**Table 6.2 – Summary of the total number of fatigue cycles obtained by each cylinder which had its liner exposed to hard water for 10 days.**

Location	DOT-SP	Time	SN	Mfg Date	Visually Condensed [Y/N]	Re-autofrettaged [Y/N]	MAE Life Extension [Y/N]	Number of Cycles	BEOP [psi]	Burst Pressure [psi]
Walker Township	10945	30	ALT639-18114	12-98	N	Y	Y	10000	13900	22100
Mid-Atlantic Fire and Air	10945	30	ALT639-9573	02-98	N	Y	Y	10000	12130	19144
Riverside	10945	30	ALT639-34075	08-99	N	Y	Y	10000	11150	20330
FDNY	10945	45	ALT695-5916	09-98	N	N	-	4142	-	-
FDNY	10945	60	ALT604-6148	10-98	N	N	-	3830	-	-
Fairfax, VA	10915	45	OM3924	08-98	N	Y	Y	10000	10140	16640
Fairfax, VA	10915	45	OM3972	08-98	N	N	-	2111	-	-
Fairfax, VA	10915	45	OM3943	08-98	N	Y	Y	10000	10371	17400
Fairfax, VA	10915	45	OM3992	08-98	N	N	-	3830	-	-
Fairfax, VA	10915	45	OM3936	08-98	N	N	-	2114	-	-

Prior to the burst pressurization of the five re-autofrettaged cylinders which successfully achieved 10,000 fatigue cycles, the test pressurization schedule and the accept/reject criteria of [5, 10] to evaluate (using MAE) the integrity of the cylinder was utilized. All five cylinders were found to meet the acceptance criteria for life extension and all five cylinders burst above the minimum required burst pressure of [1], even after 15 years of service life and an additional simulated 20 years of service life (Table 6.2).

All cylinders were found to respond in a bi-modulus fashion in both the hoop and axial directions. Figure 6 provides the stress-strain response of ALT639 – 18114, from which the bi-modulus response in each of the principal directions can be observed. Up to 8500 psi (the new test pressure of the re-autofrettaged cylinders), the aluminum liner is contributing to the stiffness of the cylinder, whereas after 8500 psi the aluminum is plastically deforming and its stiffness contribution to the cylinder wall becomes negligible. Appendix B provides the stress-strain response of all cylinders during the burst pressurization ramp, while Table 6.3 summarizes the primary and secondary hoop and axial moduli for all tested cylinders.

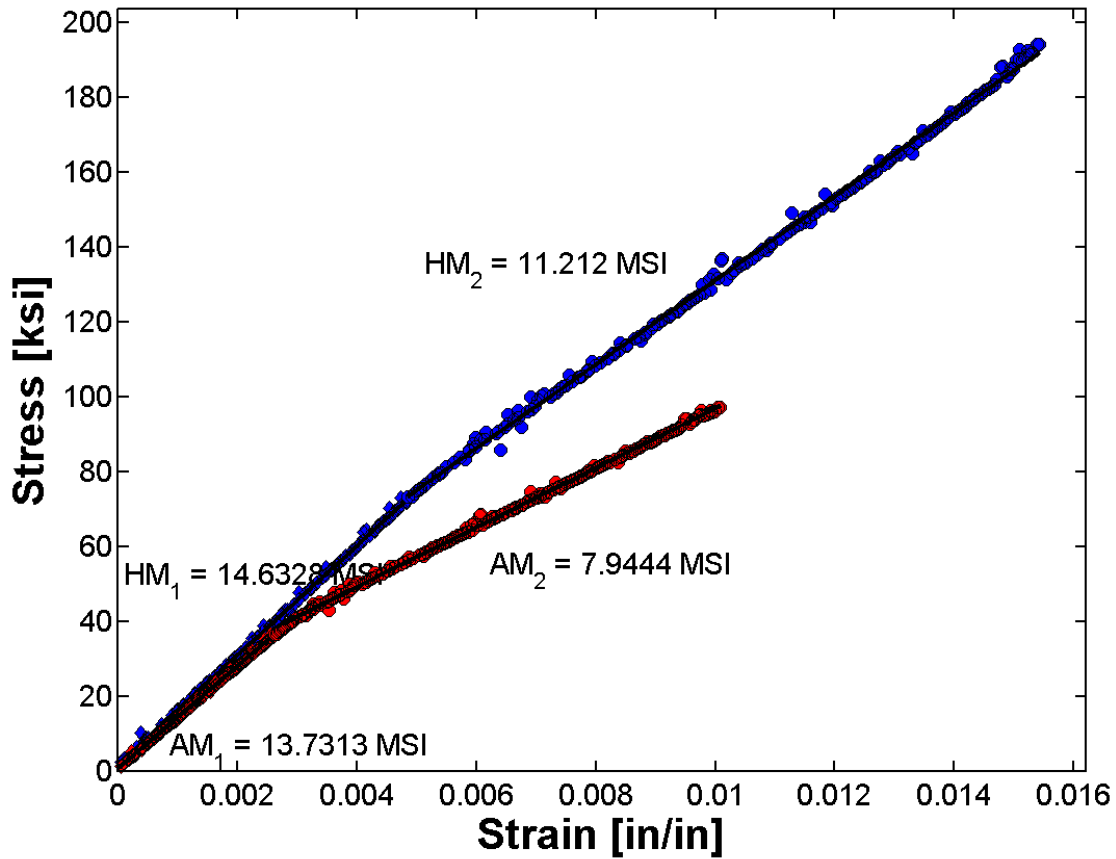


Figure 6.4 – Stress-strain response of ALT639 – 18114 during the burst ramp pressurization. Note, the blue markers are hoop response data points, while the red markers are axial response data points.

Table 6.3 – Summary of primary and secondary hoop and axial moduli measured on all burst cylinders.

Location	DOT-SP	Time	SN	Re-autofrettaged [Y/N]	MAE Life Extension [Y/N]	Number of Cycles	BEOP [psi]	Burst Pressure [psi]	BEOP/BP [%]	Primary Hoop Modulus [MSI]	Secondary Hoop Modulus [MSI]	Primary Axial Modulus [MSI]	Secondary Axial Modulus [MSI]
Walker Township	10945	30	ALT639-18114	Y	Y	10000	13900	22100	63%	14.6	11.2	13.7	7.9
Mid-Atlantic Fire and Air	10945	30	ALT639-9573	Y	Y	10000	12130	19144	63%	12.7	9.6	12.8	7.1
Riverside	10945	30	ALT639-34075	Y	Y	10000	11150	20330	55%	14.0	9.9	12.1	7.6
FDNY	10945	45	ALT695-5916	N	-	4142	-	-	-	-	-	-	-
FDNY	10945	60	ALT604-6148	N	-	3830	-	-	-	-	-	-	-
Fairfax, VA	10915	45	OM3924	Y	Y	10000	10140	16640	61%	12.6	9.2	12	6.5
Fairfax, VA	10915	45	OM3972	N	-	2111	-	-	-	-	-	-	-
Fairfax, VA	10915	45	OM3943	Y	Y	10000	10371	17400	60%	13.7	9.6	11.9	6.5
Fairfax, VA	10915	45	OM3992	N	-	3830	-	-	-	-	-	-	-
Fairfax, VA	10915	45	OM3936	N	-	2114	-	-	-	-	-	-	-

### 6.3 Chemical Exposure

The hoop stiffness of cylinders was monitored via strain and pressure measurement throughout the entire fatigue cycle testing. Figure 6.5 shows the hoop modulus determination during a single fatigue cycle of ALT639 – 9765, while Figure 6.6 shows the hoop modulus as a function of the number of cycles applied to ALT639 – 9765. The hoop modulus as a function of number of applied fatigue cycles for all monitored cylinders in which strain data was available is provided in Appendix A. From Figure 6.6 it is clear that the stiffness of the cylinder was not deteriorating during fatigue cycling. Further, in Appendix A it is shown that no cylinder which

was subjected to chemical exposure exhibited and degradation in stiffness during fatigue cycling. Additional confirmation of the lack of any composite degradation during fatigue cycling was found via analysis of the MAE waveforms. During cycling to maximum developed pressure no events related to composite material failure were detected, with all detected waveforms being very low frequency and attributed to mechanical rubbing against the containment saddles. All five (5) cylinders which were subjected to fatigue cycle testing achieved the required 10,000 fatigue cycles (equivalent to a simulated 20 additional years of service). Again, the re-autofrettage process of the aluminum liner prior to the fatigue cycling test completely mitigated liner leakage.

Of the five cylinders that were subjected to fatigue cycling, three (3) of the cylinders leaked during the EOL Burst test (Table 6.4). Such findings indicate that re-autofrettage process sufficiently retards crack growth when stress levels are kept to normal operating levels. However, when a burst pressurization is attempted on a fatigue cycled cylinder the remaining ligament in the aluminum liner may be small enough such that the liner plastically tears, causing the cylinder to leak during the burst test. It is pointed out that all three of the cylinders that leaked were 30 minute air capacity cylinders, which have a thinner aluminum liner than larger air capacity cylinders (0.080" thickness, versus 0.100"+ thickness for larger volume cylinders). The three (3) cylinders that leaked during the burst test did meet the acceptance criteria of Section 8.5.8 of ISO 11119.2:2002 [9].

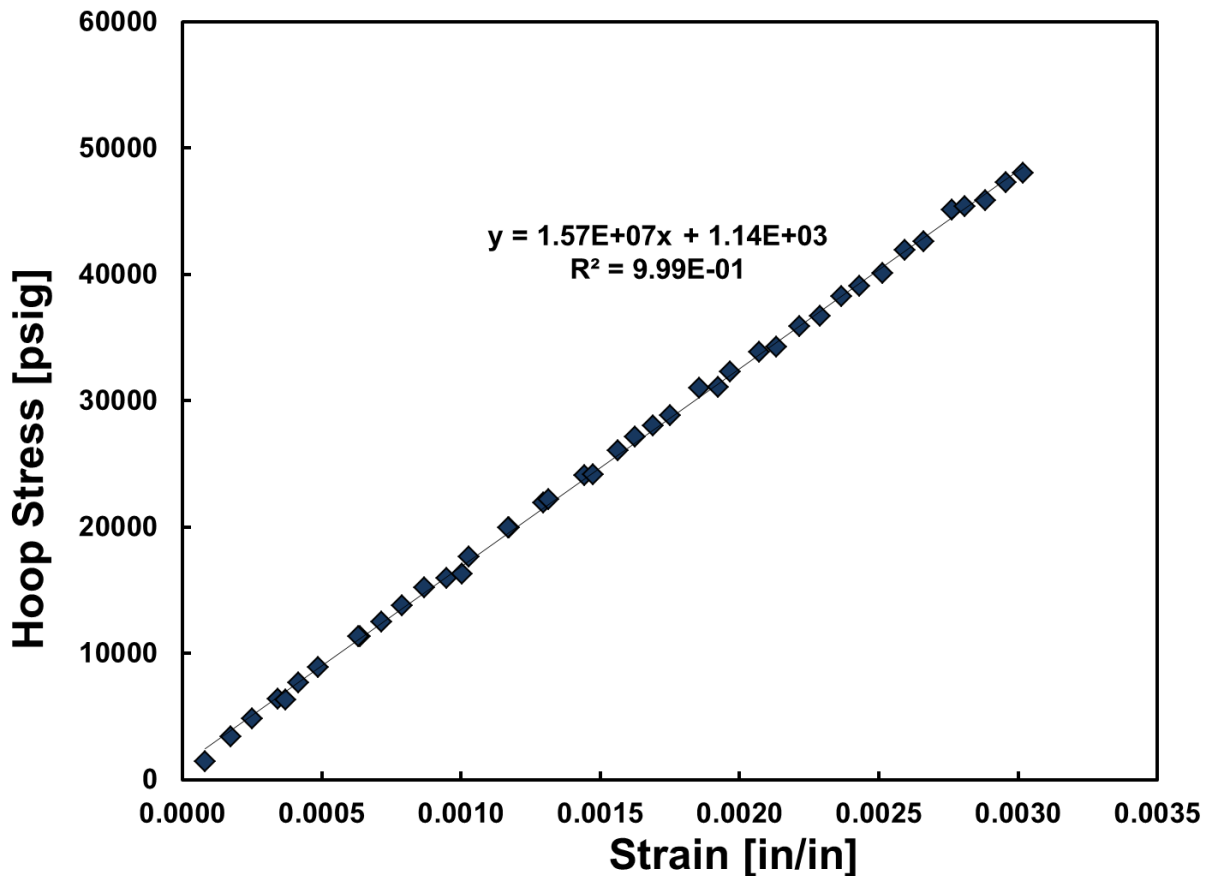


Figure 6.5 – Hoop modulus fit from a single cycle for ALT639 – 9765.

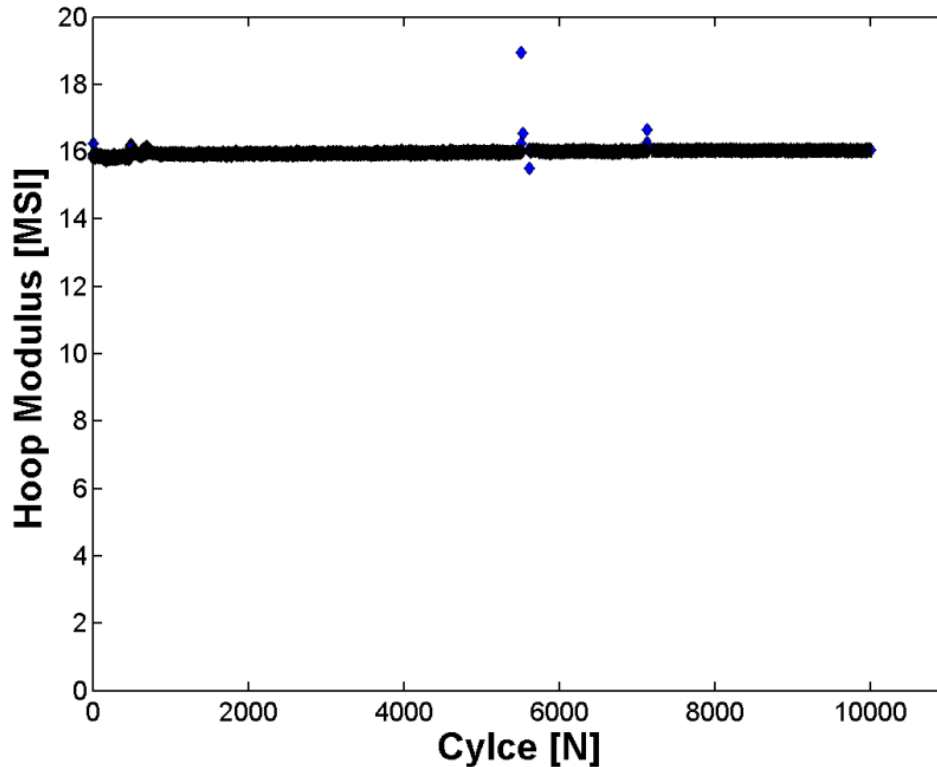


Figure 6.6 – Hoop modulus as a function of the number of applied fatigue cycles for ALT639 – 9675.

During burst testing all cylinders were found to respond in a bi-modulus fashion in both the hoop and axial directions. Figure 6.7 provides the stress-strain response of ALT639 – 70015, from which the bi-modulus response in each of the principal directions can be observed. Up to the autofrettage pressure of the cylinders, the aluminum liner is contributing to the stiffness of the cylinder, whereas after the autofrettage pressure (7500 psig for normal cylinders, 8500 psig for the re-autofrettaged cylinders) the aluminum is plastically deforming and its stiffness contribution to the cylinder wall becomes negligible. Appendix B provides the stress-strain response of all cylinders during the burst pressurization ramp, while Table 6.4 summarizes the primary and secondary hoop and axial moduli for all tested cylinders.

Also summarized in Table 6.4 is the burst pressure of all cylinders, from which it is observed that chemical exposure or chemical exposure followed by a simulated twenty (20) additional years of service life had no detrimental effects on the cylinder burst strengths. All twelve (12) cylinders which could actually be burst had a burst strength well above the minimum required burst strength of the DOT-CFFC 5th Revision (15,300 psig). Further, fourteen (14) of the fifteen (15) cylinders achieved a pressure greater than that required by DOT special permits allowing for service life extension up to thirty (30) years [14, 15]; one cylinder (ALT639-17946) leaked during the re-qualification portion of the EOL burst test.

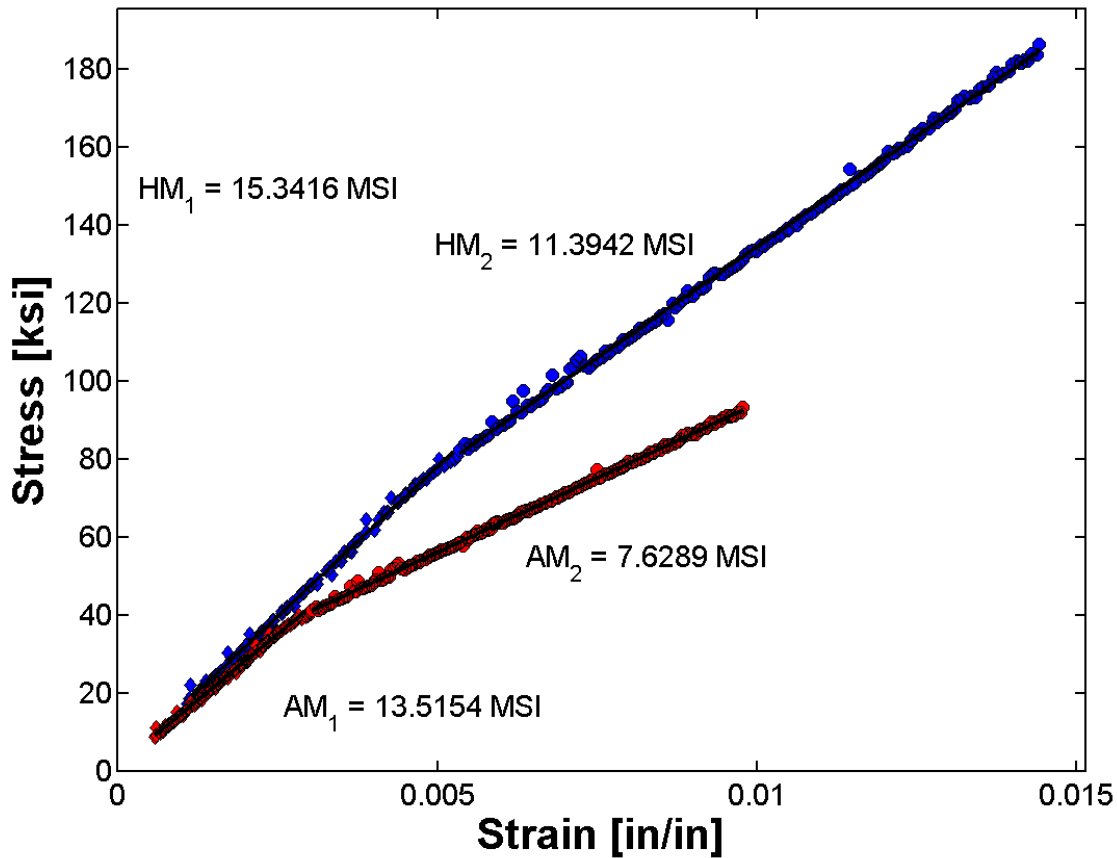


Figure 6.7 – Stress-strain response of ALT639 – 70015 during the burst ramp pressurization. Note, the blue markers are hoop response data points, while the red markers are axial response data points.

Table 6.4 – Summary of primary and secondary hoop and axial moduli measured on all burst cylinders which were exposed to chemical attack.

Location	DOT-SP	Time	SN	Chemical Exposure	MAE Life Extension [Y/N]	Number of Cycles	BEOP [psi]	Burst Pressure [psi]	BEOP/BP [%]	Primary Hoop Modulus [MSI]	Secondary Hoop Modulus [MSI]	Primary Axial Modulus [MSI]	Secondary Axial Modulus [MSI]
Walker Township	10945	30	ALT639-70015	Sulfuric Acid	Y	N/A	11690	19305	60.6%	15.3	13.5	11.4	7.6
FDNY	10945	45	ALT695-5660	Sulfuric Acid	Y	N/A	11850	19270	61.5%	15.3	11.3	11.9	6.8
FDNY	10945	45	ALT695-1665	Sulfuric Acid	Y	N/A	10209	18610	54.9%	14.7	12.6	11.1	7.5
Riverside	10945	30	ALT639-29405	Sulfuric Acid	Y	10k	10740	18935	56.7%	15.2	14.2	10.9	8.2
Mid-Atlantic Fire and Air	10945	30	ALT639-9765	Sulfuric Acid	Y	10k	12025	14670*	N/A	18.9	12.4	13.6	6.7
Riverside	10945	30	ALT639-33989	Bleach	Y	N/A	11485	19490	58.9%	15.0	14.5	11.7	9.7
Walker Township	10945	30	ALT639-18726	Bleach	Y	N/A	12011	21080	57.0%	16.5	13.4	12.3	7.7
Riverside	10945	30	ALT639-34079	Bleach	Y	N/A	9900	17600	56.3%	14.8	13.4	10.7	7.7
Fairfax	10915	45	OM3909	Bleach	Y	N/A	9550	15371	62.1%	14.8	12.3	10.7	6.4
Riverside	10945	30	ALT639-34011	Bleach	Y	N/A	12525	21400	58.5%	13.3	13.6	9	7.6
Walker Township	10945	30	ALT639-19026	Bleach	Y	N/A	9990	19720	50.7%	16.5	13.2	12.1	7.9
Mid-Atlantic Fire and Air	10945	30	ALT639-9605	Bleach	Y	N/A	12240	18350	66.7%	16.3	13.7	12.3	7.7
FDNY	10945	45	ALT695-5483	Bleach	Y	10k	12700	19520	65.1%	14.9	12.8	12	7.4
Mid-Atlantic Fire and Air	10945	30	ALT639-9948	Bleach	N <sup>†</sup>	10k	N/A	12300*	N/A	15.3	13.5	11.1	12
Walker Township	10945	30	ALT639-17946	Bleach	N/A	10k	N/A	5600*	N/A	17.3	13.2	-	-

\* Vessel leaked prior to burst during the EOL Burst procedure at the pressure indicated

<sup>†</sup> Fiber fracture failure criteria exceeded on 2nd TPC

## 6.4 Salt Water Immersion

The hoop stiffness of all salt water immersed cylinders was monitored via strain and pressure measurement throughout the entire fatigue cycle testing. Figure 6.8 shows the hoop modulus as a function of the number of cycles applied to ALT639 – 9987. The hoop modulus as a function of number of applied fatigue cycles for all monitored cylinders in which strain data was available is provided in Appendix A. From Figure 6.8 it is clear that the stiffness of the cylinder was not deteriorating during fatigue cycling. Further, in Appendix A it is shown that no cylinder which was subjected to the salt water immersion testing exhibited and degradation in stiffness during to fatigue cycle testing. Additional confirmation of the lack of any composite degradation during fatigue cycling was found via analysis of the MAE waveforms. During cycling to maximum developed pressure no events related to composite material failure were detected, with all detected waveforms being very low frequency and attributed to mechanical rubbing against the containment saddles. All five (5) cylinders which were subjected to fatigue cycle testing achieved the required 10,000 fatigue cycles (equivalent to a simulated 20 additional years of service). Once again the re-autofrettage process of the aluminum liner prior to the fatigue cycling test completely mitigated liner leakage.

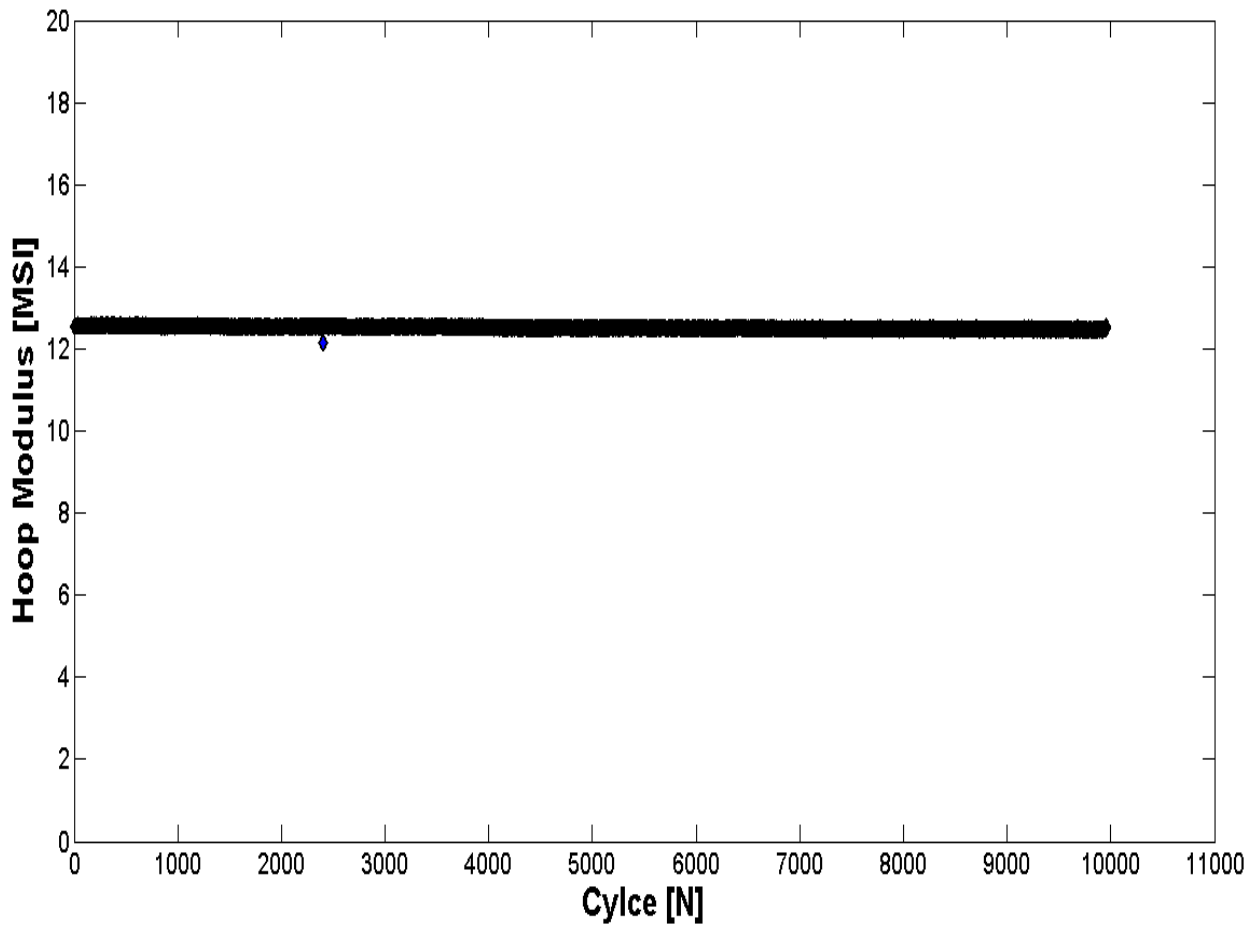


Figure 6.8 – Hoop modulus as a function of the number of applied fatigue cycles for ALT639 – 9987.

From a mechanical response perspective, all cylinders were found to respond in a bi-modulus fashion in both the hoop and axial directions. Figure 6.9 provides the stress-strain response of ALT639 – 95898, from which the bi-modulus response in each of the principal directions can be observed. Up to the autofrettage pressure of the cylinders, the aluminum liner is contributing to the stiffness of the cylinder, whereas after the autofrettage pressure the aluminum is plastically deforming and its stiffness contribution to the cylinder wall becomes negligible. Appendix B provides the stress-strain response of all cylinders during the burst pressurization ramp, while Table 6.5 summarizes the primary and secondary hoop and axial moduli for all tested cylinders.

Also summarized in Table 6.5 is the burst pressure of all cylinders, from which it is observed that salt water immersion had no detrimental effects on the cylinder burst strength. Nine (9) of the ten (10) cylinders had a burst strength well above the minimum required burst strength of the DOT-CFFC 5th Revision (15,300 psig) [1]. The aluminum liner of ALT695-5031, which was subjected to an additional 10,000 fatigue cycles, tore at 12,000 psig during the burst pressurization; it is highlighted that the composite overwrap was still structurally sound at 12,000 psig, but the aluminum liner tore during the burst pressurization due to an active flaw within the aluminum and was thus no longer able to build pressure. It is pointed out that ALT695-5031 passed the ISO 11119.2:2002 fatigue cycling requirements of Section 8.5.8 for an additional twenty (20) years of service life [9].

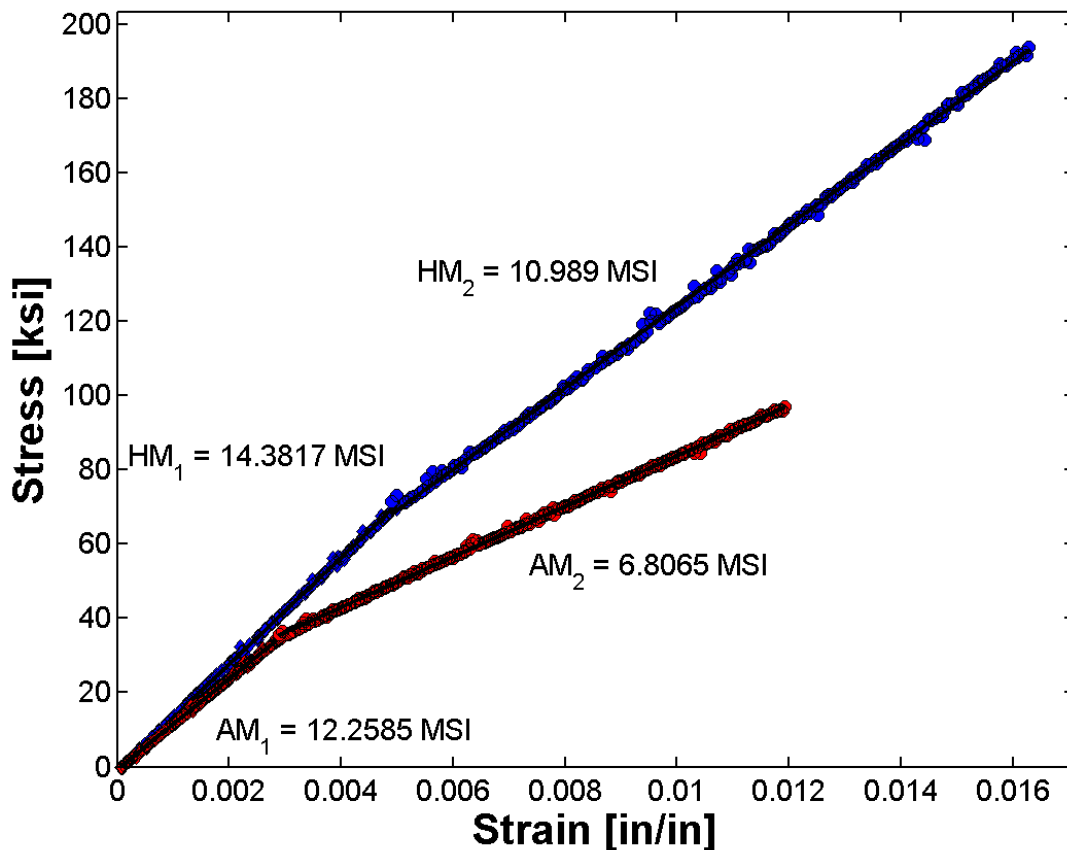


Figure 6.9 – Stress-strain response of ALT639 – 95898 during the burst ramp pressurization. Note, the blue markers are hoop data points, while the red markers are axial data points.

**Table 6.5 – Summary of primary and secondary hoop and axial moduli measured on all burst cylinders.**

Location	DOT-SP	Time	SN	Mfg Date	MAE Life Extension [Pass/Fail]	# Cycles	BEOP [psi]	Burst Pressure [psi]	BEOP/BP [%]	Primary Hoop Modulus [MSI]	Secondary Hoop Modulus [MSI]	Primary Axial Modulus [MSI]	Secondary Axial Modulus [MSI]
Walker Township	10945	30	ALT639-18030	12-98	Pass	10000	10590	20250	52.3%	17.1	12.9	13.5	7.5
Walker Township	10945	30	ALT639-18454	01-99	Pass	-	11210	18885	59.4%	15.8	11.4	10.8	7.0
Mid-Atlantic Fire and Air	10945	30	ALT639-9987	02-98	Pass	10000	12440	18880	65.9%	15.2	11.1	14.5	7.6
Mid-Atlantic Fire and Air	10945	30	ALT639-9959	02-98	Pass	10000	11340	18420	61.6%	15.4	11.6	13.3	7.2
Mid-Atlantic Fire and Air	10945	30	ALT639-9465	02-98	Pass	-	11740	18960	61.9%	13.3	10.4	12.3	6.6
Riverside	10945	30	ALT639-95898	09-01	Pass	-	11960	21600	55.4%	14.4	11.0	12.3	6.8
Riverside	10945	30	ALT639-34081	08-99	Pass	10000	12040	19390	62.1%	16.5	12.3	13.9	7.8
FDNY	10945	45	ALT695-5031	08-98	Pass	10000	-	12,000*	-	14.9	11.7	12.0	6.8
FDNY	10945	45	ALT695-5020	08-98	Pass	-	12045	19940	60.4%	15.1	11.0	11.0	6.5
Fairfax, VA	10915	45	OM3966	08-98	Pass	-	10540	18560	56.8%	14.7	10.6	12.5	6.4

\* Liner tear during burst test

### 6.5 Fire Exposure

The hoop stiffness of cylinders was monitored via strain and pressure measurement throughout the entire fatigue cycle testing. Figure 6.10 shows the hoop modulus as a function of the number of cycles applied to ALT639 – 9753. The hoop modulus as a function of number of applied fatigue cycles for all monitored cylinders in which strain data was available is provided in Appendix A. From Figure 6.10 it is clear that the stiffness of the cylinder was not deteriorating during fatigue cycling. Further, in Appendix A it is shown that no cylinder which was subjected to fire exposure testing demonstrated stiffness degradation during fatigue cycle testing. Additional confirmation of the lack of any composite degradation during fatigue cycling was found via analysis of the MAE waveforms. During cycling to maximum developed pressure no events related to composite material failure were detected, with all detected waveforms being very low frequency and attributed to mechanical rubbing against the containment saddles.

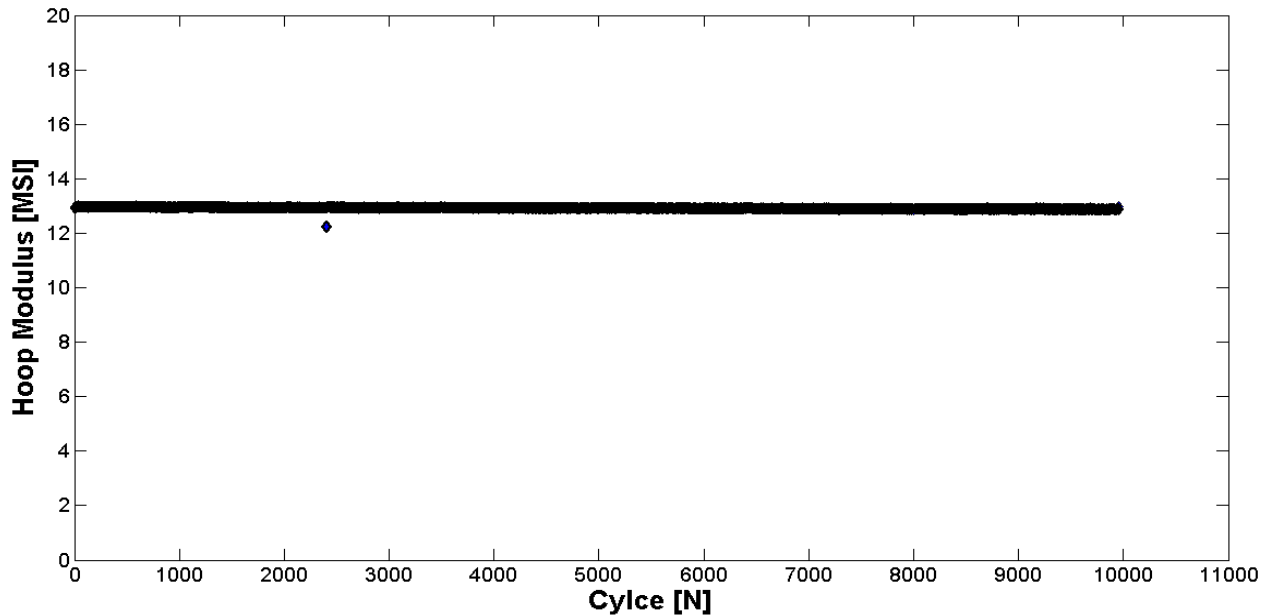


**Figure 6.10 – Hoop modulus as a function of the number of applied fatigue cycles for ALT639 – 9753.**

Of the five (5) cylinders which were subjected to fatigue cycle testing after fire exposure, only one cylinder achieved the required 10,000 fatigue cycles (equivalent to a simulated 20 additional years of service), with the other four cylinders leaking prior to achieving 10,000 fatigue cycles. The total number of fatigue cycles to maximum developed pressure during fast fill for the five fatigue cycled cylinders is summarized in Table 6.6. The reason four of the five cylinders leaked during fatigue cycling was due to annealing the 6061-T6 Aluminum liner. It is well known that for the 6061 Aluminum alloy, increased levels of annealing result in a diminished fatigue endurance limit and accelerated crack growth rates [16, 17]. Hence, while the re-autofrettage process of the DOT-CFFC aluminum liner prior to the fatigue cycling test has repeatedly been shown to enhance liner fatigue performance (Section 6.2 - 6.4 and [5]), it was unable to mitigate liner leakage on fire exposed DOT-CFFC cylinders due to the aluminum being annealed.

**Table 6.6 – Summary of fire exposed cylinder hoop and axial stiffness values, accumulated plastic strain, and MAE performance.**

Location	DOT-SP	Time	SN	Fire Exposure Level	MAE Life Extension [Y/N]	# Cycles	Cycle 1 BEOP [psi]	Burst Cycle BEOP [psi]	Burst Pressure [psi]	BEOP/BP [%]	Primary Hoop Modulus [MSI]	Secondary Hoop Modulus [MSI]	Primary Axial Modulus [MSI]	Secondary Axial Modulus [MSI]	Accumulated Hoop Plastic Strain [µε]	Accumulated Axial Plastic Strain [µε]
Walker Township	10945	30	ALT639-17716	Moderate	N-1,2,3 (All on first cycle)	-	995	8745	15690	56%	18	13.1	14.2	8	209	246
Walker Township	10945	30	ALT639-17831	Severe	N-1,2,3 (Both TPCs)	-	1395	4936	7730	64%	15.6	-	12.7	-	-	-
Walker Township	10945	30	ALT639-38556	Minor	N-1,2,3 (All on first cycle)	9177	3500	-	-	-	-	-	-	-	1200	-
Walker Township	10945	30	ALT639-18768	Moderate	N-1,2,3 (All on first cycle)	-	1700	11760	18600	63%	15.3	11.9	12.1	6.4	1194	425
Mid-Atlantic Fire and Air	10945	30	ALT639-9747	Moderate	N-1,2,3 (All on first cycle)	-	1215	9180	14535	63%	15	10.5	11.3	6	1100	810
Mid-Atlantic Fire and Air	10945	30	ALT639-9769	Severe	N-1,2,3 (All on only cycle)	-	791	1875	5115	37%	-	-	6.7	-	-	-
Mid-Atlantic Fire and Air	10945	30	ALT639-9753	Moderate	N-1,2,3 (All on first cycle)	10000	6900	10795	19440	56%	16.5	11.9	21	13.4	688	-
Riverside	10945	30	ALT639-31064	Moderate	N-1,2,3 (All on first cycle)	-	5050	11280	19160	59%	15.1	10.6	12.1	7	820	515
Riverside	10945	30	ALT639-30041	Moderate	N-1,2,3 (All on first cycle)	8551	7100	-	-	-	-	-	-	-	845	-
Riverside	10945	30	ALT639-23371	Minor	N-1,3 (First TPC) N1,2, (Second TPC)	-	1640	9008	17740	51%	14.5	10.7	15.1	7.4	970	455
FDNY	10945	45	ALT695-3669	Moderate	N-1,2,3 (All on first cycle)	-	2021	9536	16740	51%	15.6	11.9	12.8	7.2	900	490
FDNY	10945	45	ALT604-3764	Severe	N-1,2,3 (All on first cycle)	3900	-	-	-	-	-	-	-	-	560	-
FDNY	10945	60	ALT604-1781	Moderate	N-1,2,3 (All on first cycle)	-	1500	10100	17930	56%	13.3	10.6	10.4	6.4	1290	890
Fairfax, VA	10915	45	OM3930	Moderate	N-1,2,3 (On first cycle)	6920	966	-	-	-	-	-	-	-	870	-
Fairfax, VA	10915	45	OM3968	Moderate	N-1,3 (On first cycle) N-2 (On both cycles)	-	1780	9565	16300	59%	13	10.1	10.7	6.2	1790	1025

Criteria Key

- 1- BEO
- 2- Fiber Fracture Energy
- 3- Frictional/Delamination Energy

To confirm that the aluminum liners were annealed due to fire exposure, the primary hoop modulus from the first pressurization of ALT695-1781 after fire exposure was compared to the primary hoop modulus measured on a subsequent loading, see Figure 6.11. Clearly from Figure 6.11, ALT695-1781 was significantly more compliant on the first pressurization of the cylinder post fire exposure as compared to subsequent pressurizations (a difference of approximately 2.8 Msi). Such an occurrence was due to the 6061-T6 Aluminum being annealed and contributing virtually no stiffness to the cylinder on the first pressurization after fire exposure; in comparing the primary hoop modulus from the first pressurization of ALT695-1781 (Figure 6.11a) to the secondary hoop modulus of ALT695-1781 during the burst pressurization (Table 6.6), it is clear that the two moduli are identical (i.e., only the composite laminate is providing stiffness to the cylinder side wall) which confirms that the aluminum liner had been significantly annealed due to fire exposure. Furthermore, the plastic strain accumulated during the first pressurization for all cylinders' post fire exposure is summarized in Table 6.6 from which it is observed that the 6061-T6 Aluminum liners for all fire exposed cylinders were significantly annealed and accumulated a considerable amount of plastic deformation.

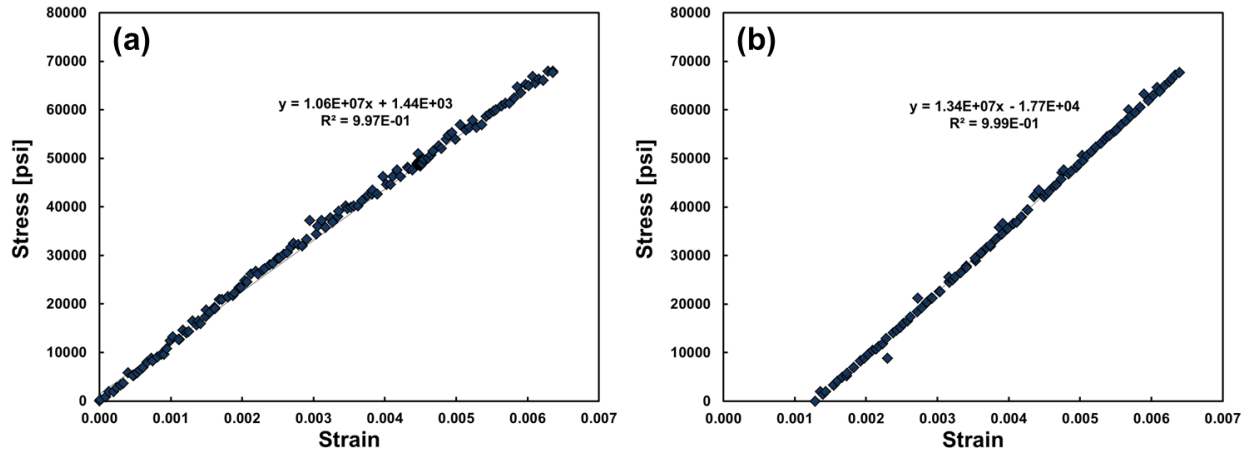


Figure 6.11 – (a) Primary hoop modulus of ALT695-1781 on the first pressurization post fire exposure, and (b) primary hoop modulus of ALT695-1781 on a subsequent pressurization.

From a mechanical response perspective, cylinders were found to respond in a bi-modulus fashion in both the hoop and axial directions. Figure 6.12 provides the stress-strain response of ALT695 – 3669, from which the bi-modulus response in each of the principal directions can be observed. Up to the test pressure of the cylinders (7500 psig or 8500 psig if fatigue tested), the aluminum liner is contributing to the stiffness of the cylinder, whereas after the test pressure the aluminum is plastically deforming and its stiffness contribution to the cylinder wall becomes negligible.

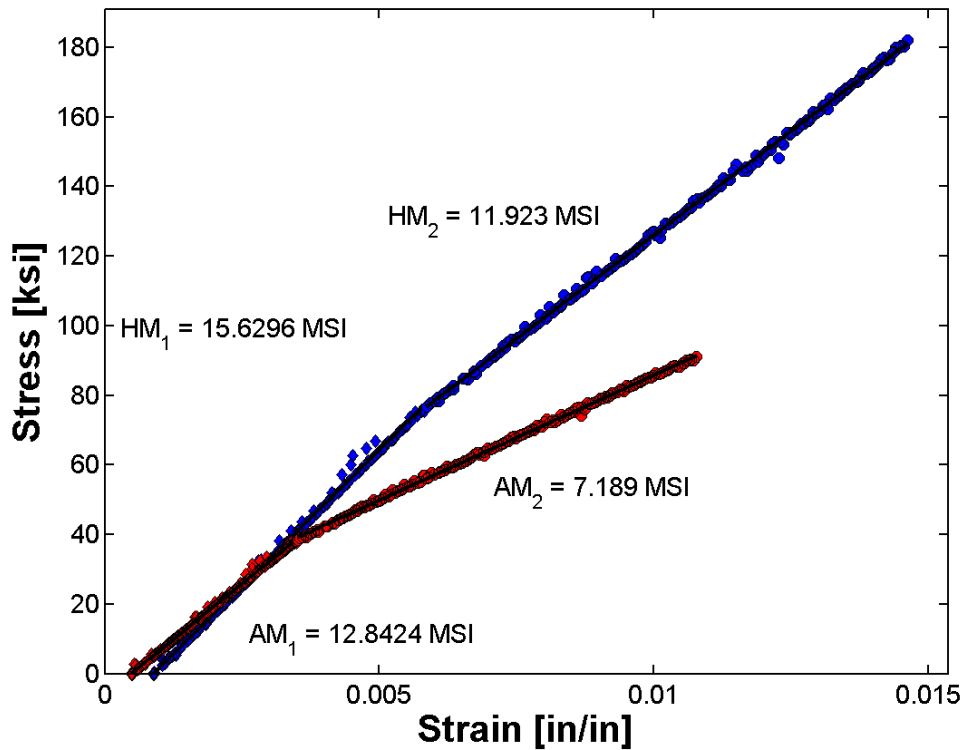


Figure 6.12 – Hoop and axial stress-strain response of ALT695-3669. Note, blue symbols are hoop data, and red symbols are axial data.

Of note in Figure 6.12, it was observed that all strictly EOL burst cylinders had accumulated a certain amount of plastic deformation during the first test pressure cycle, which is measured by a residual tensile strain being present in the composite overwrap. Because the cylinders got so warm during the fire exposure, the 6061 Aluminum was annealed to a degree which lowered the yield strength of the liner. By subjecting the cylinders to a test pressure cycle prior to burst, the yield stress of the liner was once again raised and the characteristic bi-modulus response that has previously been observed [5] was again observed. The effects of annealing the 6061 T6 Aluminum liner were discussed in depth previously in this section. Appendix B provides the stress-strain response of all cylinders during the burst pressurization ramp, while Table 6.6 summarizes the primary and secondary hoop and axial moduli for all tested cylinders measured during the burst pressurization, as well as the measured plastic strain in each DOT-CFFC cylinder which was subjected to fire exposure.

Also shown in Table 6.6 is the burst strength of the fire exposed cylinders, from which it is observed that cylinder burst strength is still adequate relative to service pressure for cylinders with minor to moderate Level 3 fire damage. Eight of nine cylinders with minor to moderate Level 3 fire exposure possessed burst strengths meeting DOT-CFFC 5<sup>th</sup> Revision, while the one cylinder which burst below DOT-CFFC 5<sup>th</sup> Revision requirements still had a burst to service pressure ratio of 3.23. While the burst strengths are adequate, Figure 6.13 shows that fire exposure damage (even minor to moderate as ranked in this report, but still to a CGA C.6.2 Level 3 damage) does statistically reduce the burst strengths of the cylinders when compared to only expired service life cylinder strength taken from [5].

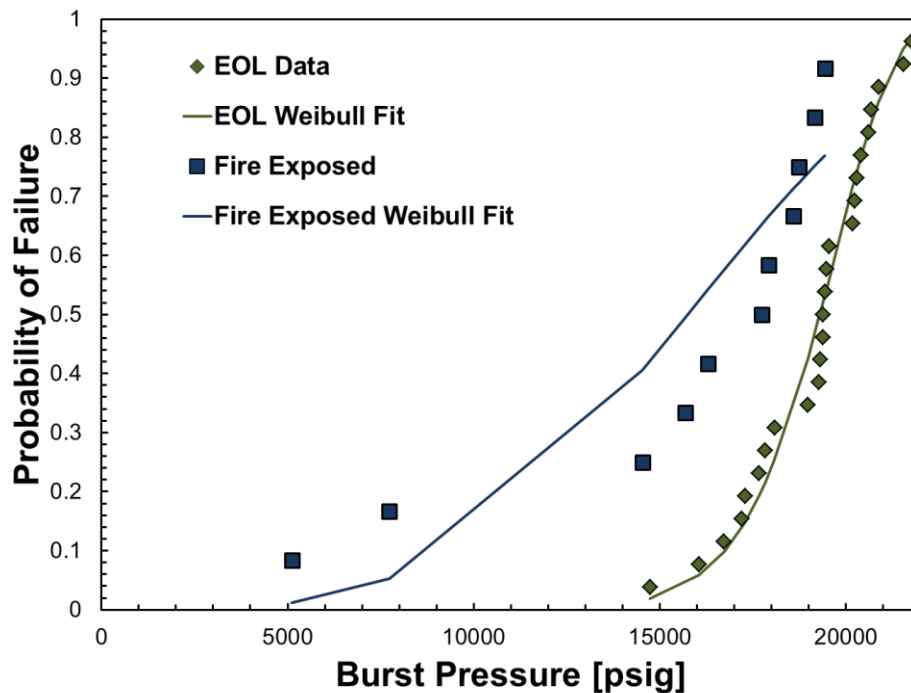


Figure 6.13 – Comparison of EOL Burst strength data from as received expired service life cylinders taken from [5] and a Weibull distribution fit of the burst strengths of the fire exposed DOT-CFFC cylinders.

## 7. Modal Acoustic Emission Results

### 7.1 Hard Water Exposure

Prior to the burst pressurization of the five re-autofrettaged cylinders which successfully achieved 10,000 fatigue cycles, the test pressurization schedule and the accept/reject criteria of [5, 10] to evaluate (using MAE) the integrity of the cylinder was utilized. All five cylinders were found to meet the acceptance criteria for life extension and all five cylinders burst above the minimum required burst pressure of [1], even after 15 years of service life and an additional simulated 20 years of service life (Table 6.3).

During the burst pressurization ramp of all five cylinders the Background Energy Oscillation Pressure (BEOP, as defined in [5]) was measured. Figure 7.1 provides the BEOP determination for cylinder OM3943 (BEOP = 10,371 psi), while all other BEOP plots are provided in Appendix C. In agreement with [5], Table 6.3 shows that the BEOP occurs at nominally 60% of the ultimate strength of a given cylinder, once again facilitating a predictive capability on the burst strength of the cylinder at pressures well below their respective strength.

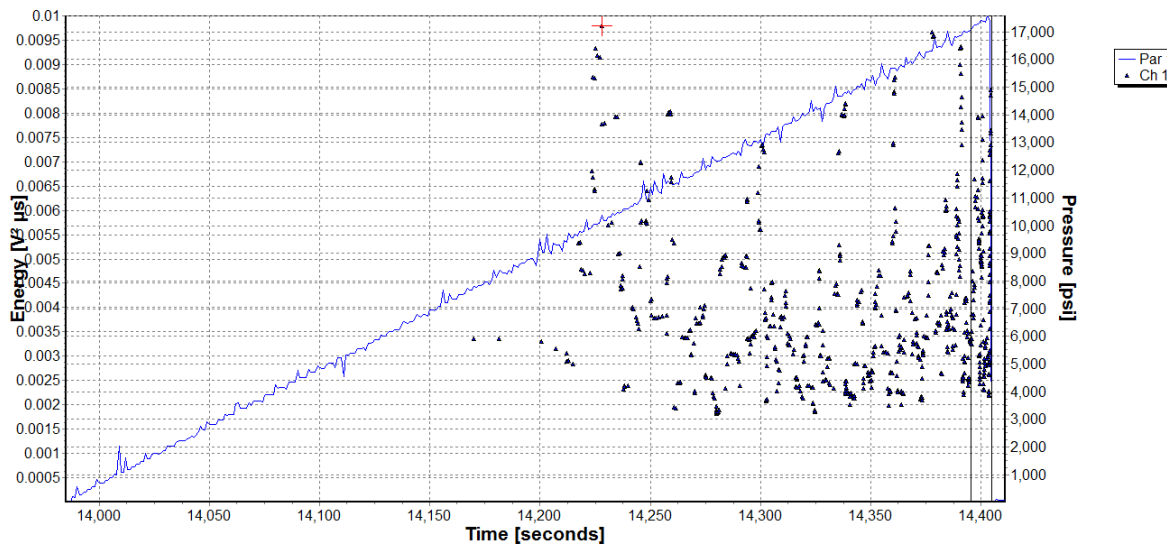


Figure 7.1 – Background Energy Oscillation Pressure (BEOP) determination for OM3943.

Source mechanism classification was achieved through digital signal processing techniques. Specifically, the Modal Acoustic Emission Frequency ( $MF$ ) and spectral standard deviation ( $\sigma_F$ ) were used as metrics of the frequency content within each signal.

Due to the significantly different moduli of the matrix and fibers of the carbon fiber composite overwrap, inherent material anisotropy, and the preferential directions of load release associated with the various damage mechanisms that occur within composite materials (e.g., fiber fracture, matrix cracking, delamination, interfacial failure, etc.) the frequency content of the captured waveforms may be thought of as a “fingerprint” of the given mechanism, hence a means of identifying the various type of failure. Thus, the  $MF$  and  $\sigma_F$  are scalar metrics of the

waveforms that show natural clustering within the frequency domain, and lend insight into the ultimate failure process of a given composite cylinder.

As an example, the spectral standard deviation versus the weighted peak frequency of ALT639 – 9573 is shown in Figure 7.2. In Figure 7.2, the blue markers are matrix cracking events, the green markers are interfacial/delamination events, the yellow markers are fiber fracture events, and the red markers are bulk mode detected fiber fracture events. As the cylinder was not subjected to any form of artificial damage (impact and/or notching) the two most prevalent types of damage mechanisms that were observed were matrix cracking and fiber fracture. Previously it has been reported that cylinders with simulated damage emit a comparatively larger number of delamination events [5]. In agreement with statistical fiber strength models, no fiber fracture events were observed for ALT639 – 9573 until the cylinder had been pressurized to 58% of its ultimate burst strength. As all five cylinders that were burst were not subjected to an artificial form of damage, all cylinders performed in a manner consistent with ALT639 – 9573. Plots of the spectral standard deviation versus *MF* are provided in Appendix D.

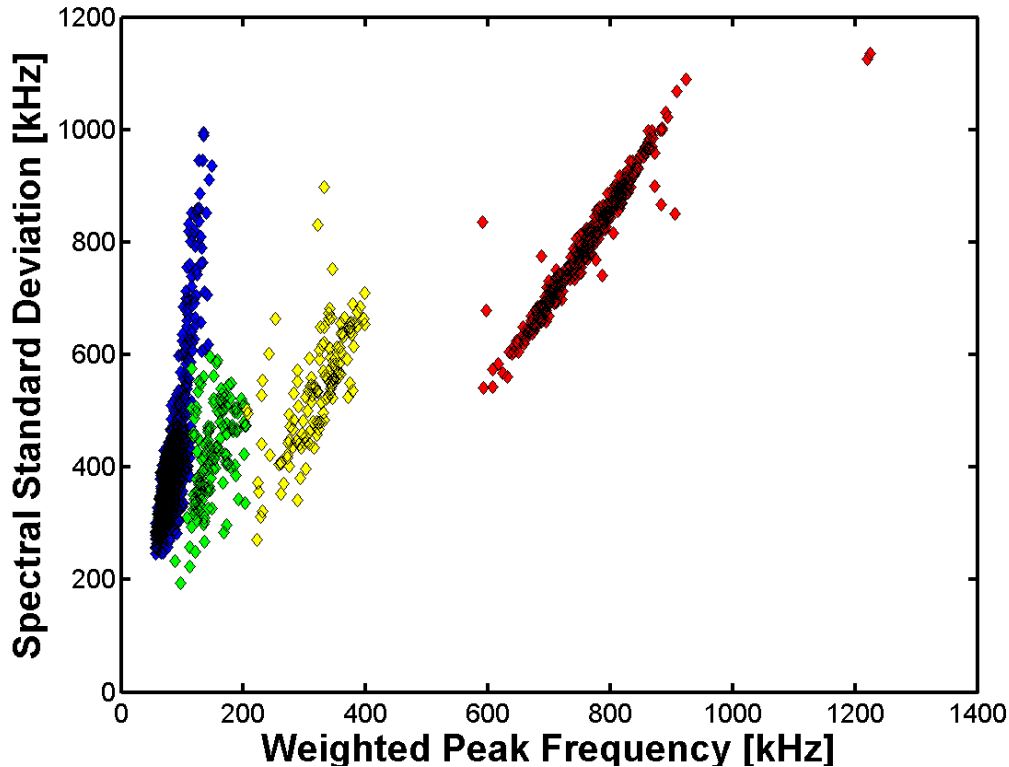


Figure 7.2 – Spectral standard deviation versus *MF* for ALT639-9573.

## 7.2 Chemical Exposure

No significant MAE was detected throughout the entire chemical exposure pressurization test. Since cylinders were only pressurized to a level that they were consistently operated at, no new damage accumulation was taking place; such a finding indicates that neither the sulfuric acid nor sodium hypochlorite exposure resulted in any detrimental physical changes to the DOT-CFFC cylinders. Once again, the gel coat incorporated into the sacrificial layers of the DOT-

CFFC design proved to be an impermeable barrier to the chemicals protecting the structural carbon fibers.

Prior to the burst pressurization of the ten (10) cylinders which were exposed to a given chemical and the five (5) cylinders which were exposed to a given chemical, re-autofrettaged, and then fatigue cycled, the test pressurization schedule and the MAE accept/reject criteria of [5, 10] were evaluated to assess the integrity of the particular cylinder. MAE analysis revealed that all three of the cylinders that leaked did so due to liner fatigue and not because the composite overwrap was compromised due to chemical exposure or fatigue; this was confirmed as all three cylinders failed via leakage in a non-catastrophic fashion.

Of the fourteen (14) cylinders in which the MAE accept/reject criteria could be evaluated, thirteen cylinders met the acceptance criteria. The cylinder (ALT639 – 9948) which was rejected by MAE examination failed the fiber fracture energy criteria on the second test pressure cycle; unfortunately, this cylinder leaked at 12,300 psig (due to Al liner tearing), not allowing for a determination as to whether or not MAE successfully identified a cylinder with compromised burst strength.

During the burst pressurization ramp of all fourteen cylinders, the Background Energy Oscillation Pressure (BEOP, as defined in [5]) was measured. Figure 7.3 provides the BEOP determination for cylinder ALT639 - 70015 (BEOP = 11,690 psig), while all other BEOP plots are provided in Appendix C. In agreement with [5], Table 6.4 shows that the BEOP occurs at an average value of 60% of the ultimate strength of a given cylinder, once again facilitating a predictive capability on the burst strength of the cylinder at pressures well below their respective strength. With such a predictive capability, cylinders with compromised burst strength may be identified and removed from service enhancing the safety of the public.

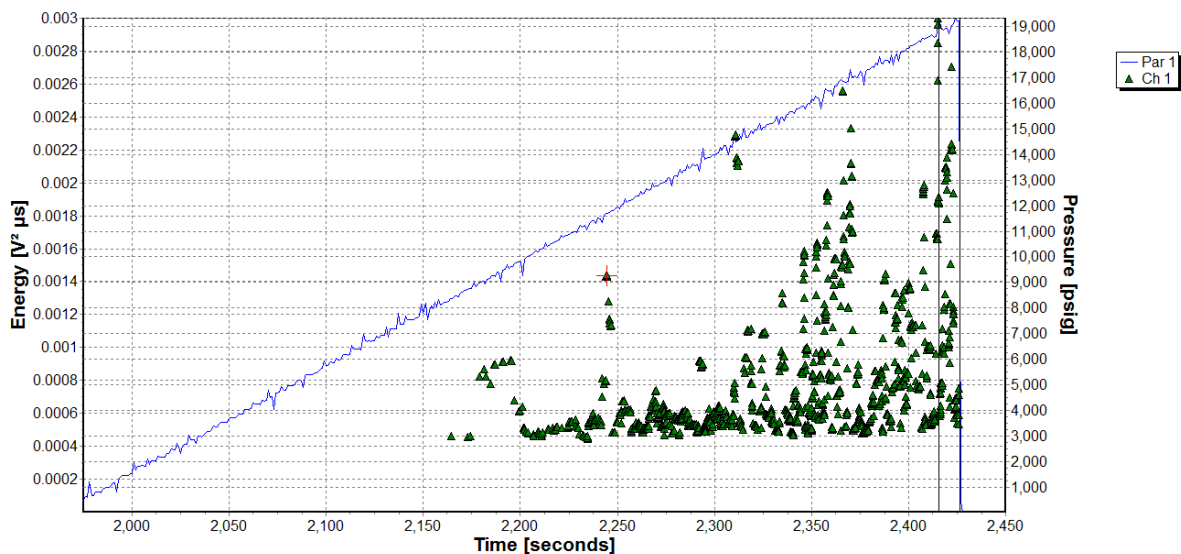


Figure 7.3 – Background Energy Oscillation Pressure (BEOP) determination for ALT639-70015.

Finally, MAE source mechanism classification was achieved through digital signal processing techniques. Specifically, the Modal Acoustic Emission Frequency ( $MF$ ) and spectral standard deviation ( $\sigma_F$ ) were used as metrics of the frequency content within each waveform captured during the EOL burst test of a given cylinder.

As an example, the spectral standard deviation versus the  $MF$  of ALT639 – 70015 is shown in Figure 7.4. In Figure 7.4, the blue markers indicate matrix cracking events, the green markers indicate interfacial failure events (fiber/matrix debonding and delamination), the yellow markers indicate fiber fracture events, and the red markers indicate bulk mode fiber fracture events. As the cylinder was not subjected to any form of artificial damage (impact and/or notching) the occurrence of damage mechanisms was more or less uniform. Previously it has been reported that cylinders with simulated damage emit a comparatively larger number of delamination events [5]. In agreement with statistical fiber strength models, no fiber fracture events were observed for ALT639 – 70015 until the cylinder had been pressurized to 56% of its ultimate burst strength. As all fourteen cylinders that were subjected to a burst pressurization were not subjected to an artificial form of damage, all cylinders performed in a manner consistent with ALT639 – 70015. Plots of the spectral standard deviation versus  $MF$  are provided in Appendix D.

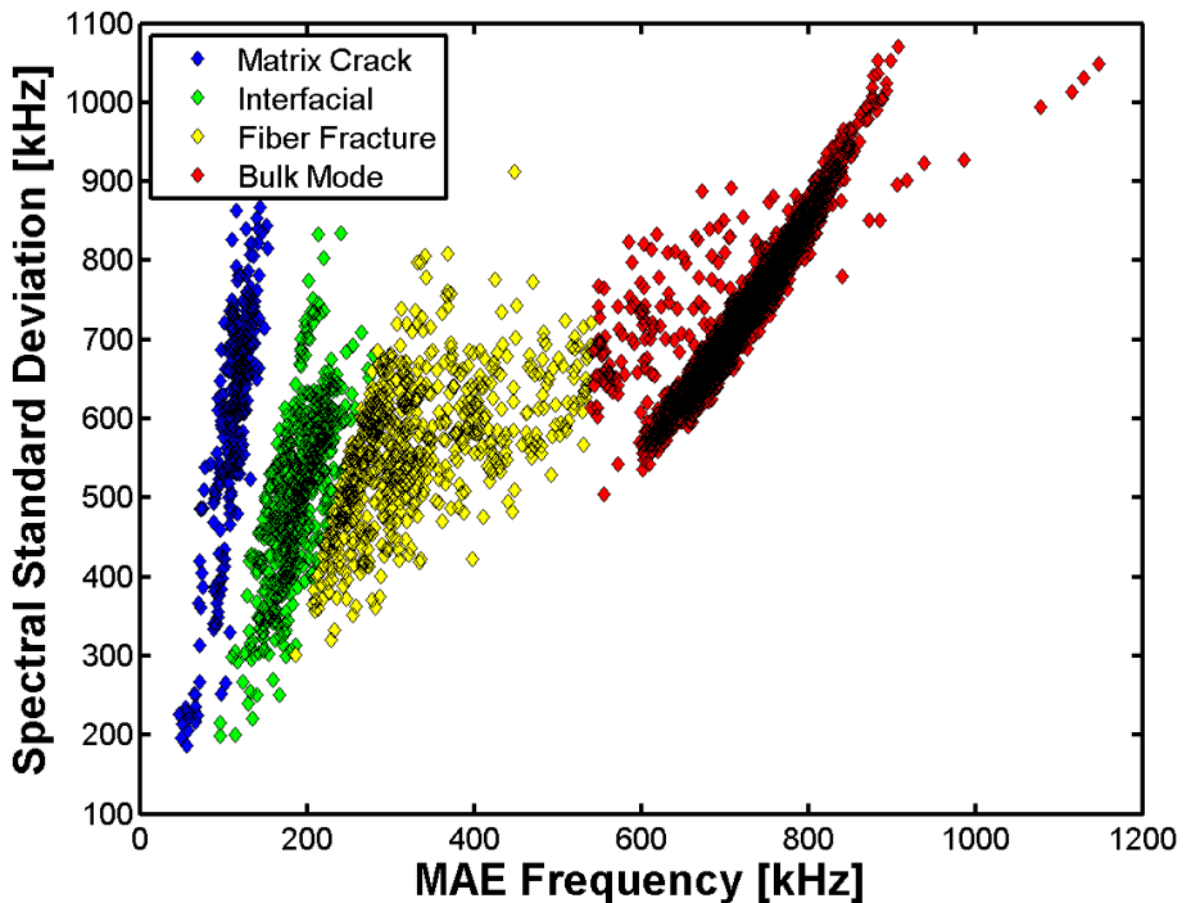


Figure 7.4 – Spectral standard deviation versus  $MF$  for ALT639 - 70015.

### 7.3 Salt Water Immersion

No visual indications or significant MAE was detected throughout the entire salt water immersion test. Since cylinders were only pressurized to a level that they were consistently operated at, no new damage accumulation was taking place; such a finding indicates that neither the salt water exposure, nor the thirty cycles up to service pressure had any detrimental effect on the DOT-CFFC cylinders. It is believed that the hydrophobic gel coat incorporated into the sacrificial layers of the DOT-CFFC design proved to be an impermeable barrier to the salt water protecting the structural carbon fibers.

During the burst pressurization ramp of all ten cylinders, the Background Energy Oscillation Pressure (BEOP, as defined in [5]) was measured. Figure 7.5 provides the BEOP determination for cylinder ALT639 - 95898 (BEOP = 11,960 psig), while all other BEOP plots are provided in Appendix C. In agreement with [5], Table 6.5 shows that the BEOP occurs at an average value of 60% of the ultimate strength of a given cylinder, once again facilitating a predictive capability on the burst strength of the cylinder at pressures well below their respective strength. With such a predictive capability, cylinders with compromised burst strength may be identified and removed from service enhancing the safety of the public.

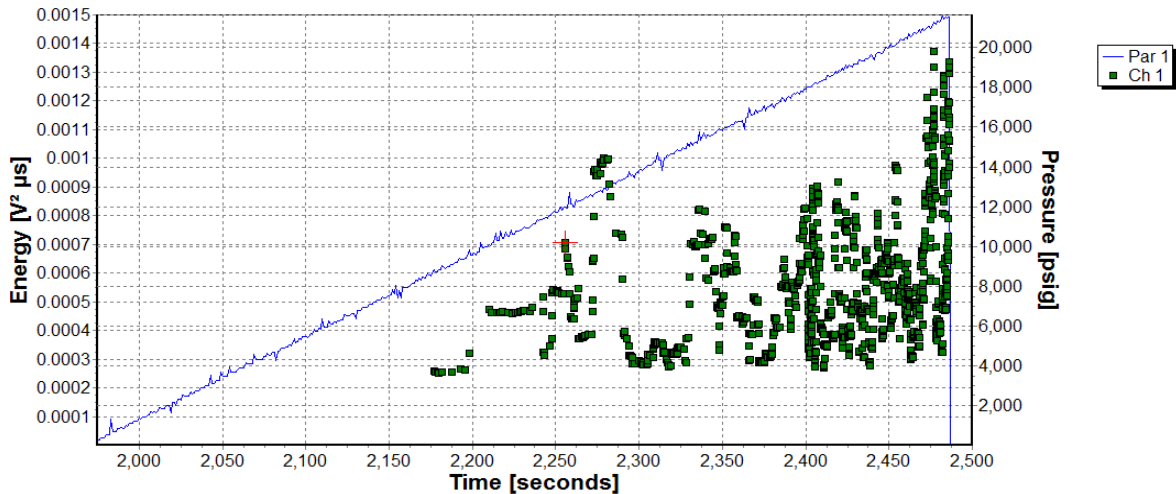


Figure 7.5 – Background Energy Oscillation Pressure (BEOP) determination for ALT639-95898.

Finally, MAE source mechanism classification was achieved through digital signal processing techniques. Specifically, the Modal Acoustic Emission Frequency ( $MF$ ) and spectral standard deviation ( $\sigma_F$ ) were used as metrics of the frequency content within each waveform captured during the EOL burst test of a given cylinder. The formulas used to compute the aforementioned metrics have been provided in [5].

As an example, the spectral standard deviation versus the  $MF$  of ALT639 – 95898 is shown in Figure 7.6. In Figure 7.6, the blue markers indicate matrix cracking events, the green markers indicate interfacial failure events (fiber/matrix debonding and delamination), the yellow markers indicate fiber fracture events, and the red markers indicate bulk mode fiber fracture events. As the cylinder was not subjected to any form of artificial damage (impact and/or notching) the

occurrence of damage mechanisms was more or less uniform. Previously it has been reported that cylinders with simulated damage emit a comparatively larger number of delamination events [5]. In agreement with statistical fiber strength models, no fiber fracture events were observed for ALT639 – 95898 until the cylinder had been pressurized to 57% of its ultimate burst strength. As all ten cylinders that were subjected to a burst pressurization were not subjected to an artificial form of damage, all cylinders performed in a manner consistent with ALT639 – 95898. Plots of the spectral standard deviation versus *MF* are provided in Appendix D.

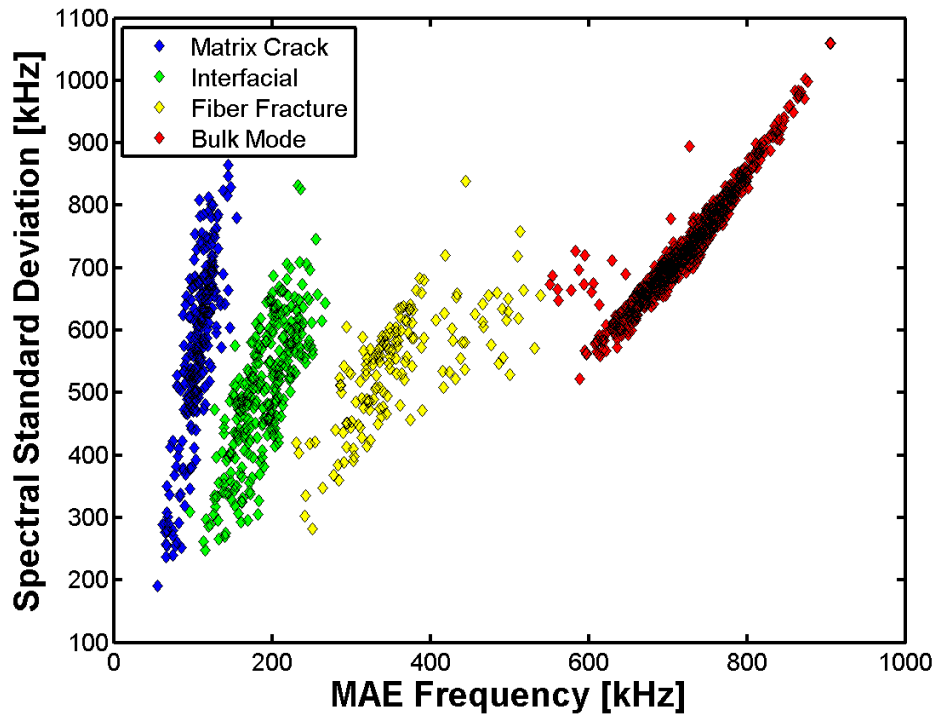
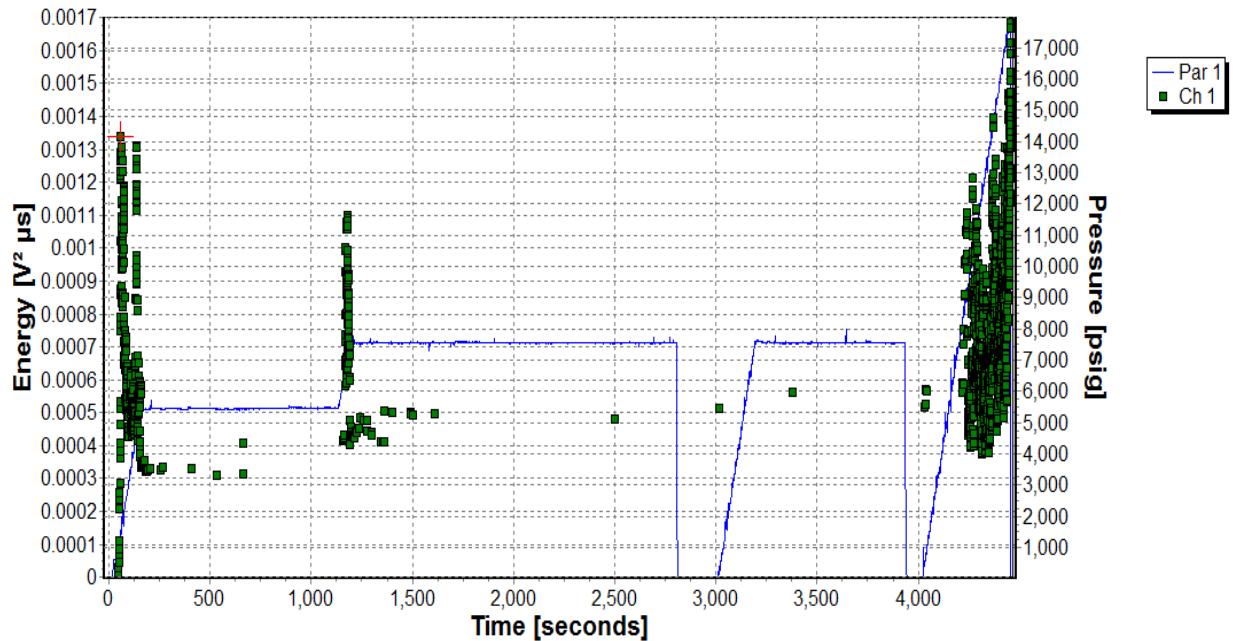


Figure 7.6- Spectral standard deviation versus *MF* for ALT639 - 95898.

#### 7.4 Fire Exposure

Prior to the burst pressurization of the fire exposed cylinders, the pressure schedule and the MAE accept/reject criteria of [5] were followed and evaluated to assess the integrity of the particular cylinder. In evaluating the MAE accept/reject criteria of [5], all fire exposed cylinders failed due to violating a multitude of the criteria on both the first and second test pressure cycles. Due to the cylinders having a new damage state introduced to the composite microstructure and not experiencing any fatigue cycles to develop their new characteristic damage state, all fire exposed cylinders violated several modal acoustic emission accept/reject criteria (see Table 6.6). Such findings indicate that MAE can be used to evaluate the severity of fire exposure as opposed to relying on the currently used visual inspection techniques of [12]. Of particular value in investigating the fire exposure of cylinders, it was found that the Background Energy began oscillating at very low pressures (Table 6.6), as compared to previously tested expired service life cylinders [5]. Figure 7.7 provides a representative Background Energy Oscillation (BEO) plot of ALT 695-1781 in which oscillation is observed on

both the first test pressure cycle, as well as on the burst pressurization. Appendix C provides BEO plots for the fire exposed cylinders addressed in this report. Due to the unique response of the fire exposed DOT-CFFC cylinders two BEOP were measured; the first BEOP measurement was taken on the first pressurization of the cylinder after being exposed to the fire, the second BEOP measurement was taken on the burst pressurization cycle of the cylinder (Table 6.6).



**Figure 7.7 – Background Energy Oscillation plot of ALT695-1781.**

From a Modal Acoustic Emission perspective, all fire exposed cylinders with minor to moderate fire damage performed in a similar fashion. Due to the oxidation of the sacrificial layer, a majority of the detected events during the first pressurization of the cylinder after the fire exposure were matrix cracking and interfacial failure (e.g., see ALT639-23371 as a representative example, Figure 7.8), whereas during the burst pressurization a far greater percentage of the detected events were fiber fracture (Figure 7.9). Burks and Kumosa have previously investigated thermally oxidized hybrid polymer matrix composite structures using Modal Acoustic Emission with Scanning Electron Microscopy confirmation, and concluded that matrix cracking of the oxidized layer and fiber/matrix debonding (interfacial failure) were the primarily observed failure mechanisms during the first loading after oxidation [19].

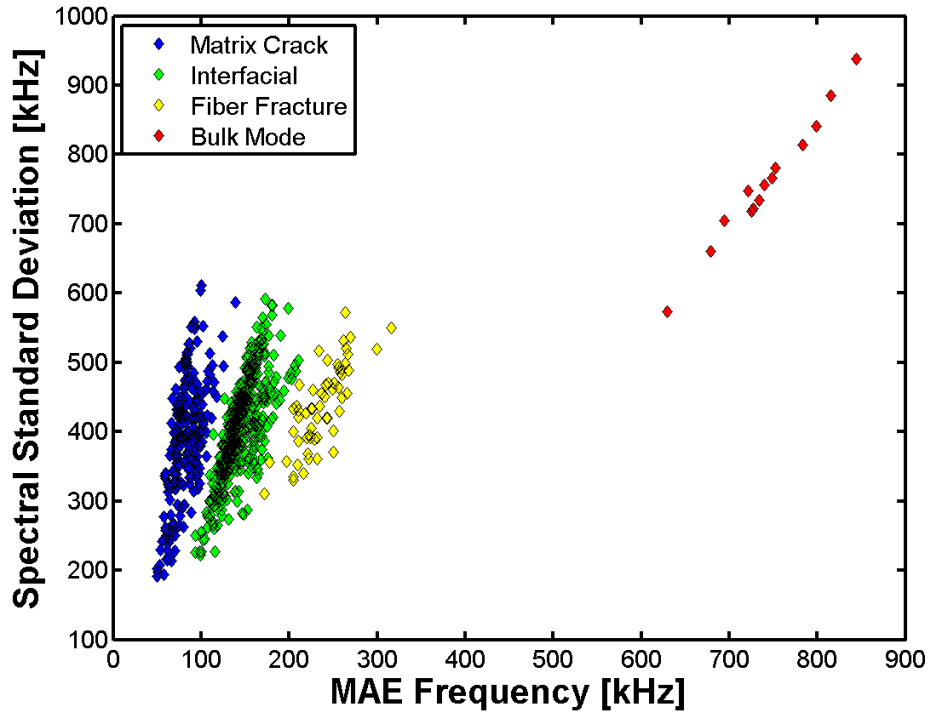


Figure 7.8 – Signal classification of detected acoustic emissions from ALT639-23371 during the first test pressure cycle after fire exposure.

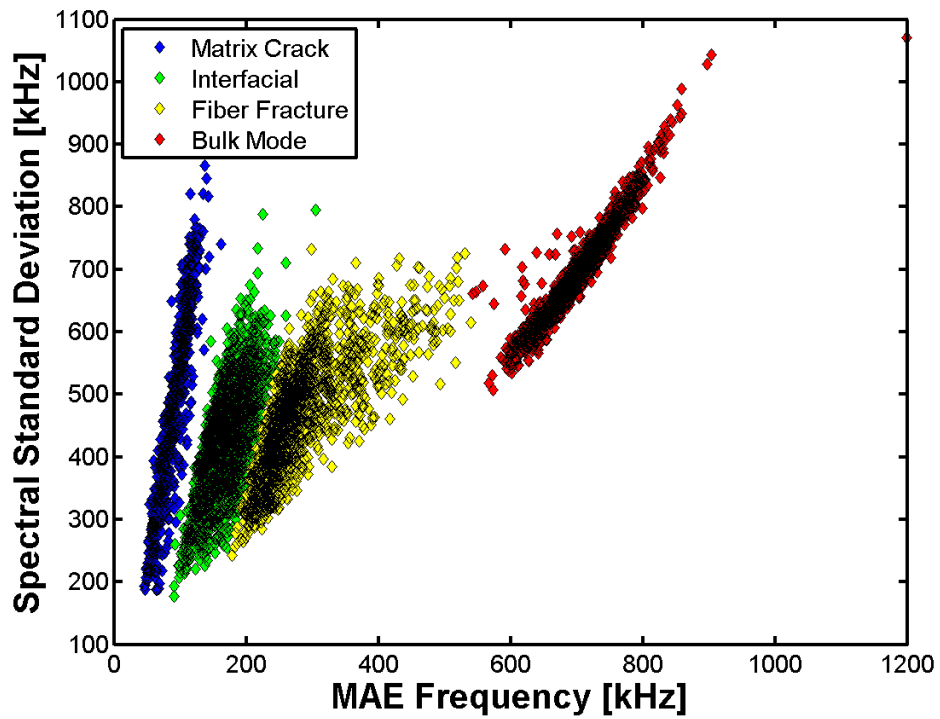
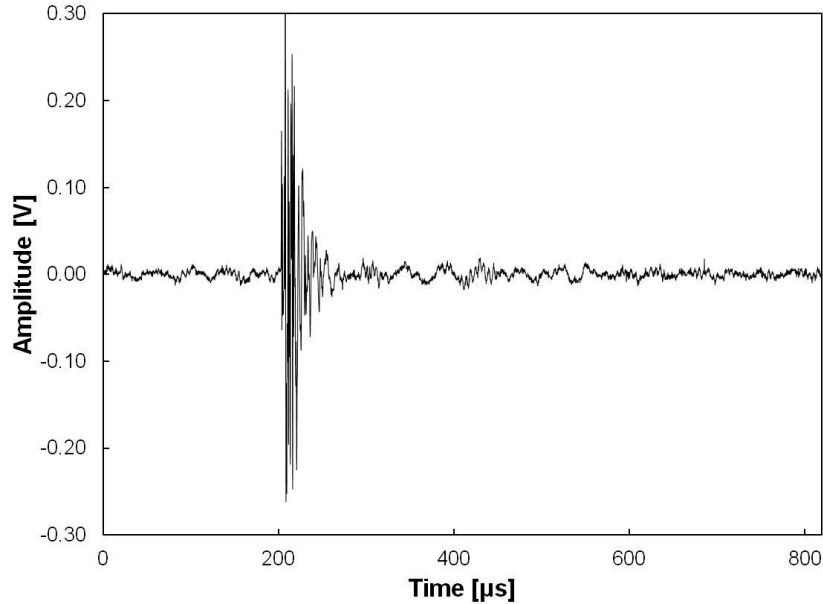


Figure 7.9 - Signal classification of detected acoustic emissions from ALT639-23371 during the burst pressure cycle.

In looking at the Modal Acoustic Emission performance of the cylinders with severe fire damage (ALT639-17831, ALT639-9769, and ALT604-3764), several key characteristics were identified that were not observed in the minor to moderately fire damaged cylinders. As compared to the minor and moderately fire damaged cylinders, the level of visual fire damage was significant with obvious fiber tow unwrapping and a loss (or decomposition) of epoxy resin (Figure 7.10). Moreover, as opposed to the cylinders with minor to moderate fire damage, cylinders with severe fire damage exhibited numerous partial-to-multiple fiber tow fracture events at extremely low pressures during the first test pressure cycle. Figure 7.11 shows a multiple fiber tow fracture event which occurred on the first pressurization of ALT639-17831 at a pressure of 1700 psig in which approximately 60k filaments (or five 12k fiber tows) fractured. Such severe fiber fracture damage occurring at only 1700 psig of a 4500 psi service pressure DOT-CFFC cylinder suggests that a significant level of damage has occurred to the cylinder; the MAE test should be suspended and the cylinder condemned immediately.



Figure 7.10 – Severe fire exposure damage showing fiber tow unraveling, and epoxy resin loss (ALT 639-9769).



**Figure 7.11 – Multiple fiber tow fracture event recorded during the first test pressure cycle of ALT639-17831 at a pressure of 1,700 psig.**

### 7.5 Predictive Capability of MAE

In looking at the ratio of Background Energy Oscillation Pressure (BEOP) on the cycle in which the cylinder burst to the cylinder's burst pressure (Figure 7.12), for all cylinders considered in this work, it is observed that the BEOP occurs on average at 58.6% of the cylinders strength, with a standard deviation of 5.6%. Such findings highlight MAE's ability to predict burst strength of the composite pressure cylinders. Figure 7.13 also shows the extremely strong correlation between BEOP from the burst pressure cycle and the cylinder ultimate burst pressure. The strong one-to-one relationship which exists between a cylinder's BEOP and its ultimate burst strength has been described in depth [5, 20], and is a key component of the MAE inspection technique insuring that compromised cylinders may be properly identified and removed from service, enhancing public safety.

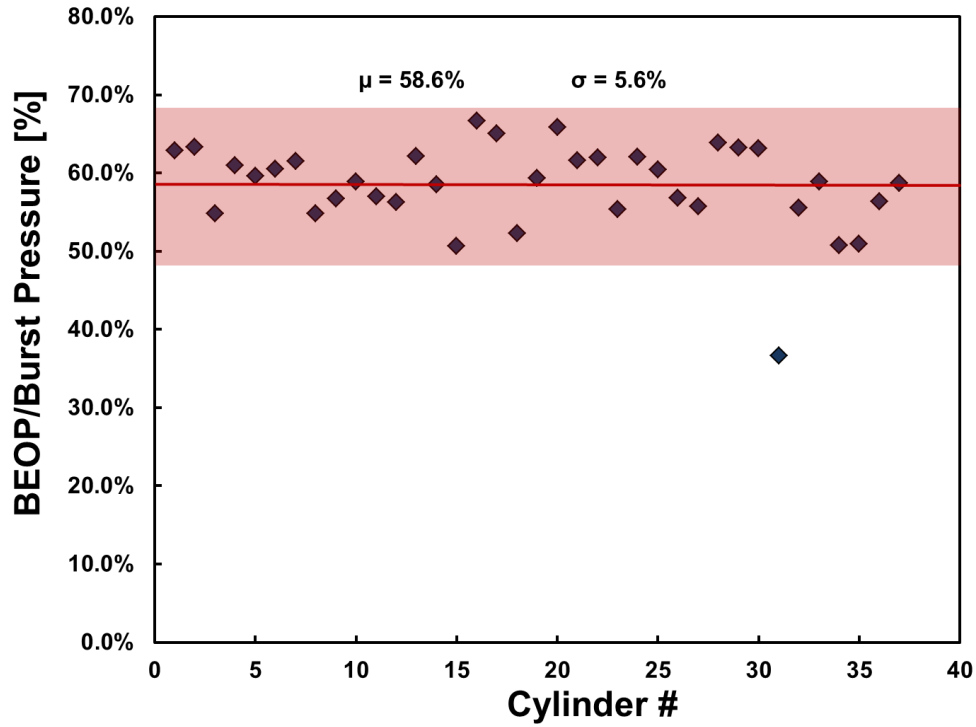


Figure 7.12 – Ratio of BEOP to Burst Pressure for all cylinders which were catastrophically burst in this study. The mean ( $\mu$ ) value and two standard deviation ( $2\sigma$ ) bounds are also included.

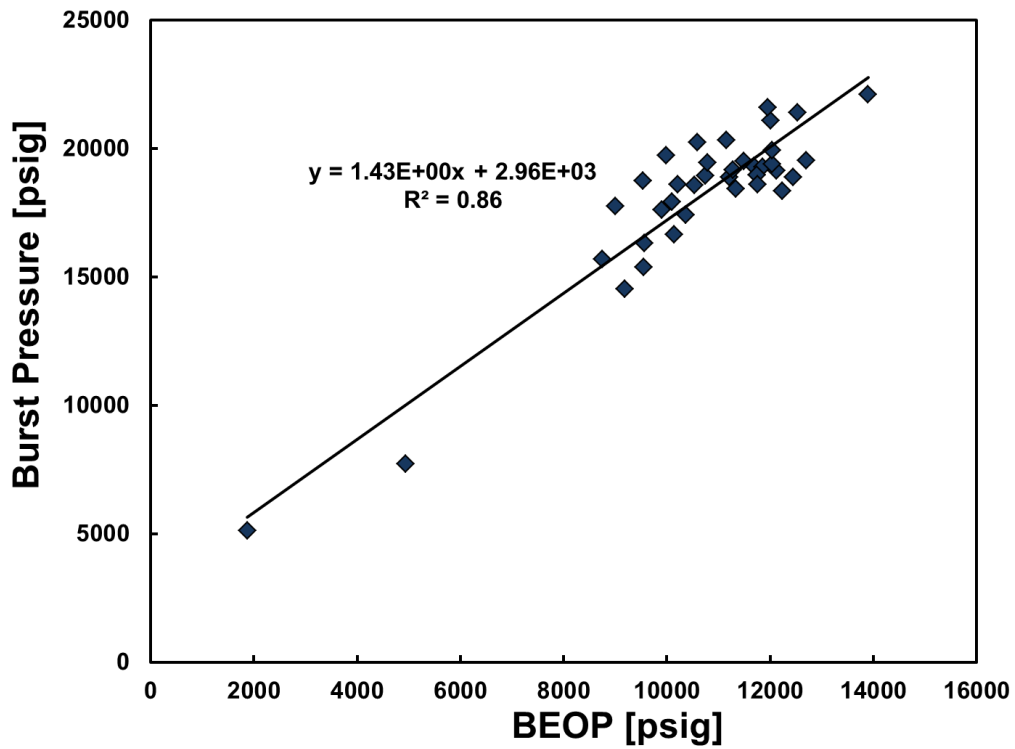


Figure 7.13 – Cylinder burst pressure vs. background energy oscillation pressure for all cylinders burst test in this environmental effects study.

## 8. Conclusions

In considering the totality of the work completed in the present study, several conclusions may be drawn.

- Prolonged hard water exposure of the 6061 T6 Al liner significantly reduces the fatigue life of a DOT-CFFC composite pressure cylinder, if a corrective action is not taken.
- The Digital Wave Corporation developed re-autofrettage process mitigates the effects of corrosion initiated flaw sites, and greatly improves fatigue performance.
- The Digital Wave Corporation developed re-autofrettage process enabled every cylinder fatigue tested in the present study (excluding fire exposed cylinders) to pass the ISO 11119.2:2002 fatigue test and achieve an additional simulated twenty (20) years of service life, even when the cylinder's liner was subjected to prolonged hard water exposure (e.g., in the hard water exposure test, the salt water immersion test, and the chemical exposure test).
- Sulfuric acid or sodium hypochlorite exposure to the overwrap of DOT-CFFC cylinders held at service pressure did not diminish the burst strength of the cylinders.
- Sulfuric acid or sodium hypochlorite exposure to the overwrap of DOT-CFFC cylinders held at service pressure did not diminish the fatigue performance of the cylinders.
- Thirty (30) days of salt water immersion testing of DOT-CFFC cylinders cycled up to service pressure did not diminish the burst strength of the cylinders.
- Thirty (30) days of salt water immersion testing of DOT-CFFC cylinders cycled up to service pressure did not diminish the subsequent fatigue performance of the five (5) tested cylinders.
- Seven minutes of simulated structural fire exposure resulted in Level 3 fire exposure damage as defined by CGA C-6.2 [12].
- Cylinders with Level 3 fire damage had diminished burst strengths as compared to expired service life cylinders, or expired service life cylinders which had experienced an additional simulated 20 years of service life.
- Cylinders with Level 3 fire damage had diminished fatigue performance due to an annealing of the 6061 T6 Aluminum liner. Even the use of a re-autofrettage process (which has proven exceptionally useful in other fatigue tests) was unsuccessful in recouping the fatigue performance of the fire exposed cylinders.
- Modal Acoustic Emission rejected every cylinder which had been exposed to a simulated structure fire on the first pressurization of the cylinder after fire exposure.

- Cylinders with severe Level 3 fire damage accumulated significant fiber tow fracture damage at much lower pressure levels than cylinders with minor to moderate Level 3 fire damage.
- Background Energy Oscillation occurred at an average value of 58.6% of a cylinder's ultimate strength with a standard deviation of 5.6%, once again facilitating a predictive metric on the burst strength of a given cylinder.
- Modal Acoustic Emission testing properly identified all cylinders with compromised burst strength ensuring that cylinders, even life-extended cylinders, could safely be transported in commerce with enhanced safety for the public.

## 9. References

- [1] Department of Transportation, "Basic requirements for fully wrapped carbon-fiber reinforced aluminum lined cylinders (DOT-CFFC)," DOT, 2007.
- [2] L. Cylinders, 28 October 2010. [Online]. Available: <http://www.luxfercylinders.com/support/technical-bulletins/5-luxfer-position-concerning-life-extension-of-dot-cffc-carbon-composite-cylinders>. [Accessed 1 June 2015].
- [3] American Society of Mechanical Engineers (ASME), "Boiler and Pressure Vessel Code," in *Section X: Fiber Reinforced Plastic Pressure Vessels*, New York, NY, 2013, pp. 129-134.
- [4] National Board of Inspectors Code (NBIC), "National Board Inspection Code, NB10-0601," Columbus, OH, 2013.
- [5] Digital Wave Corporation (DWC), "Use of Modal Acoustic Emission (MAE) for life extension of civilian self-contained breathing apparatus (SCBA) DOT-CFFC cylinders," DOT/PHMSA, Centennial, CO, 2014.
- [6] Compressed Gas Association (CGA), "CGA C-22 Water Corrosion of Composites AA6061 Liners," Compressed Gas Association, Inc., Chantilly, VA, 2012.
- [7] R. Frankle and H. Wachob, "Investigation of the Failure of an SCBA Cylinder," Failure Analysis Associates, Fremont, CA, 1996.
- [8] (ISO), International Standards Organization, "11515 Gas cylinders - Refillable composite reinforced tubes of water capacity between 150 L and 3 000 L - Design, construction, and testing," International Standards Organization (ISO), 2010.
- [9] (ISO), International Standards Organization, "11119.2 Gas cylinders of composite construction - specification and test methods Part 2: Fully wrapped fibre reinforced composite gas cylinders with load-sharing metal liners," ISO, Geneva, Switzerland, 2002.
- [10] Department of Transportation, "DOT-SP 15720," Washington D.C., 2013.
- [11] Department of Transportation, "DOT-SP 16343," Washington, DC, 2015.
- [12] C. G. A. (CGA), "CGA C-6.2 - 2013 Standard for Visual Inspection and Requalification of Fiber Reinforced High Pressure Cylinders," CGA, Chantilly, VA, 2013.
- [13] J. Wagner, "Optical Detection of Ultrasound," in *Ultrasonic Measurement Methods*, San Diego, Academic Press, 1990, pp. 201-240.

- [14] Department of Transportation, "DOT-SP 14232," Washington D.C., 2014.
- [15] Department of Transportation, "DOT-SP 13583," Washington D.C., 2011.
- [16] A. Brammer, Experiments and modeling of the effects of heat exposure on fatigue of 6061 and 7075 Aluminum alloys, Tuscaloosa: University of Alabama, 2013.
- [17] ASM, Metals Handbook vol. 1 - Properties and Selection of Metals, Metals Park, OH: American Society for Metals, 1961.
- [18] Digital Wave Corporation, "10162014 Hard Water Exposure Update," Digital Wave Corporation, Centennial, CO, 2014.
- [19] B. Burks and M. Kumosa, "A modal acoustic emission signal classification scheme derived from finite element simulations," *International Journal of Damage Mechanics*, vol. 23, no. 1, pp. 43-62, 2014.
- [20] M. Gorman, "Modal AE analysis of fracture and failure in composite materials, and the quality and life of high pressure composite cylinders," *Journal of Acoustic Emission*, vol. 29, pp. 1-28, 2011.
- [21] R. I. Stephens, A. Fatemi, R. R. Stephens and H. O. Fuchs, Metal Fatigue in Engineering 2nd Edition, New York: Wiley Inter-Science, 2001.
- [22] B. Burks, "Salt water exposure of DOT-CFFC cylinders," Digital Wave Corporation, Centennial, CO, 2015.
- [23] B. Burks, "Hard water exposure of DOT-CFFC cylinders and the subsequent fatigue performance," Digital Wave Corporation, Centennial, CO, 2014.
- [24] Department of Transportation, "DOT-SP 15720," DOT, Washington D.C., 2014.

## APPENDIX A

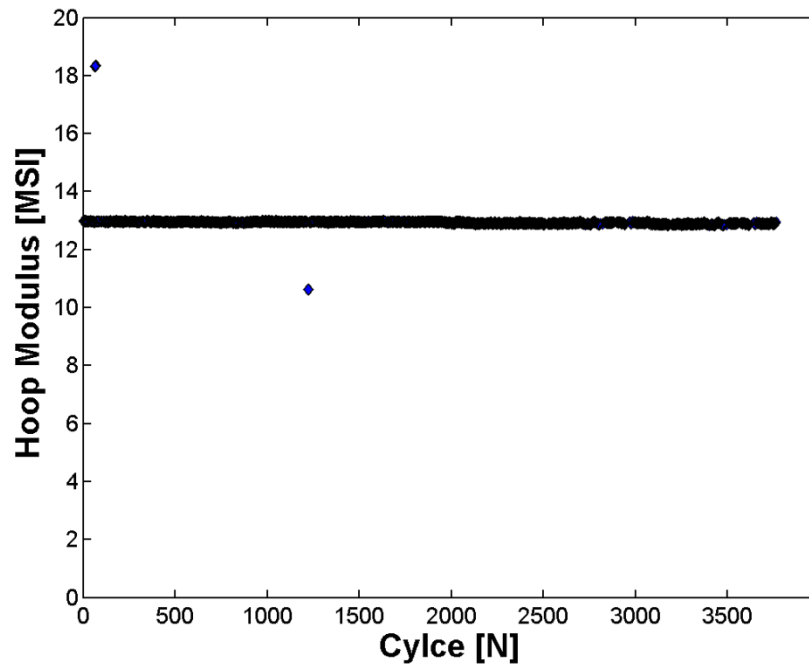


Figure A.1 – Hoop modulus as a function of number of fatigue cycles for ALT604-6148.

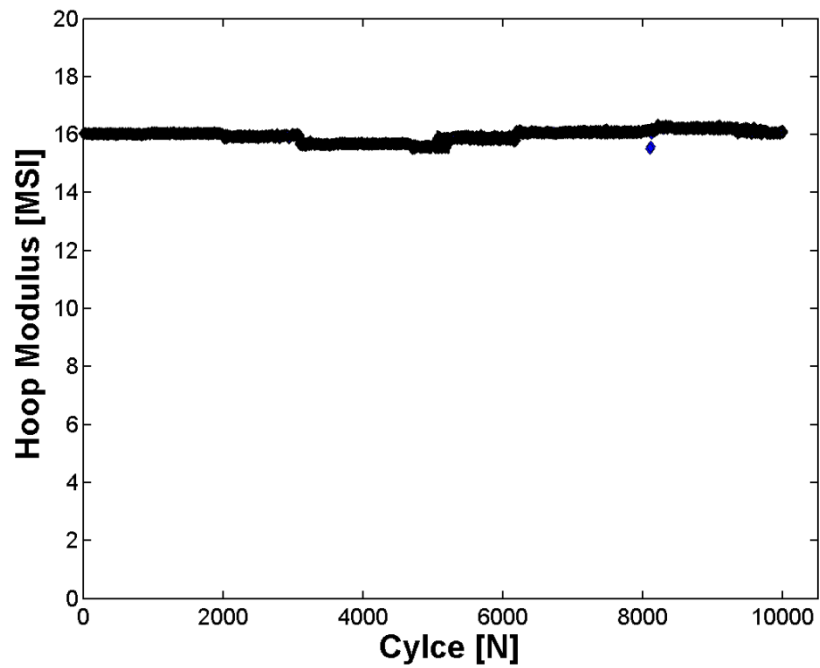


Figure A.2 – Hoop modulus as a function of number of fatigue cycles for ALT639-9573.

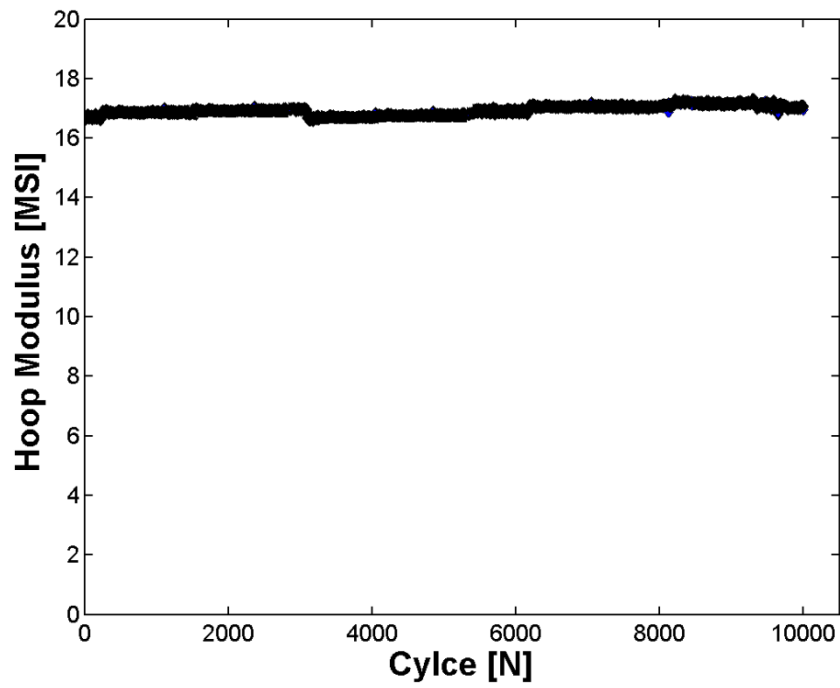


Figure A.3 – Hoop modulus as a function of number of fatigue cycles for ALT639-18114.

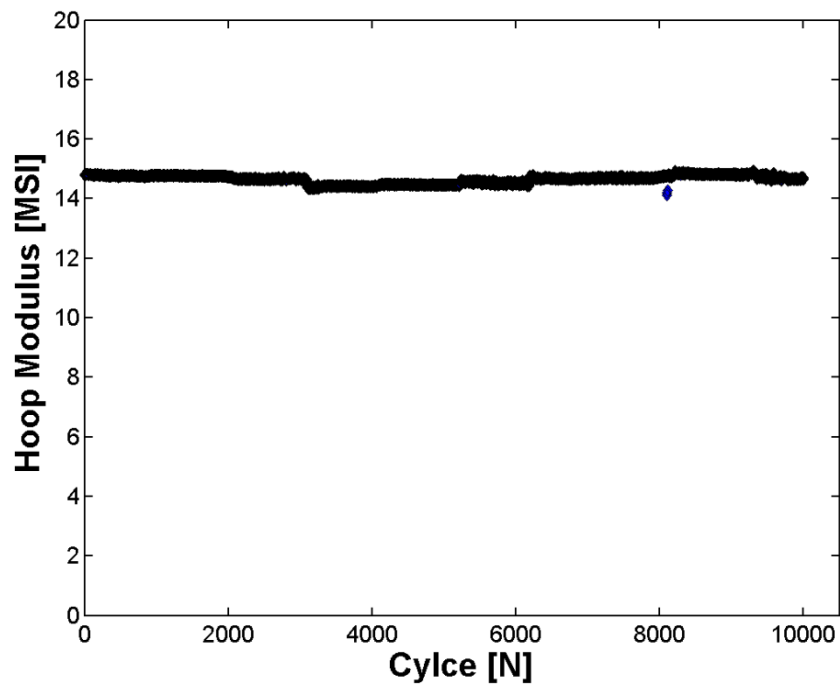


Figure A.4 – Hoop modulus as a function of number of fatigue cycles for ALT639-34075.

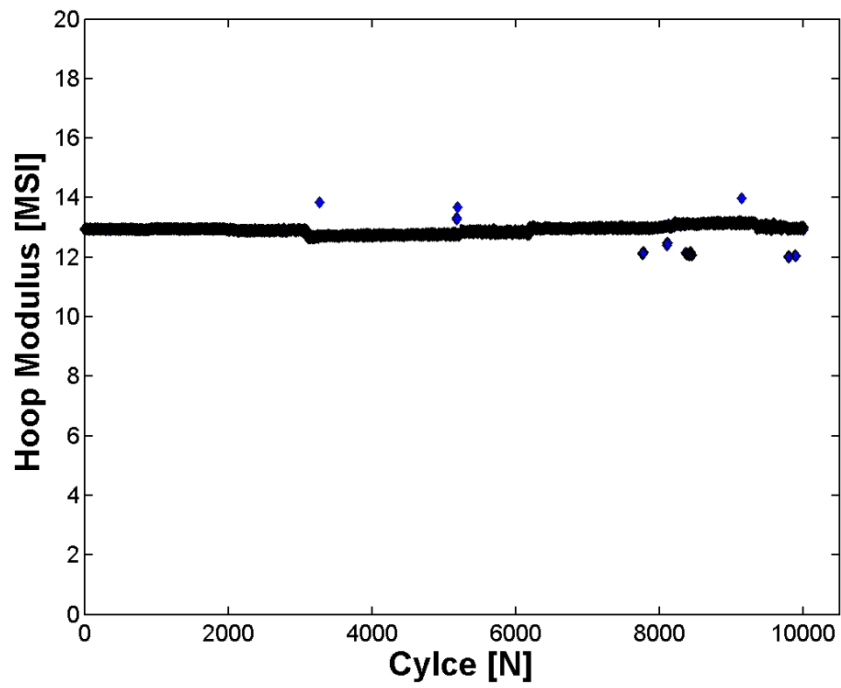


Figure A.5 – Hoop modulus as a function of number of fatigue cycles for OM3924.

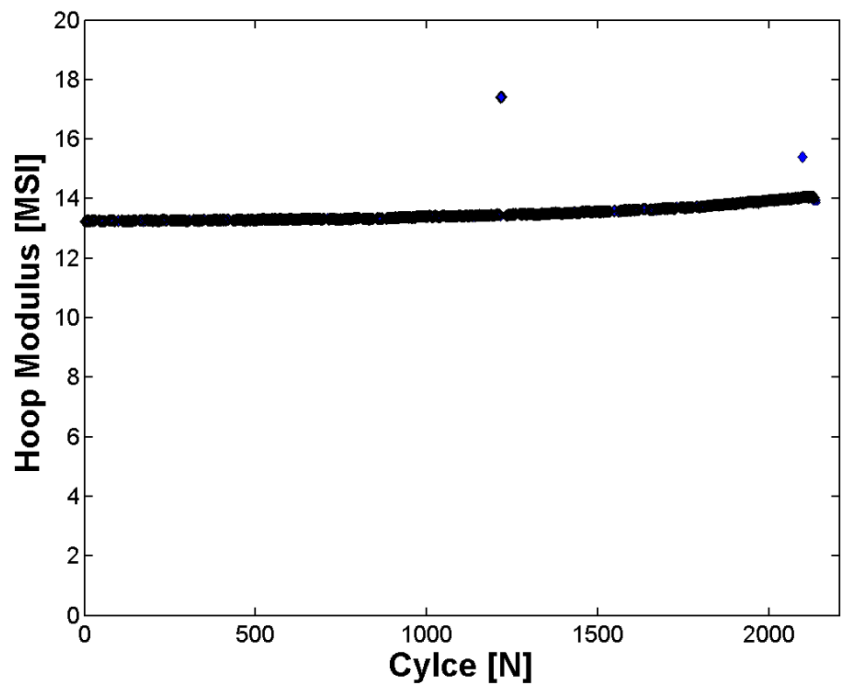


Figure A.6 – Hoop modulus as a function of number of fatigue cycles for OM3936.

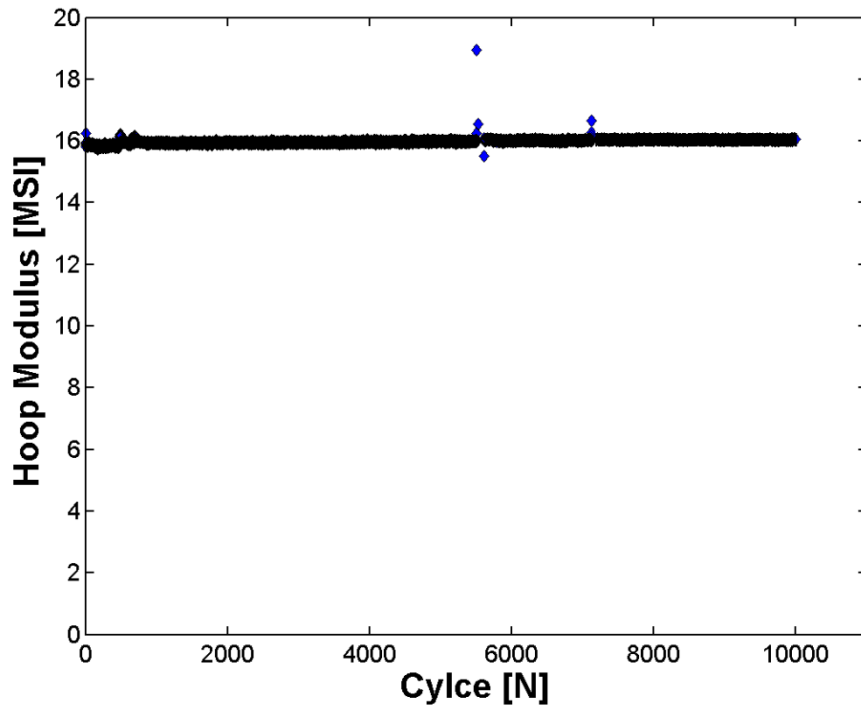


Figure A.7 – Hoop modulus as a function of number of fatigue cycles for ALT639-9765.

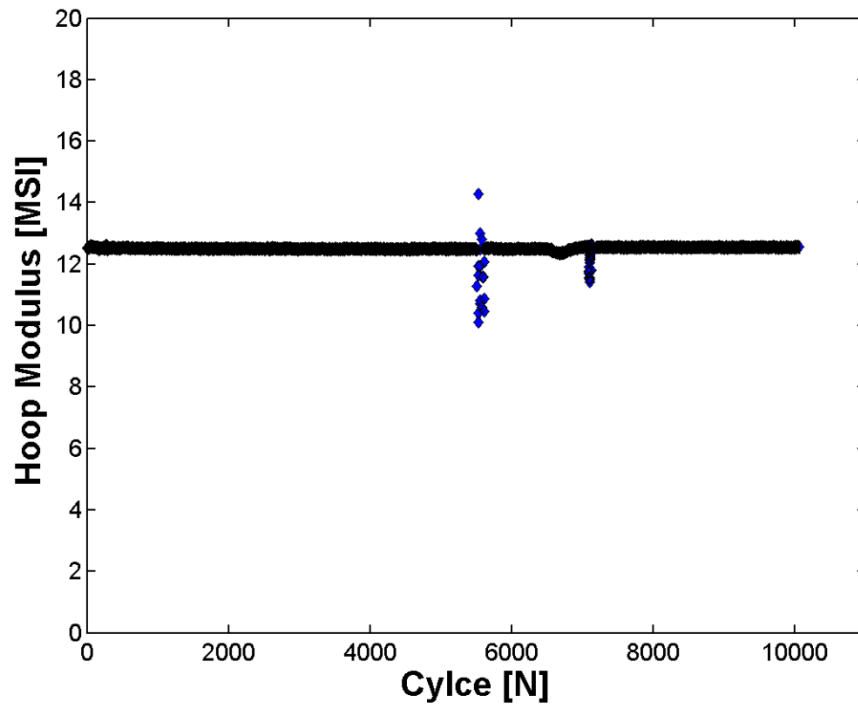


Figure A.8 – Hoop modulus as a function of number of fatigue cycles for ALT639-17946.

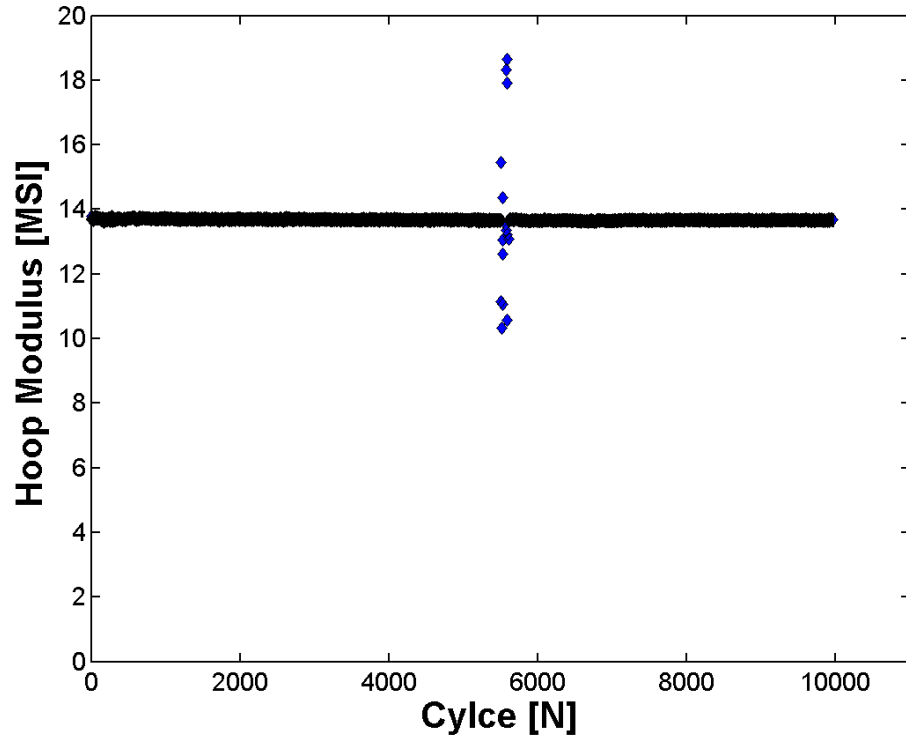


Figure A.9 – Hoop modulus as a function of number of fatigue cycles for ALT695-5483.

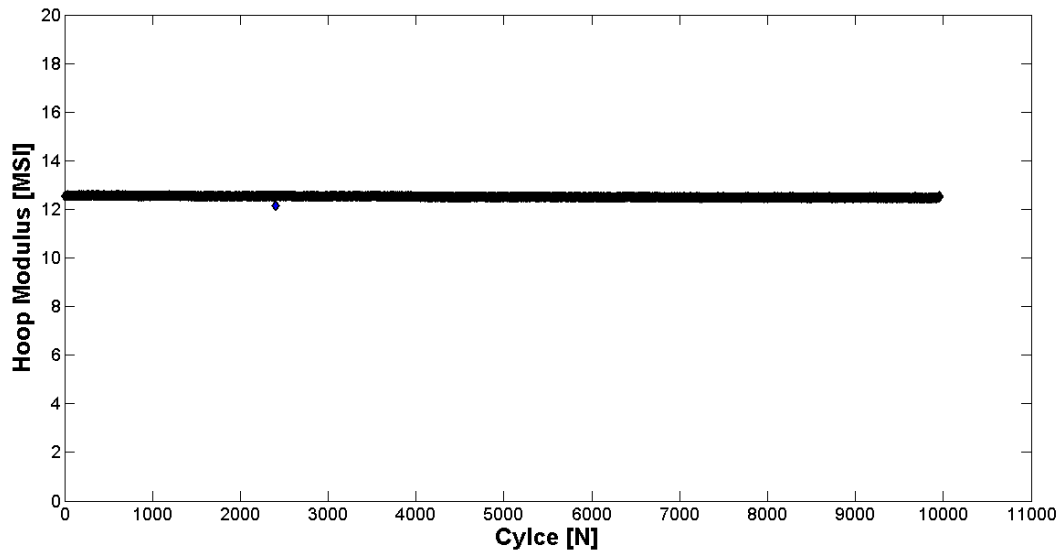


Figure A.10 – Hoop modulus as a function of applied fatigue cycles for ALT639-9987.

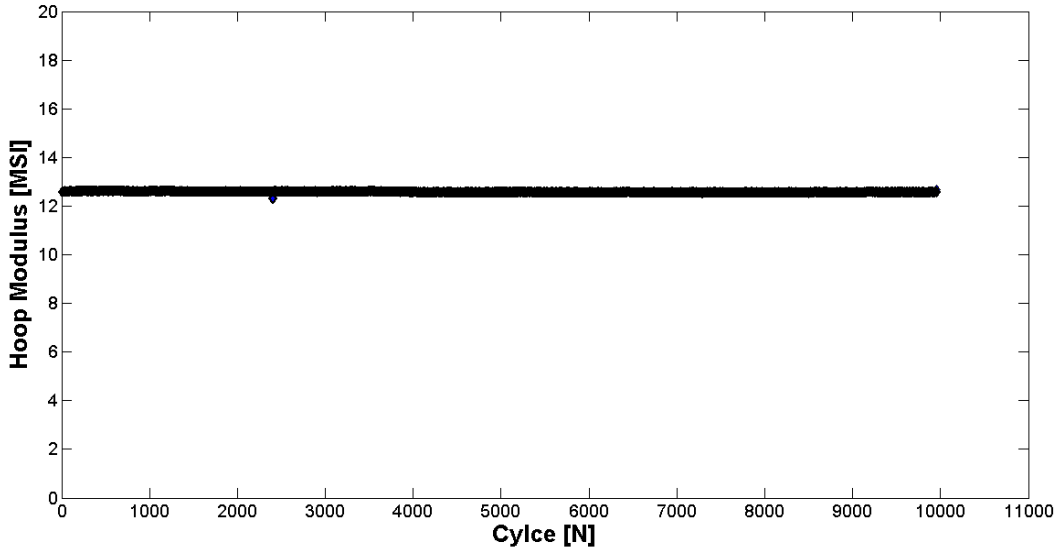


Figure A.11 – Hoop modulus as a function of applied fatigue cycles for ALT639-9959.

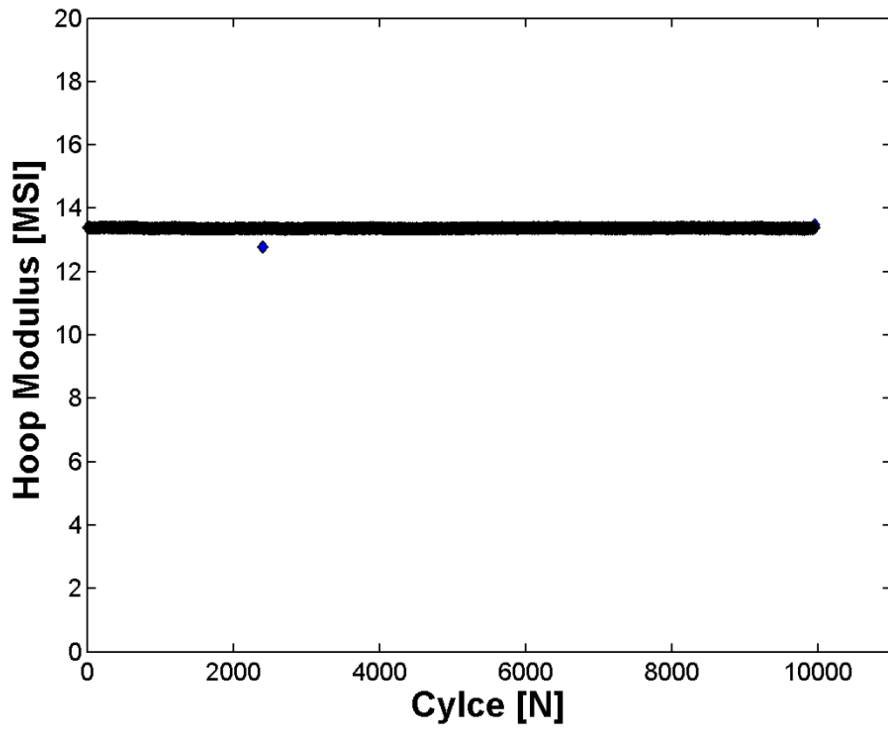


Figure A.12 – Hoop modulus as a function of applied fatigue cycles for ALT639-34081.

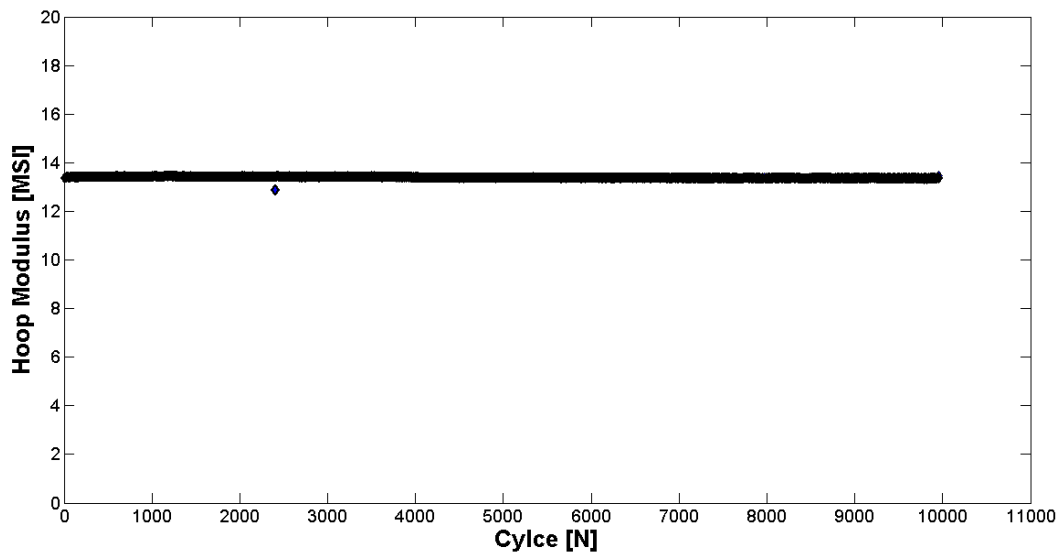


Figure A.13 – Hoop modulus as a function of applied fatigue cycles for ALT695-5031.

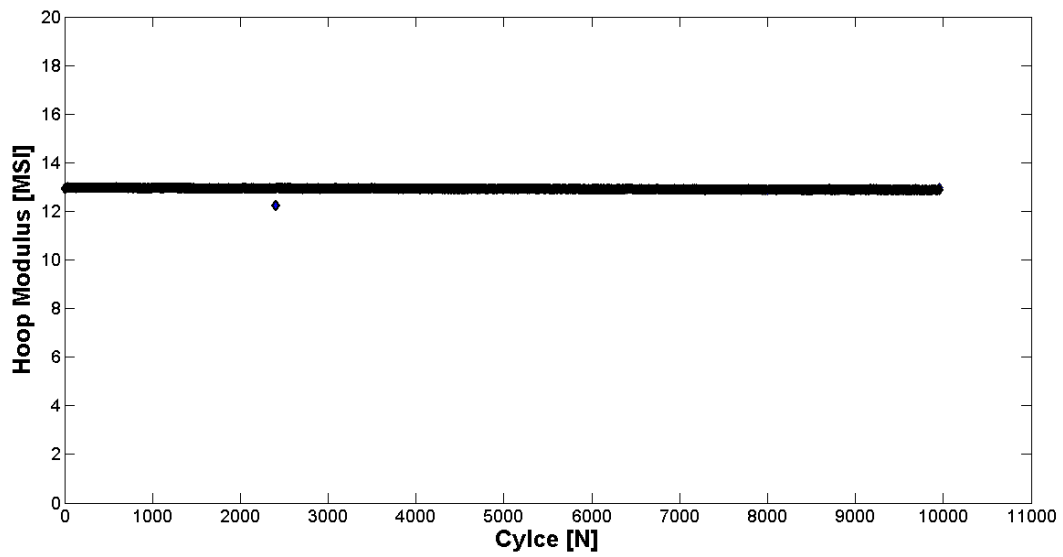


Figure A.14 – Hoop modulus as a function of applied fatigue cycles of ALT639-9753.

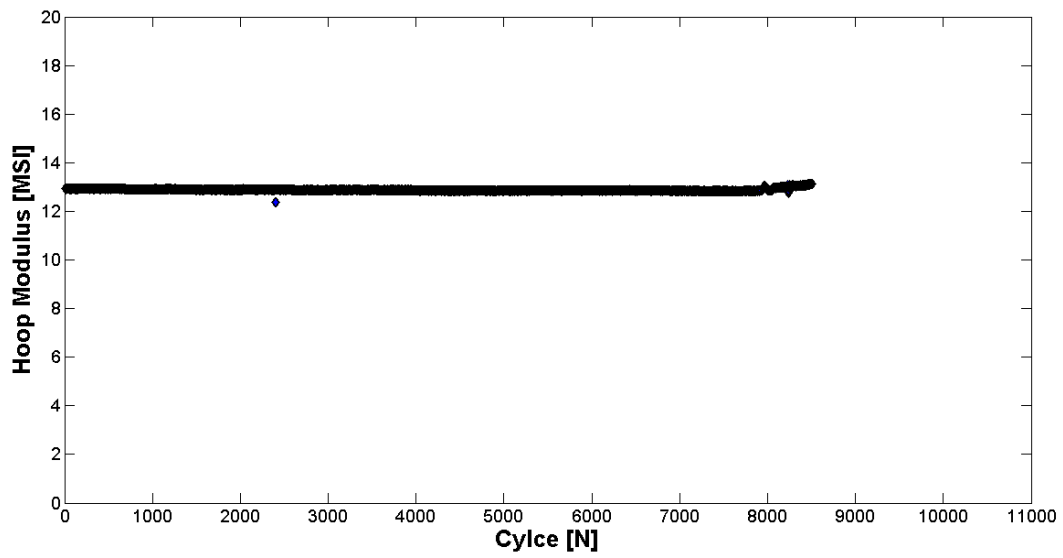


Figure A.15 – Hoop modulus as a function of applied fatigue cycles of ALT639-30041.

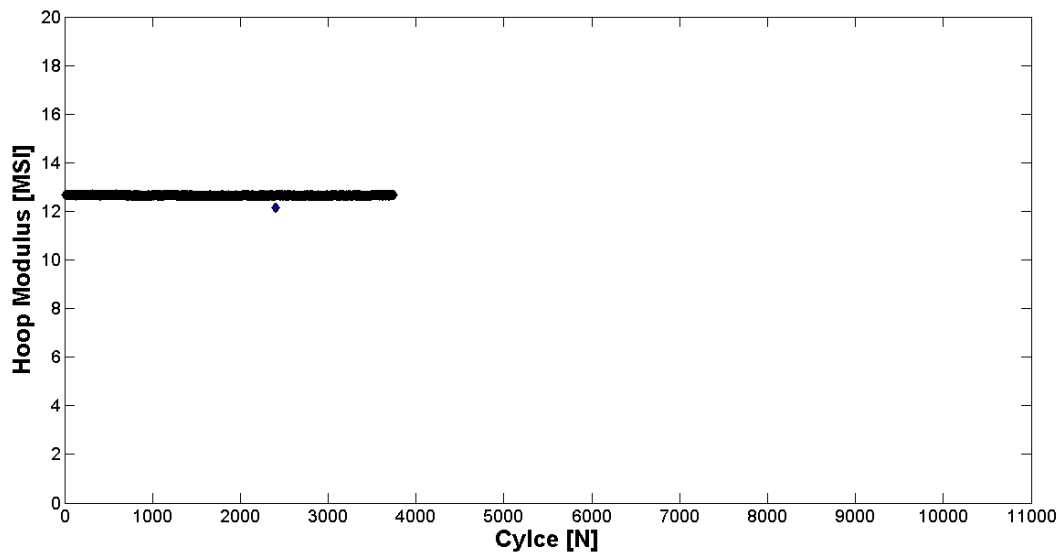


Figure A. 16 – Hoop modulus as a function of applied fatigue cycles of ALT604-3764.

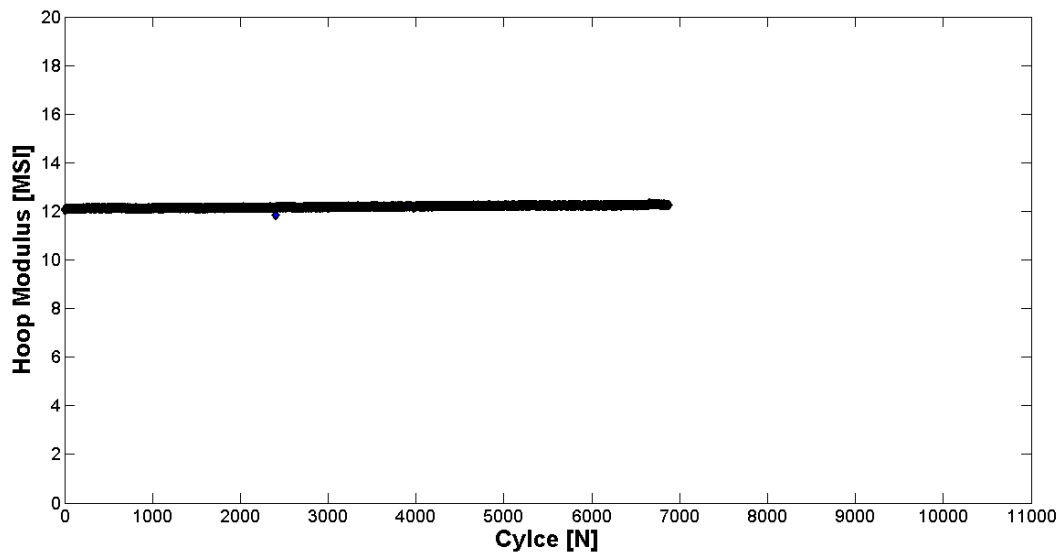


Figure A.17 – Hoop modulus as a function of applied fatigue cycles of OM3930.

## APPENDIX B

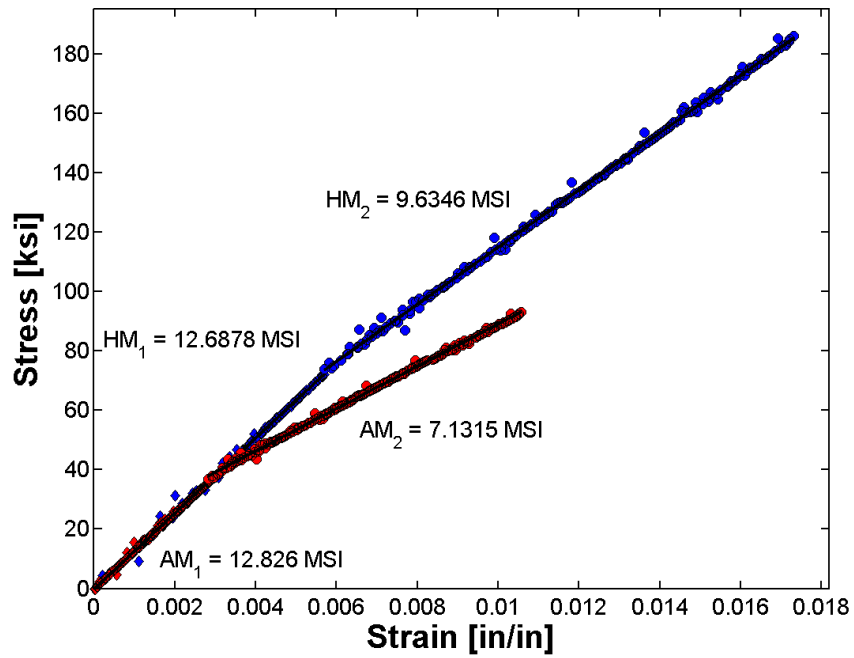


Figure B.1 – Hoop and axial modulus for ALT639-9573. Note, blue symbols are hoop data and red symbols are axial data.

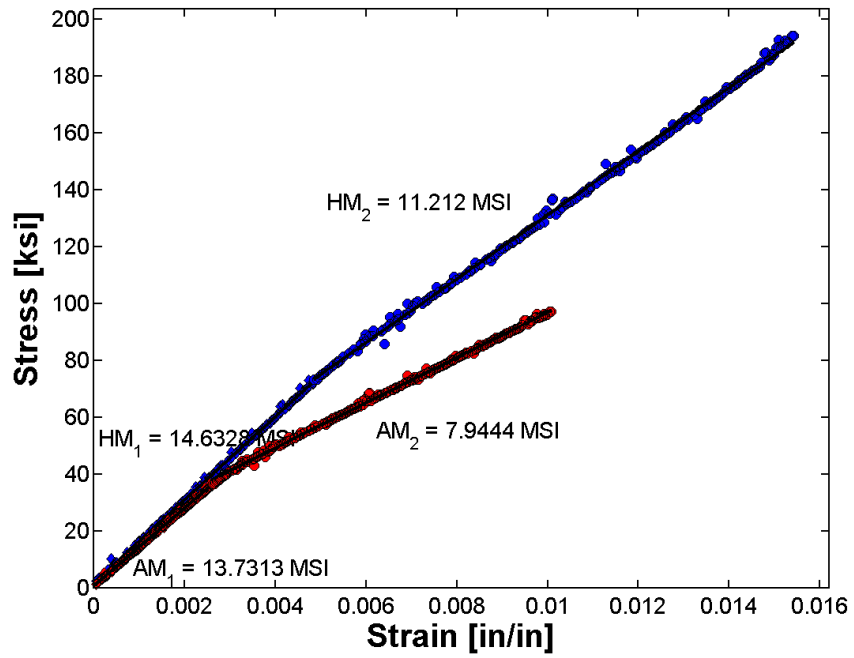


Figure B.2 – Hoop and axial modulus for ALT639-18114. Note, blue symbols are hoop data and red symbols are axial data.

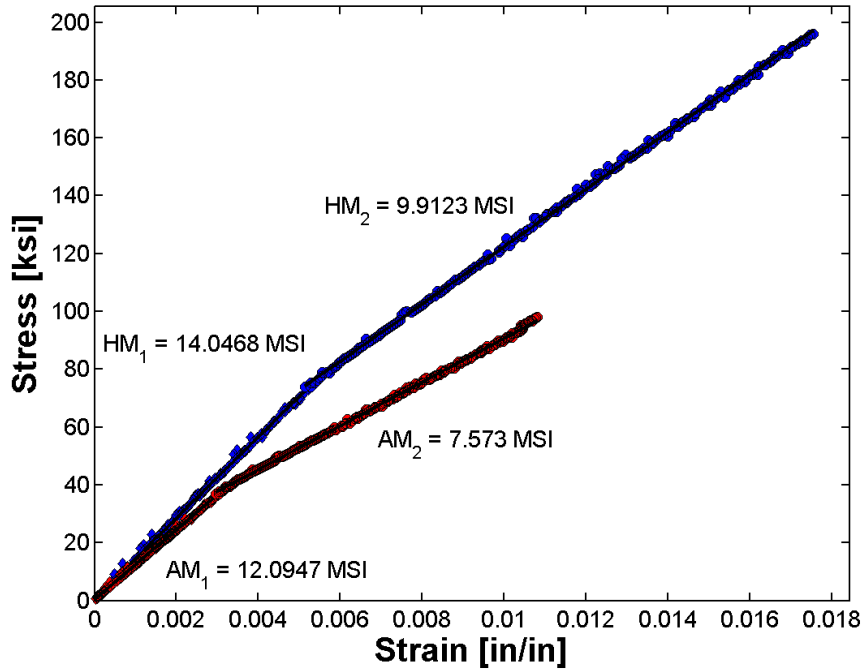


Figure B.3 – Hoop and axial modulus for ALT639-34075. Note, blue symbols are hoop data and red symbols are axial data.

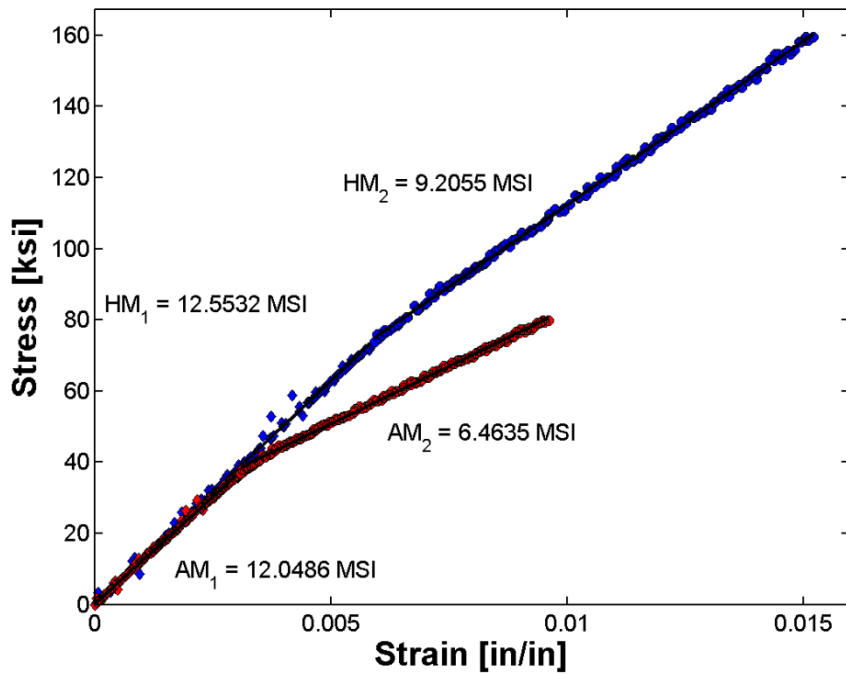


Figure B.4 – Hoop and axial modulus for OM3924. Note, blue symbols are hoop data and red symbols are axial data.

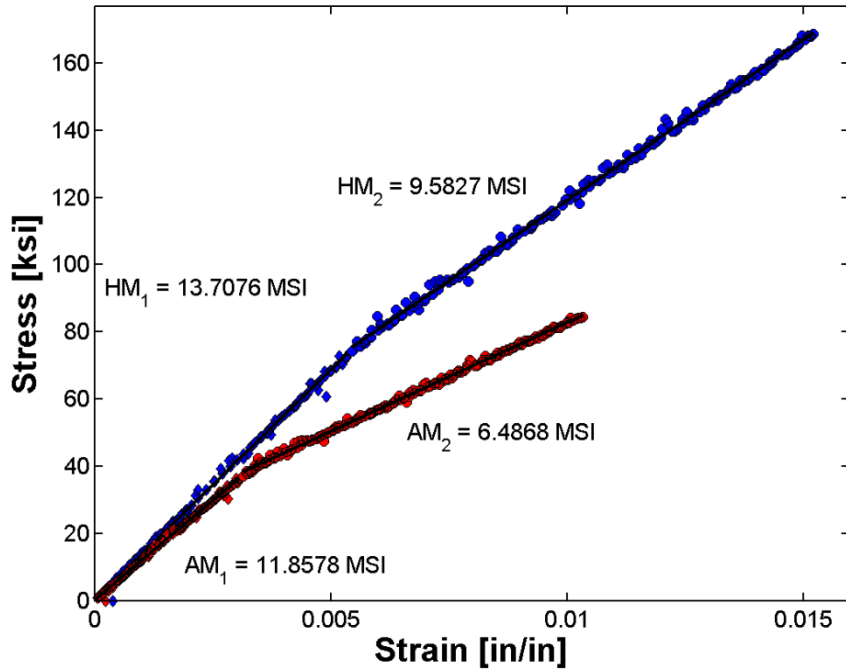


Figure B.5 – Hoop and axial modulus for OM3943. Note, blue symbols are hoop data and red symbols are axial data.

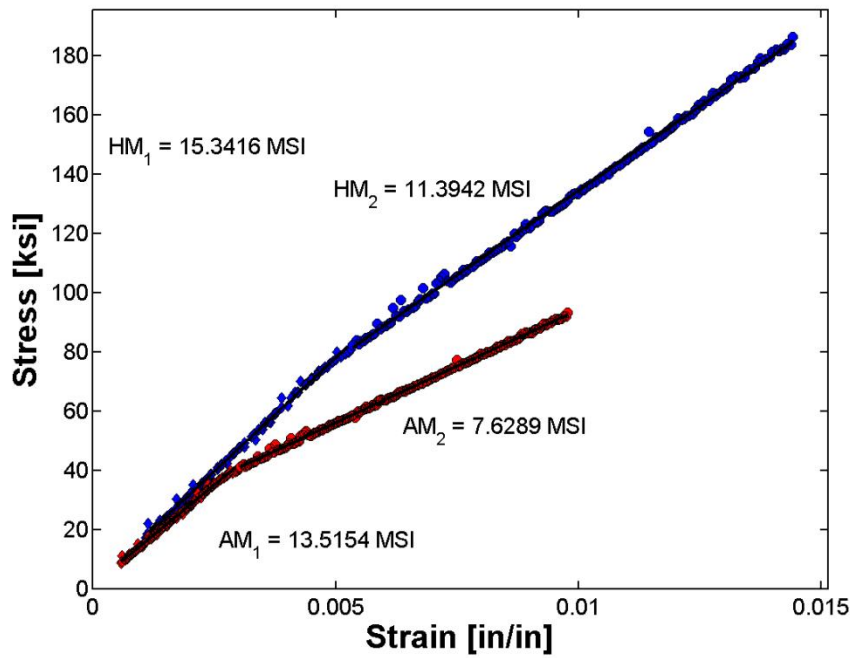


Figure B.6 – Hoop and axial modulus for ALT639-70015. Note, blue symbols are hoop data and red symbols are axial data.

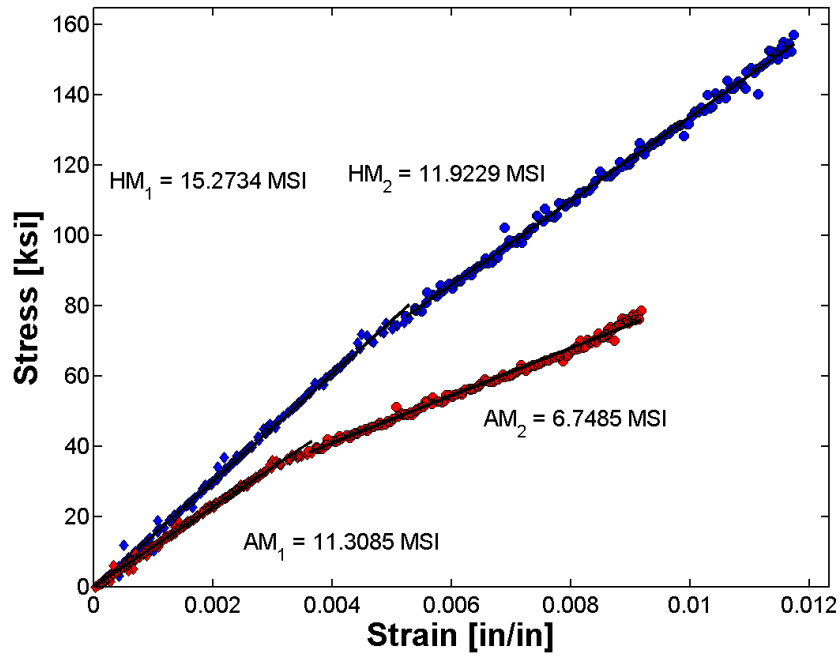


Figure B.7 – Hoop and axial modulus for ALT695-5660. Note, blue symbols are hoop data and red symbols are axial data.

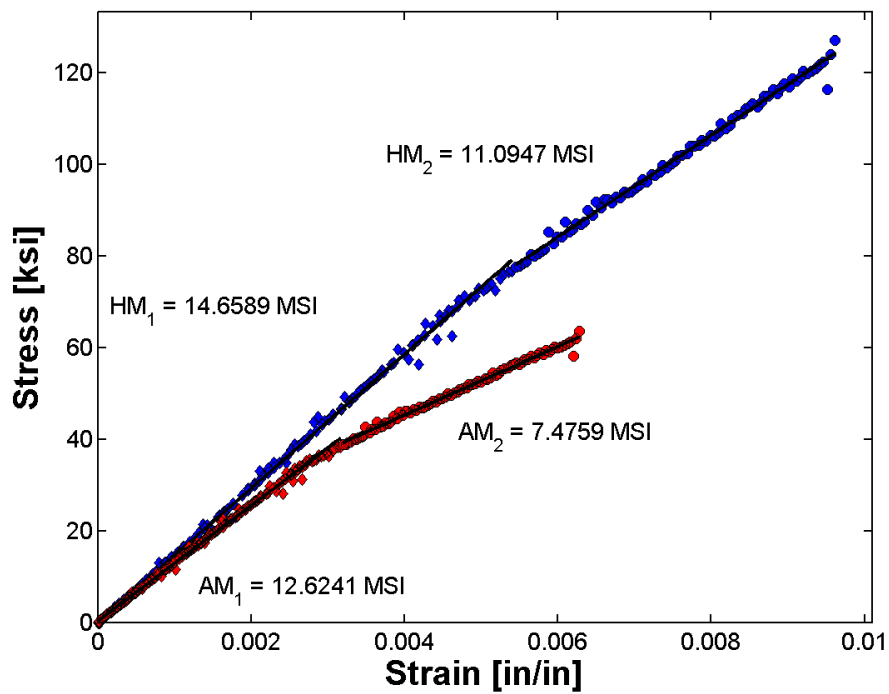


Figure B.8 – Hoop and axial modulus for ALT695-1665. Note, blue symbols are hoop data and red symbols are axial data.

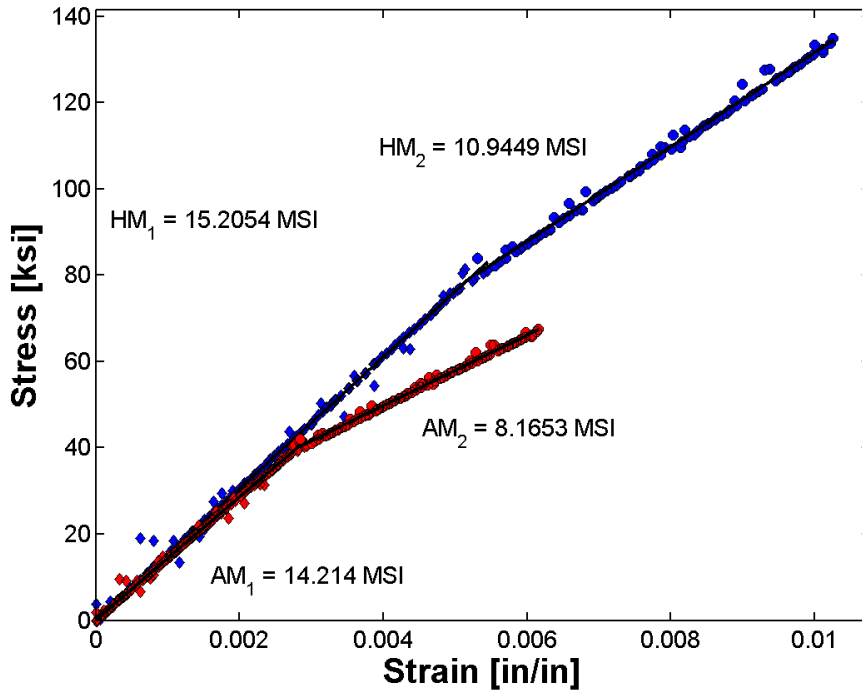


Figure B.9 – Hoop and axial modulus for ALT639-29405. Note, blue symbols are hoop data and red symbols are axial data.

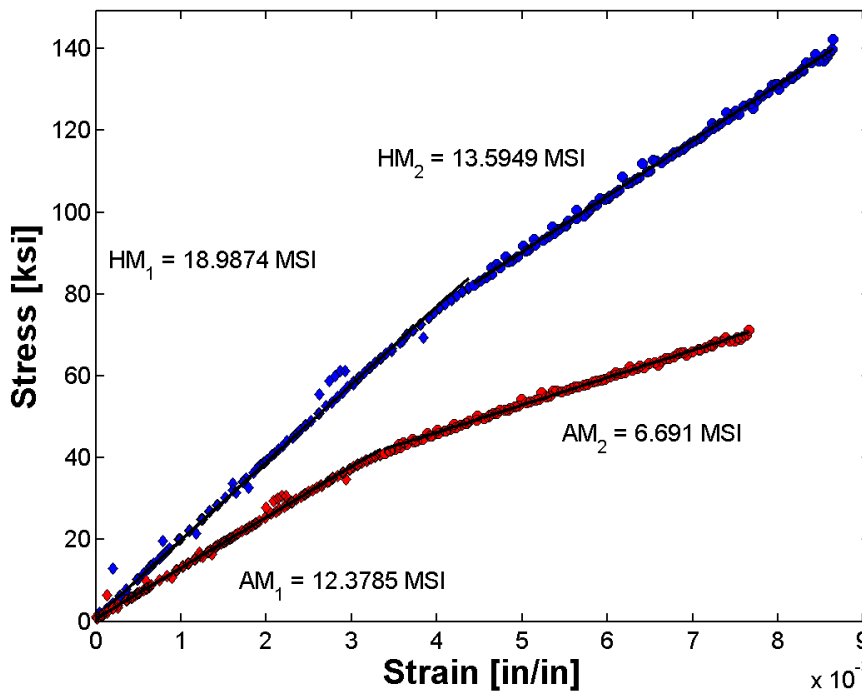


Figure B.10 – Hoop and axial modulus for ALT639-9765. Note, blue symbols are hoop data and red symbols are axial data.

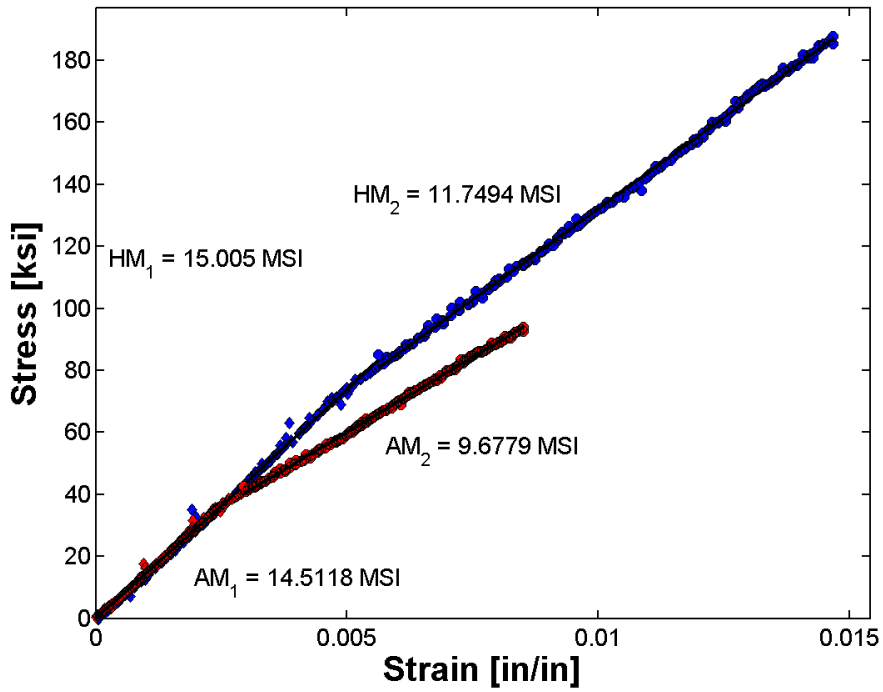


Figure B.11 – Hoop and axial modulus for ALT639-33989. Note, blue symbols are hoop data and red symbols are axial data.

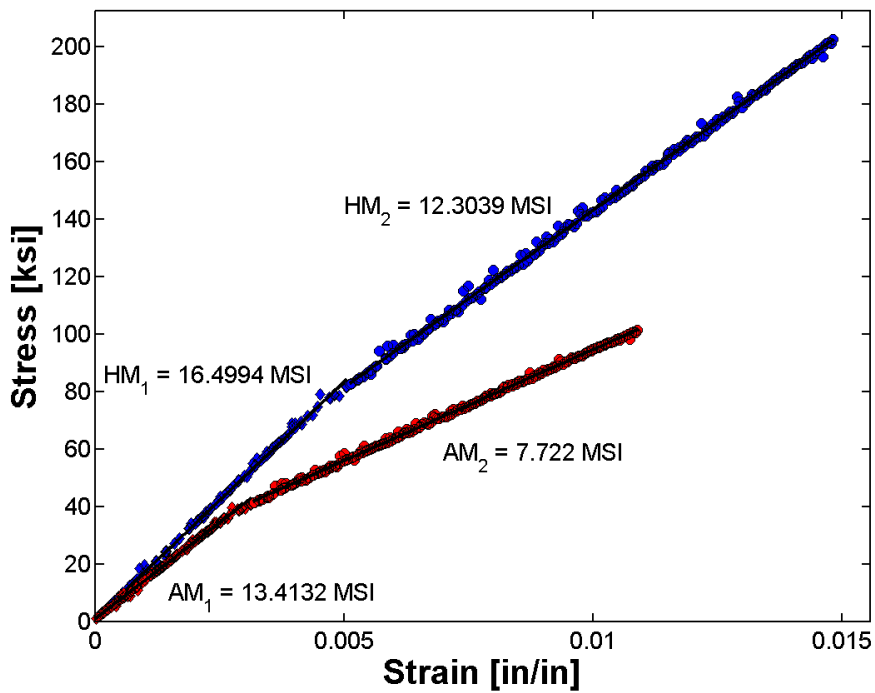


Figure B.12 – Hoop and axial modulus for ALT639-18726. Note, blue symbols are hoop data and red symbols are axial data.

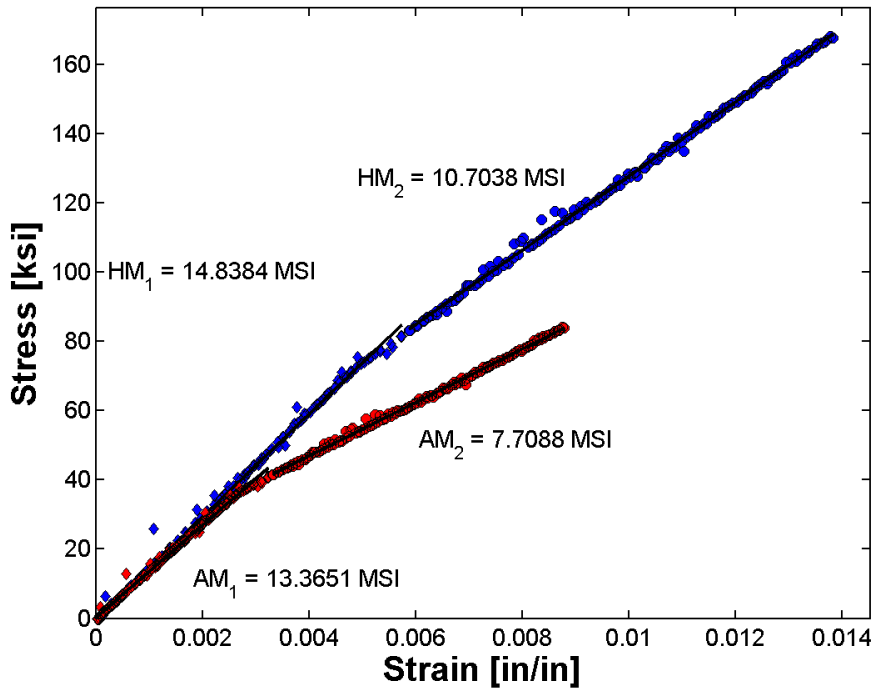


Figure B.13 – Hoop and axial modulus for ALT639-34079. Note, blue symbols are hoop data and red symbols are axial data.

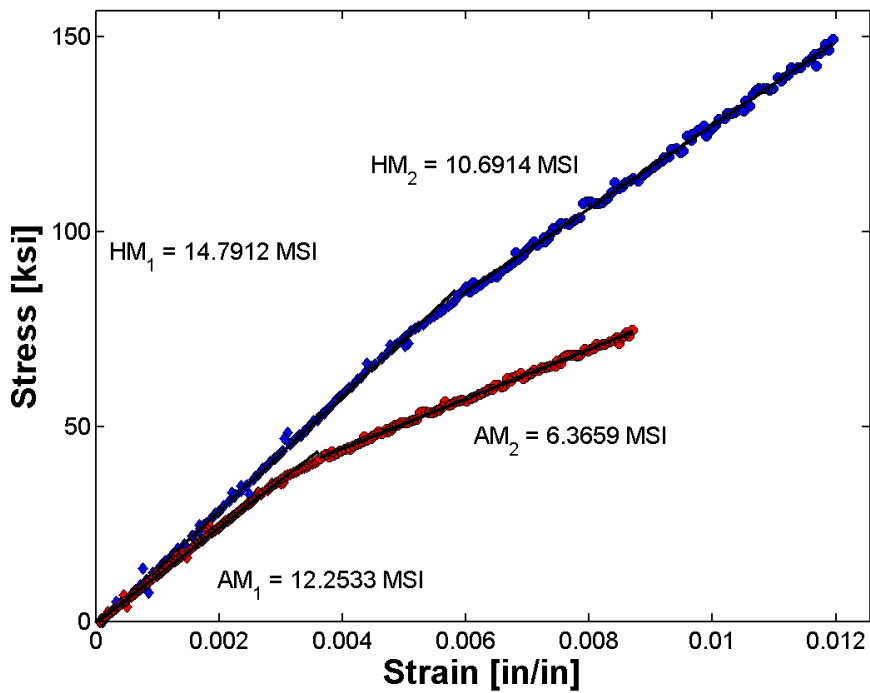


Figure B.14 – Hoop and axial modulus for OM3909. Note, blue symbols are hoop data and red symbols are axial data.

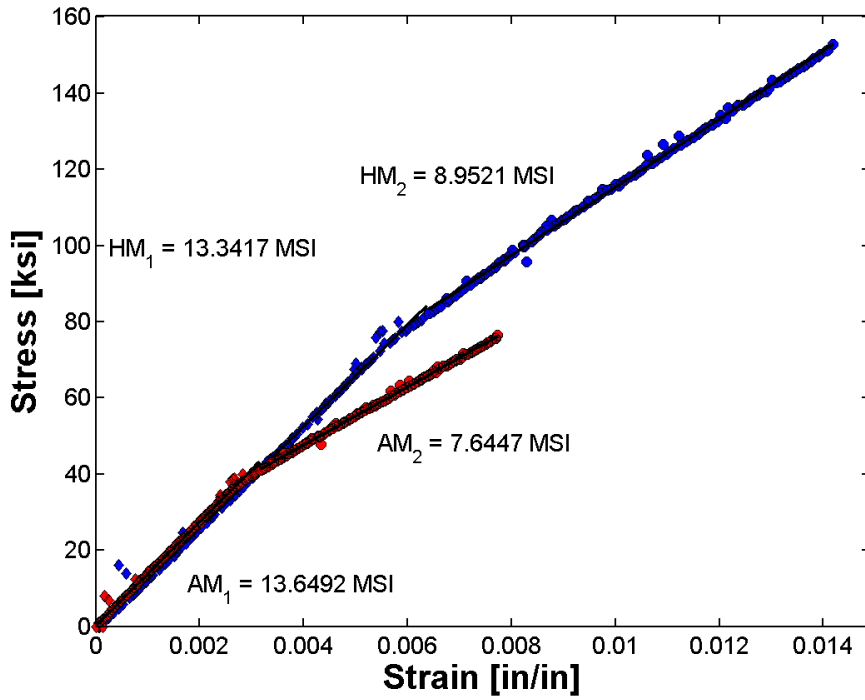


Figure B.15 – Hoop and axial modulus for ALT639-34011. Note, blue symbols are hoop data and red symbols are axial data.

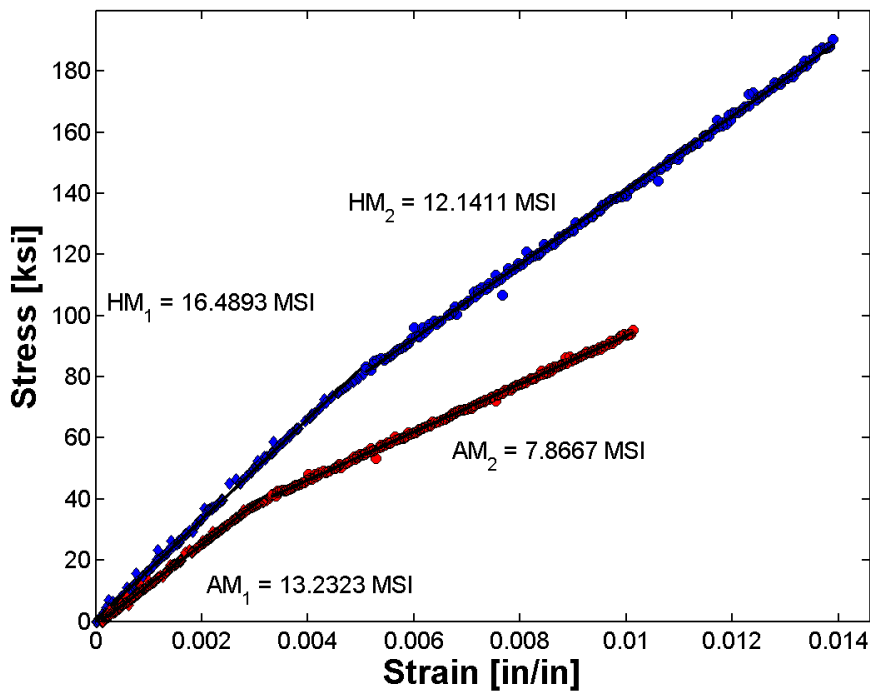


Figure B.16 – Hoop and axial modulus for ALT639-19026. Note, blue symbols are hoop data and red symbols are axial data.

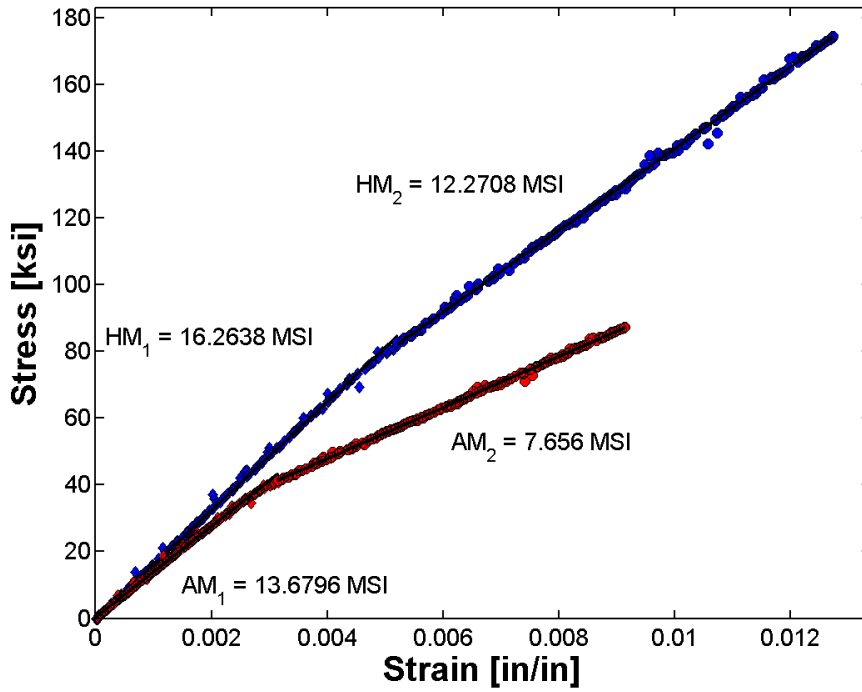


Figure B.17 – Hoop and axial modulus for ALT639-9605. Note, blue symbols are hoop data and red symbols are axial data.

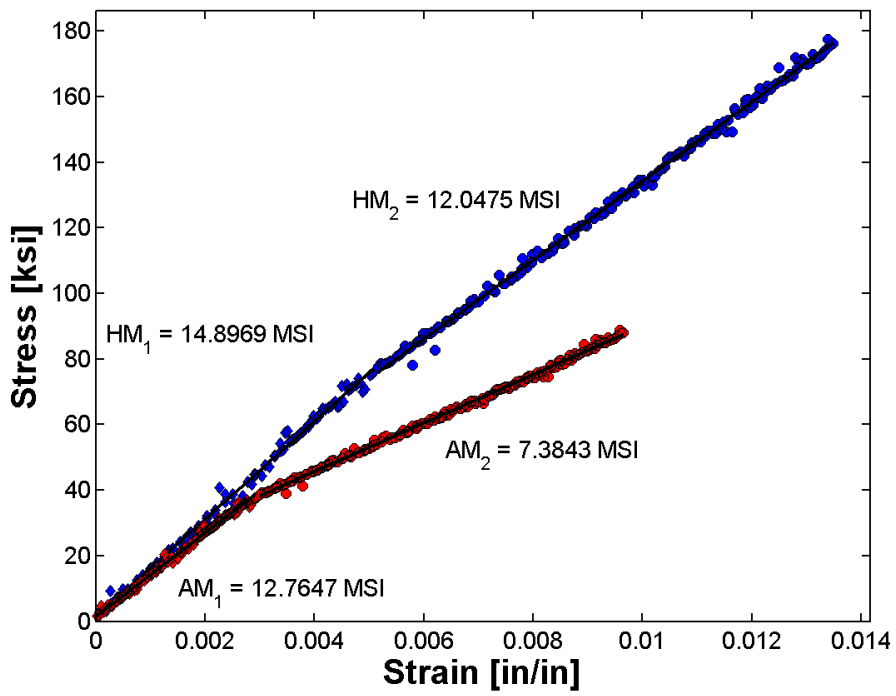


Figure B.18 – Hoop and axial modulus for ALT695-5483. Note, blue symbols are hoop data and red symbols are axial data.

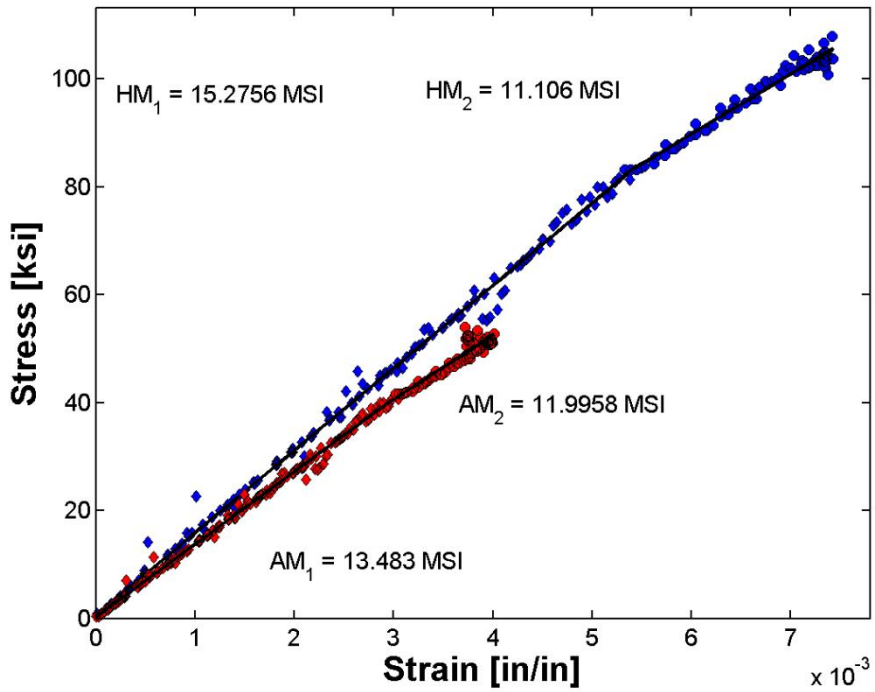


Figure B.19 – Hoop and axial modulus for ALT639-9948. Note, blue symbols are hoop data and red symbols are axial data.

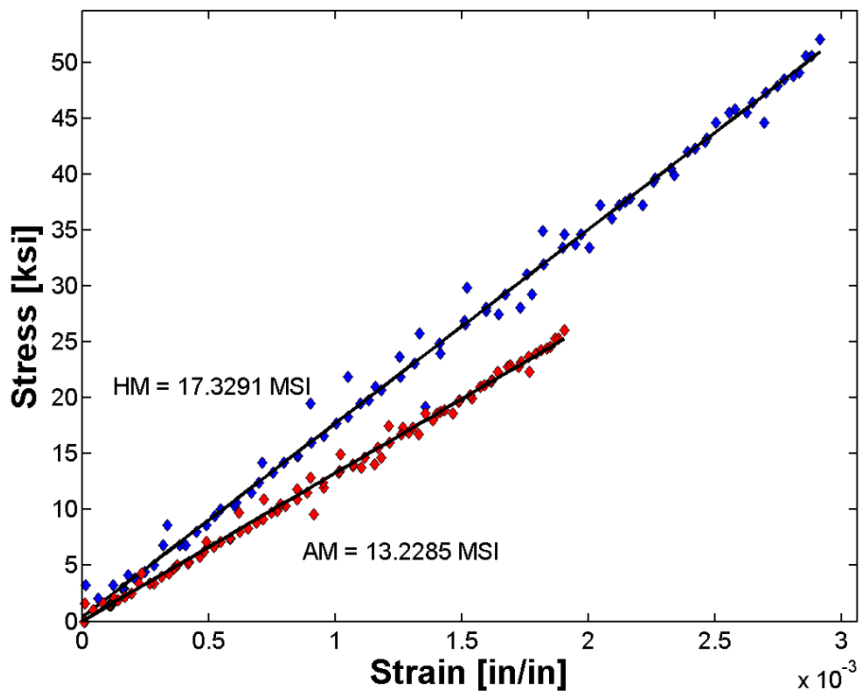


Figure B.20 – Hoop and axial modulus for ALT639-17946. Note, blue symbols are hoop data and red symbols are axial data.

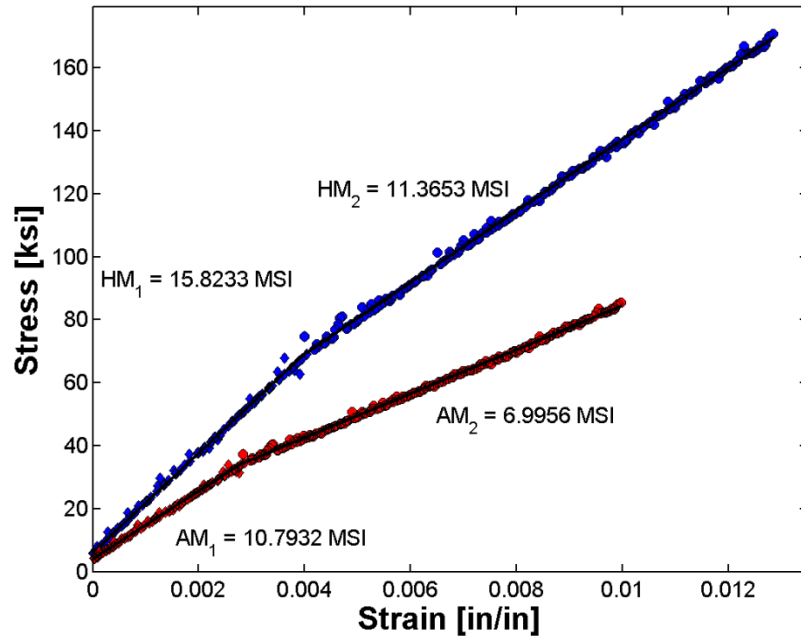


Figure B.21 – Hoop and axial modulus for ALT639-18454. Note, blue symbols are hoop data and red symbols are axial data.

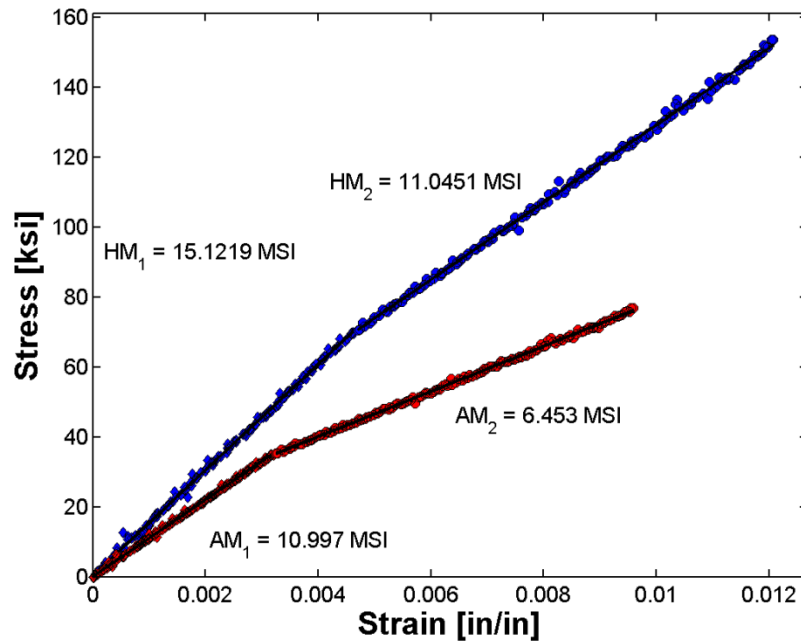


Figure B.22 – Hoop and axial modulus for ALT695-5020. Note, blue symbols are hoop data and red symbols are axial data.

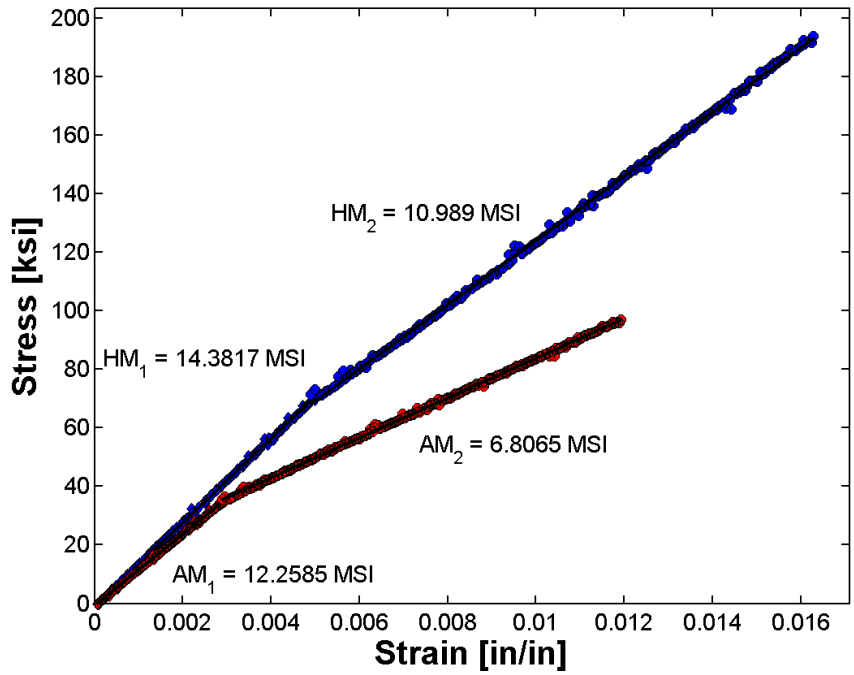


Figure B.23 – Hoop and axial modulus for ALT639-95898. Note, blue symbols are hoop data and red symbols are axial data.

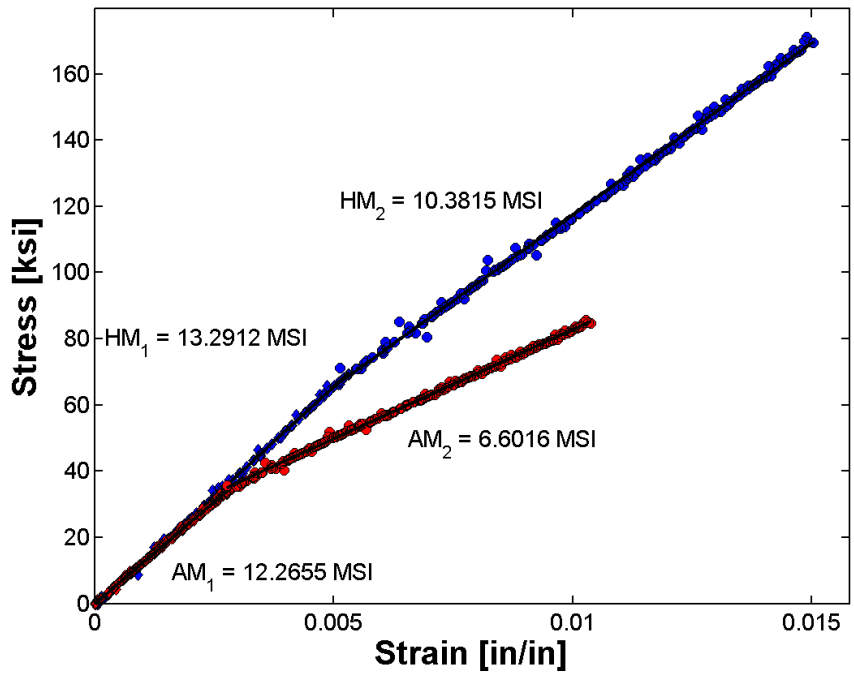


Figure B.24 – Hoop and axial modulus for ALT639-9465. Note, blue symbols are hoop data and red symbols are axial data.

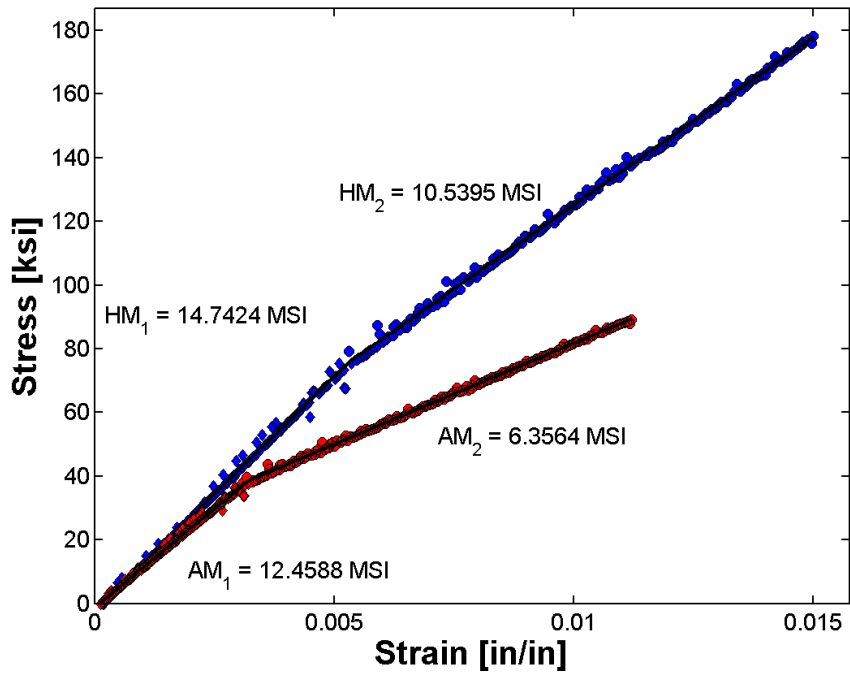


Figure B.25 – Hoop and axial modulus for OM3966. Note, blue symbols are hoop data and red symbols are axial data.

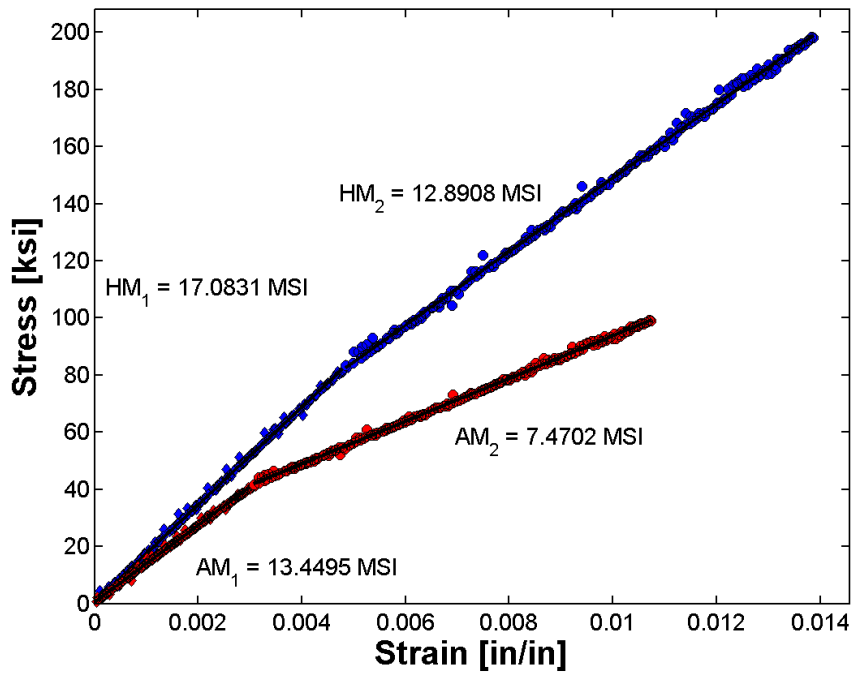


Figure B.26 – Hoop and axial modulus for ALT639-18030. Note, blue symbols are hoop data and red symbols are axial data.

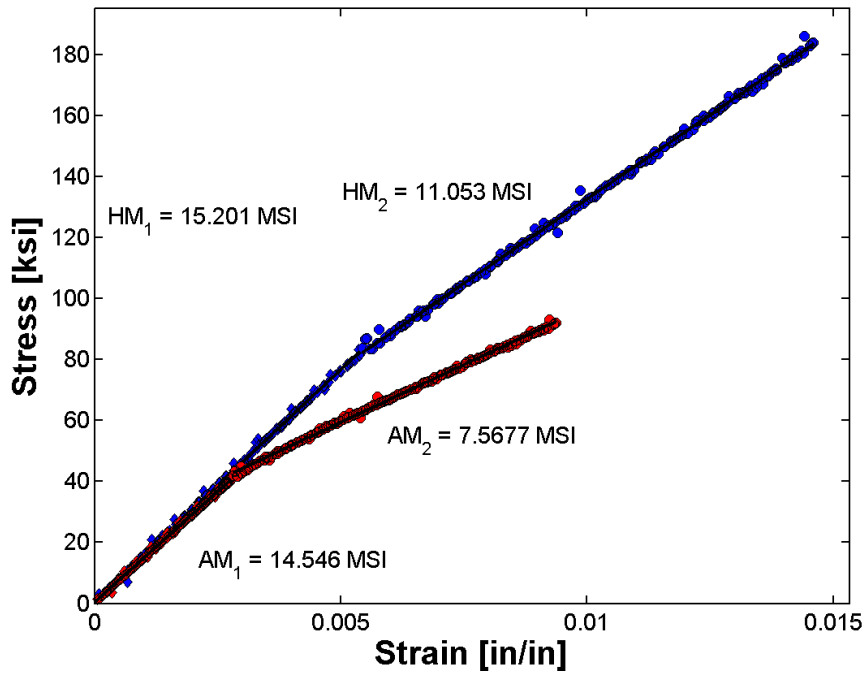


Figure B.27 – Hoop and axial modulus for ALT639-9987. Note, blue symbols are hoop data and red symbols are axial data.

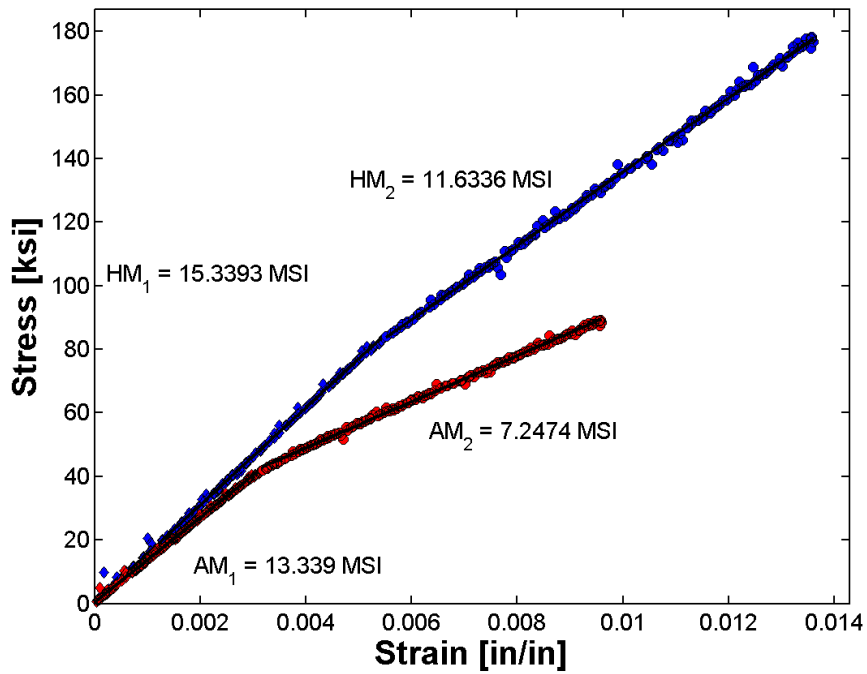


Figure B.28 – Hoop and axial modulus for ALT639-9959. Note, blue symbols are hoop data and red symbols are axial data.

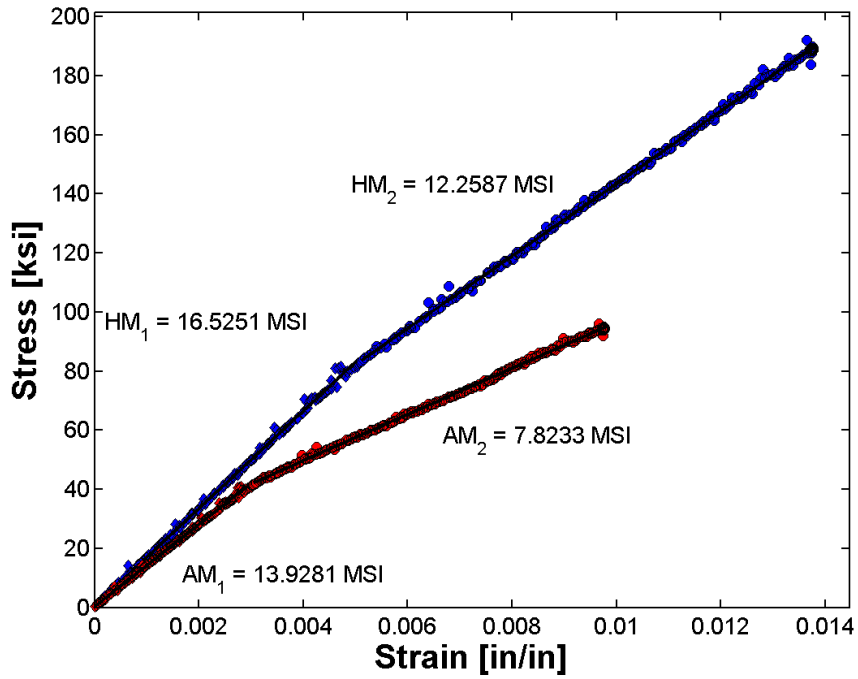


Figure B.29 – Hoop and axial modulus for ALT639-34061. Note, blue symbols are hoop data and red symbols are axial data.

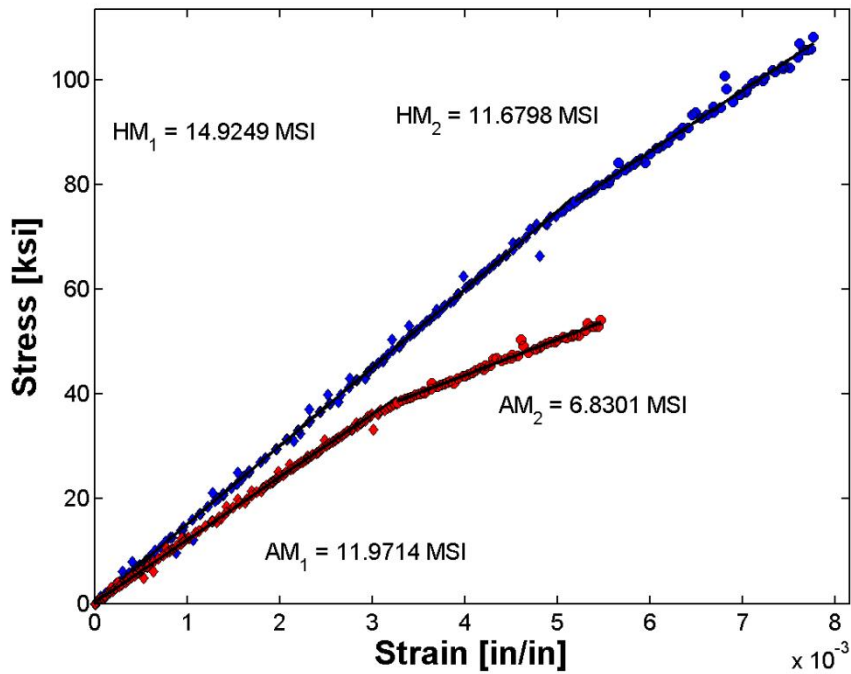


Figure B.30 – Hoop and axial modulus for ALT695-5031. Note, blue symbols are hoop data and red symbols are axial data.

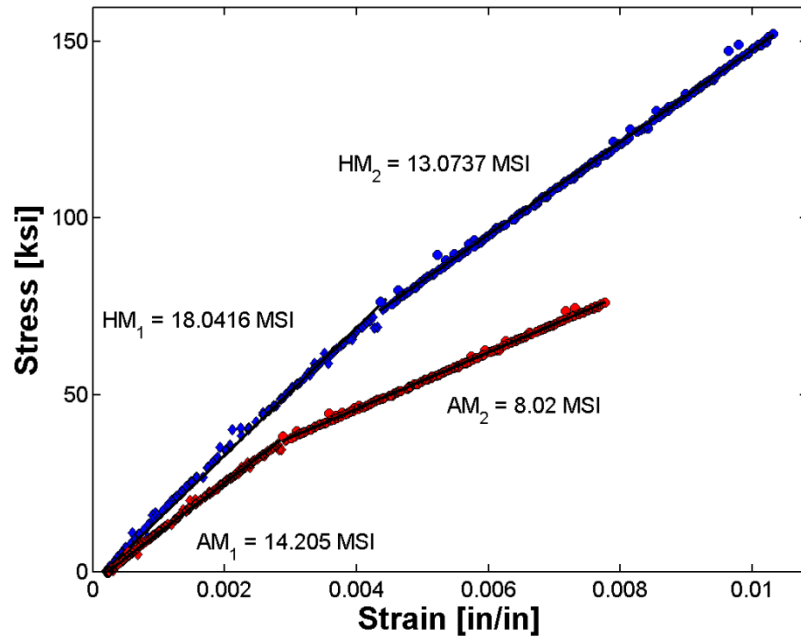


Figure B.31 – Primary (1) and Secondary (2) stiffness plot for ALT639 – 17716. Note, blue symbols are hoop data and red symbols are axial data.

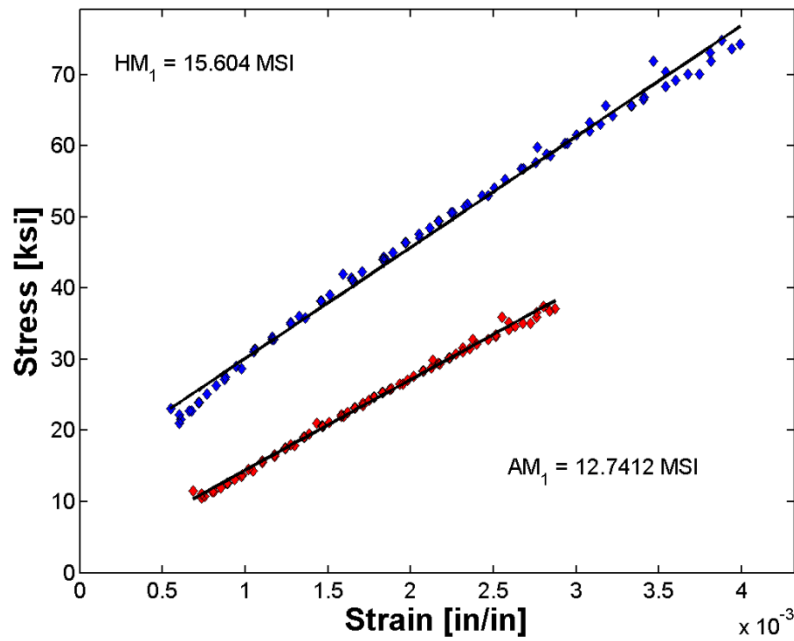


Figure B.32 - Primary (1) stiffness plot for ALT639 – 17831. Note, blue symbols are hoop data and red symbols are axial data.

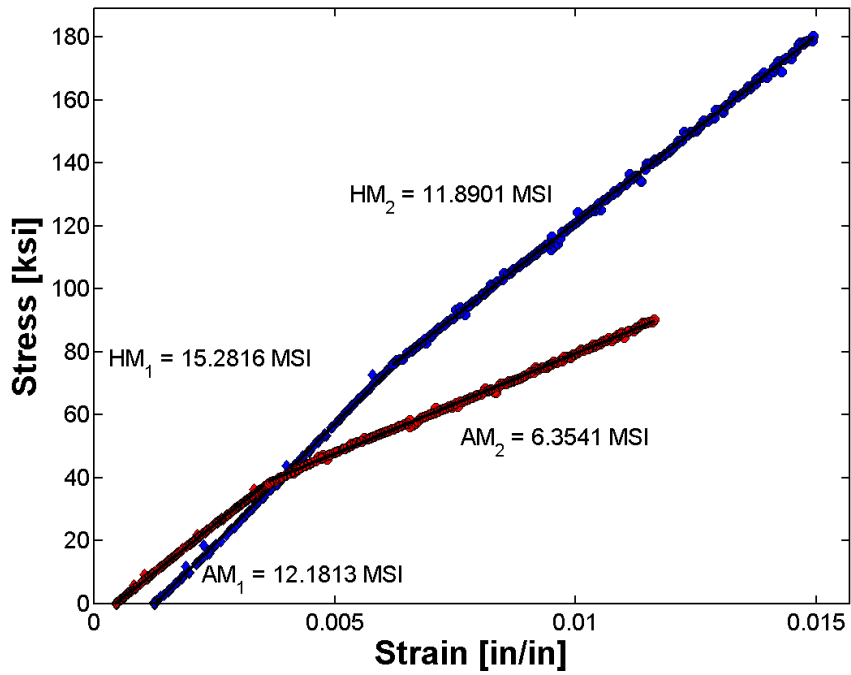


Figure B.33 - Primary (1) and Secondary (2) stiffness plot for ALT639 – 18768. Note, blue symbols are hoop data and red symbols are axial data.

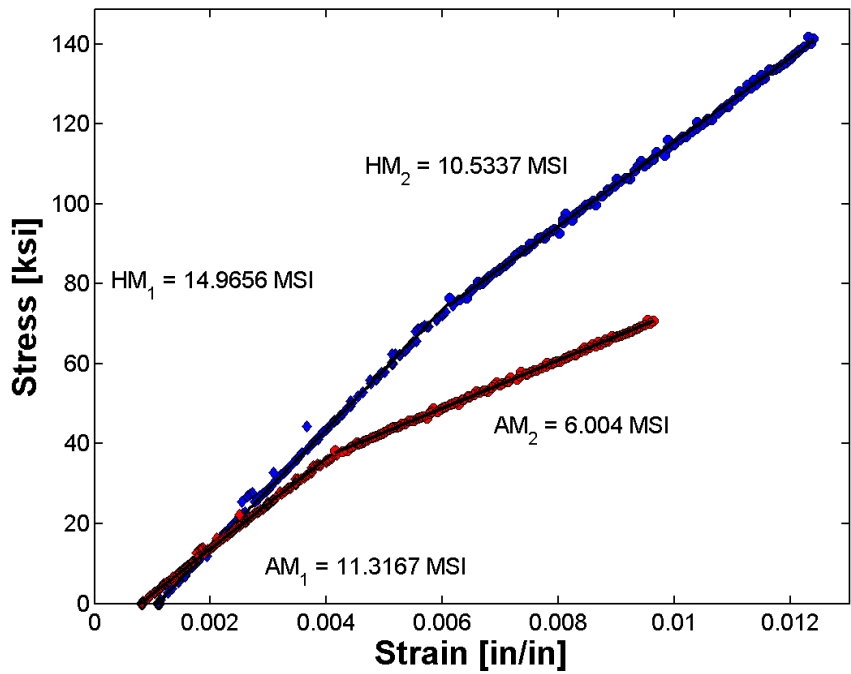


Figure B.34 - Primary (1) and Secondary (2) stiffness plot for ALT639 – 9747. Note, blue symbols are hoop data and red symbols are axial data.

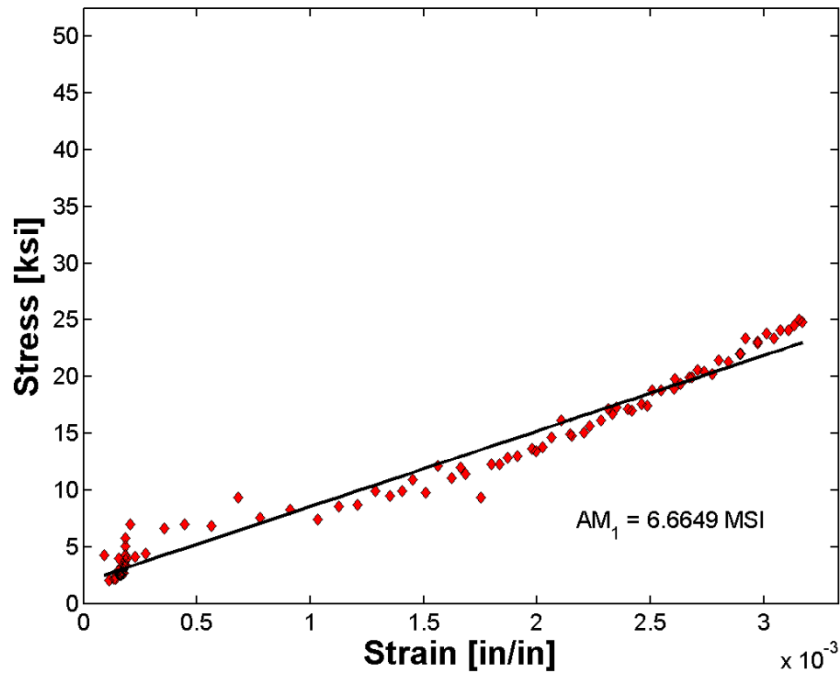


Figure B.35 - Primary (1) stiffness plot for ALT639 – 9769. Note, only primary axial modulus data was available due to severe fire exposure.

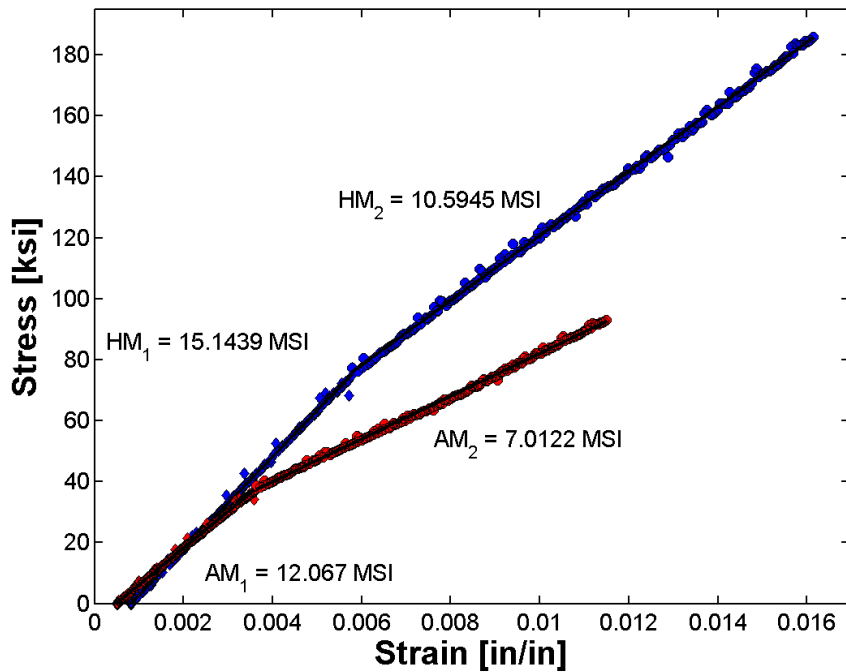


Figure B.36 - Primary (1) and Secondary (2) stiffness plot for ALT639 – 31064. Note, blue symbols are hoop data and red symbols are axial data.

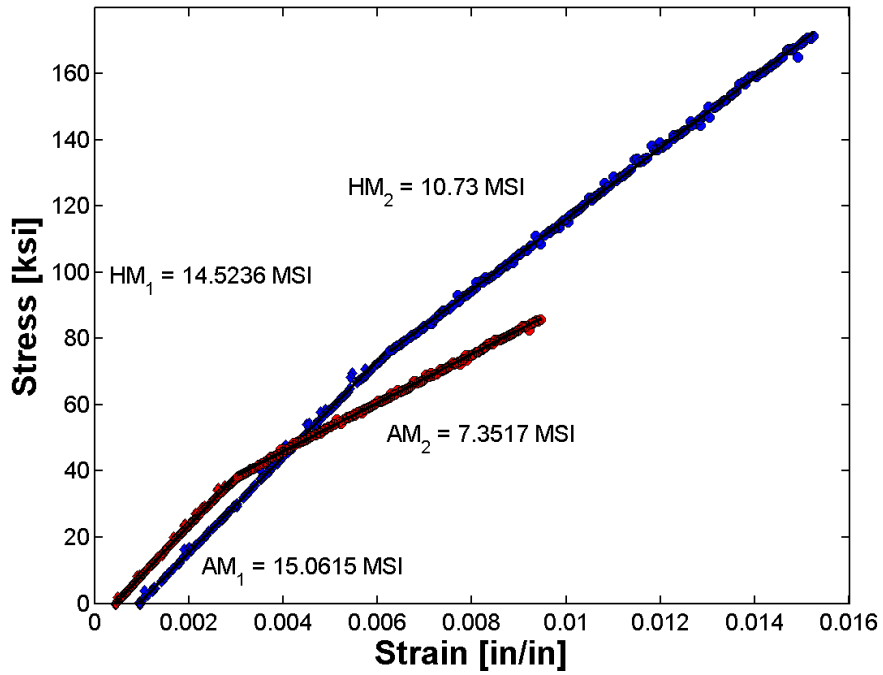


Figure B.37 - Primary (1) and Secondary (2) stiffness plot for ALT639 – 23371. Note, blue symbols are hoop data and red symbols are axial data.

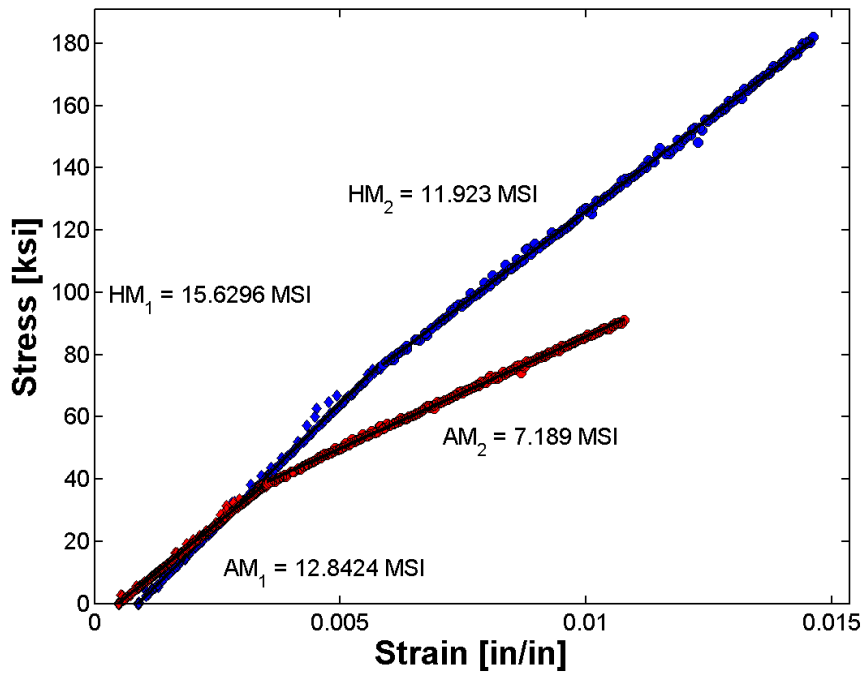


Figure B.38 - Primary (1) and Secondary (2) stiffness plot for ALT695 – 3669. Note, blue symbols are hoop data and red symbols are axial data.

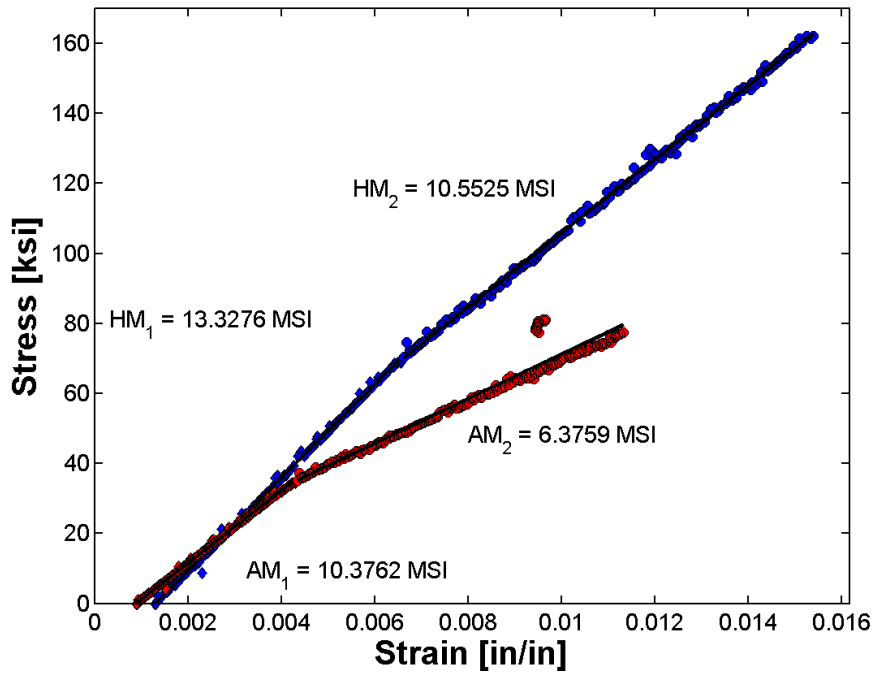


Figure B.39 - Primary (1) and Secondary (2) stiffness plot for ALT695-1781. Note, blue symbols are hoop data and red symbols are axial data.

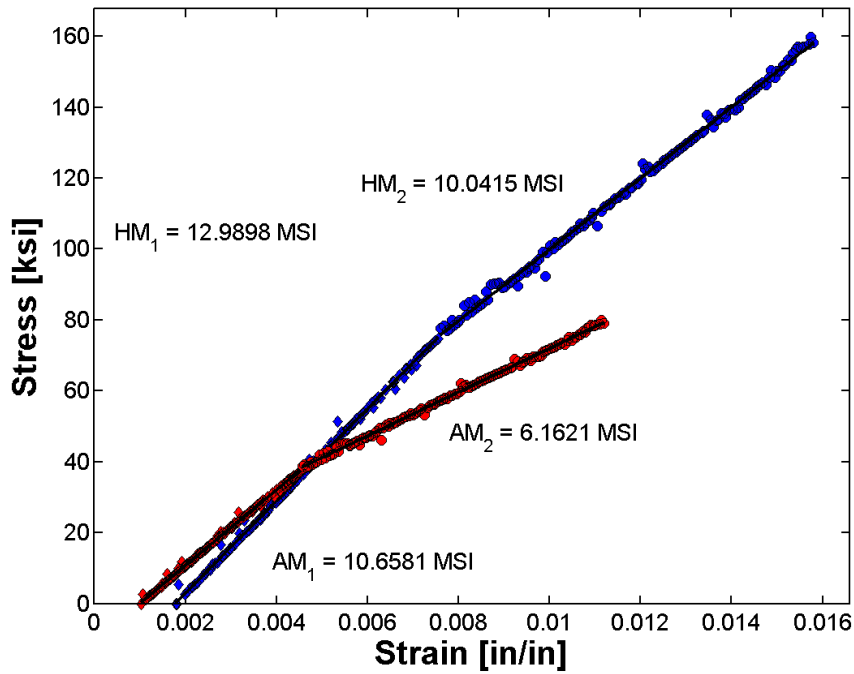


Figure B.40 - Primary (1) and Secondary (2) stiffness plot for OM3930. Note, blue symbols are hoop data and red symbols are axial data.

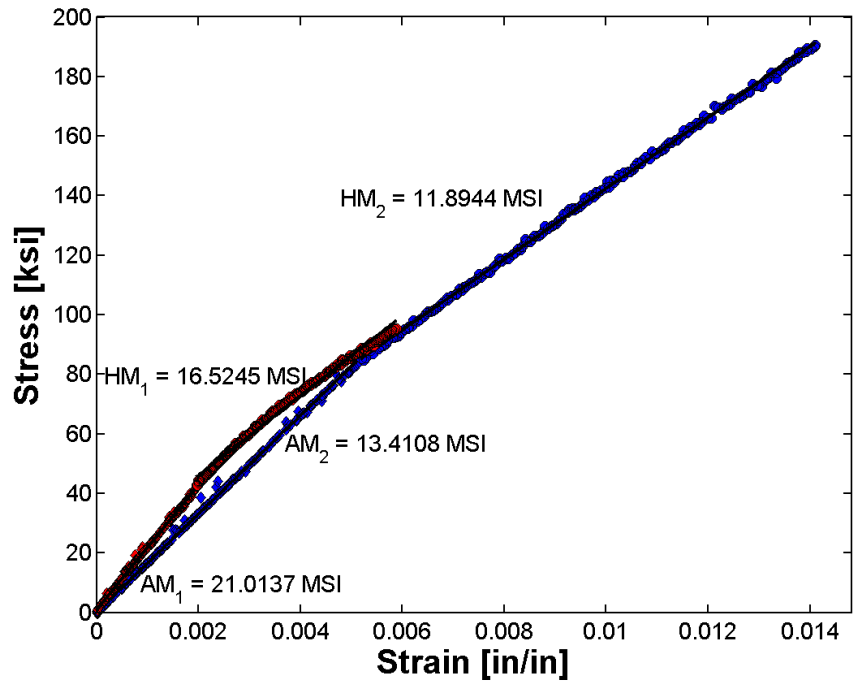


Figure B.41 - Primary (1) and Secondary (2) stiffness plot for ALT639-9753. Note, blue symbols are hoop data and red symbols are axial data.

# APPENDIX C

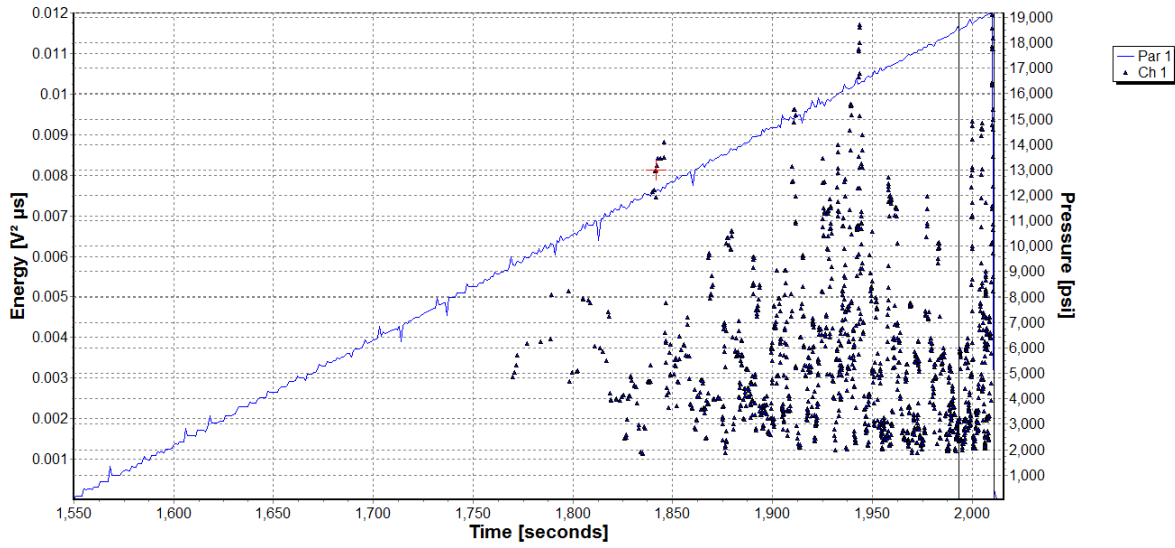


Figure C.1 – Background Energy Oscillation Pressure determination of ALT639 - 9573.

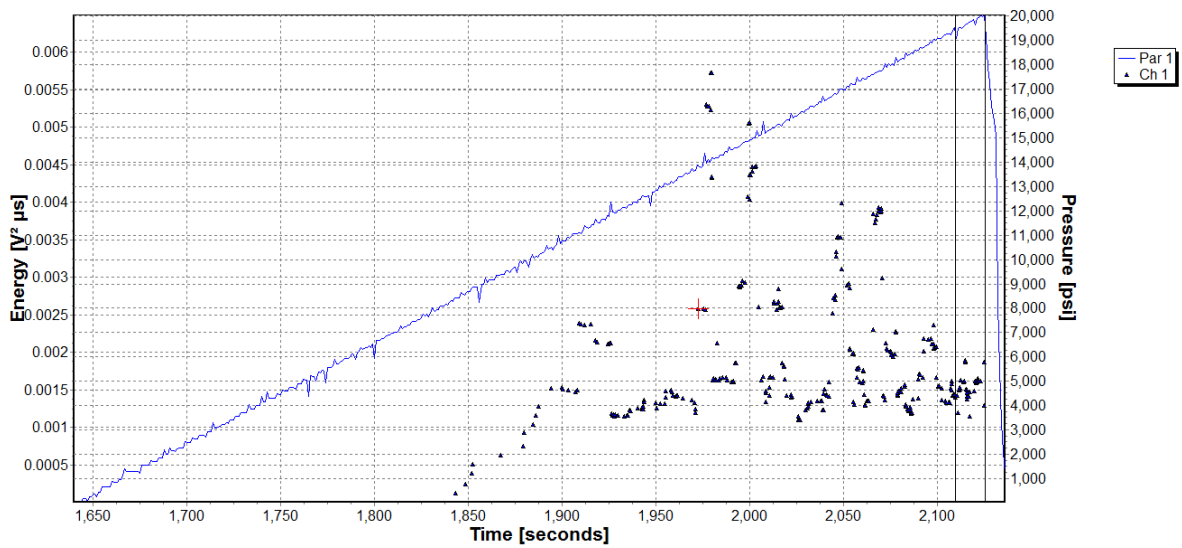


Figure C.2 – Background Energy Oscillation Pressure determination of ALT639 - 18114.

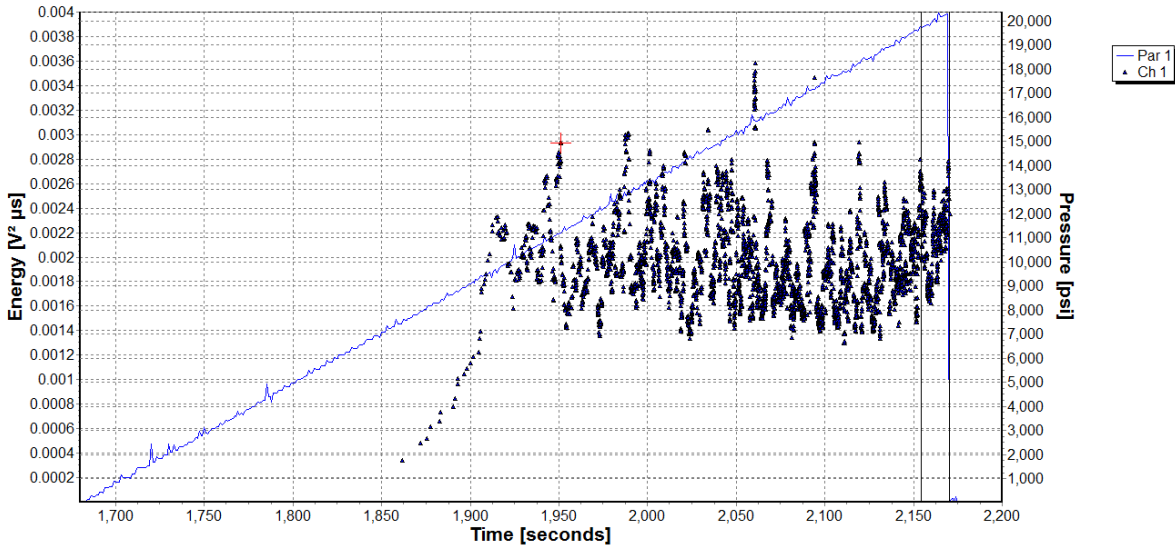


Figure C.3 – Background Energy Oscillation Pressure determination of ALT639 - 34075.

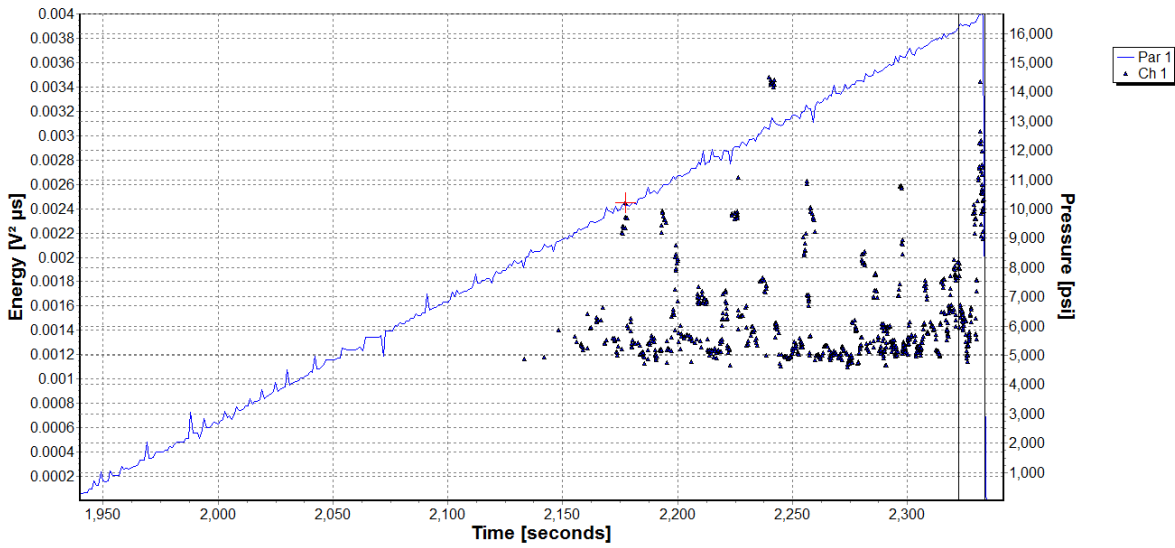


Figure C.4 – Background Energy Oscillation Pressure determination of OM3924.

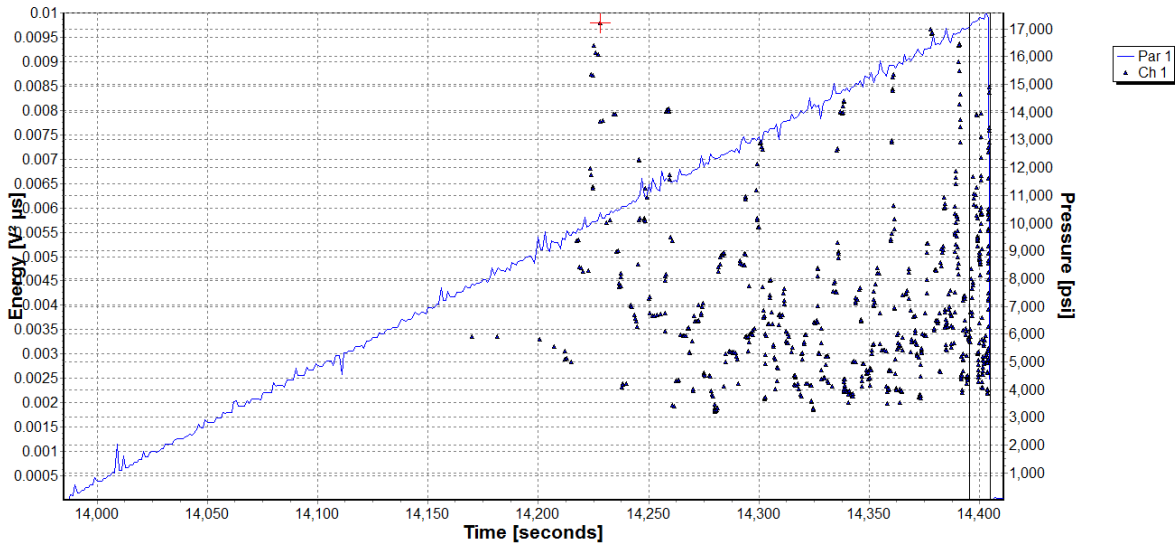


Figure C.5 – Background Energy Oscillation Pressure determination of OM3943.

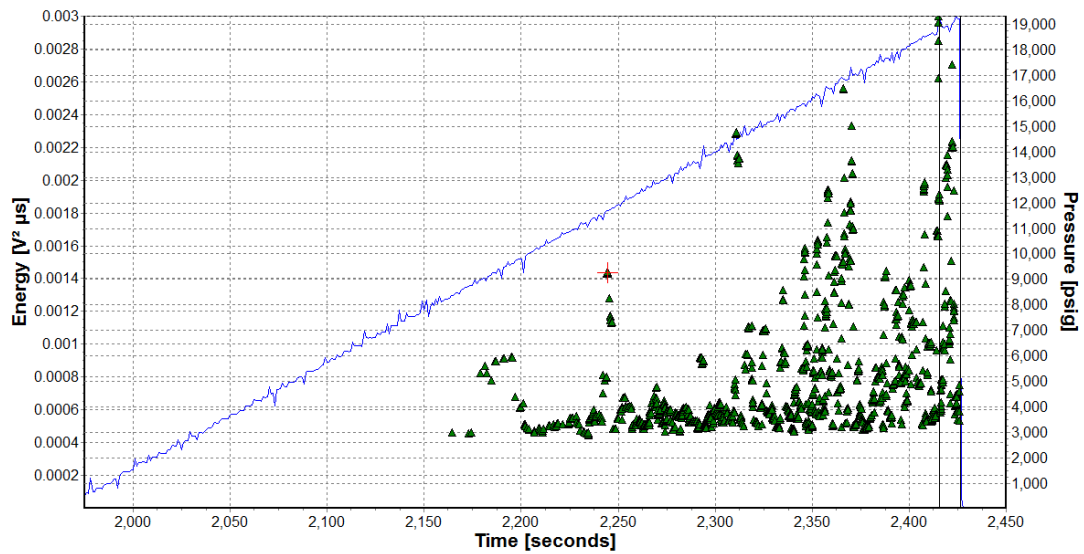


Figure C.6 – Background Energy Oscillation Pressure determination of ALT639 - 70015.

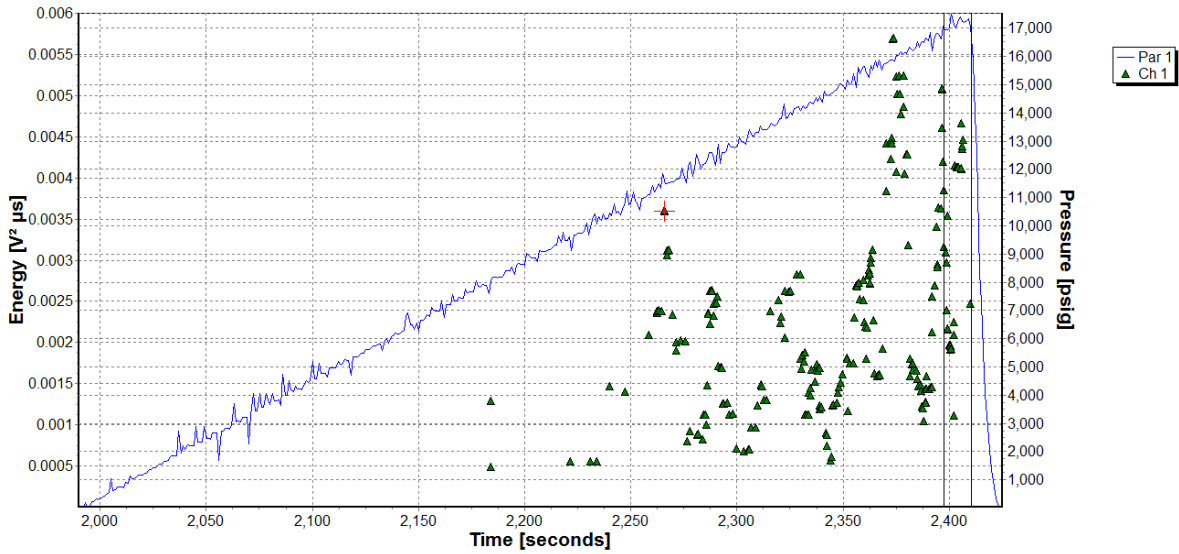


Figure C.7 – Background Energy Oscillation Pressure determination of ALT695 - 5660.

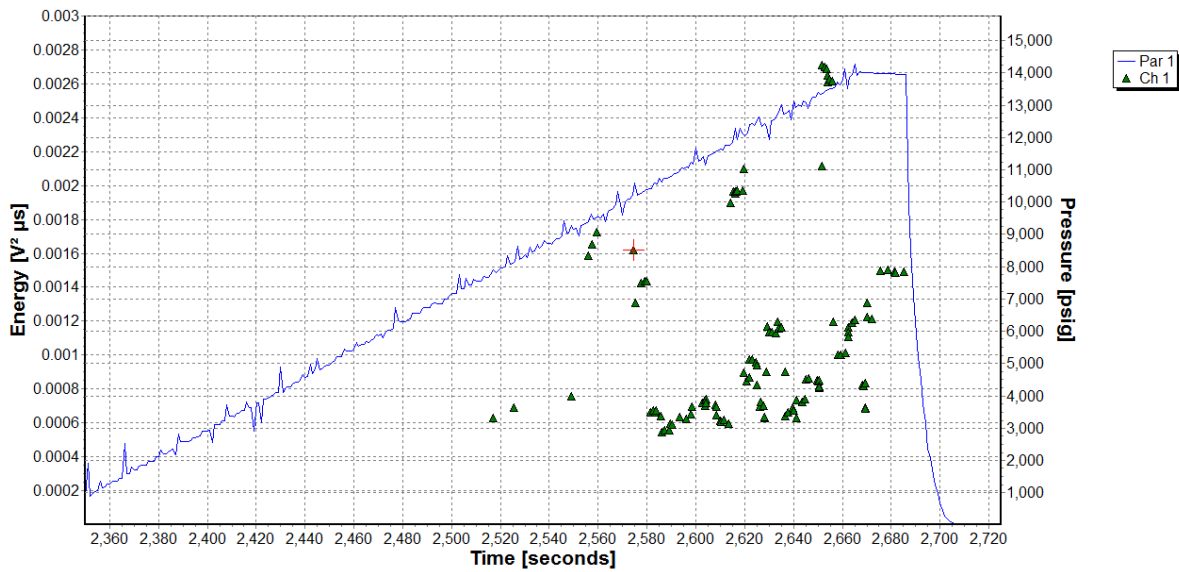


Figure C.8 – Background Energy Oscillation Pressure determination of ALT695 - 1665.

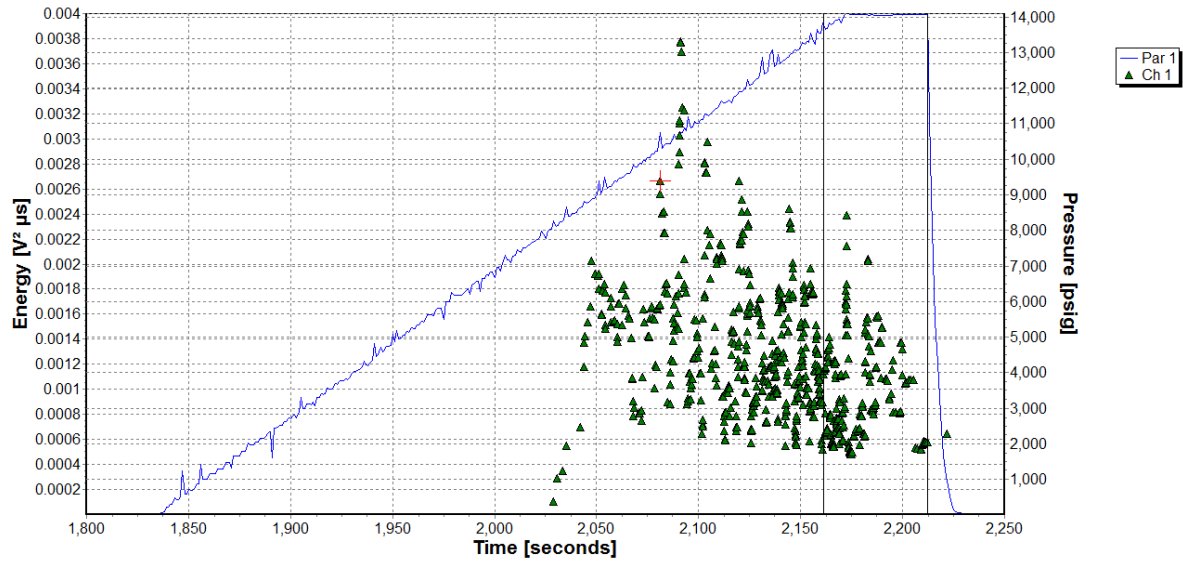


Figure C.9 – Background Energy Oscillation Pressure determination of ALT639 - 29405.

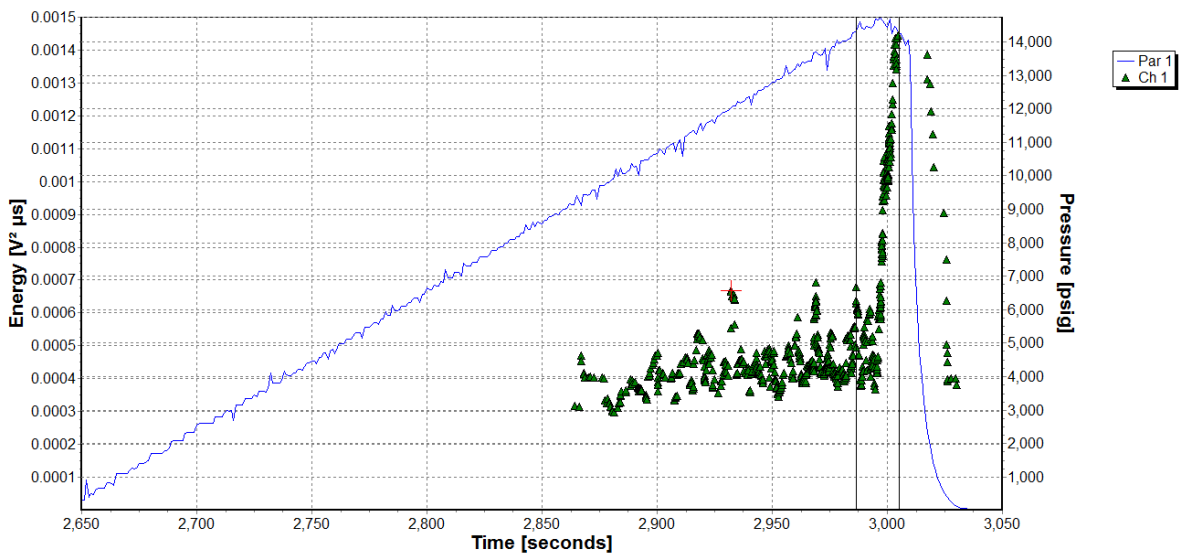


Figure C.10 – Background Energy Oscillation Pressure determination of ALT639 - 9765.

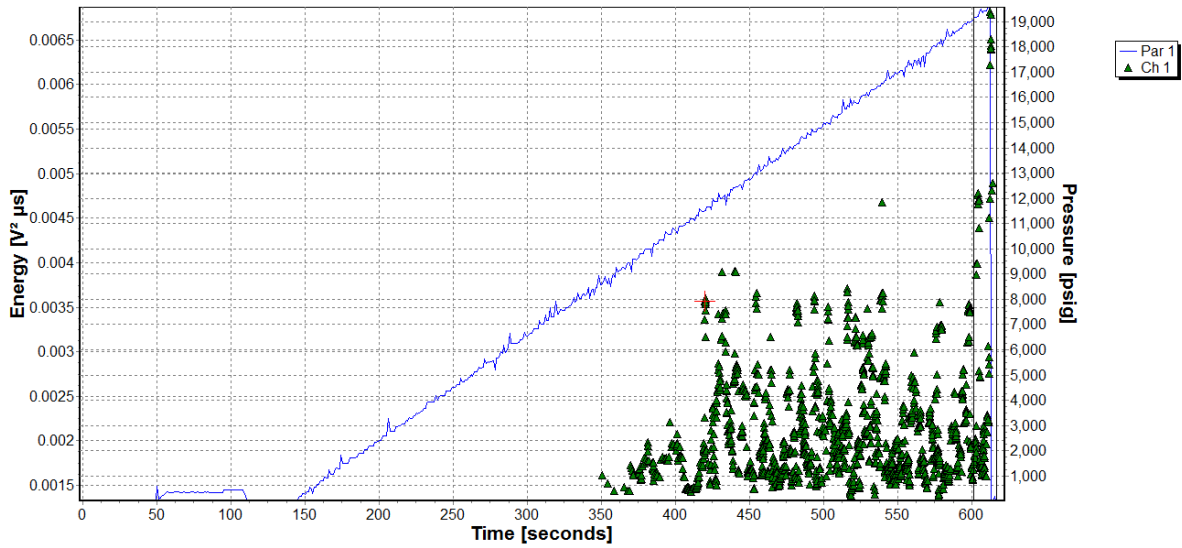


Figure C.11 – Background Energy Oscillation Pressure determination of ALT639 - 33989.

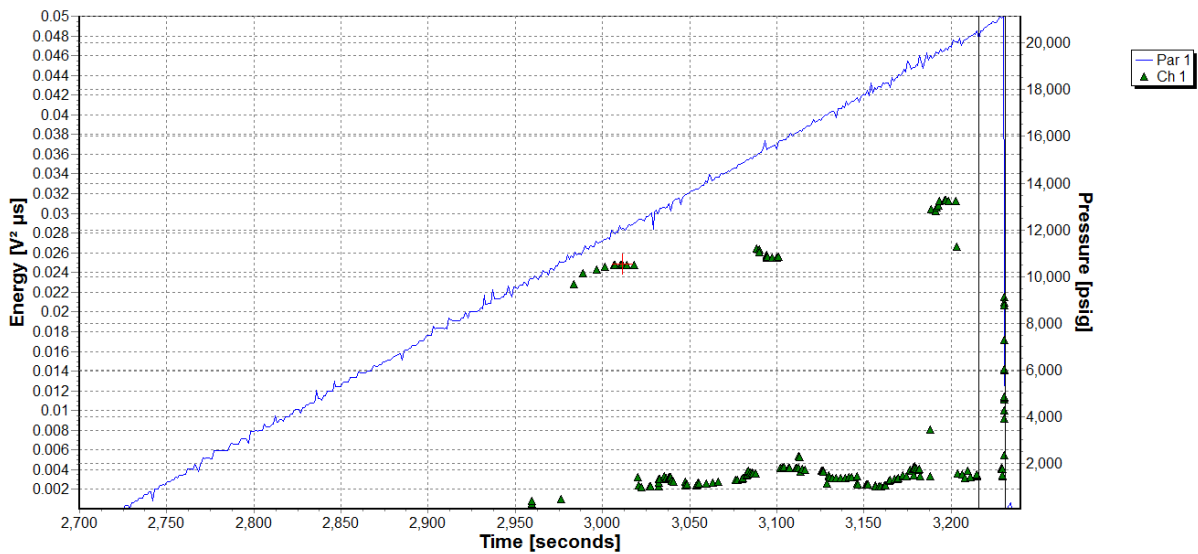


Figure C.12 – Background Energy Oscillation Pressure determination of ALT639 - 18726.

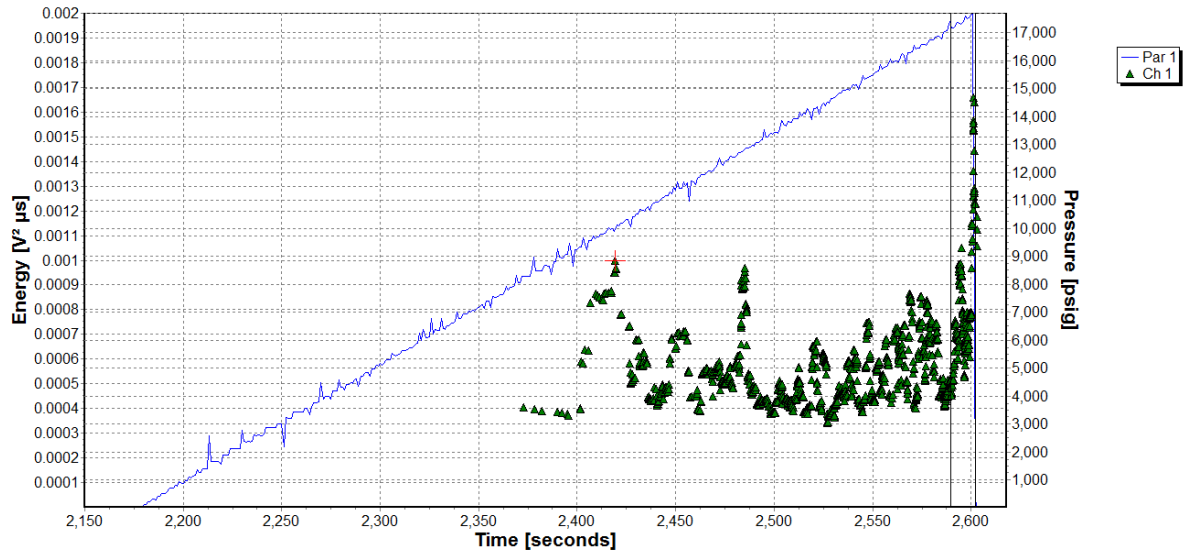


Figure C.13 – Background Energy Oscillation Pressure determination of ALT639 - 34079.

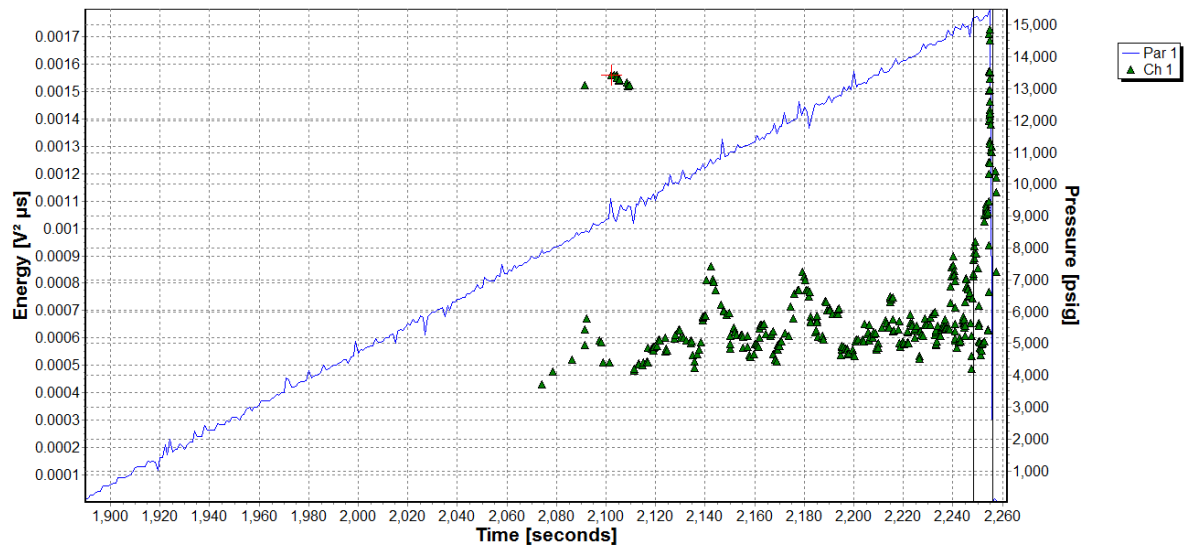


Figure C.14 – Background Energy Oscillation Pressure determination of OM3909.

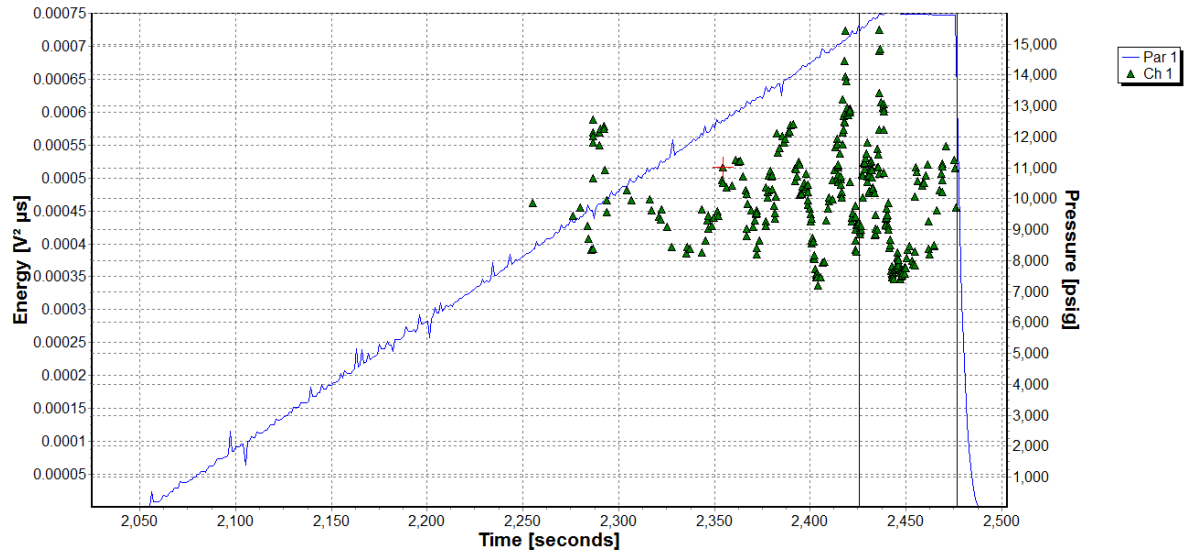


Figure C.15 – Background Energy Oscillation Pressure determination of ALT639 - 34011.

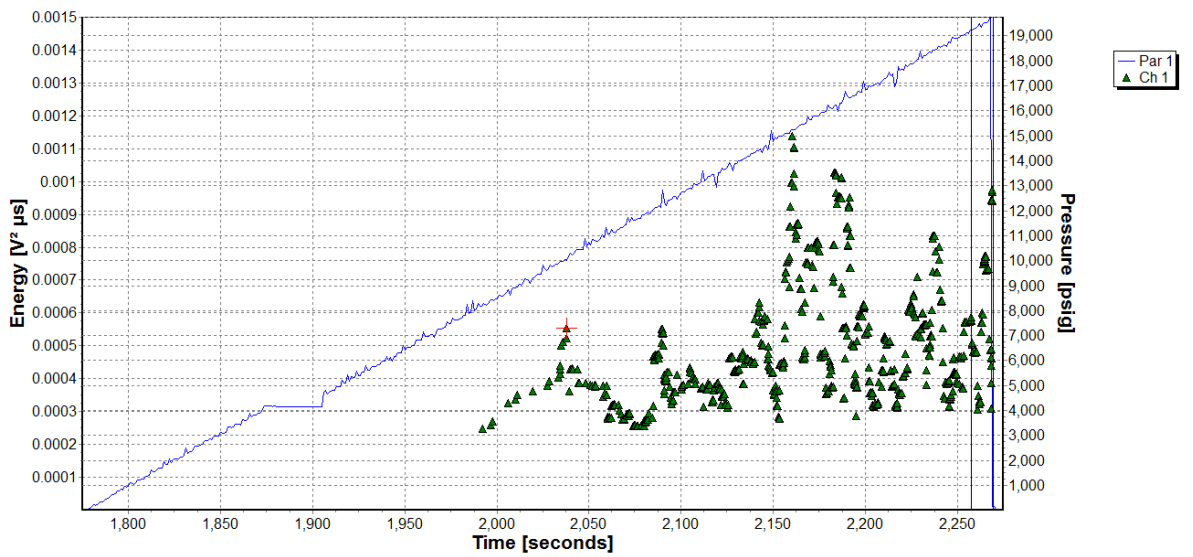


Figure C.16 – Background Energy Oscillation Pressure determination of ALT639 - 19026.

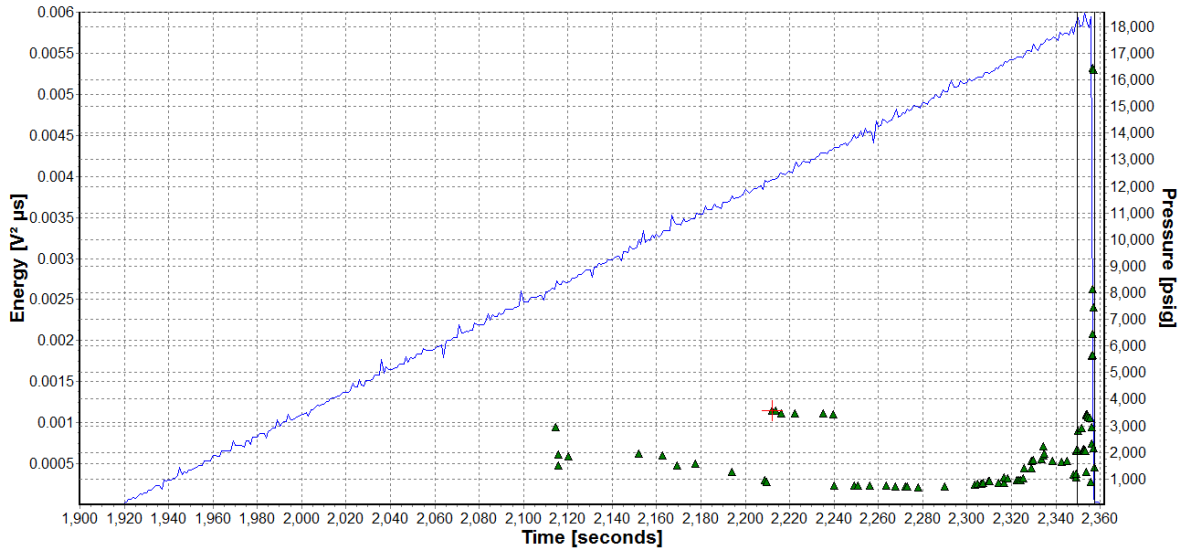


Figure C.17 – Background Energy Oscillation Pressure determination of ALT639 - 9605.

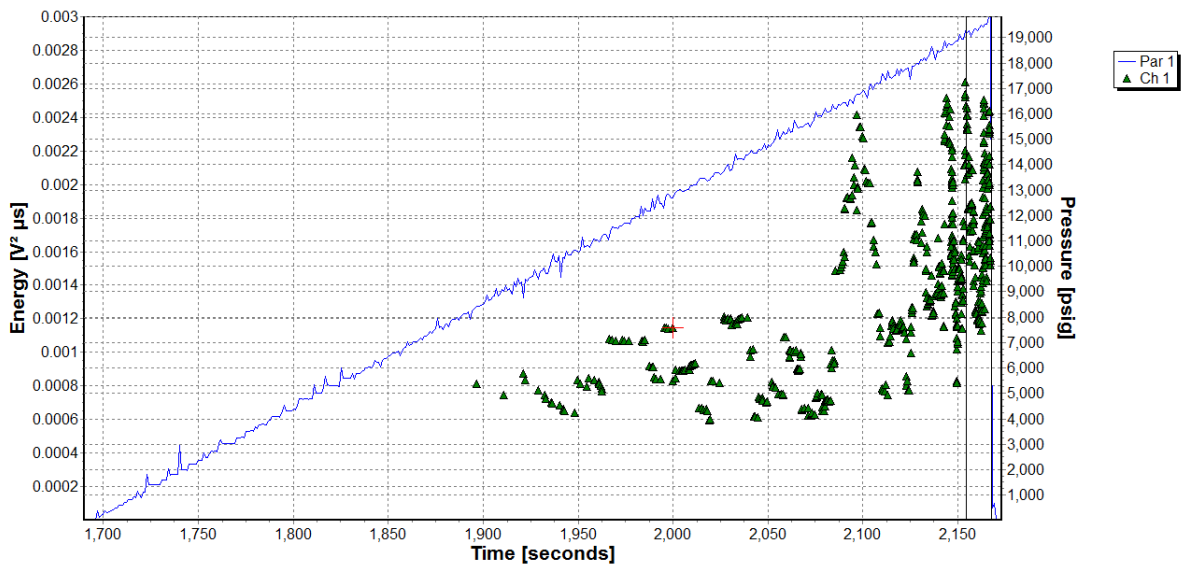


Figure C.18 – Background Energy Oscillation Pressure determination of ALT695 - 5483.

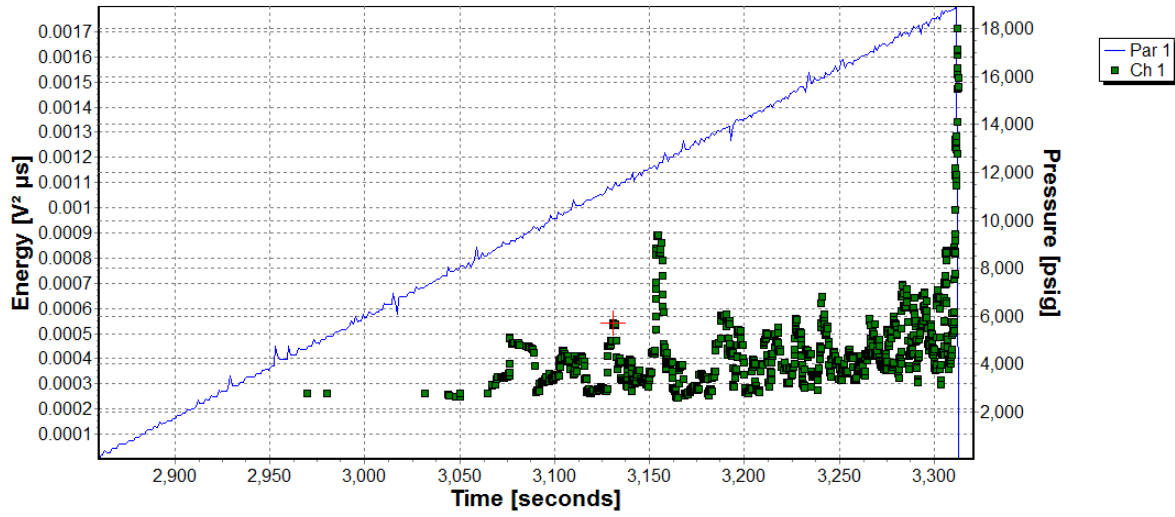


Figure C.19 – Background Energy Oscillation Pressure determination of ALT639 - 18454.

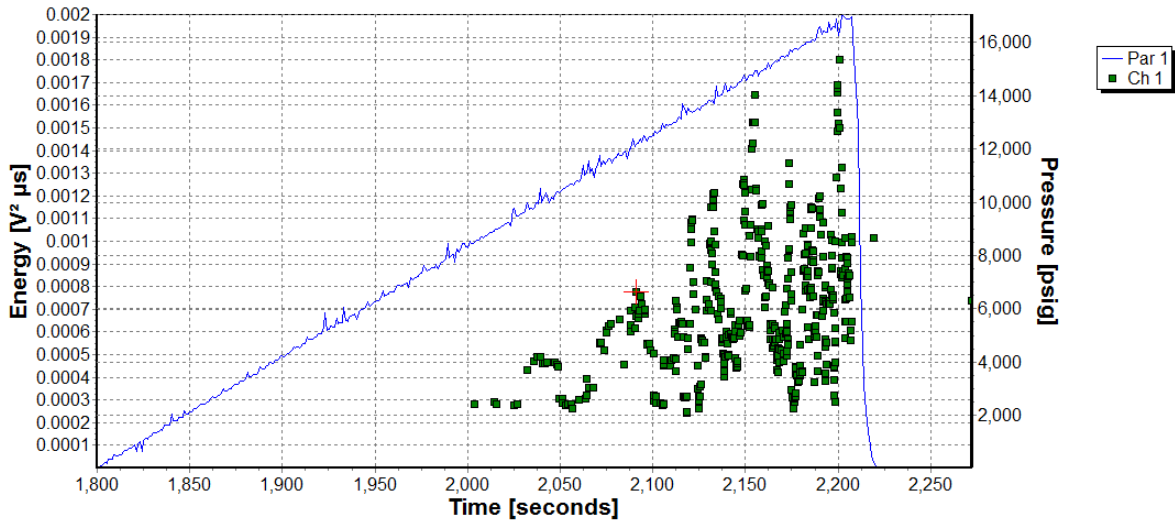


Figure C.20 – Background Energy Oscillation Pressure determination of ALT695 - 5020.

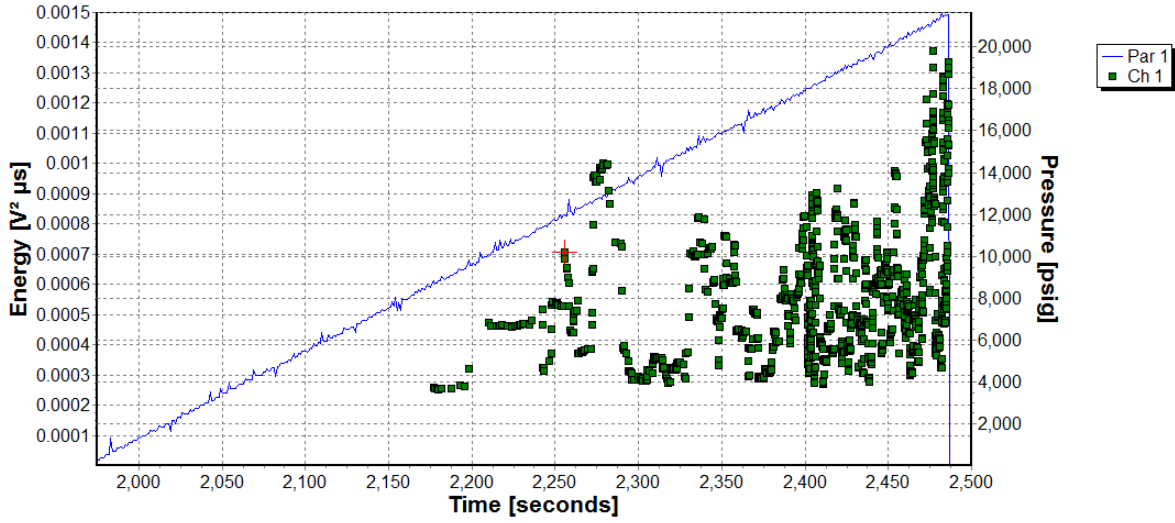


Figure C.21 – Background Energy Oscillation Pressure determination of ALT639 - 95898.

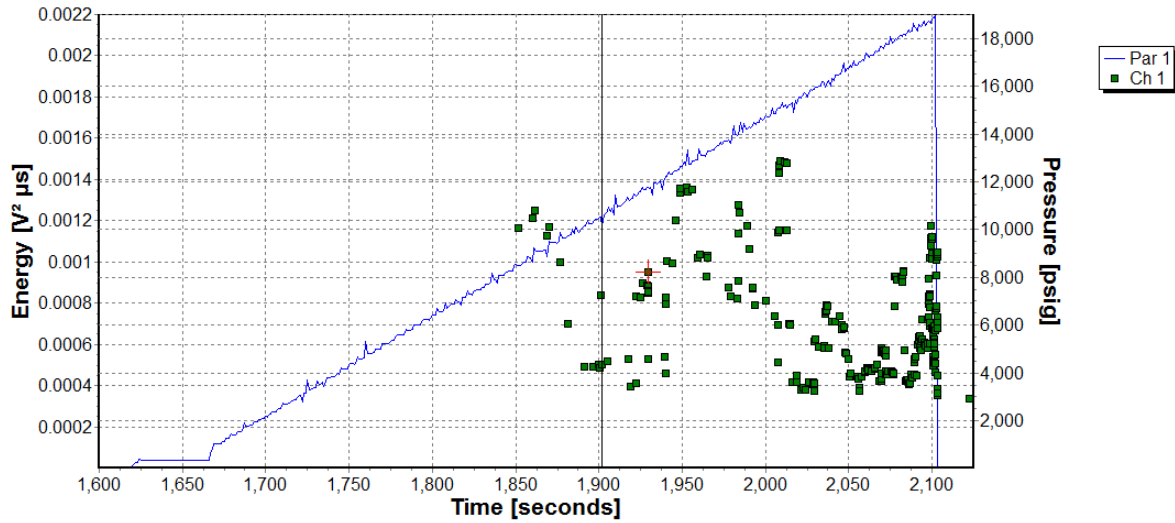


Figure C.22 – Background Energy Oscillation Pressure determination of ALT639 - 9465.

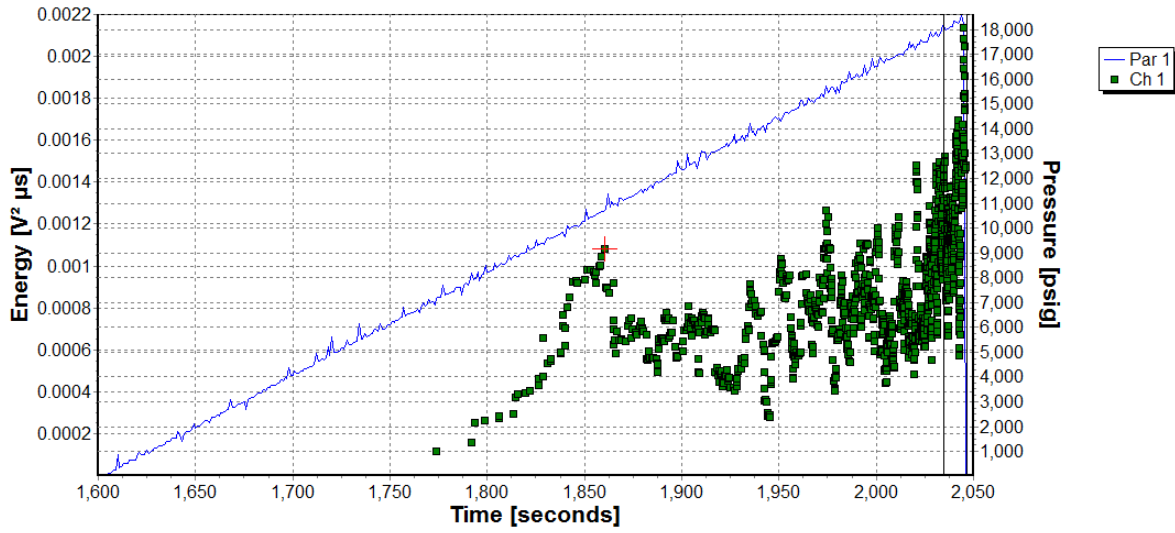


Figure C.23 – Background Energy Oscillation Pressure determination of OM3966.

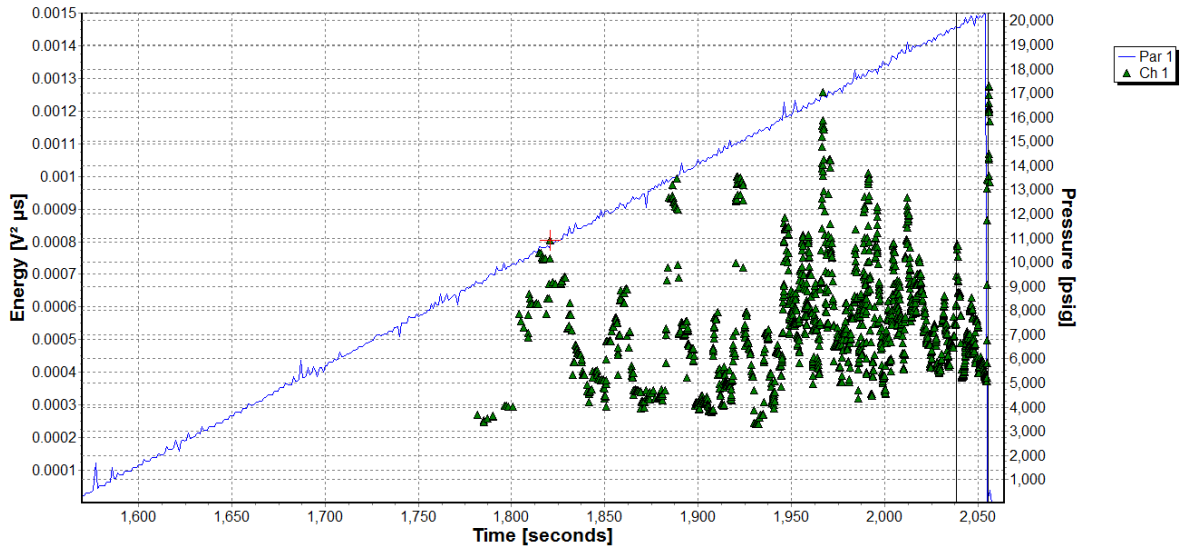


Figure C.24 – Background Energy Oscillation Pressure determination of ALT639 - 18030.

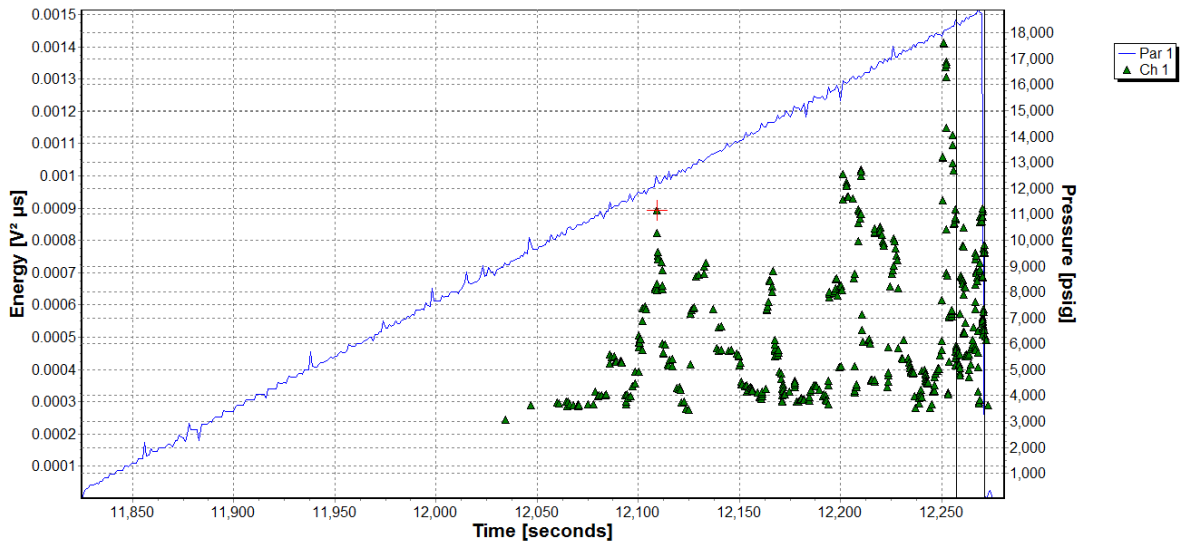


Figure C.25 – Background Energy Oscillation Pressure determination of ALT639 - 9987.

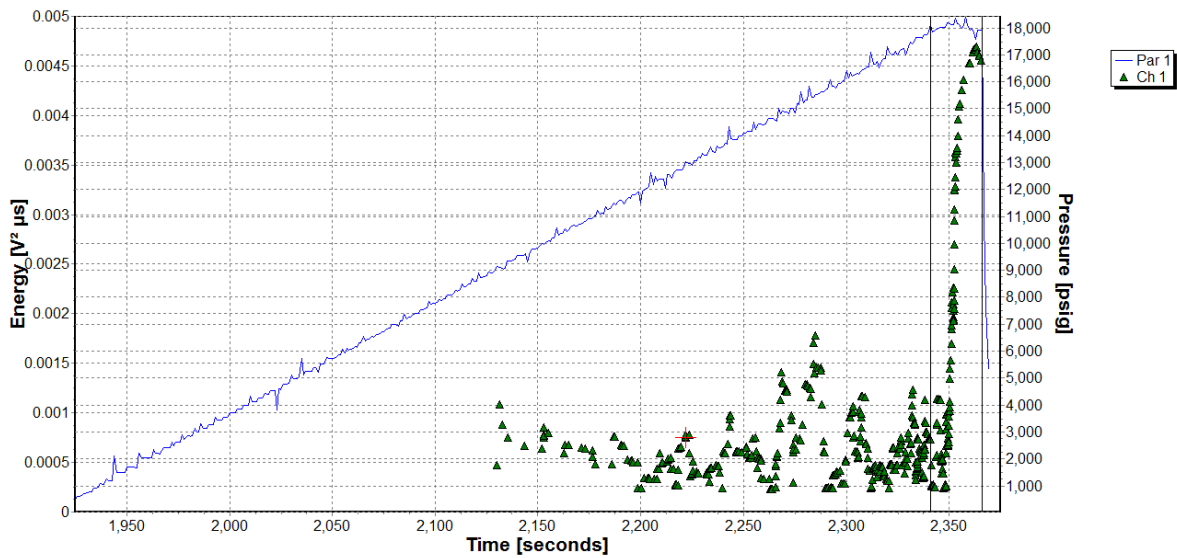


Figure C.26 – Background Energy Oscillation Pressure determination of ALT639 - 9959.

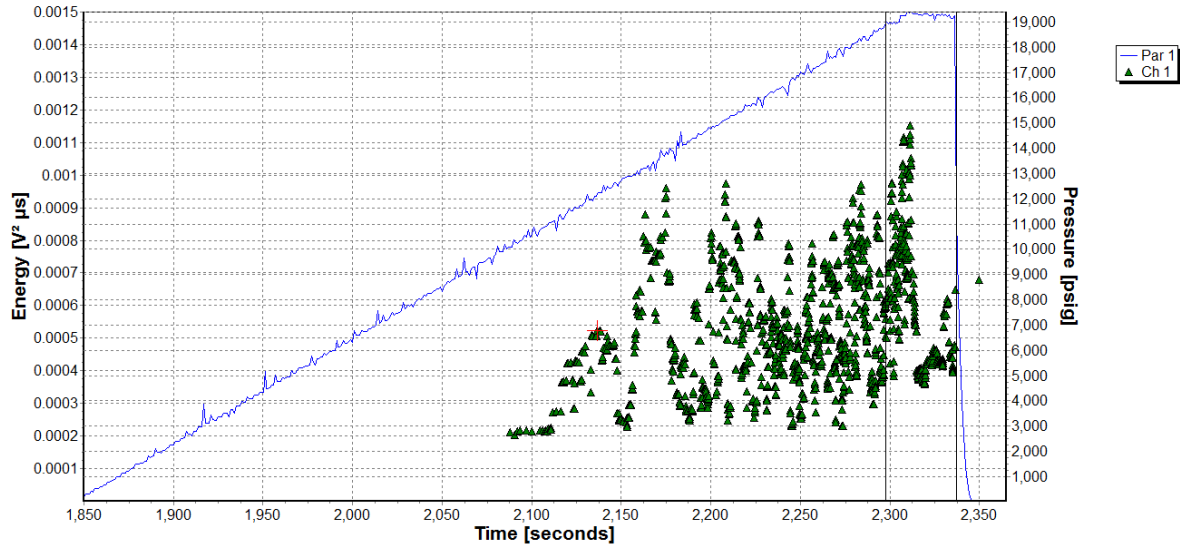


Figure C.27 – Background Energy Oscillation Pressure determination of ALT639 - 34061.

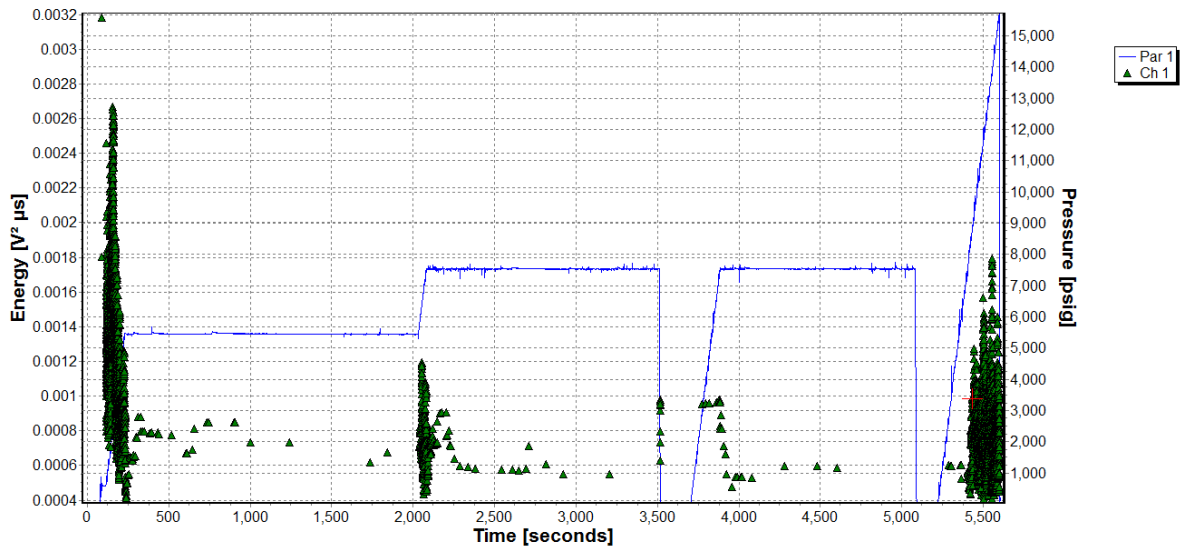


Figure C.28 – Background Energy Oscillation Pressure plot of ALT639-17716.

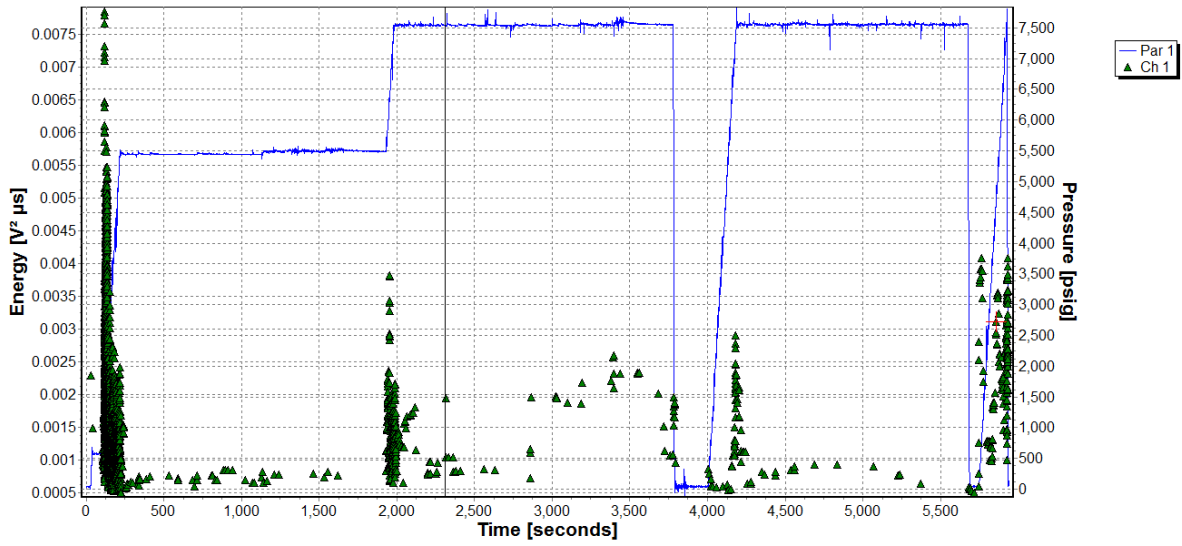


Figure C.29 – Background Energy Oscillation Pressure plot of ALT639-17831.

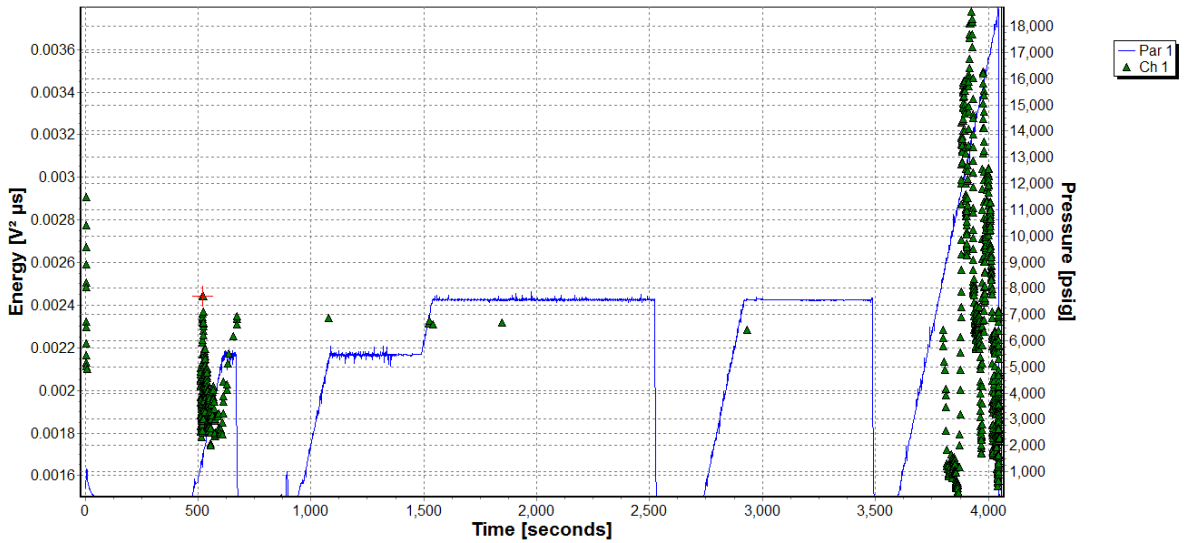


Figure C.30 – Background Energy Oscillation Pressure plot of ALT639-18768.

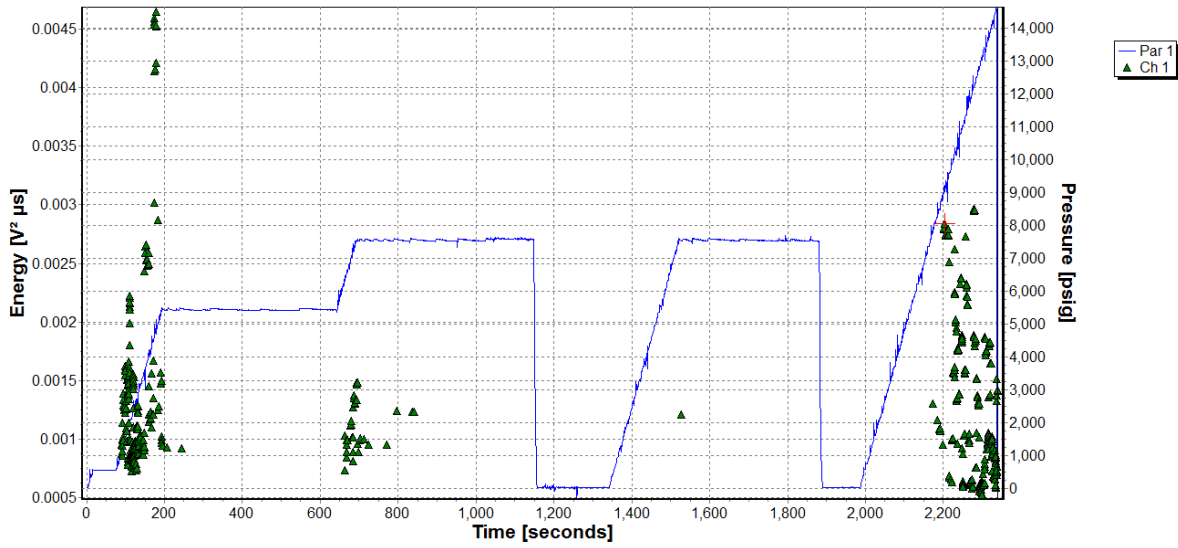


Figure C.31 – Background Energy Oscillation Pressure plot of ALT639-9747.

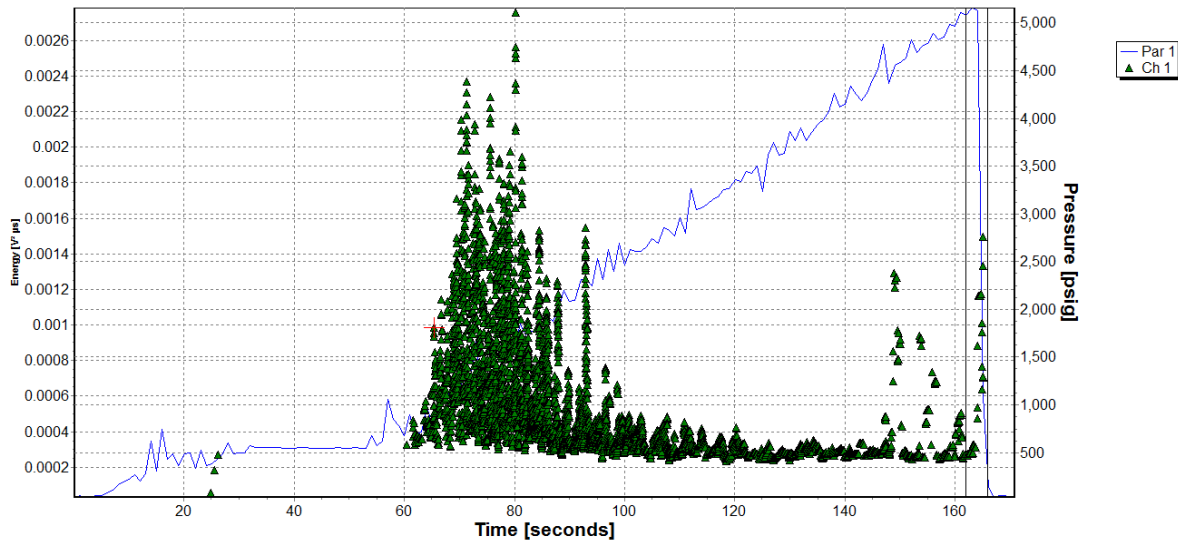


Figure C.32 – Background Energy Oscillation Pressure plot of ALT639-9769.

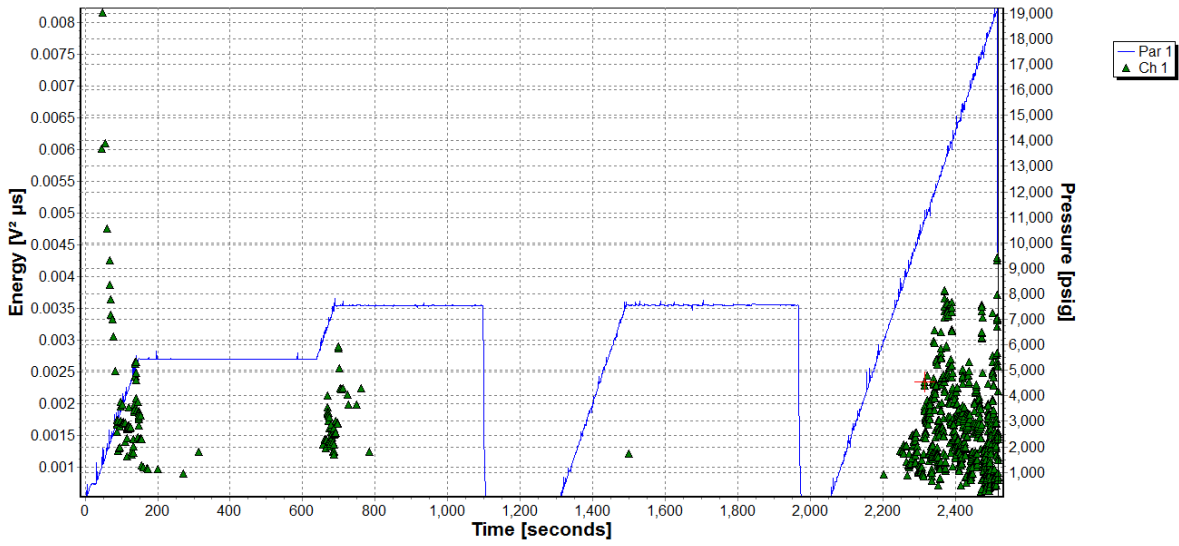


Figure C.33 – Background Energy Oscillation Pressure plot of ALT639-31064.

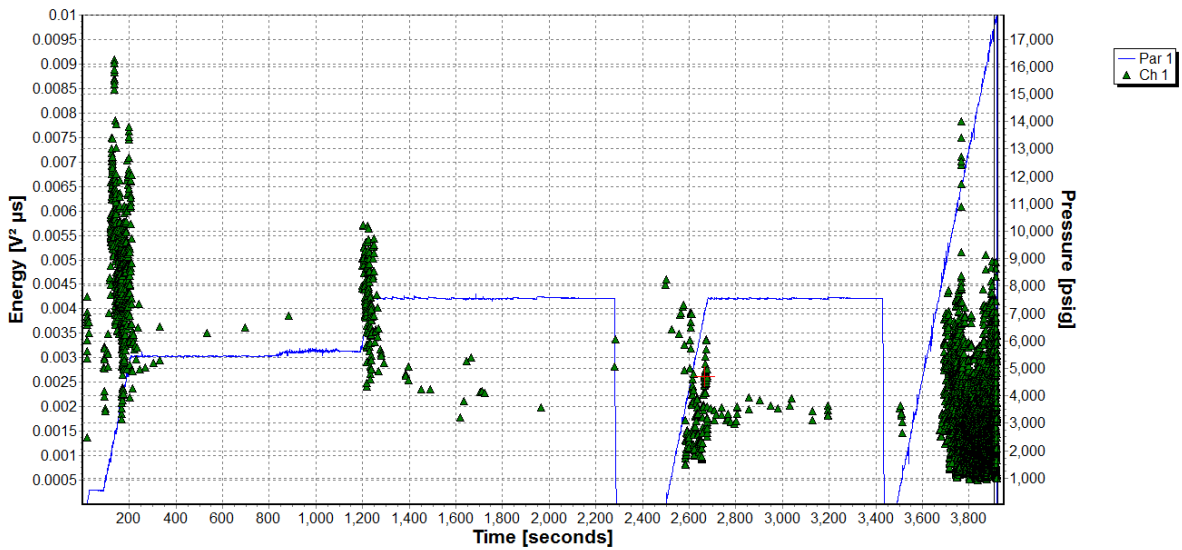


Figure C.34 – Background Energy Oscillation Pressure plot of ALT639-23371.

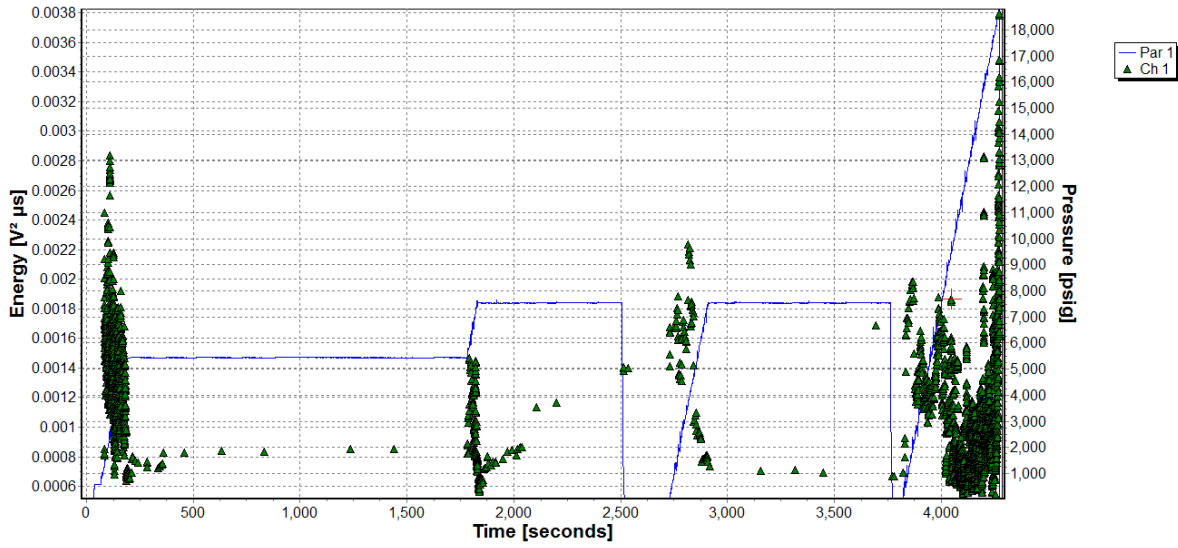


Figure C.35 – Background Energy Oscillation Pressure plot of ALT695-3669.

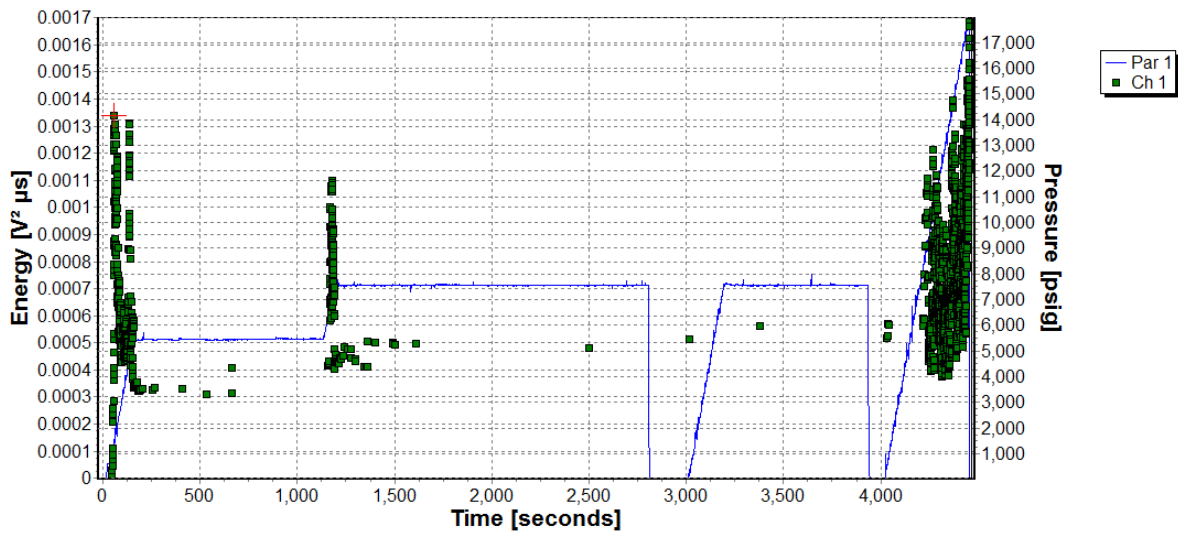


Figure C.36 – Background Energy Oscillation Pressure plot of ALT695-1781.

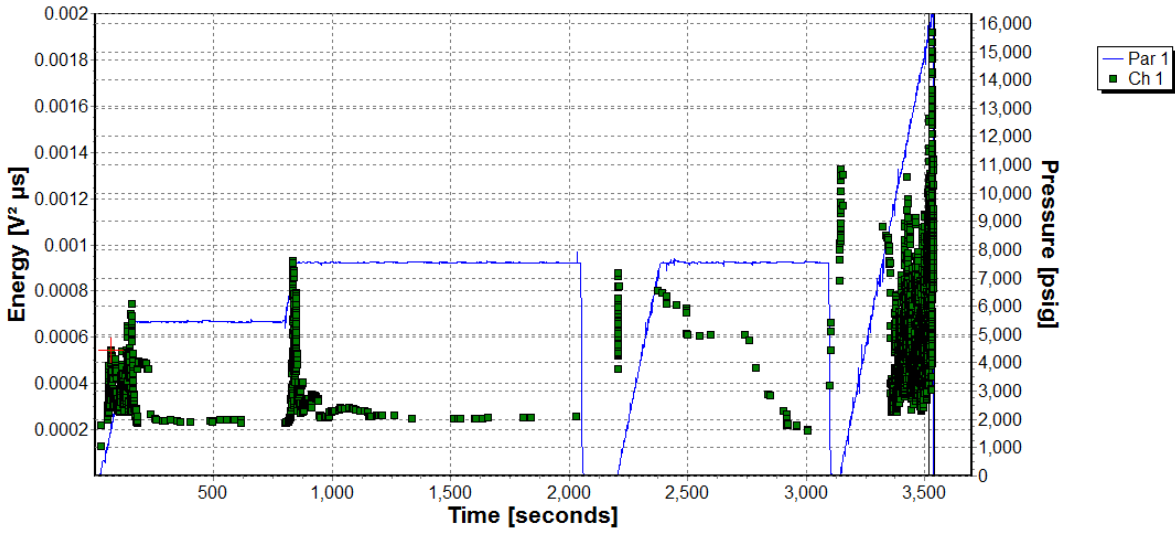


Figure C.37 – Background Energy Oscillation Pressure plot of OM3930.

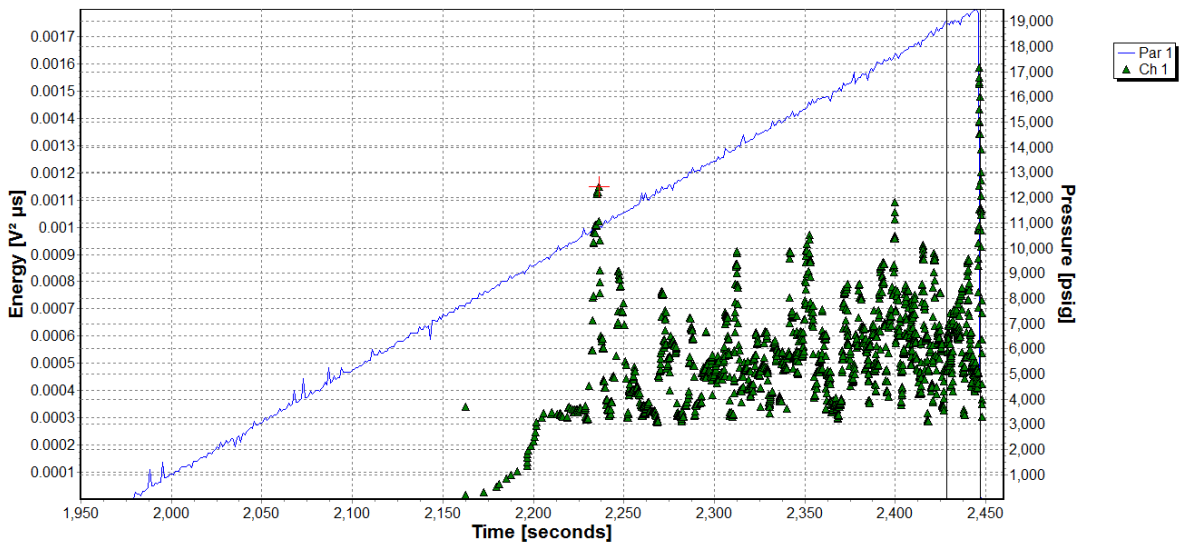


Figure C.38 – Background Energy Oscillation Pressure plot of ALT639-9753.

## APPENDIX D

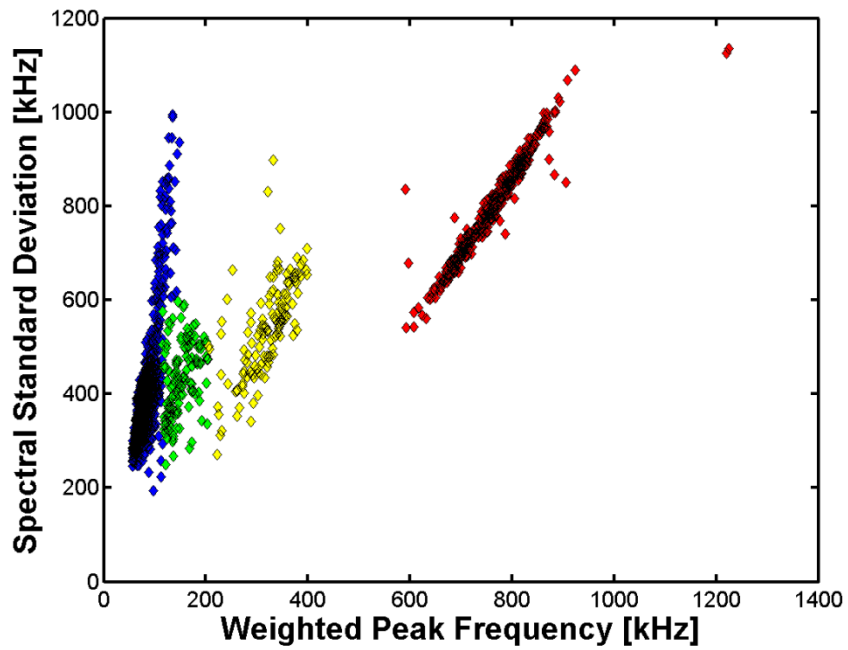


Figure D.1 – Spectral standard deviation versus weighted peak frequency for ALT639 - 9573.

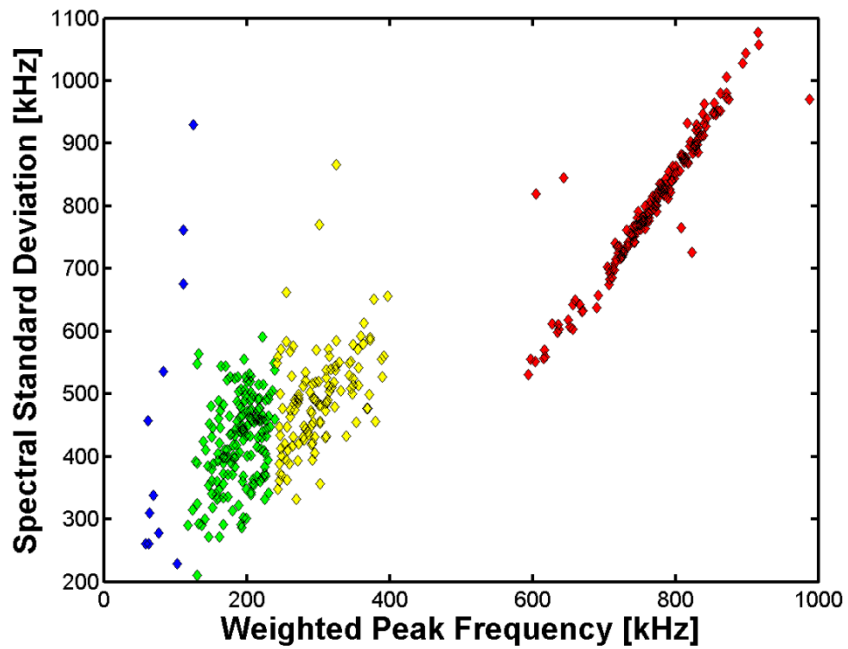


Figure D.2 – Spectral standard deviation versus weighted peak frequency for ALT639 - 18114.

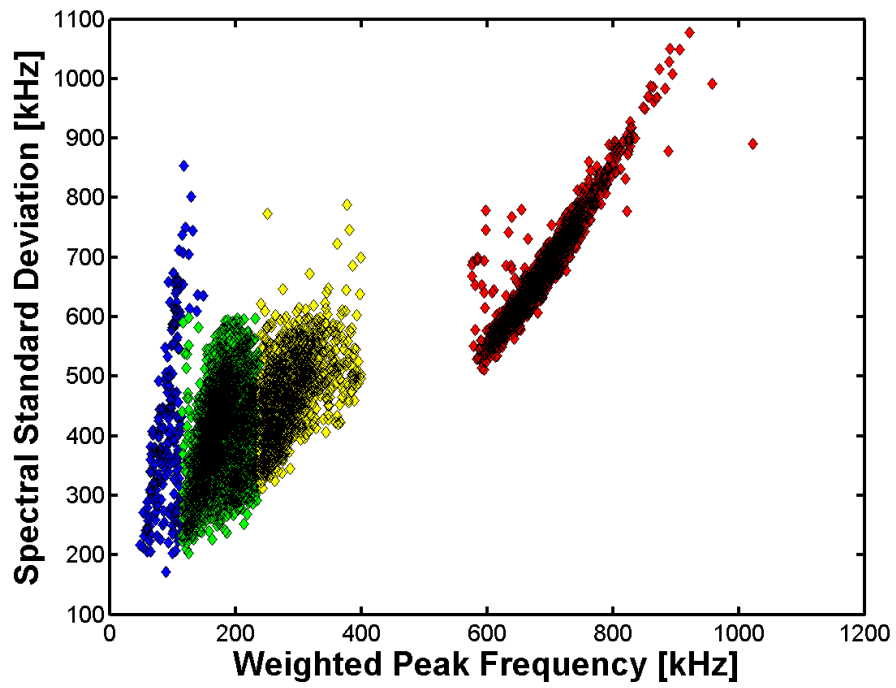


Figure D.3 – Spectral standard deviation versus weighted peak frequency for ALT639 - 34075.

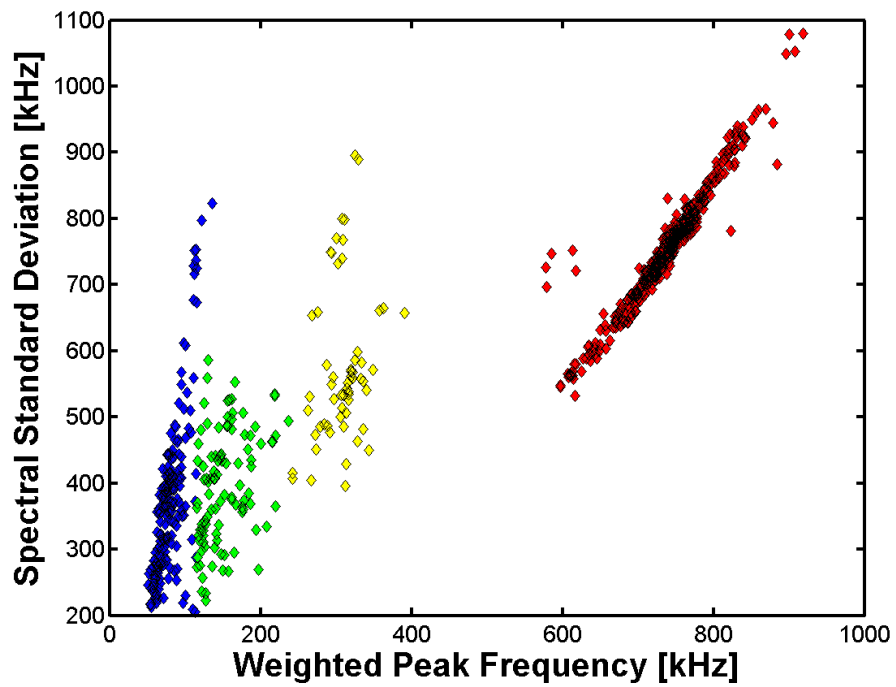


Figure D.4 – Spectral standard deviation versus weighted peak frequency for OM3924.

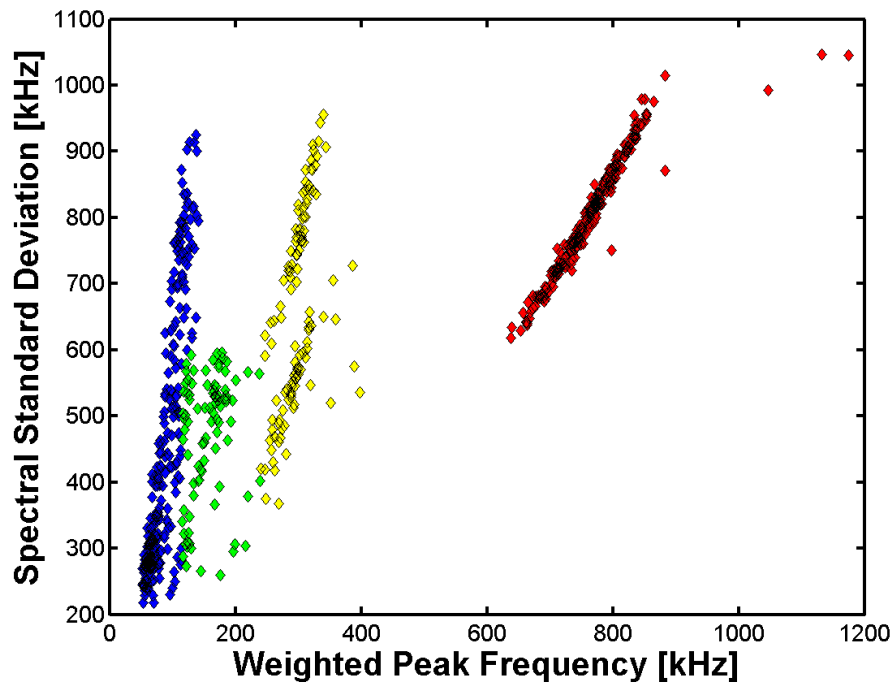


Figure D.5 – Spectral standard deviation versus weighted peak frequency for OM3943.

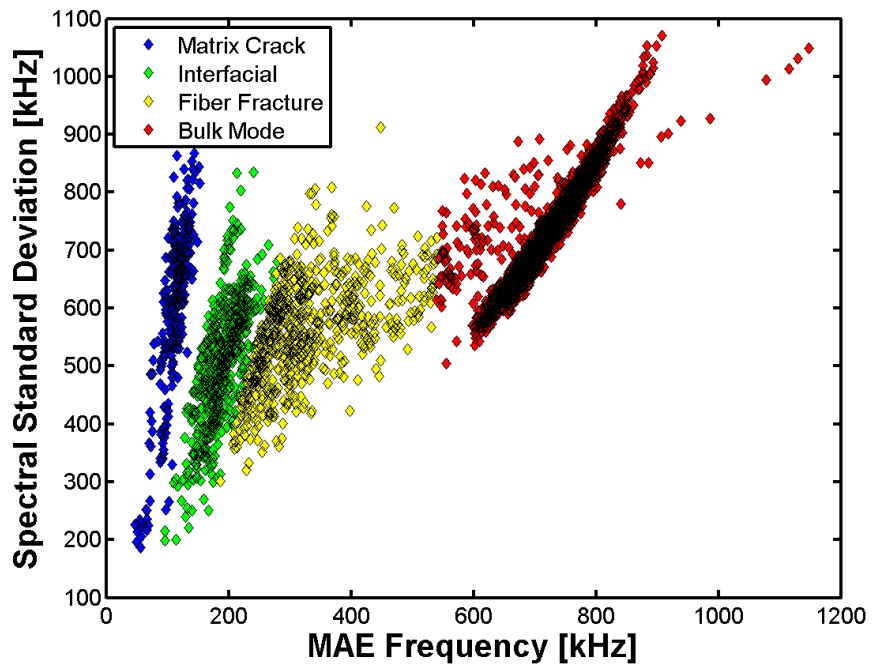


Figure D.6 – Spectral standard deviation versus Modal Acoustic Emission Frequency for ALT639 - 70015.

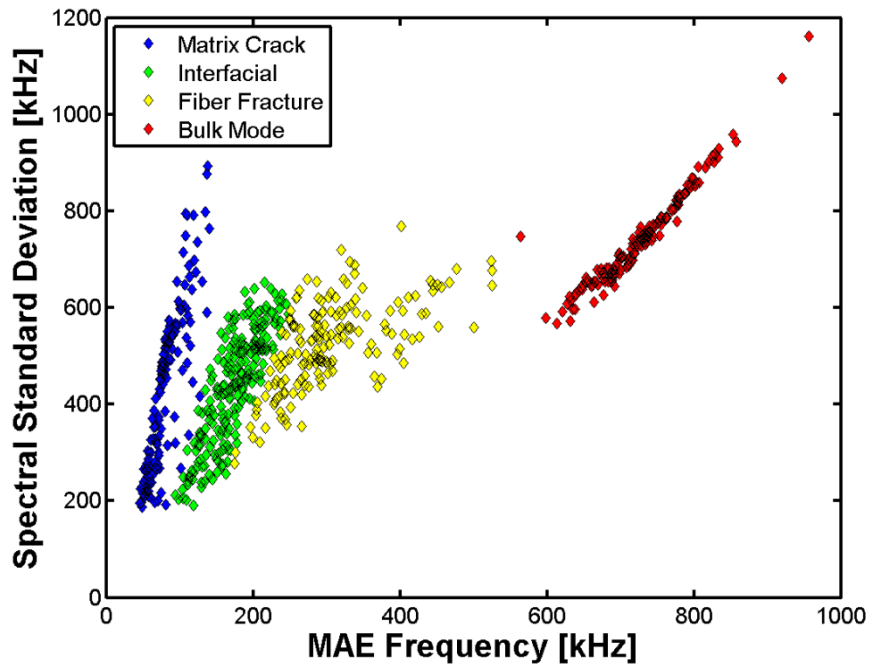


Figure D.7 – Spectral standard deviation versus Modal Acoustic Emission Frequency for ALT695 - 5660.

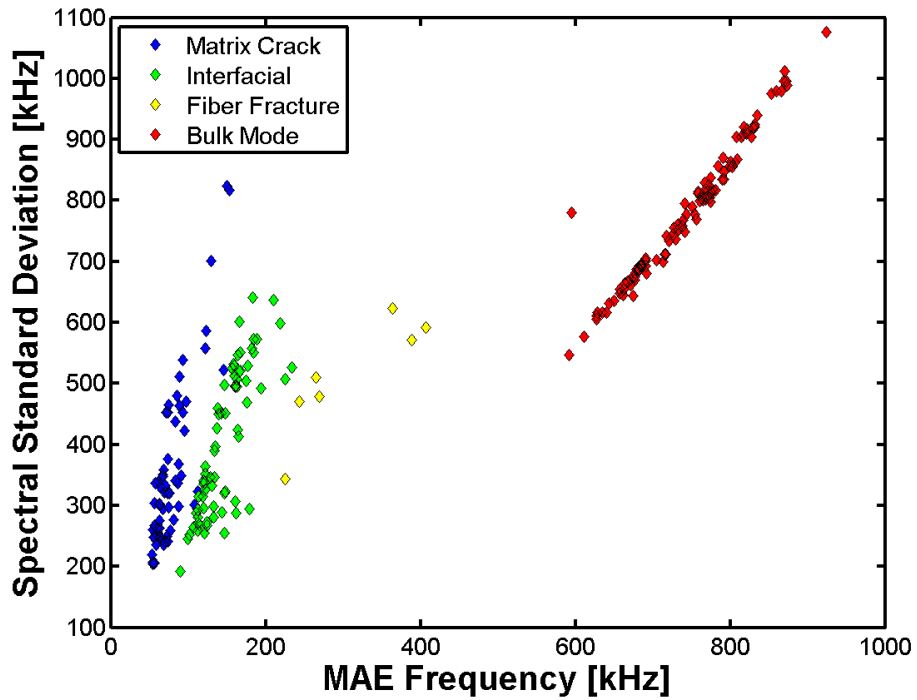


Figure D.8 – Spectral standard deviation versus Modal Acoustic Emission Frequency for ALT695 - 1665.

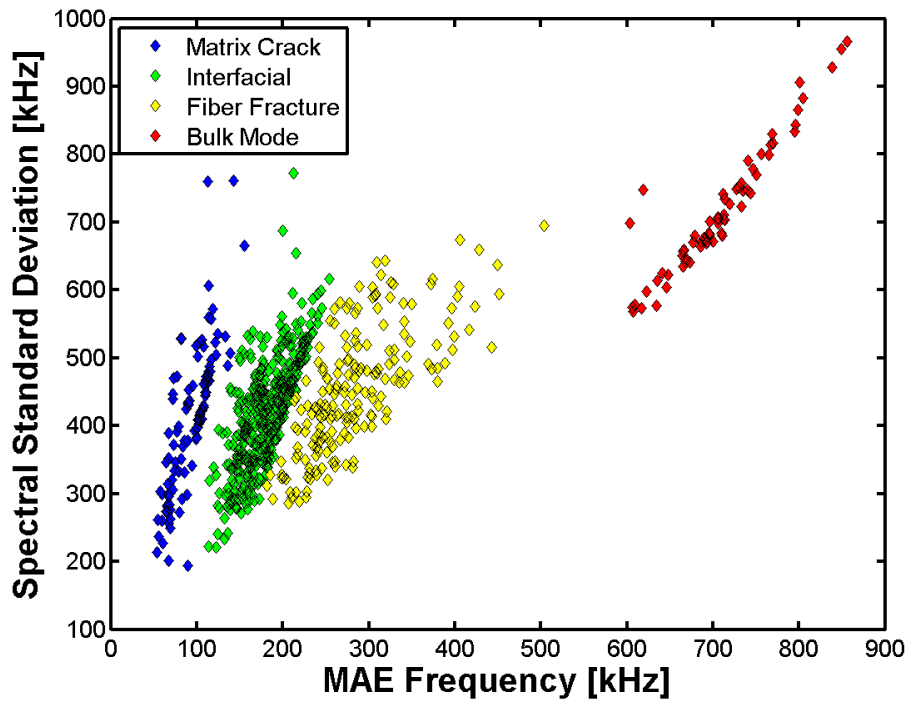


Figure D.9 – Spectral standard deviation versus Modal Acoustic Emission Frequency for ALT639 - 29405.

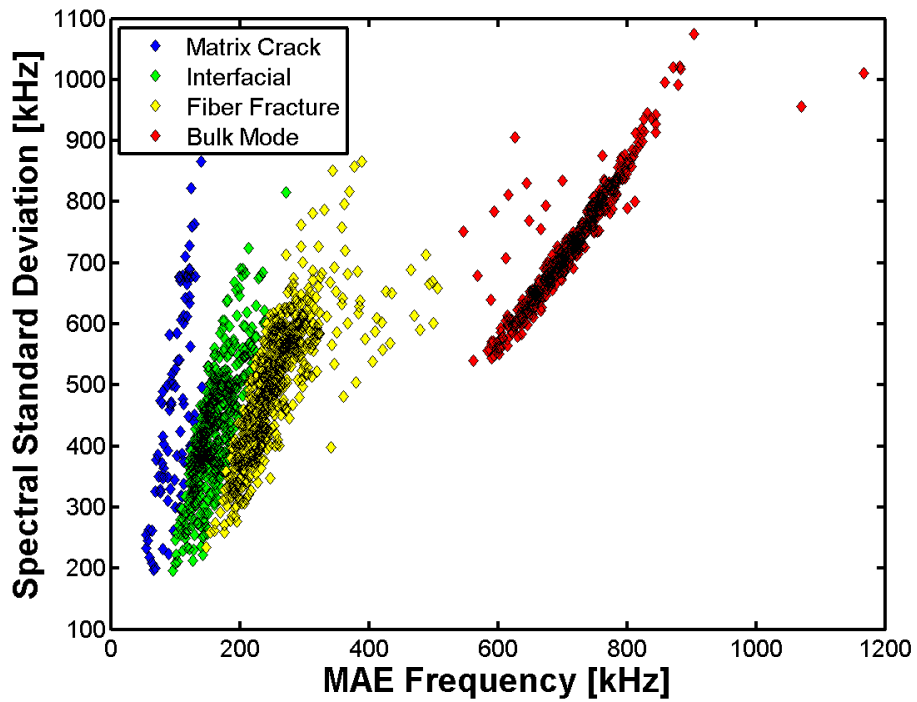


Figure D.10 – Spectral standard deviation versus Modal Acoustic Emission Frequency for ALT639 - 9765.

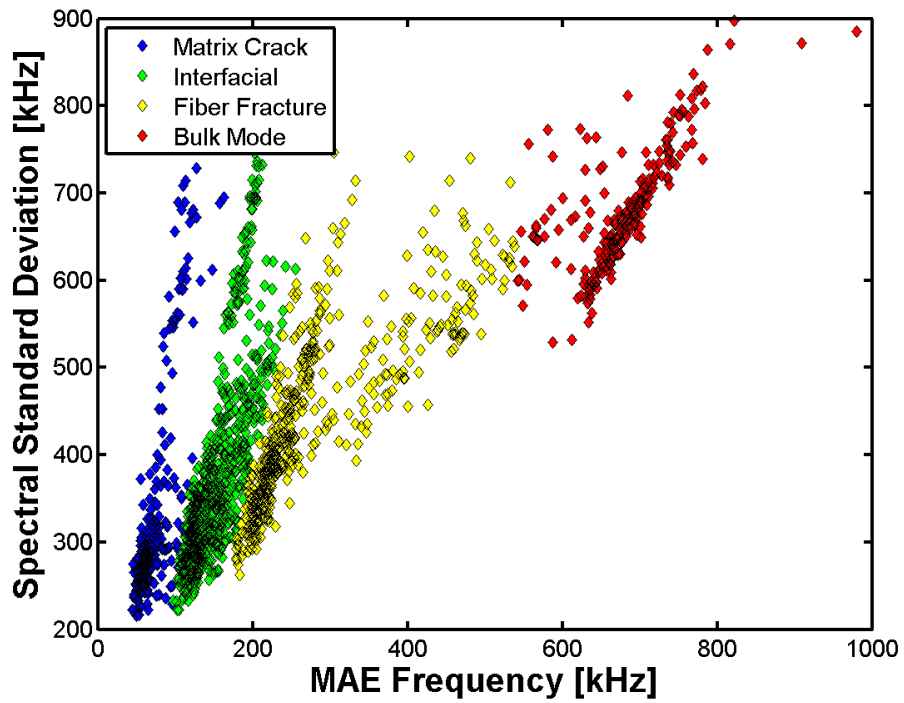


Figure D.11 – Spectral standard deviation versus Modal Acoustic Emission Frequency for ALT639 - 33989.

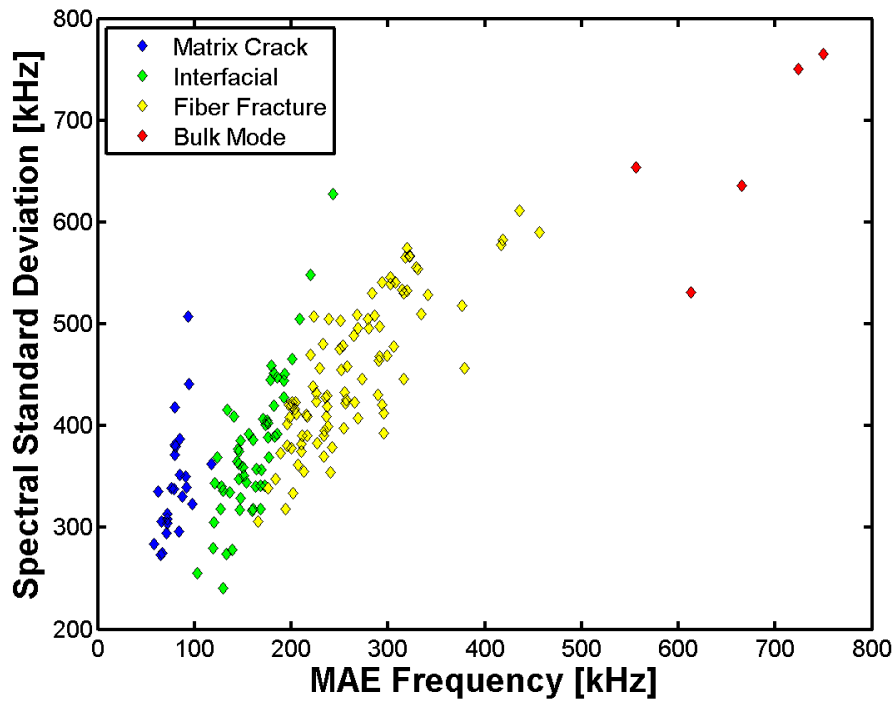


Figure D.12 – Spectral standard deviation versus Modal Acoustic Emission Frequency for ALT639 - 18726.

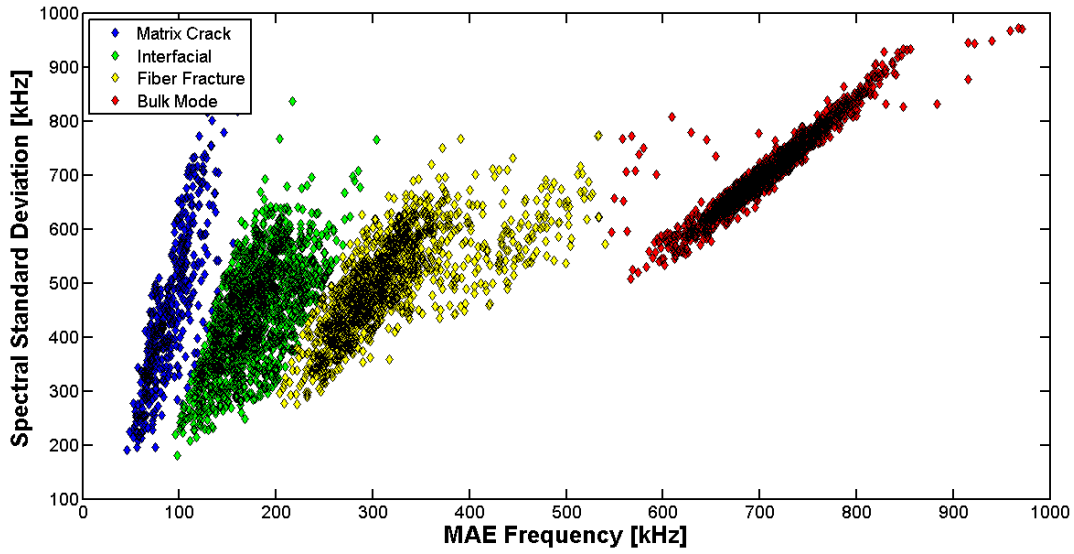


Figure D.13 – Spectral standard deviation versus Modal Acoustic Emission Frequency for ALT639 - 34079.

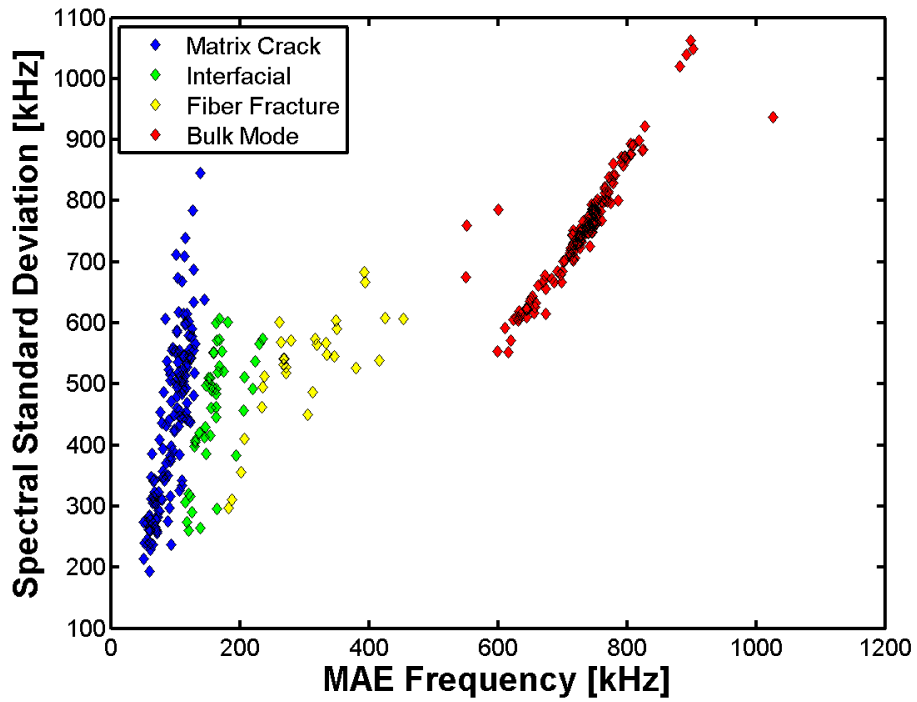


Figure D.14 – Spectral standard deviation versus Modal Acoustic Emission Frequency for OM3909.

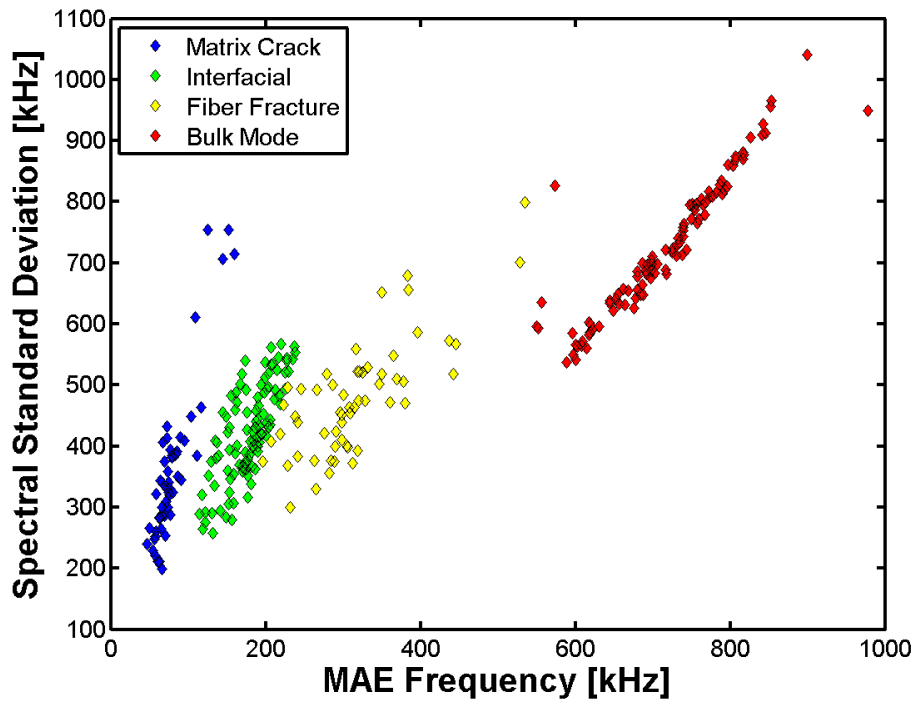


Figure D.15 – Spectral standard deviation versus Modal Acoustic Emission Frequency for ALT639 - 34011.

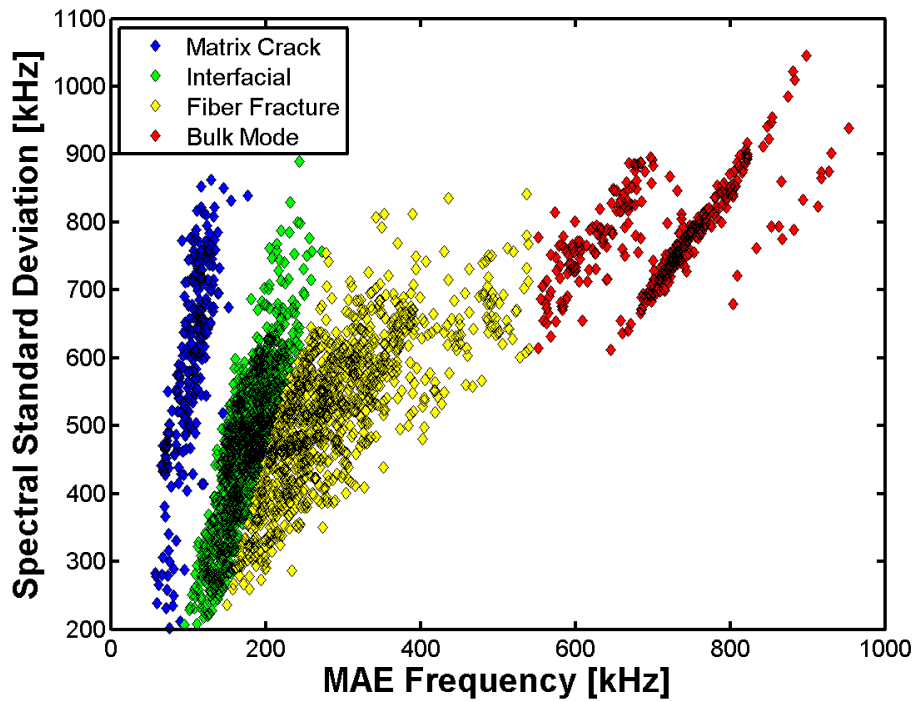


Figure D.16 – Spectral standard deviation versus Modal Acoustic Emission Frequency for ALT639 - 19026.

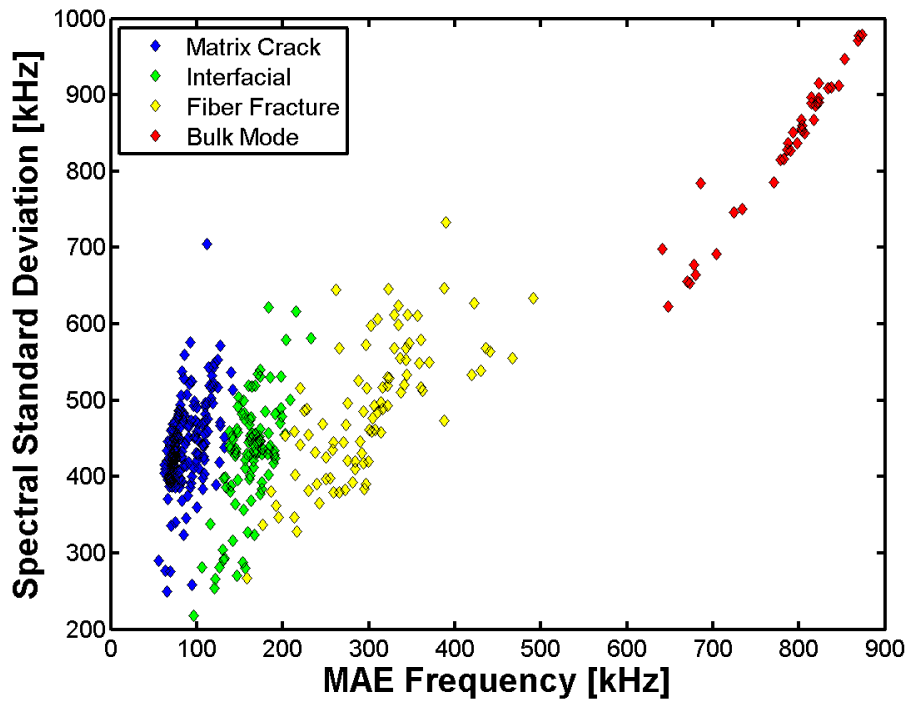


Figure D.17 – Spectral standard deviation versus Modal Acoustic Emission Frequency for ALT639 - 9605.

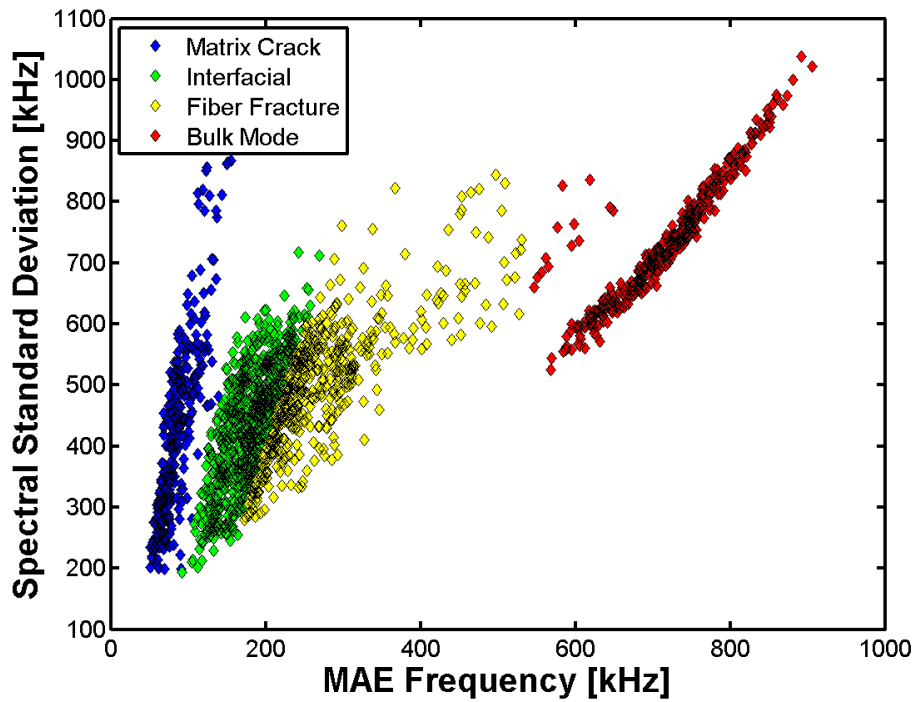


Figure D.18 – Spectral standard deviation versus Modal Acoustic Emission Frequency for ALT695 - 5483.

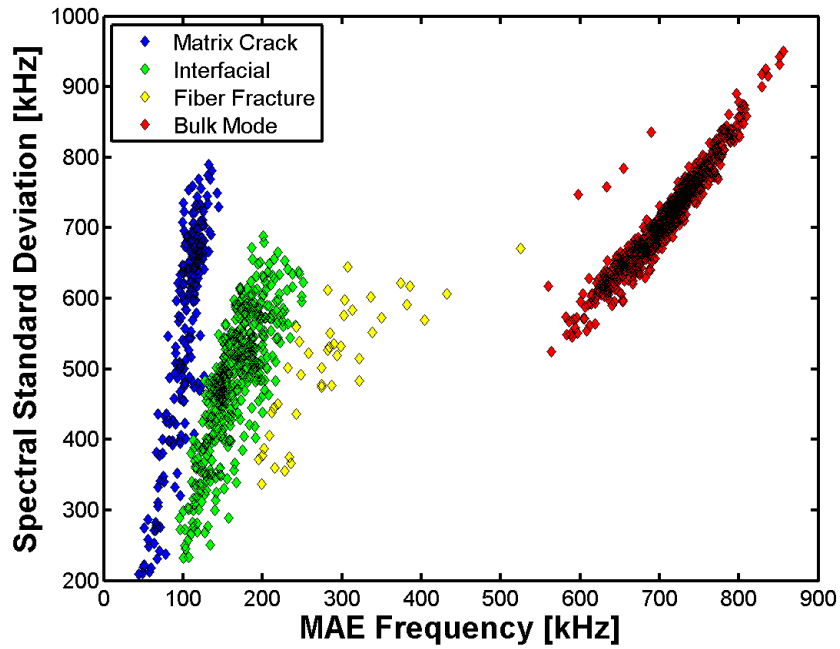


Figure D.19 – Spectral standard deviation versus Modal Acoustic Emission Frequency for ALT639 - 18454.

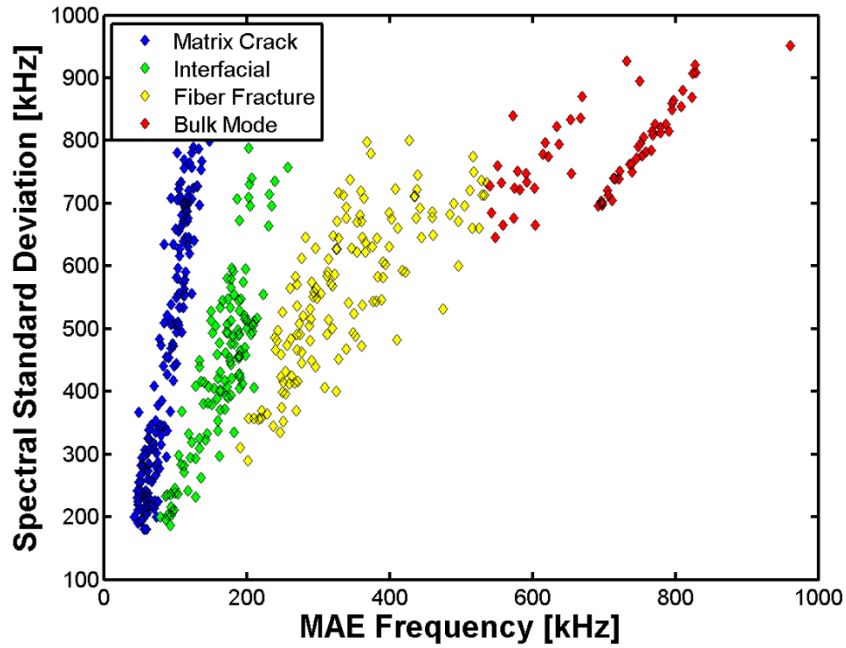


Figure D.20 – Spectral standard deviation versus Modal Acoustic Emission Frequency for ALT695 - 5020.

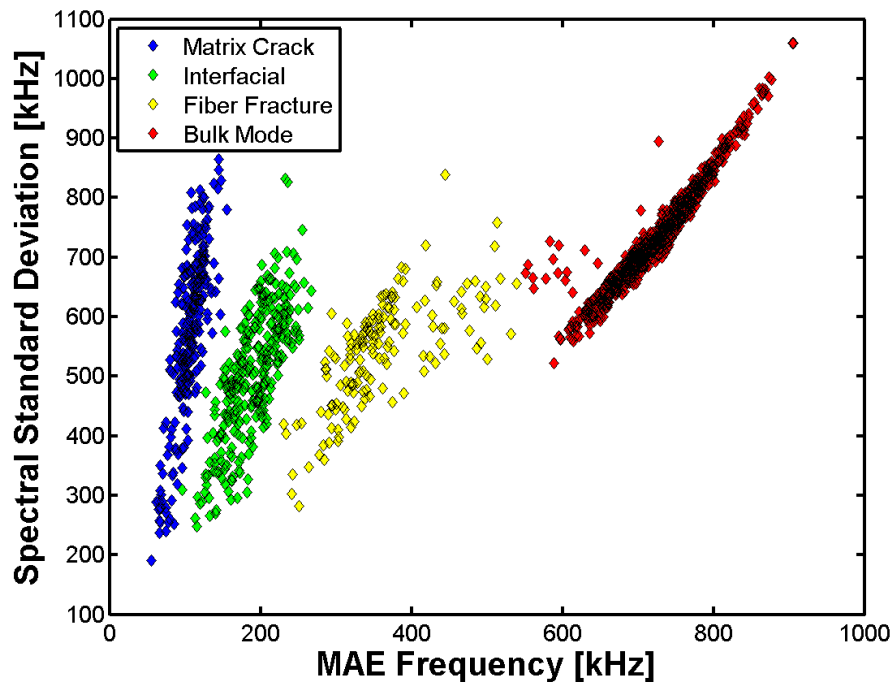


Figure D.21 – Spectral standard deviation versus Modal Acoustic Emission Frequency for ALT639 - 95898.

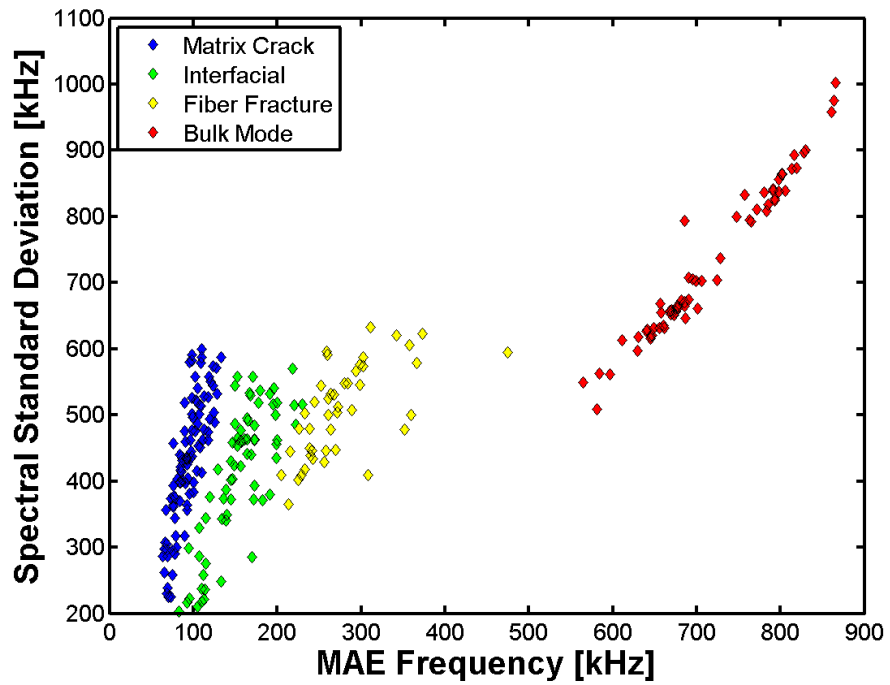


Figure D.22 – Spectral standard deviation versus Modal Acoustic Emission Frequency for ALT639 - 9465.

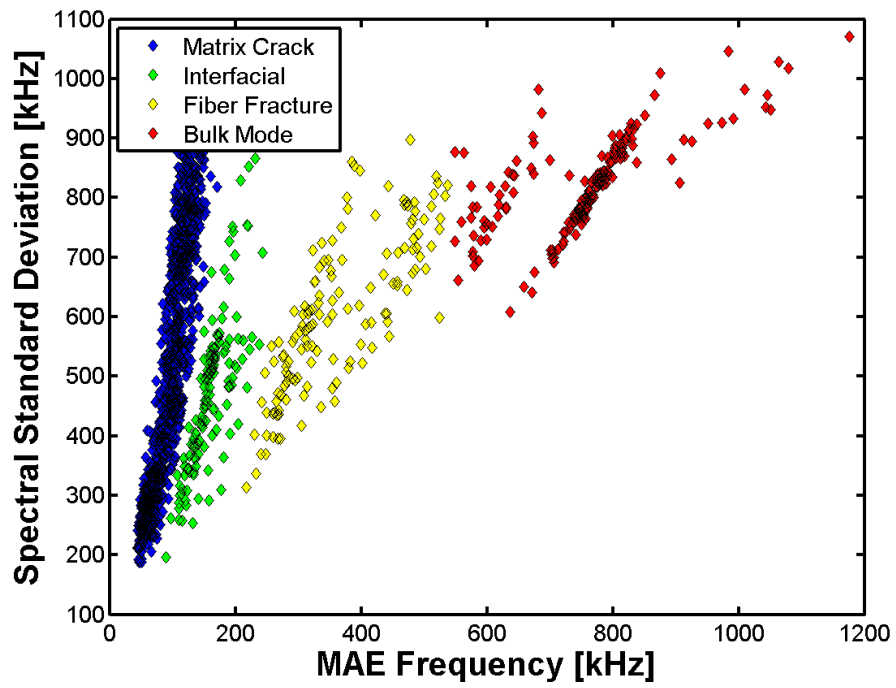


Figure D.23 – Spectral standard deviation versus Modal Acoustic Emission Frequency for OM3966.

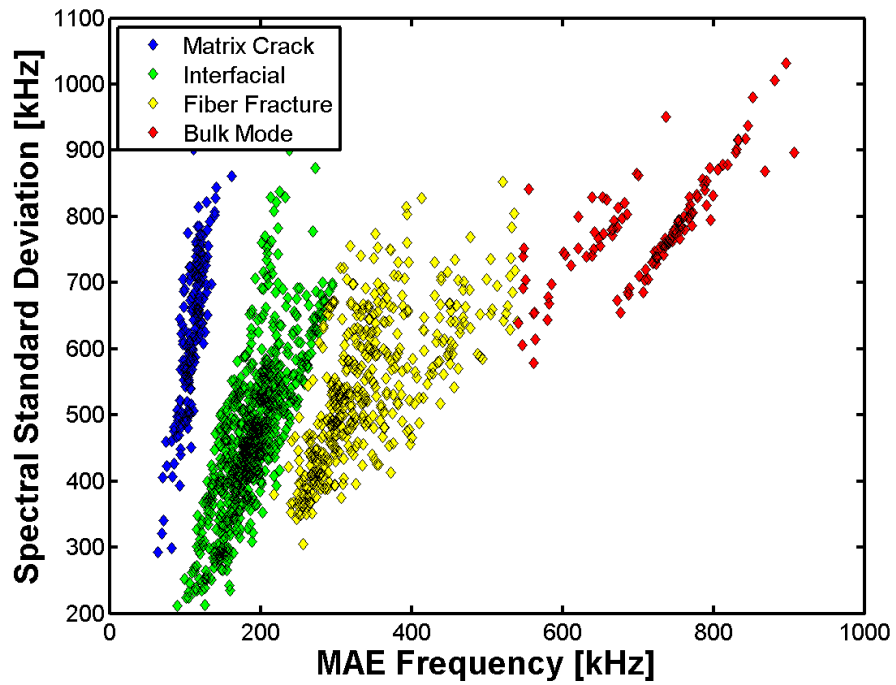


Figure D.24 – Spectral standard deviation versus Modal Acoustic Emission Frequency for ALT639-18030.

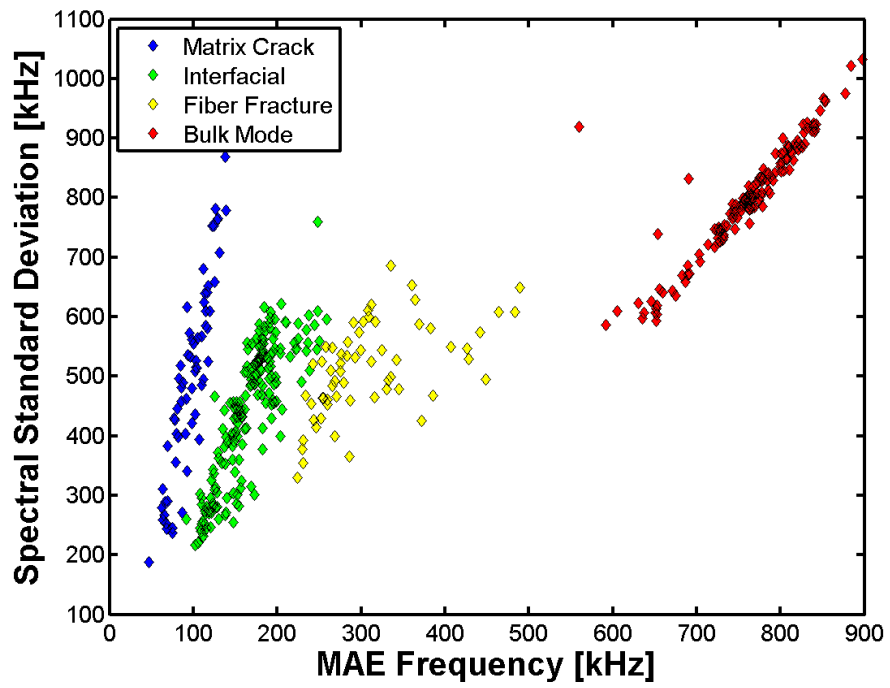


Figure D.25 – Spectral standard deviation versus Modal Acoustic Emission Frequency for ALT639-9987.

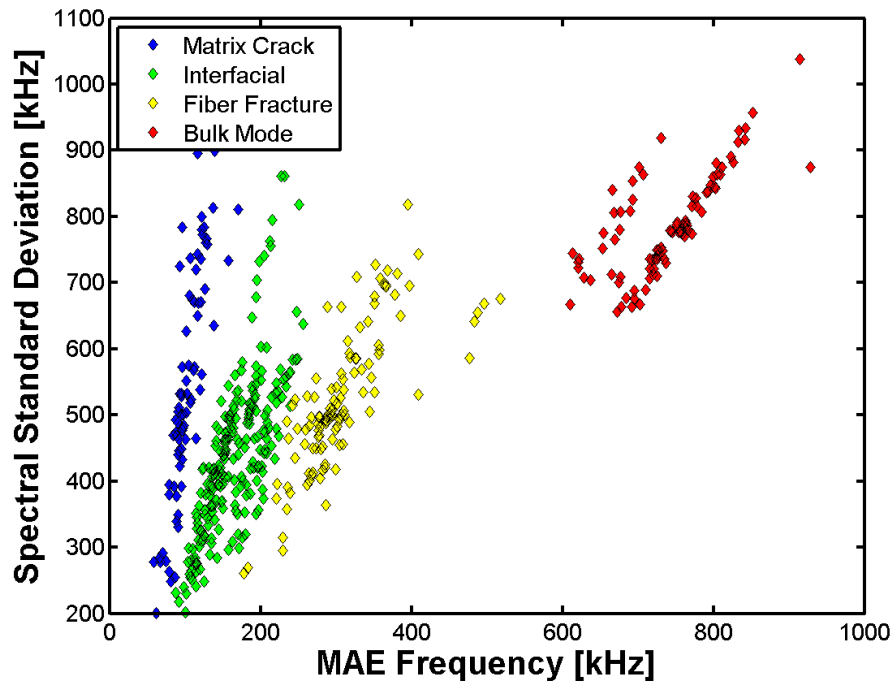


Figure D.26 – Spectral standard deviation versus Modal Acoustic Emission Frequency for ALT639-9959.

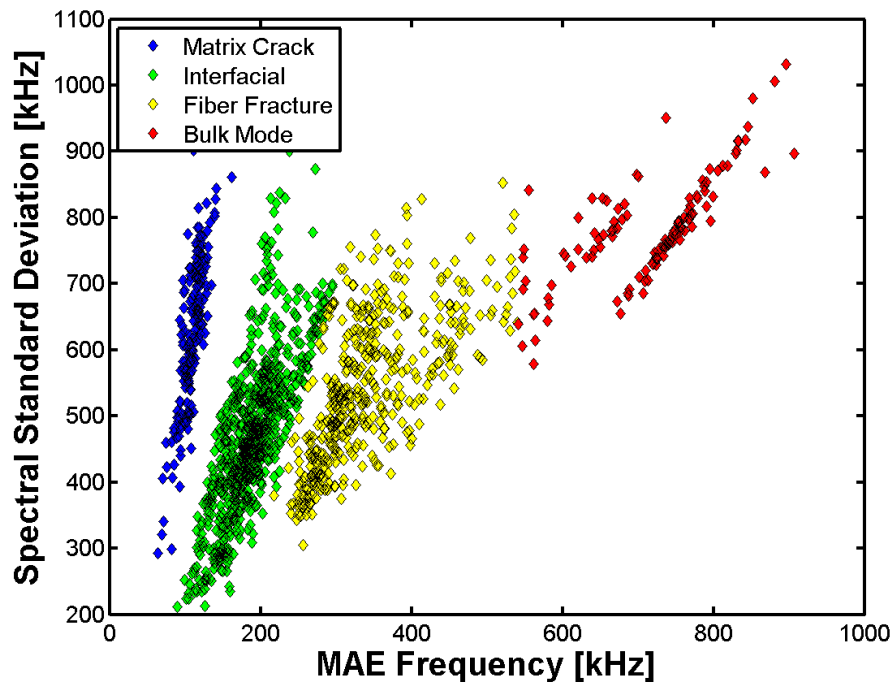


Figure D.27 – Spectral standard deviation versus Modal Acoustic Emission Frequency for ALT639-34081.

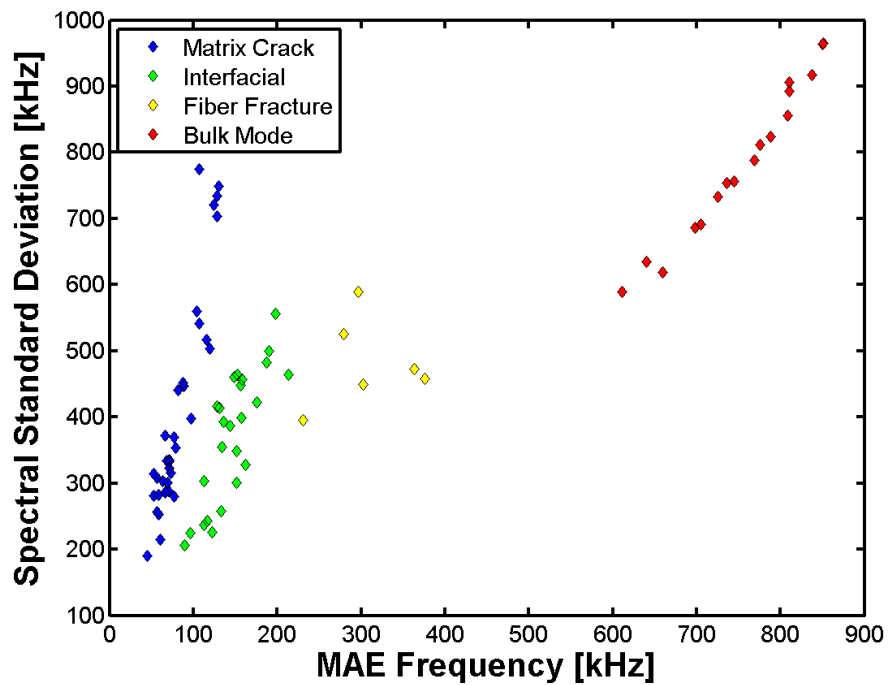


Figure D.28 – Spectral standard deviation versus Modal Acoustic Emission Frequency for ALT695-5031.

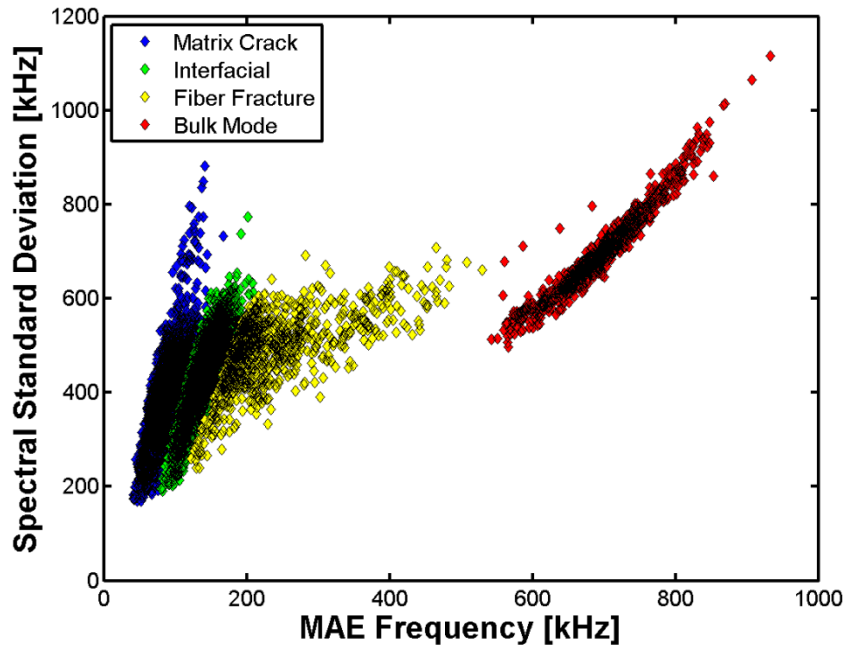


Figure D.29 – Source mechanism classification plot for ALT639-17716.

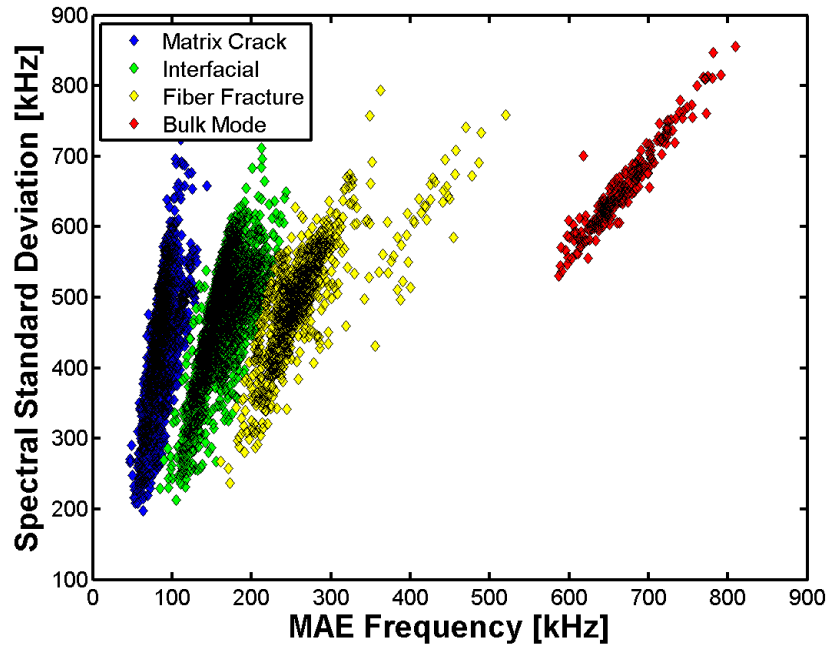


Figure D.30 – Source mechanism classification plot for ALT639-17831.

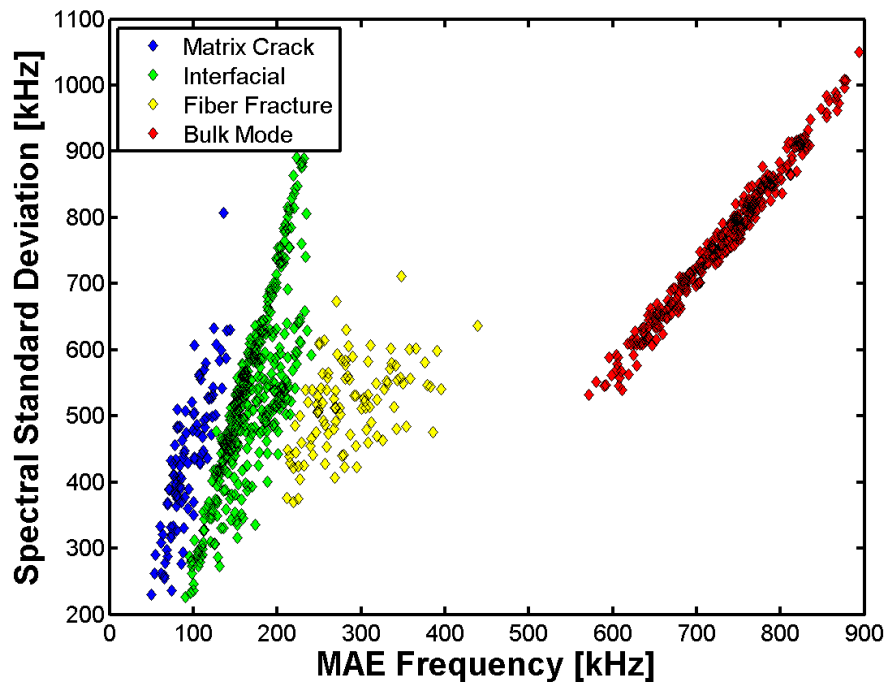


Figure D.31 – Source mechanism classification plot for ALT639-18768.

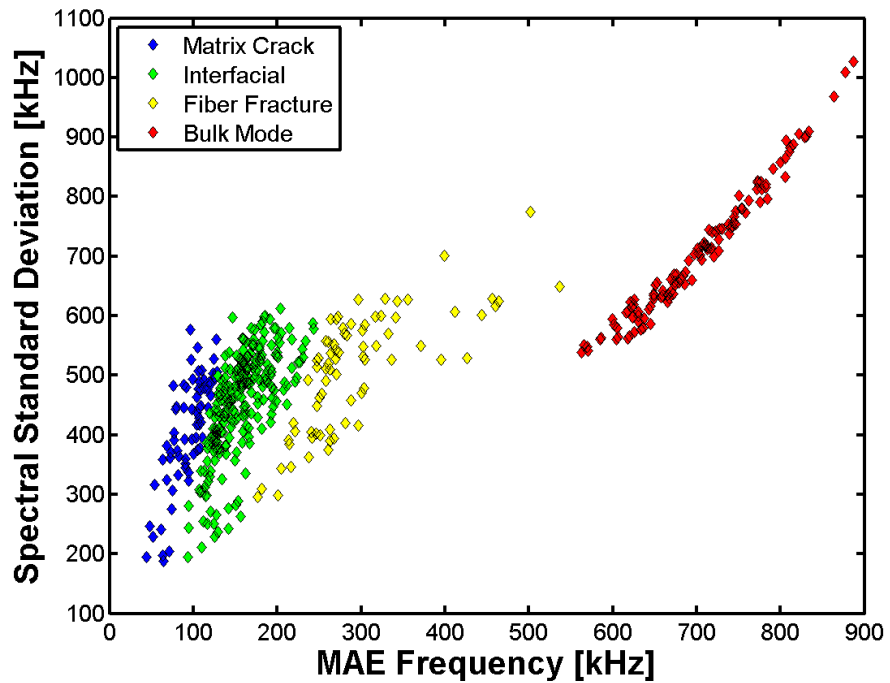


Figure D.32 – Source mechanism classification plot for ALT639-9747.

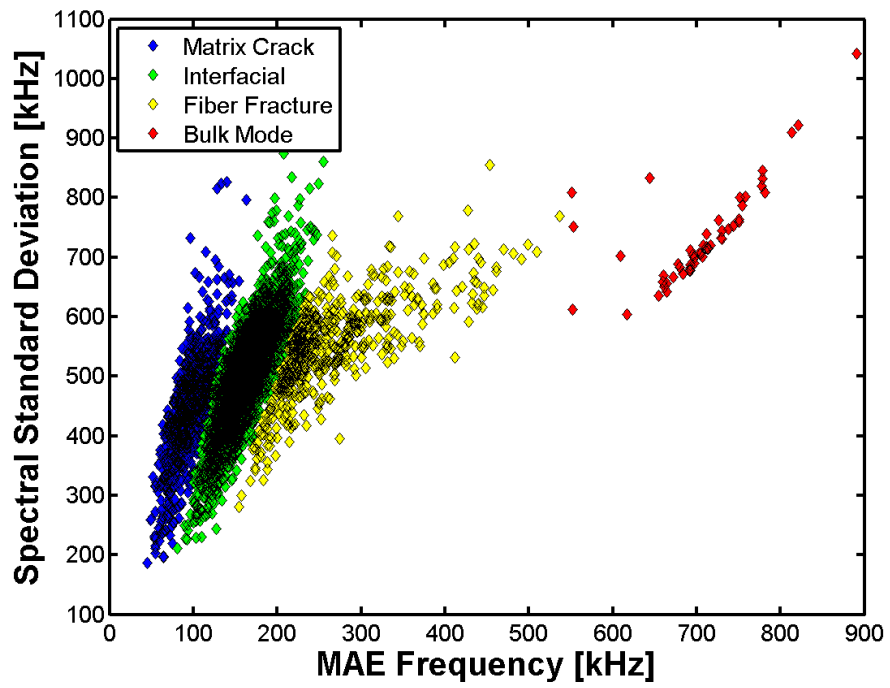


Figure D.33 – Source mechanism classification plot for ALT639-9769.

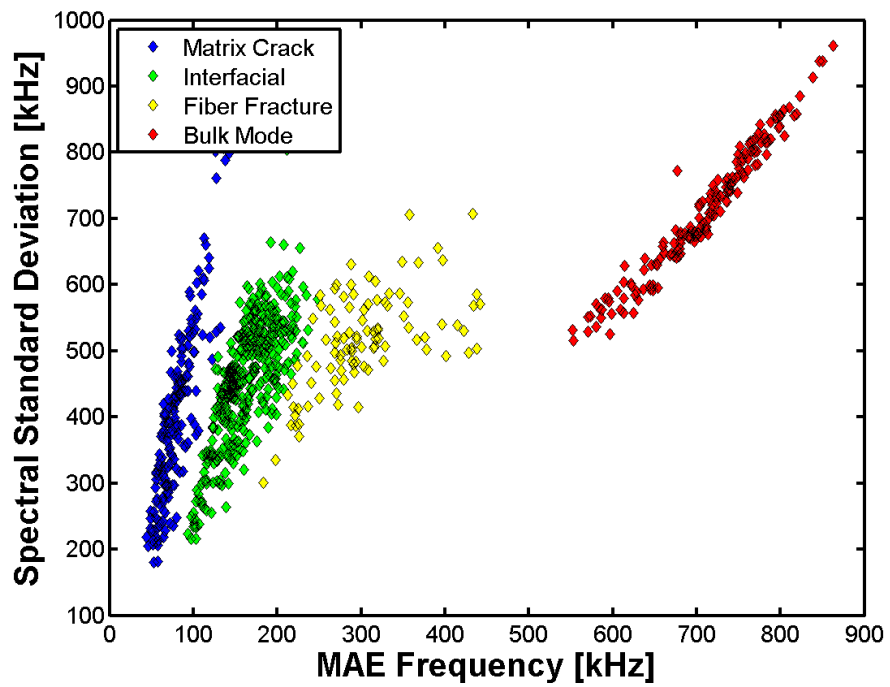


Figure D.34 – Source mechanism classification plot for ALT639-31064.

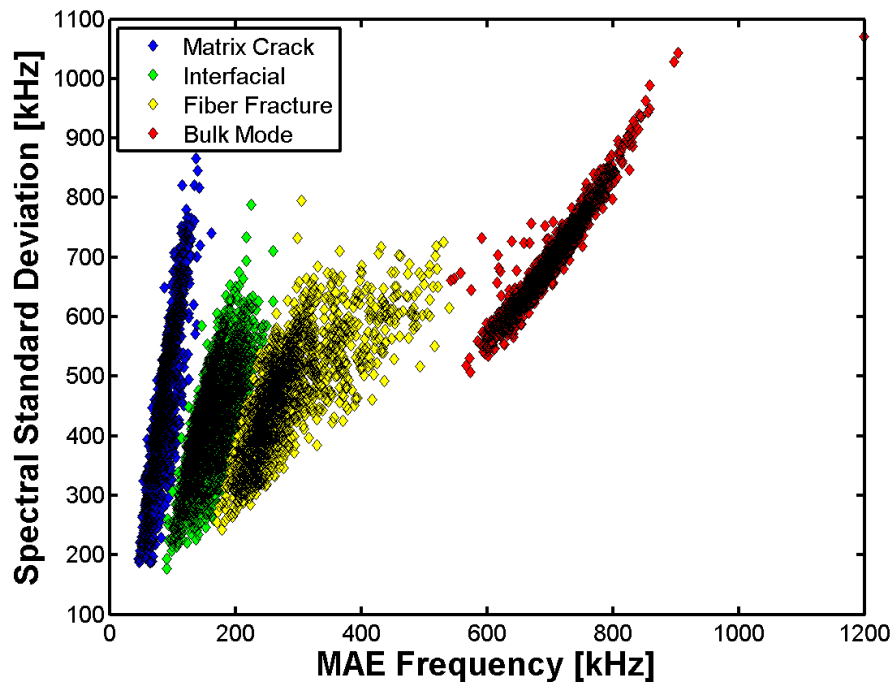


Figure D.35 – Source mechanism classification plot for ALT639-23371.

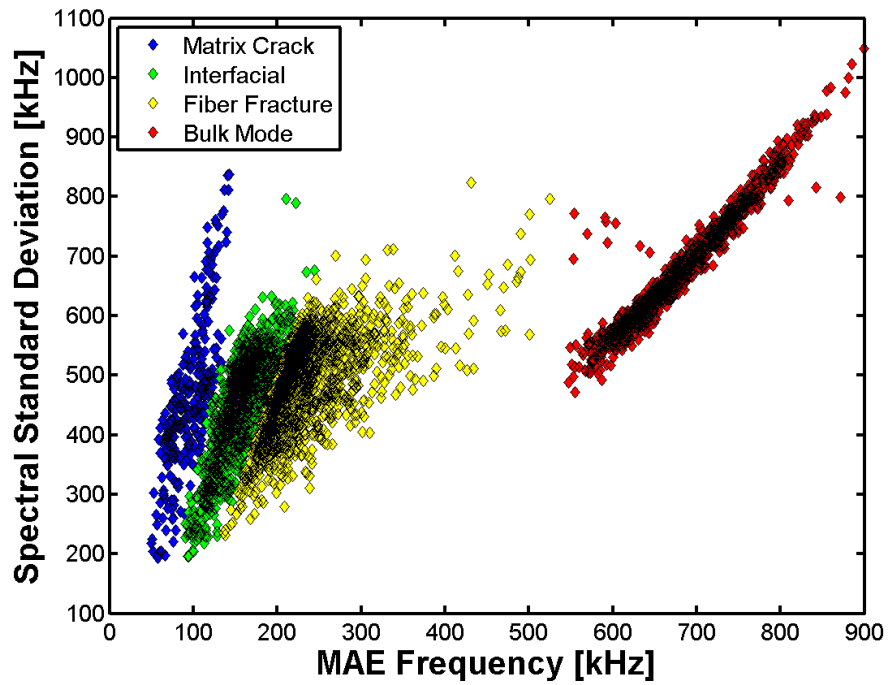


Figure D.36 – Source mechanism classification plot for ALT695-3669.

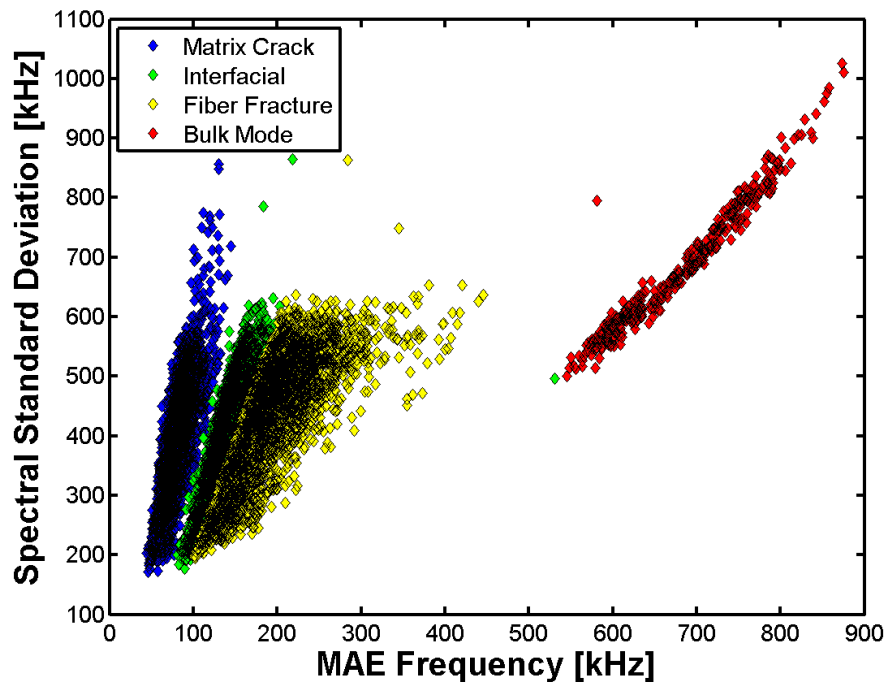


Figure D.37 – Source mechanism classification plot for ALT695-1781.

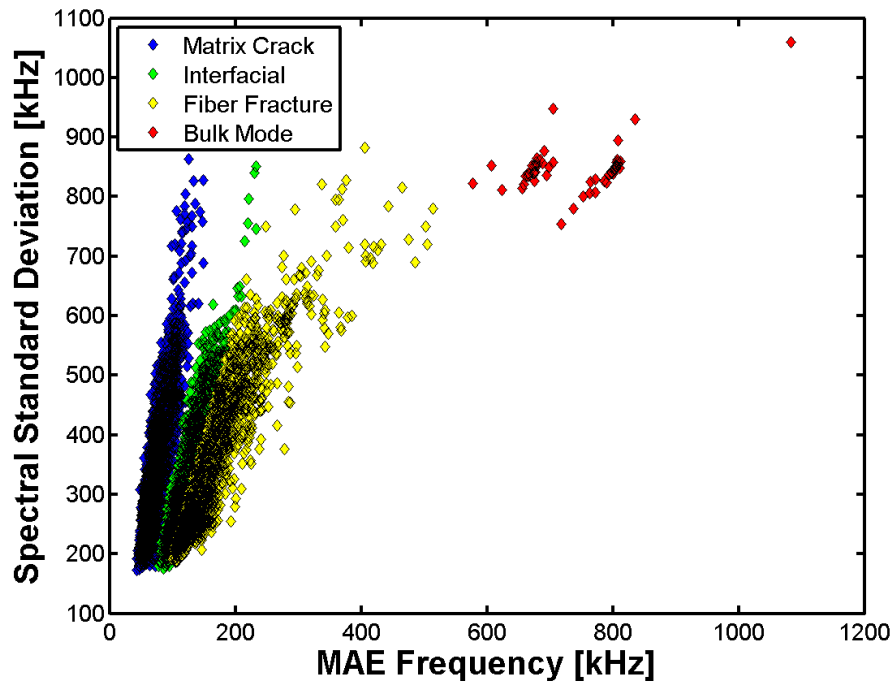


Figure D.38 – Source mechanism classification plot for OM3930.

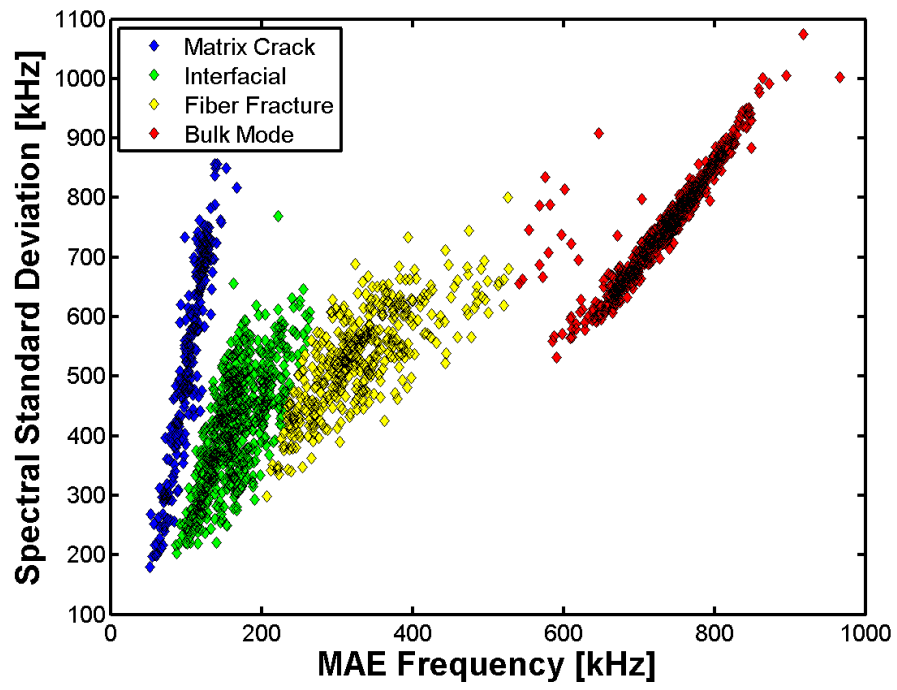


Figure D.39 – Source mechanism classification plot for ALT639-9753.

## APPENDIX E

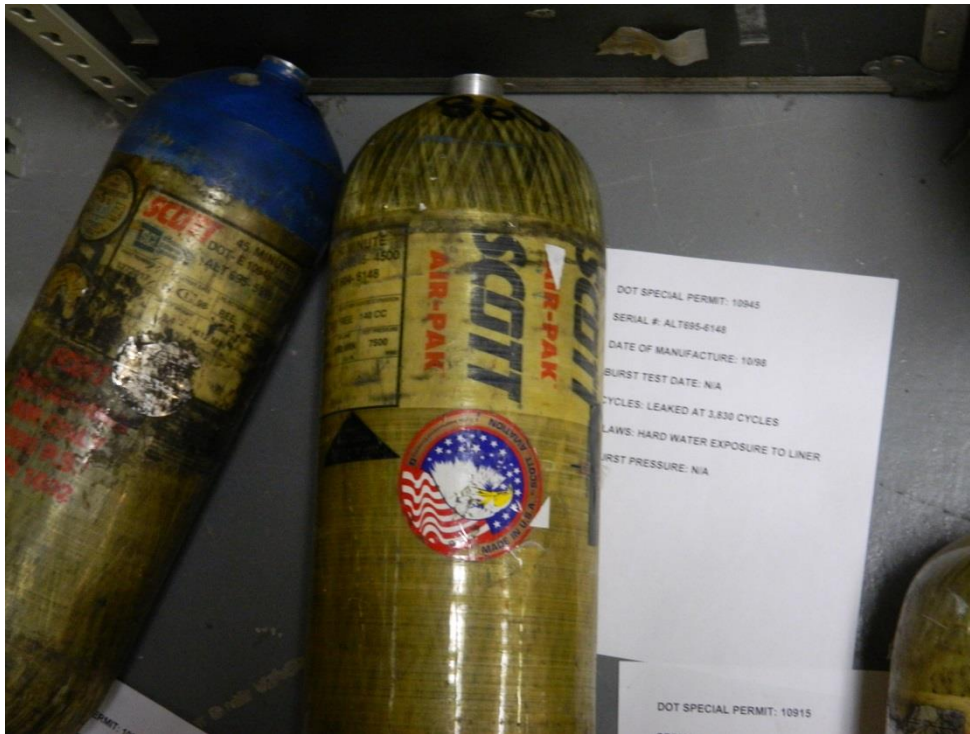


Figure E.1 – EOL photo of ALT604-6148.



Figure E.2 – EOL Burst of ALT639-9573.

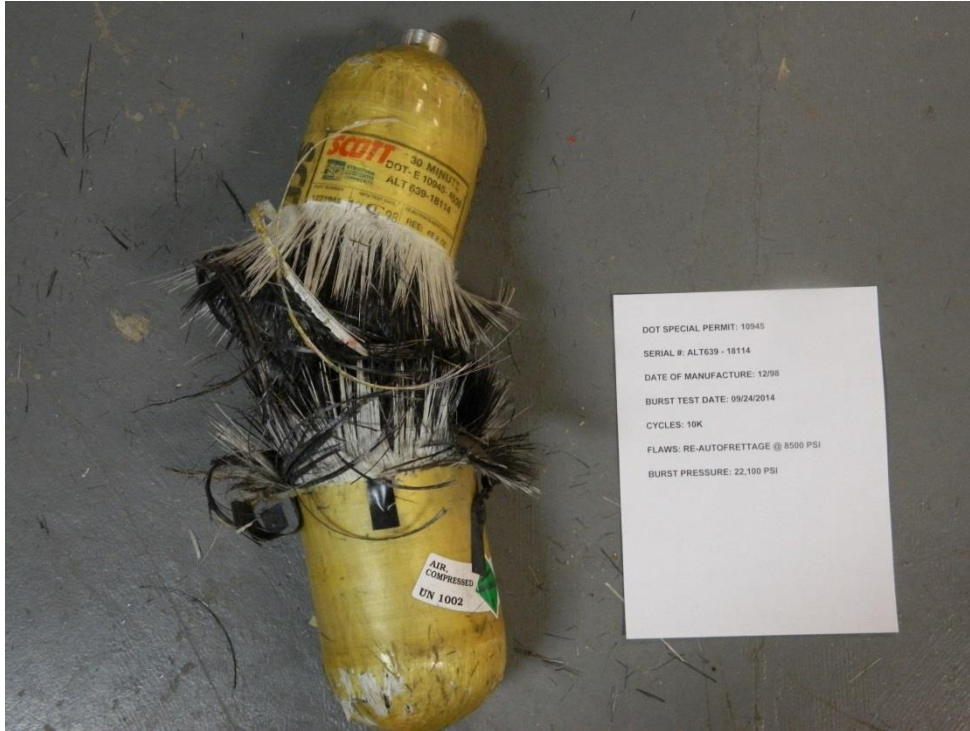


Figure E.3 – EOL Burst of ALT639-18114.

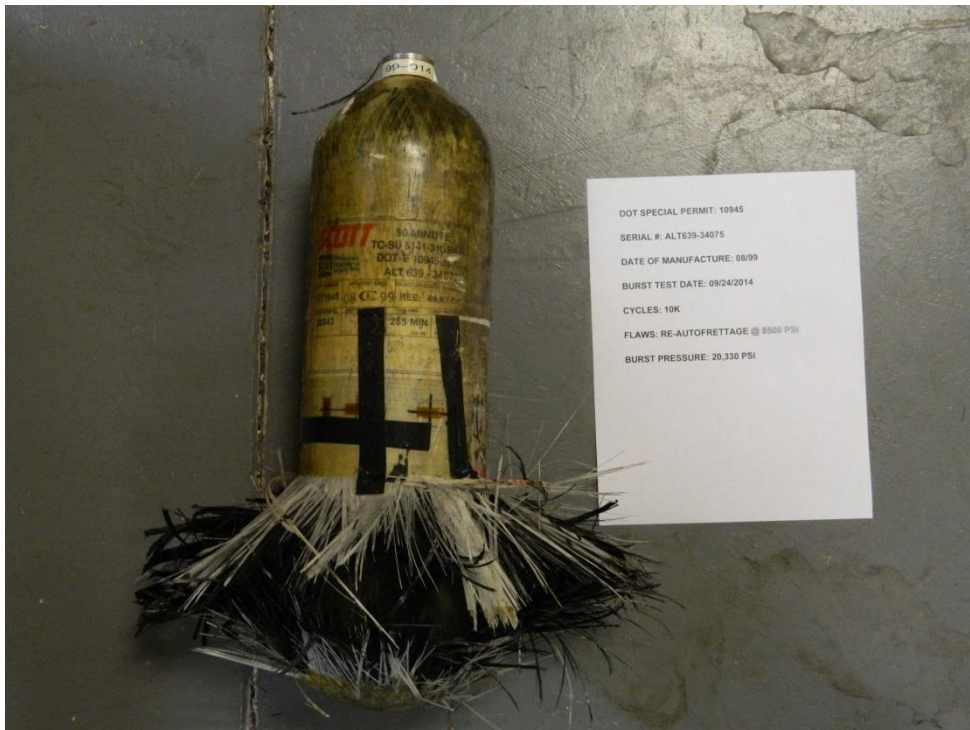


Figure E.4 – EOL Burst of ALT639-34075.

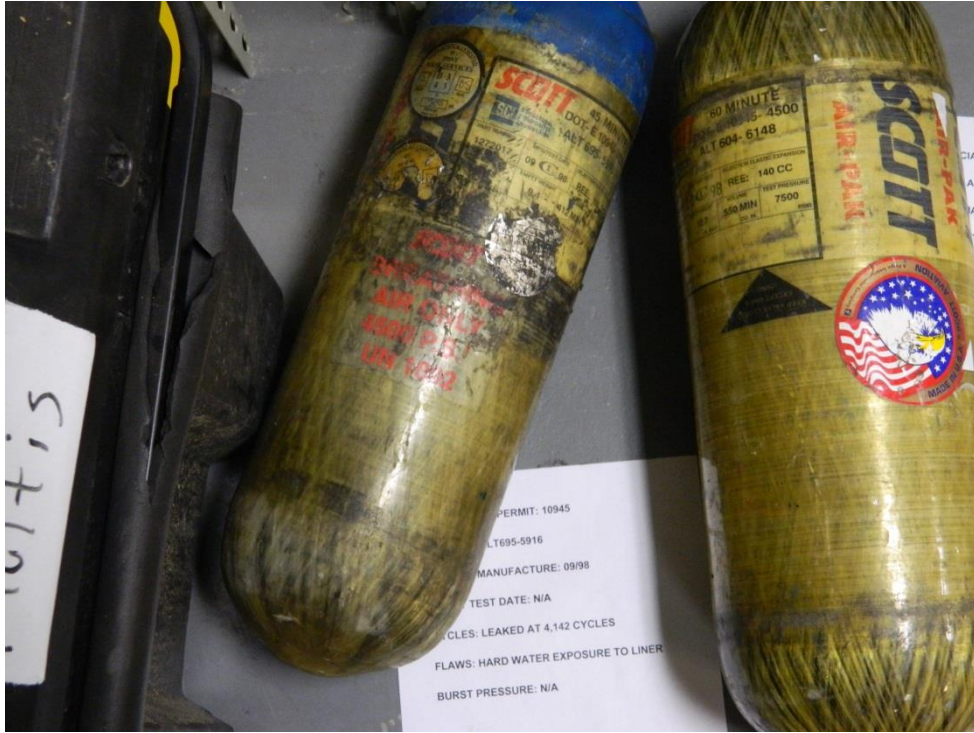


Figure E.5 – EOL photo of ALT695-5916.

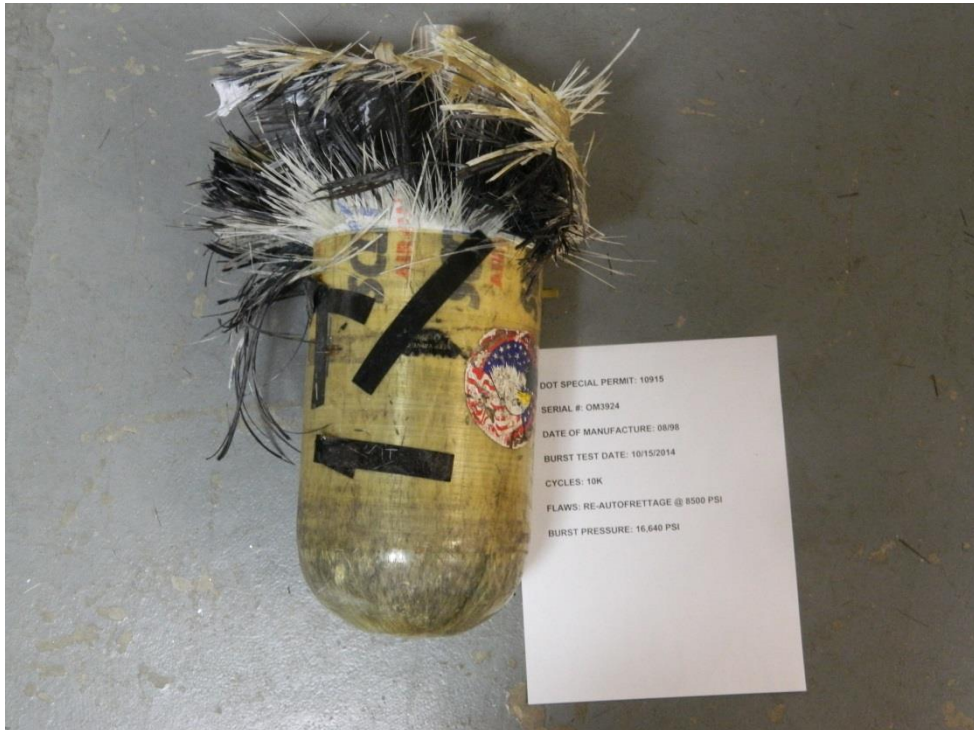


Figure E.6 – EOL Burst of OM3924.

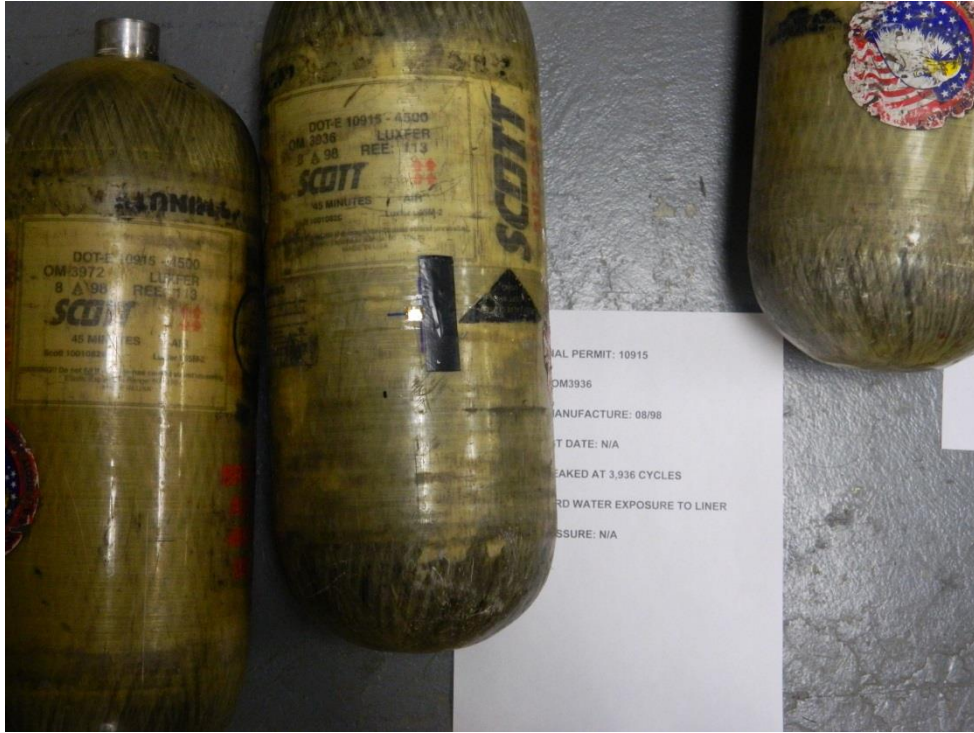


Figure E.7 – EOL photo of OM3936.

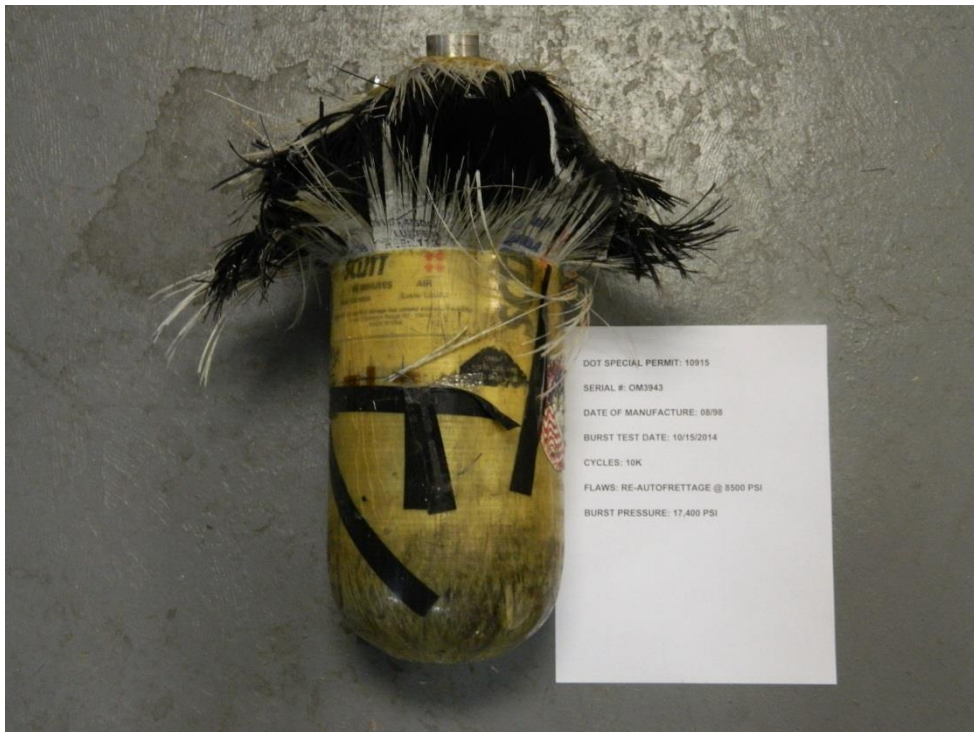


Figure E.8 – EOL Burst of OM3943.

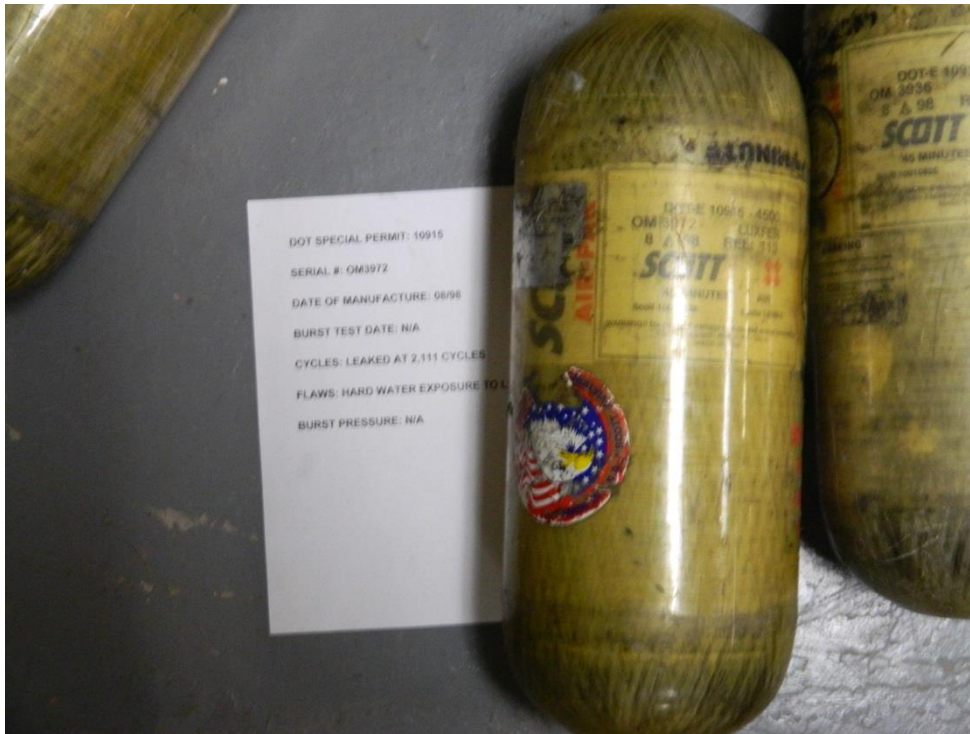


Figure E.9 – EOL photo of OM3972.



Figure E.10 – EOL photo of OM3992.



Figure E.11 – EOL Burst of ALT639-9605.

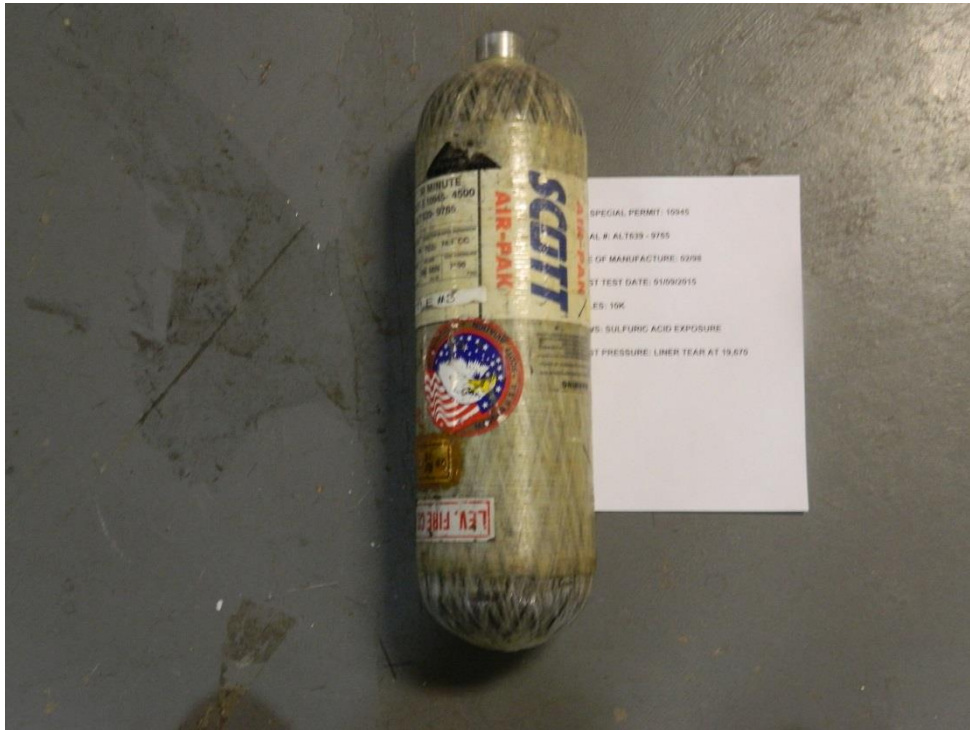


Figure E.12 – EOL Burst of ALT639-9765.

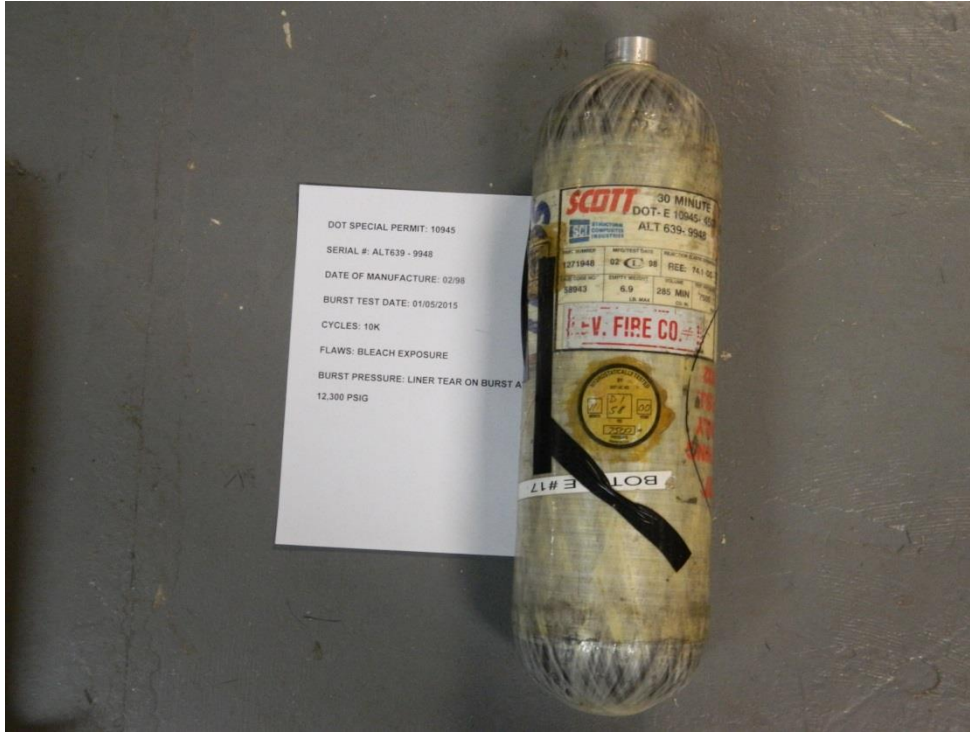


Figure E.13 – EOL Burst of ALT639-9948.

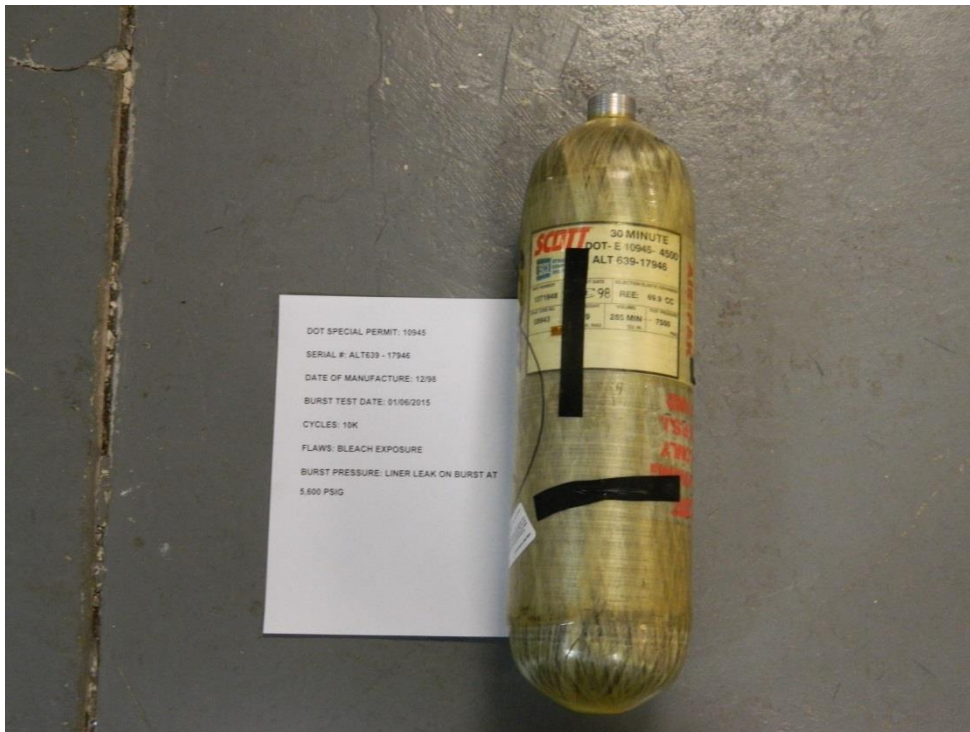


Figure E.14 – EOL Burst of ALT639-17946.

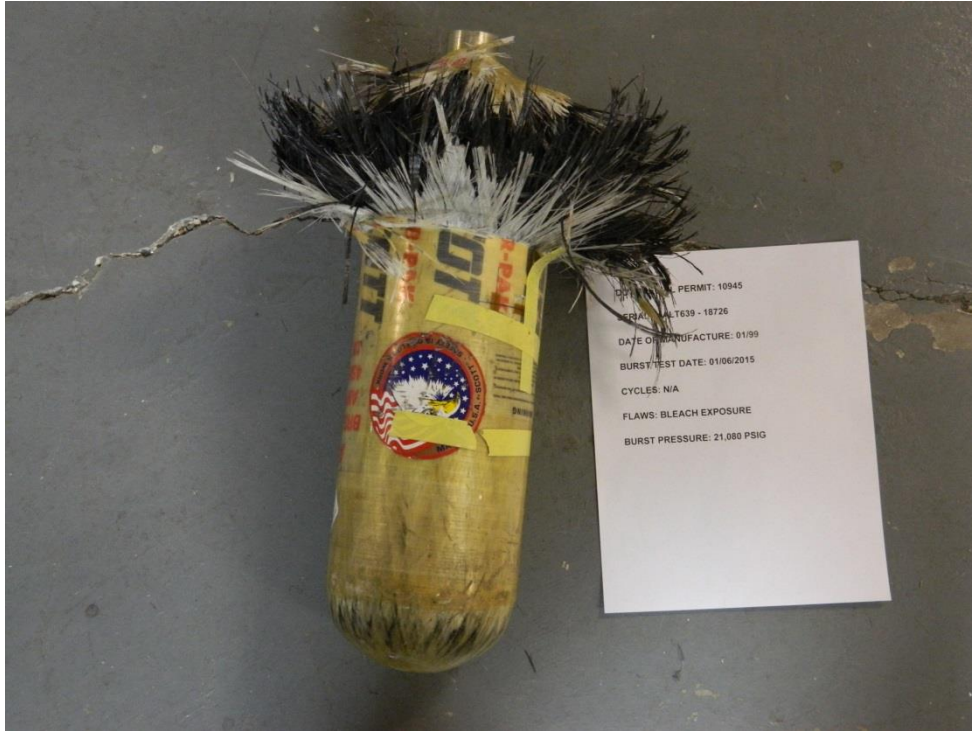


Figure E.15 – EOL Burst of ALT639-18726.

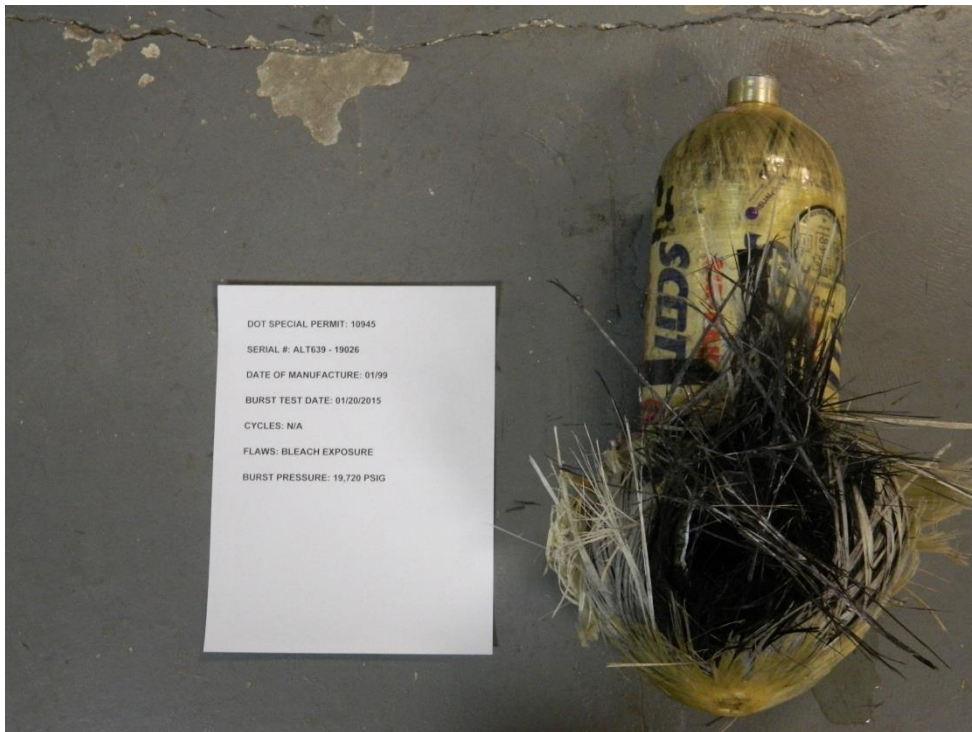


Figure E. 16 – EOL Burst of ALT639-19026.

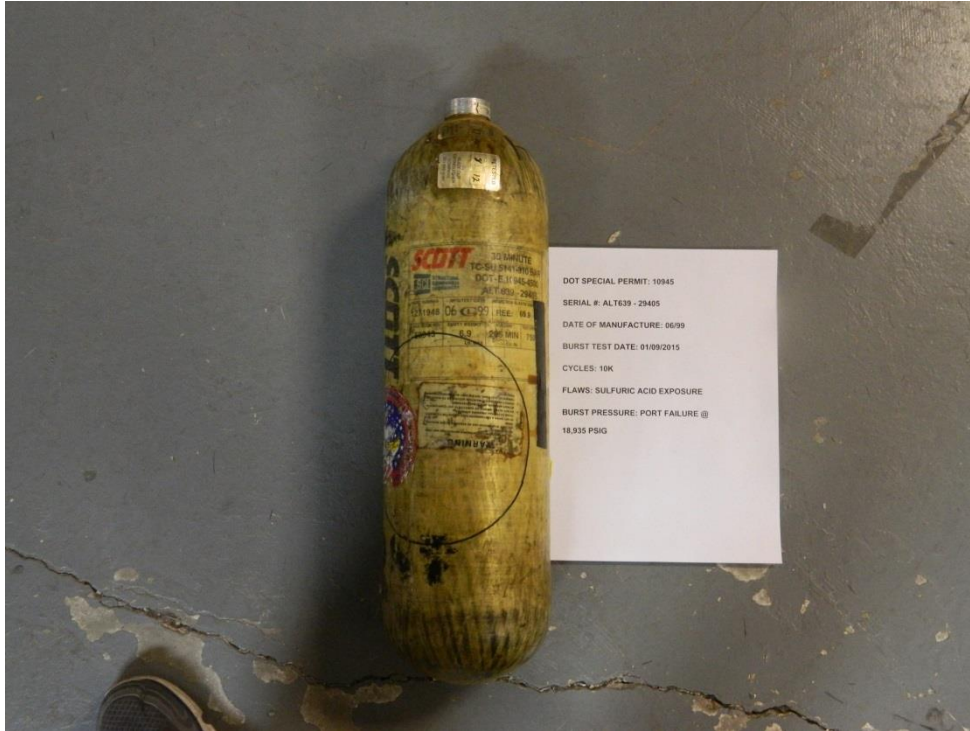


Figure E.17 – EOL Burst of ALT639-29405.

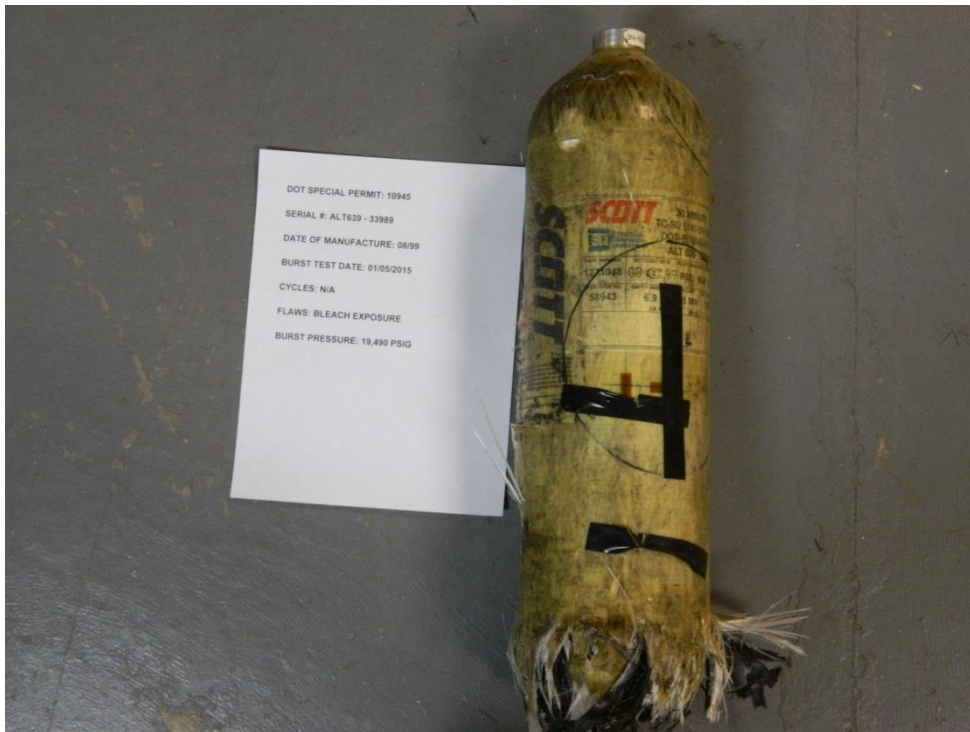


Figure E.18 – EOL Burst of ALT639-33989.



Figure E.19 – EOL Burst of ALT639-34011.



Figure E.20 – EOL Burst of ALT639-34079.

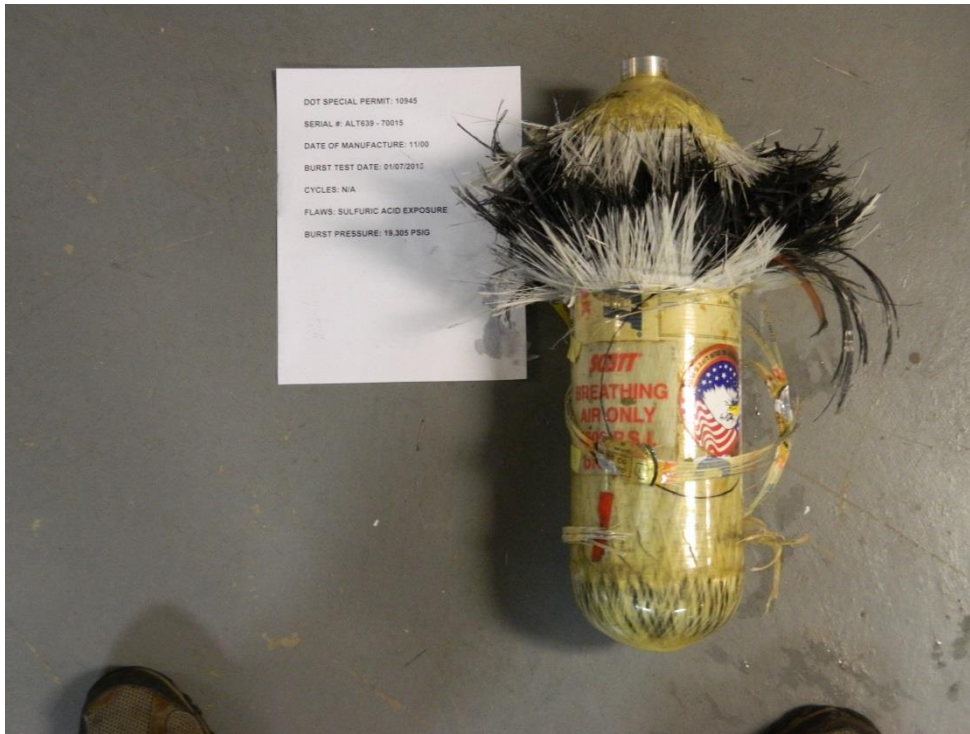


Figure E.21 – EOL Burst of ALT639-70015.



Figure E.22 – EOL Burst of ALT695-1665.

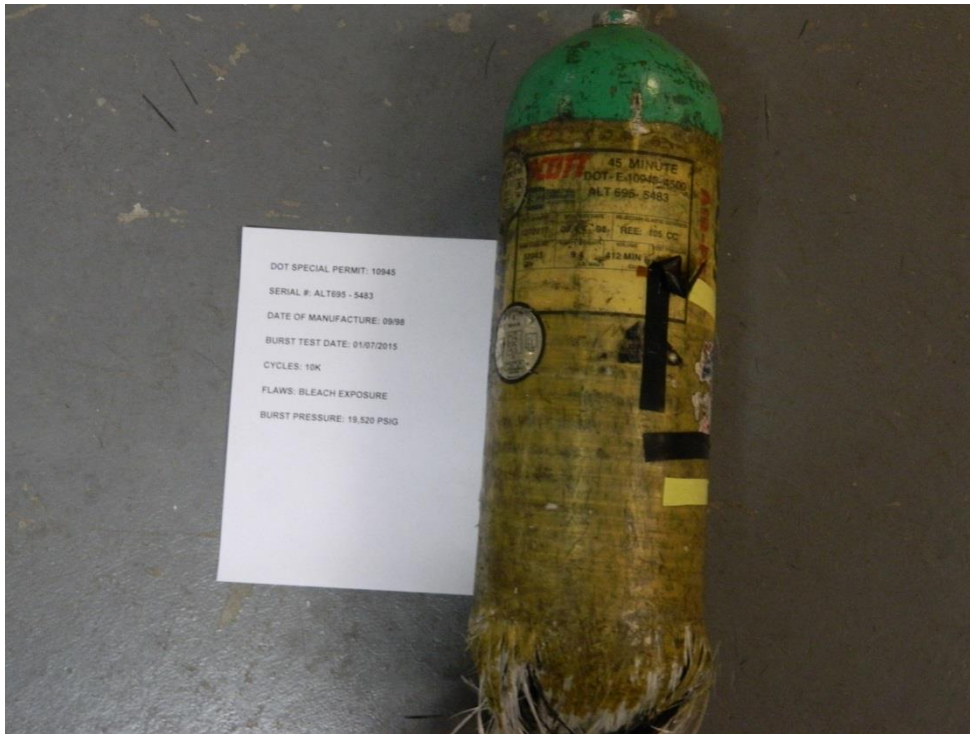


Figure E.23 – EOL Burst of ALT695-5483.

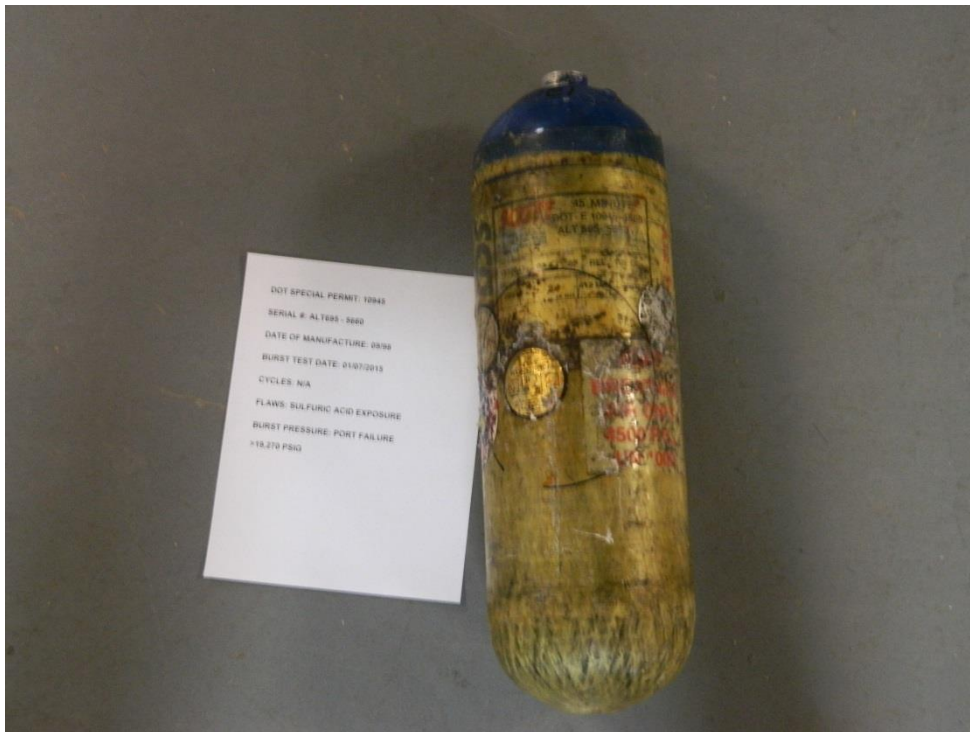
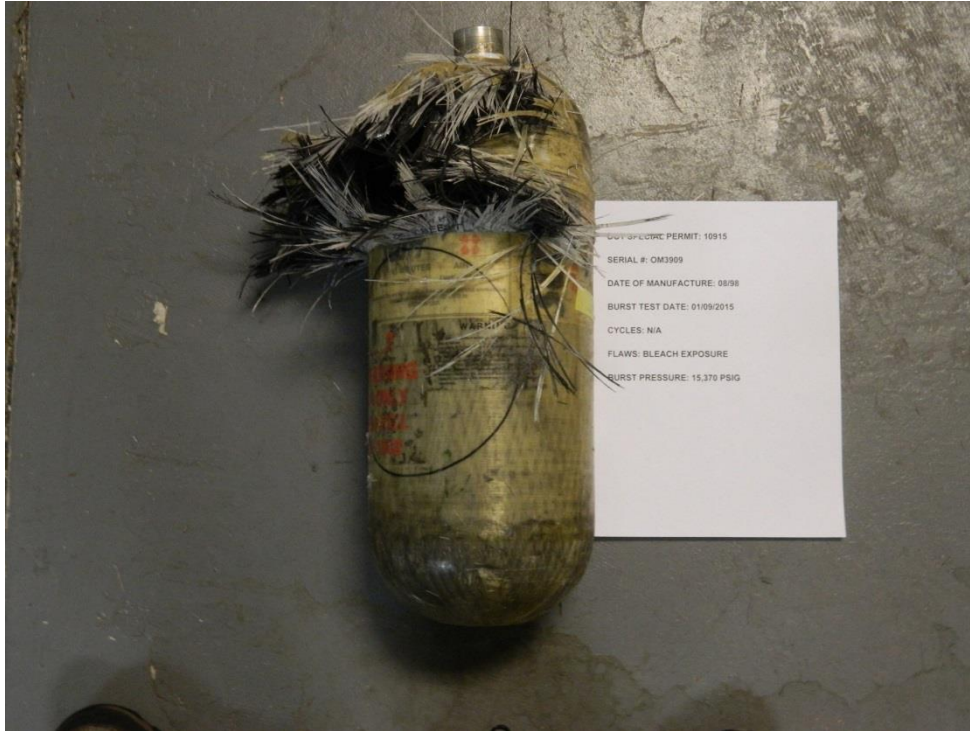
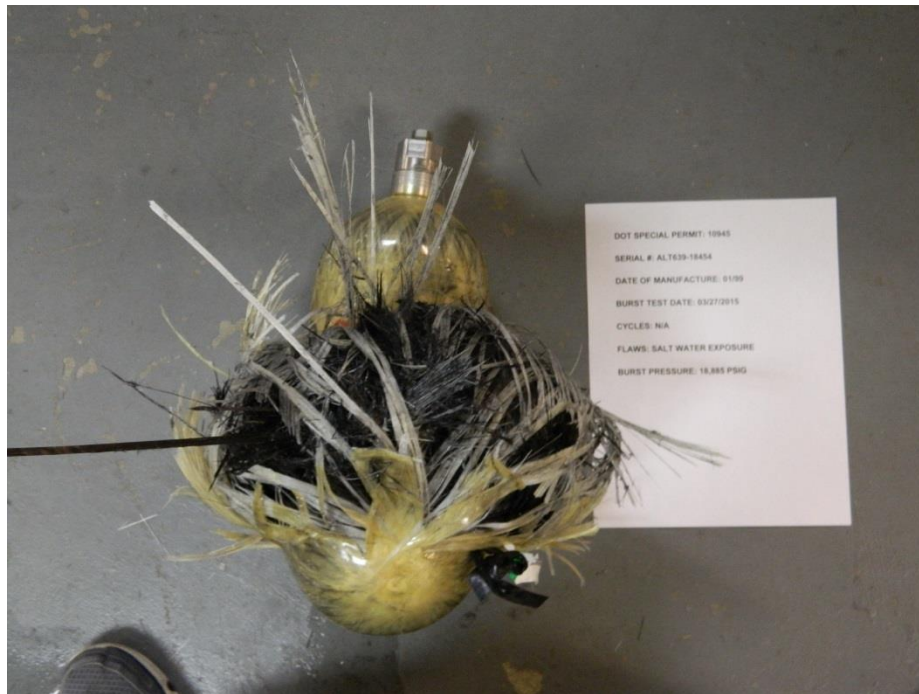


Figure E.24 – EOL Burst of ALT695-5660.



DOT SPECIAL PERMIT: 10915  
SERIAL #: OM3909  
DATE OF MANUFACTURE: 08/98  
BURST TEST DATE: 01/09/2015  
CYCLES: N/A  
FLAWS: BLEACH EXPOSURE  
BURST PRESSURE: 15,370 PSIG

**Figure E.25 – EOL Burst of OM3909.**



DOT SPECIAL PERMIT: 10945  
SERIAL #: ALT639-18454  
DATE OF MANUFACTURE: 01/99  
BURST TEST DATE: 03/27/2015  
CYCLES: N/A  
FLAWS: SALT WATER EXPOSURE  
BURST PRESSURE: 15,955 PSIG

**Figure E.26 – EOL Burst of ALT639-18454.**

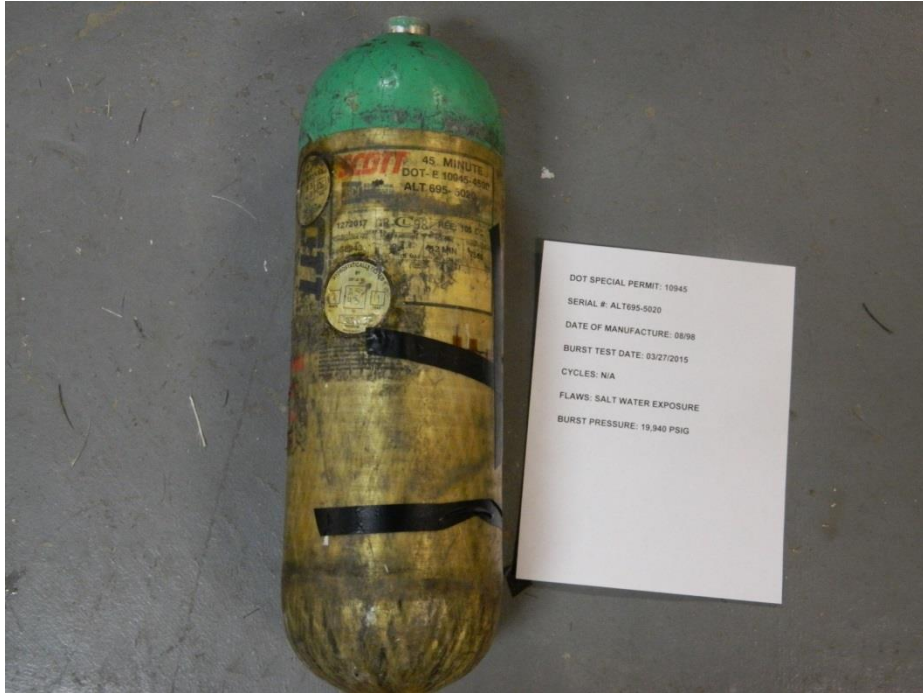


Figure E.27 – EOL Burst of ALT695-5020.

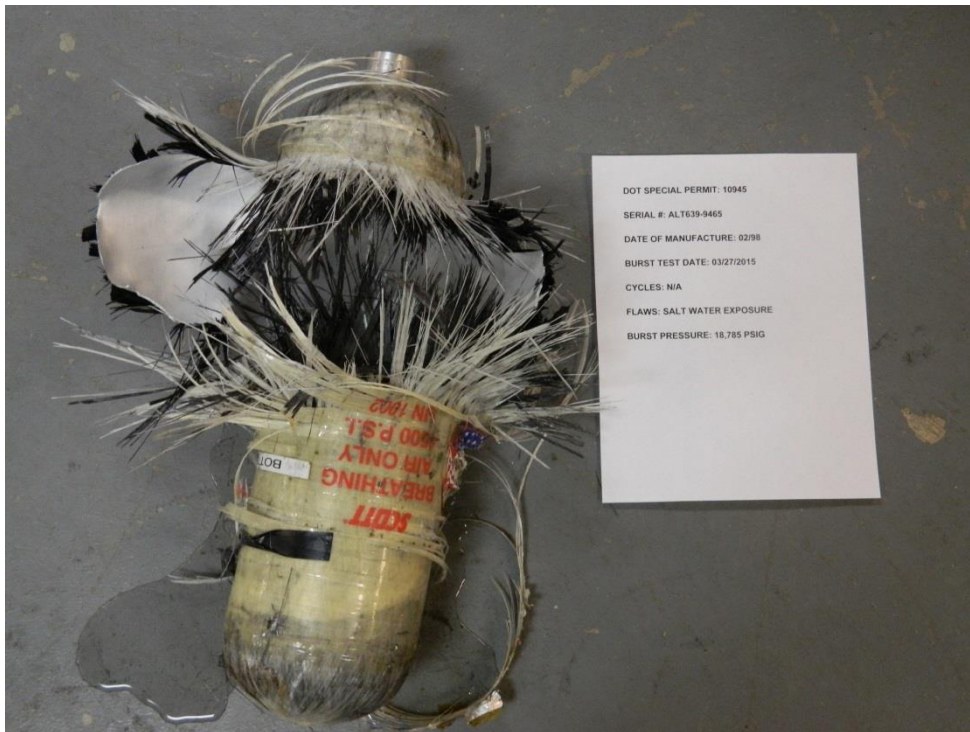


Figure E.28 – EOL Burst of ALT639-9465.



Figure E.29 – EOL Burst of ALT639-95898.

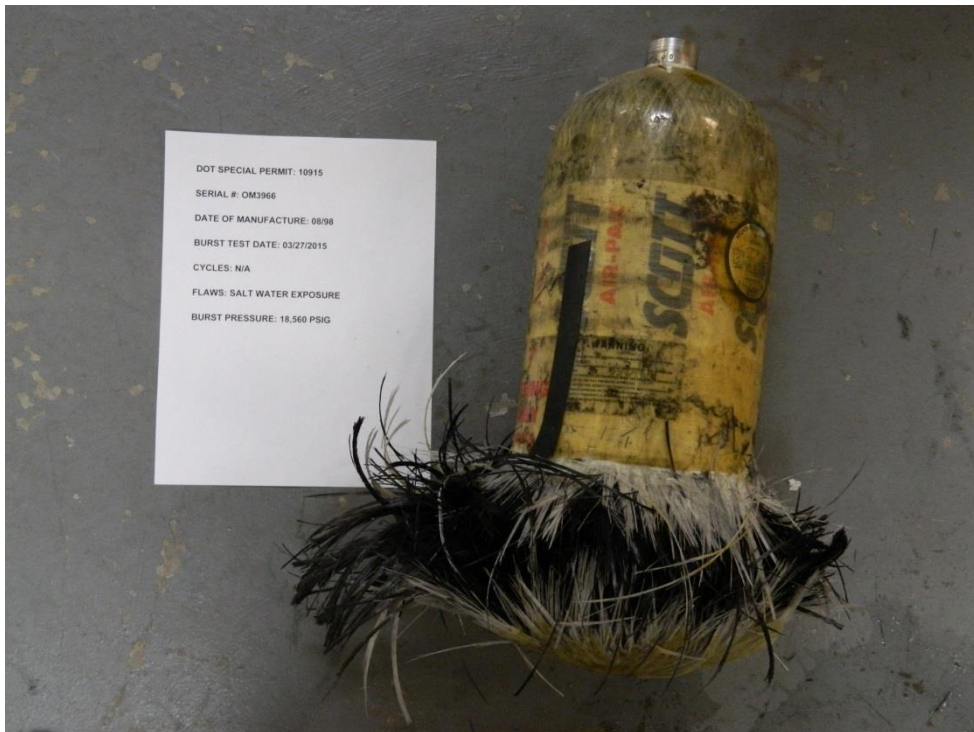


Figure E.30 – EOL Burst of OM3966.



Figure E.31 – EOL Burst of ALT639-18030.

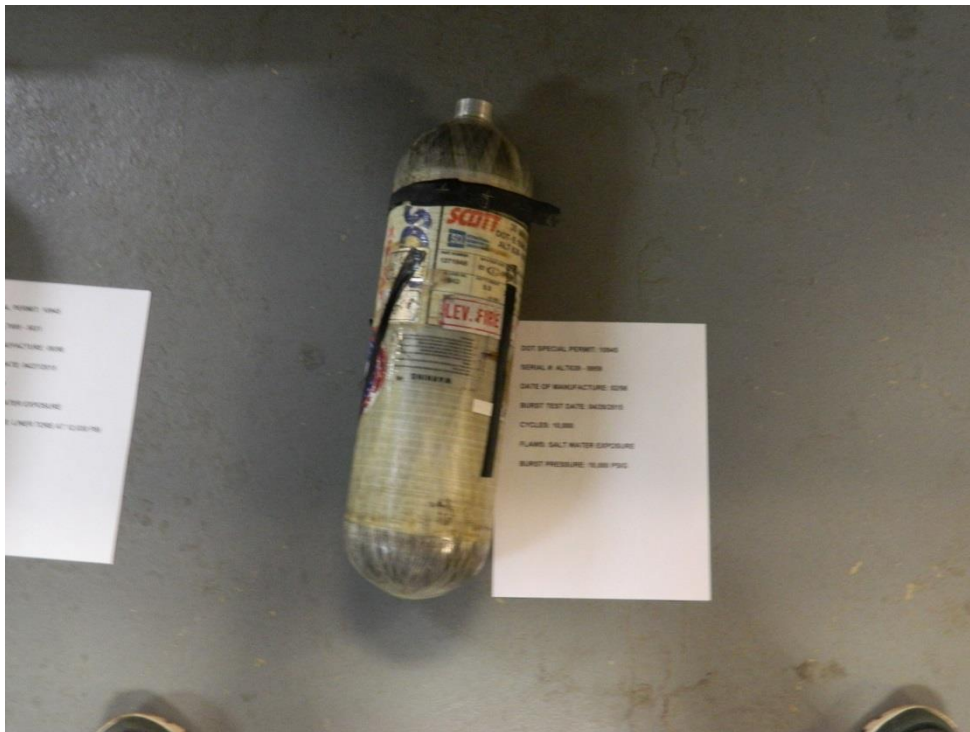


Figure E.32 – EOL Burst of ALT639-9959.

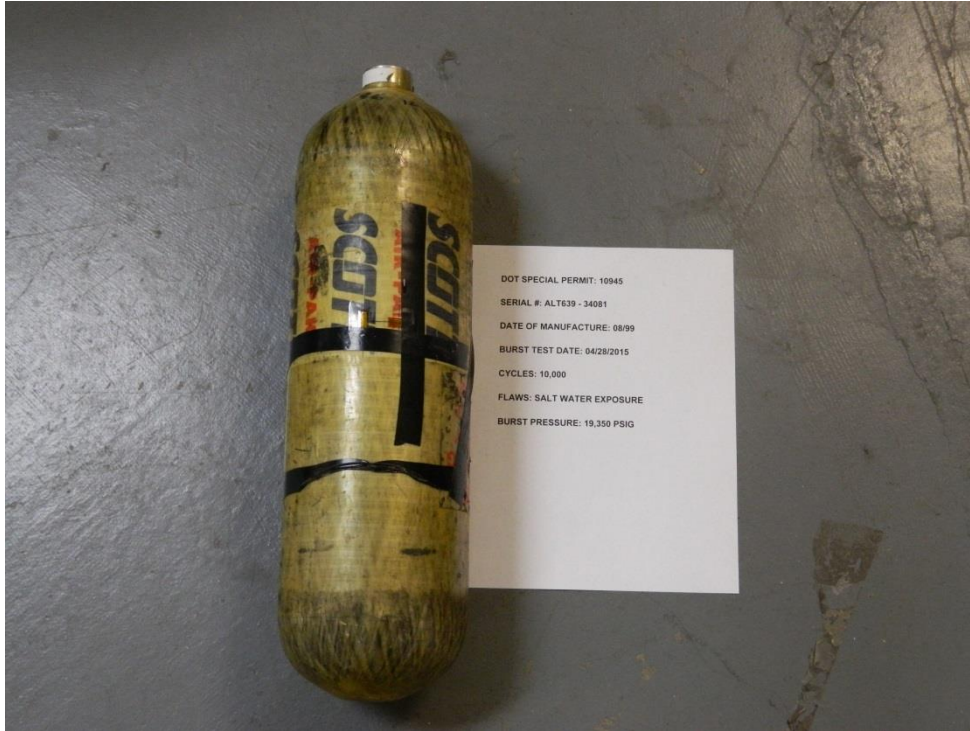


Figure E.33 – EOL Burst of ALT639-34081.

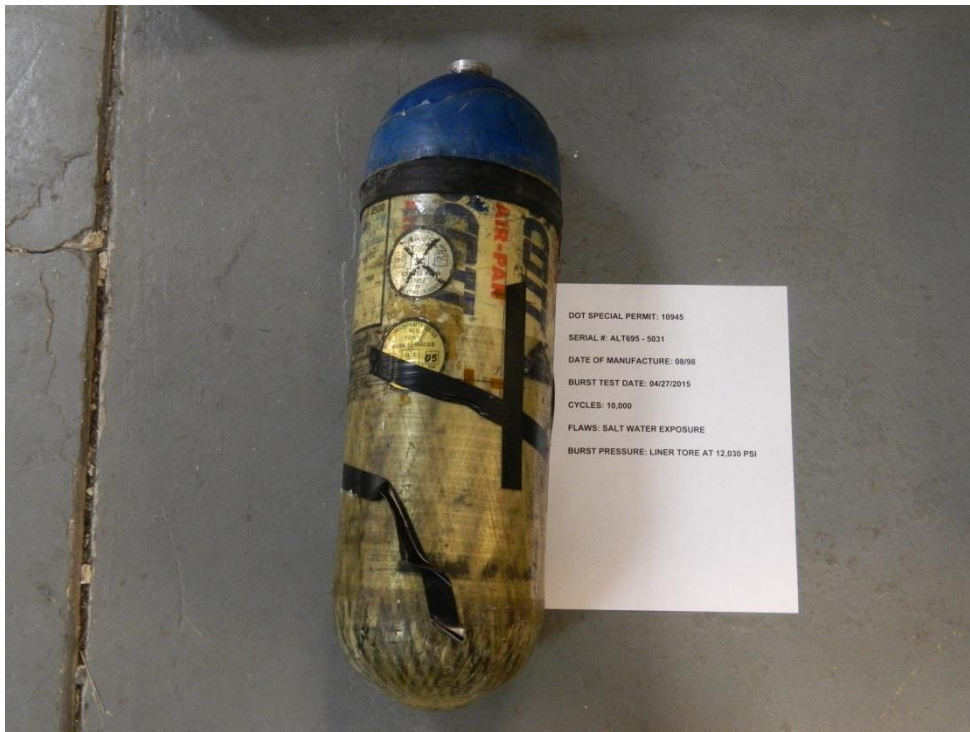
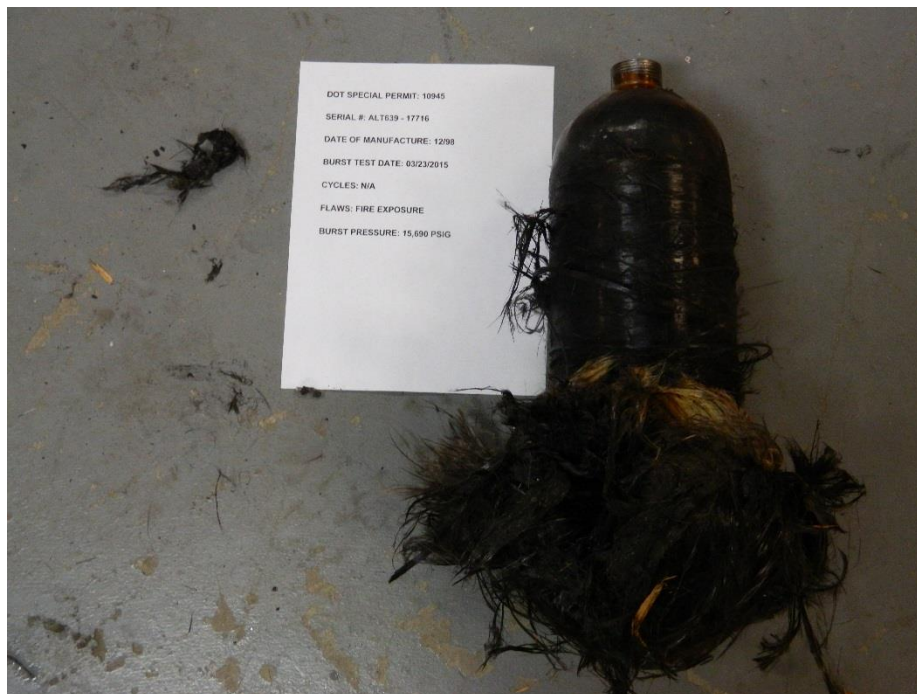


Figure E.34 – EOL Burst of ALT695-5031.



**Figure E.35 – EOL Burst of ALT639-9987.**



**Figure E.36 – End-of-Life burst of ALT639-17716.**

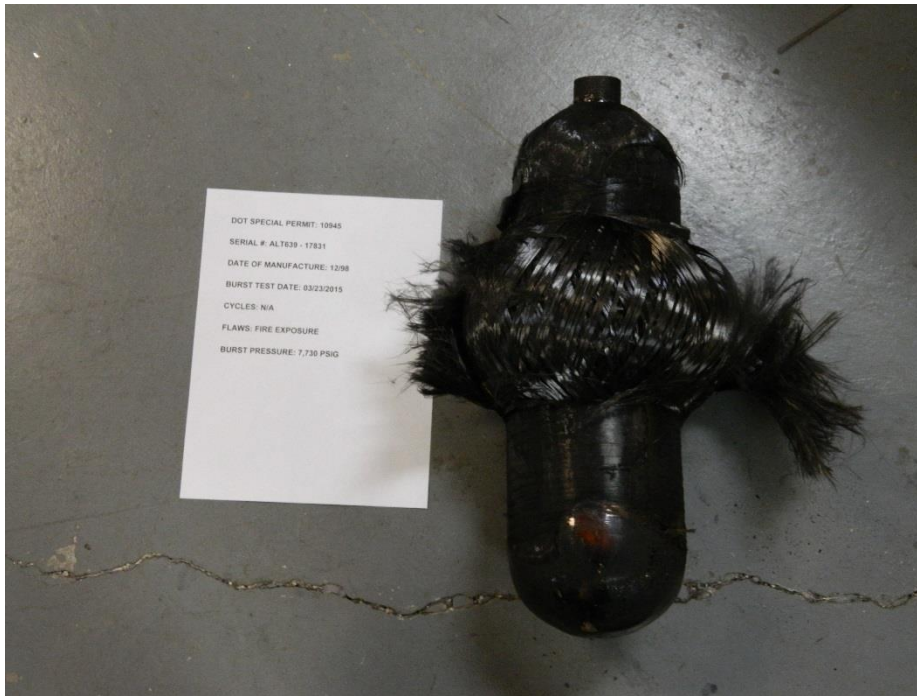


**Figure E.37 – End-of-Life burst of ALT639-17831.**

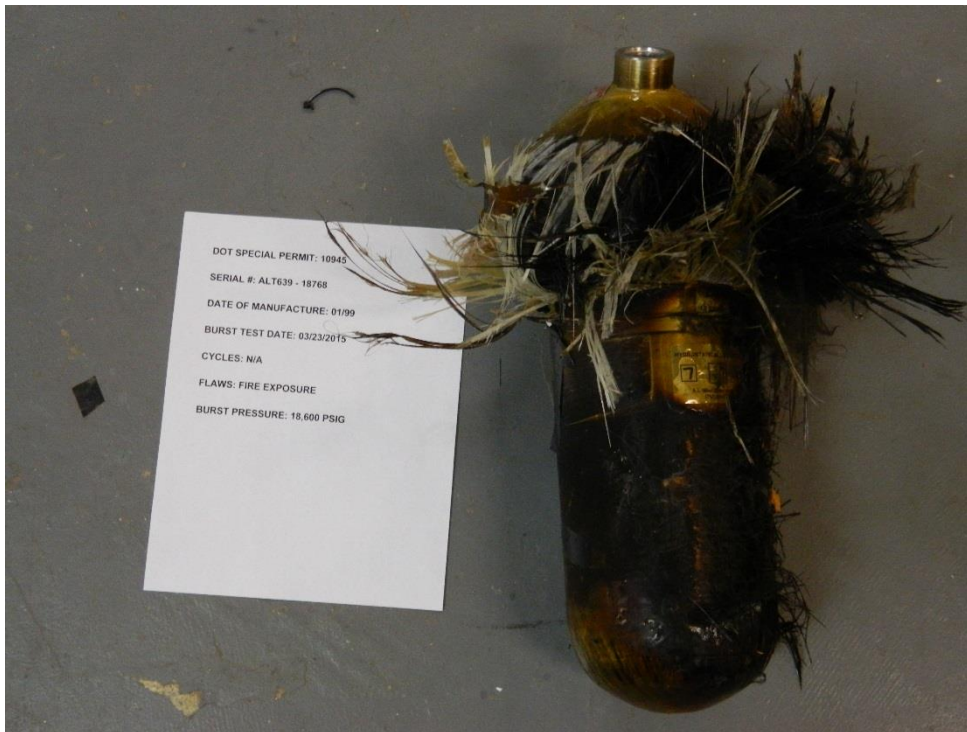


**Figure E.38 – End-of-Life burst of ALT639-18768.**

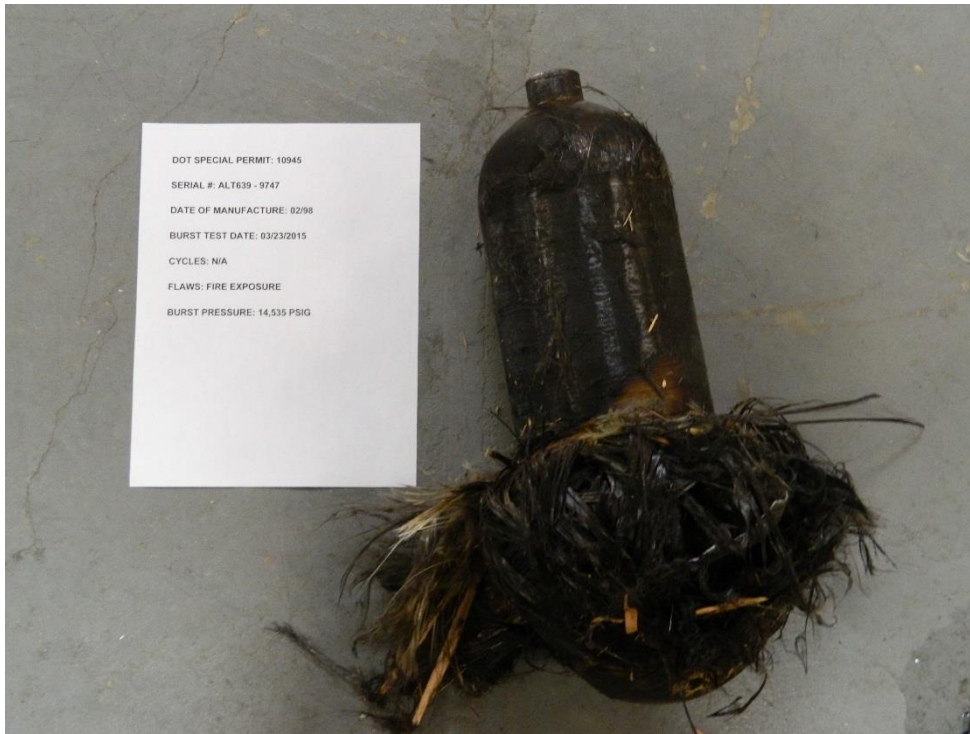


**Figure E.39 – End-of-Life burst of ALT639-9747.**



**Figure E.40 – End-of-Life burst of ALT639-9769.**

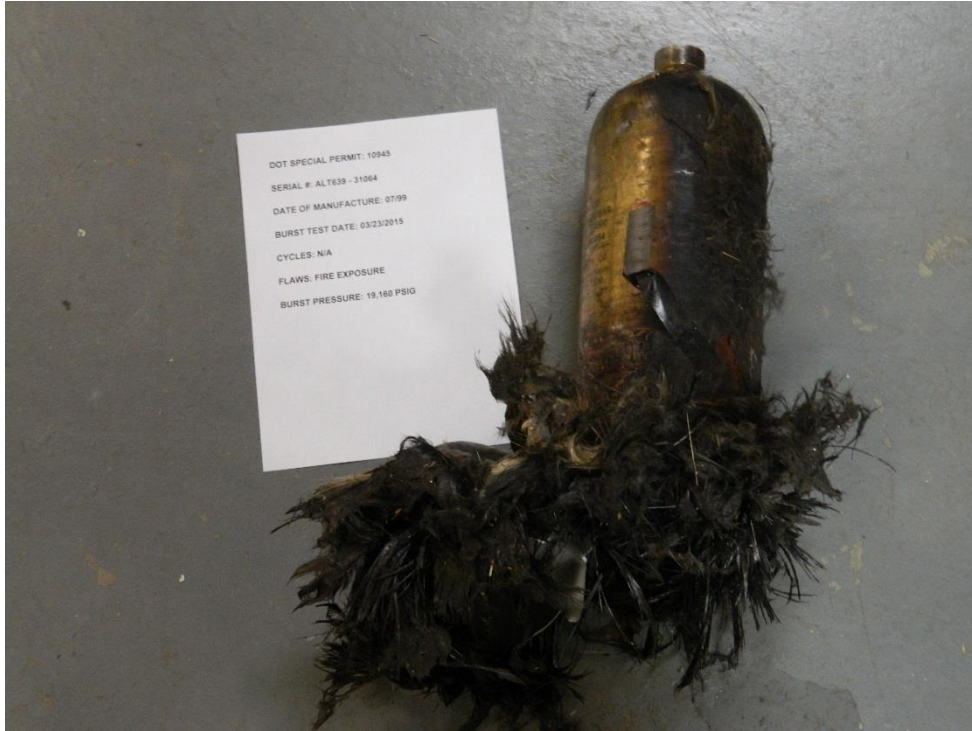


**Figure E.41 – End-of-Life burst of ALT639-31064.**



**Figure E. 42 – End-of-Life burst of ALT639-23371.**



Figure E.43 – End-of-Life burst of ALT695-3669.

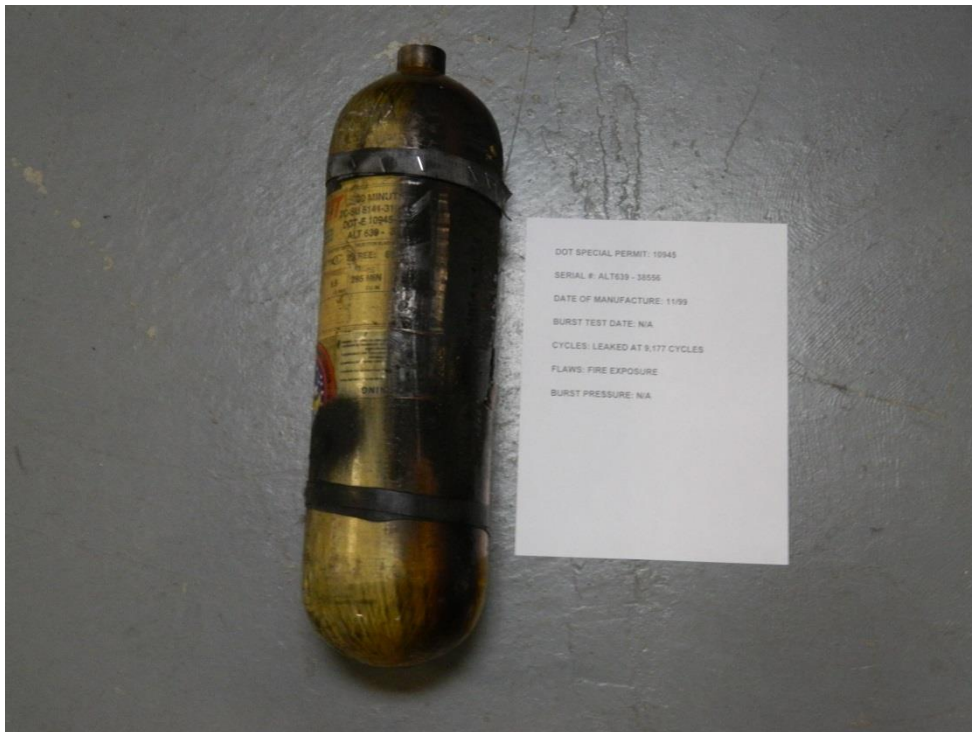


Figure E.44 – End-of-Life burst of ALT695-1781.



DOT SPECIAL PERMIT: 10015  
SERIAL #: OM3920  
DATE OF MANUFACTURE: 08/98  
BURST TEST DATE: 03/28/2015  
CYCLES: N/A  
FLAWS: FIRE EXPOSURE  
BURST PRESSURE: 16,180 PSIG

**Figure E.45 – End-of-Life burst of OM3968.**



DOT SPECIAL PERMIT: 10045  
SERIAL #: ALT639 - 38556  
DATE OF MANUFACTURE: 11/99  
BURST TEST DATE: N/A  
CYCLES: LEAKED AT 9,177 CYCLES  
FLAWS: FIRE EXPOSURE  
BURST PRESSURE: N/A

**Figure E.46 – End-of-Life burst of ALT639-38556.**

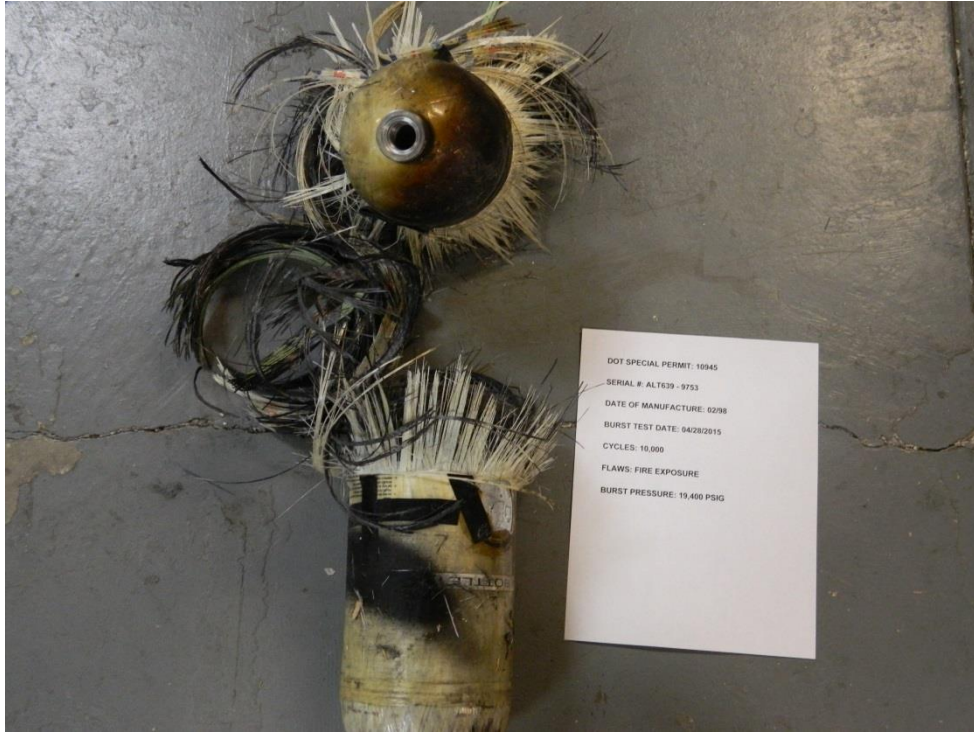


Figure E.47 – End-of-Life burst of ALT639-9753.

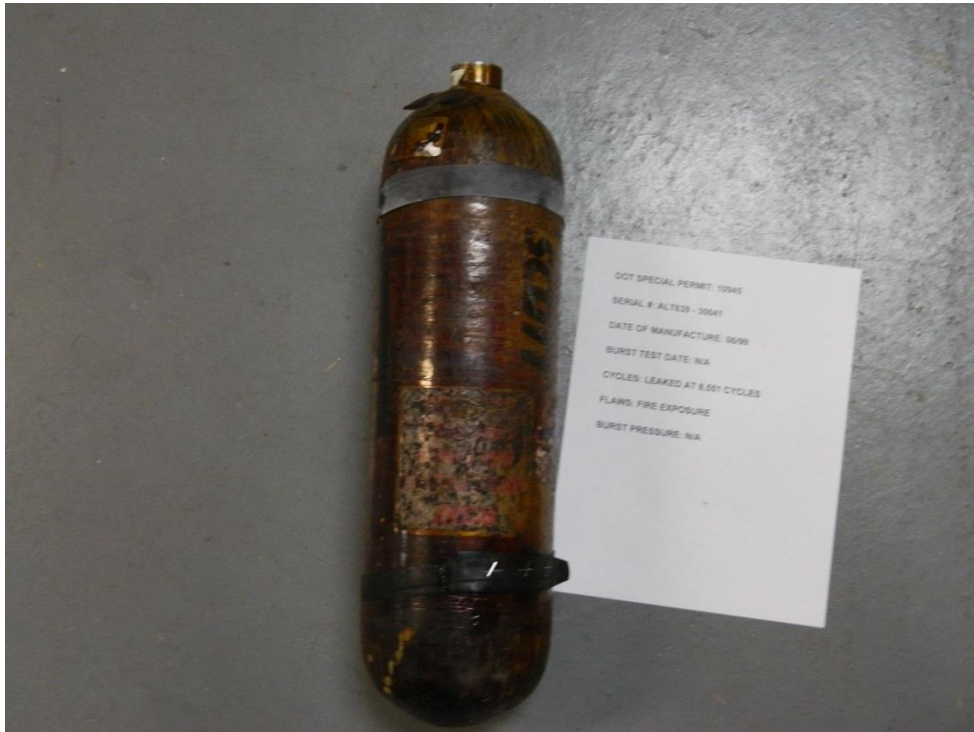
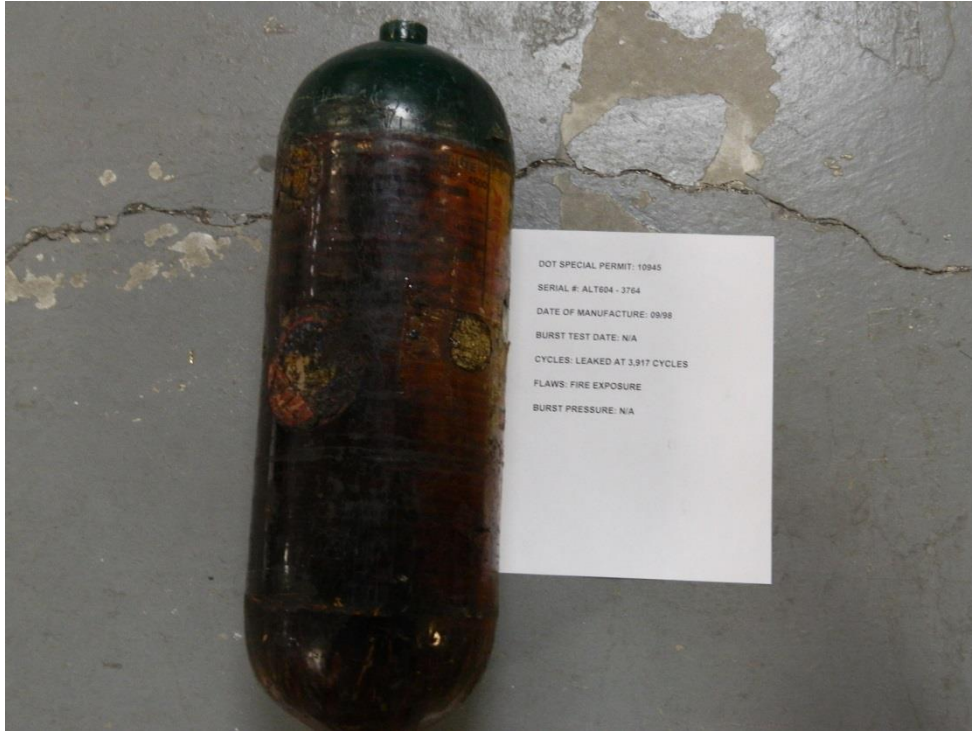
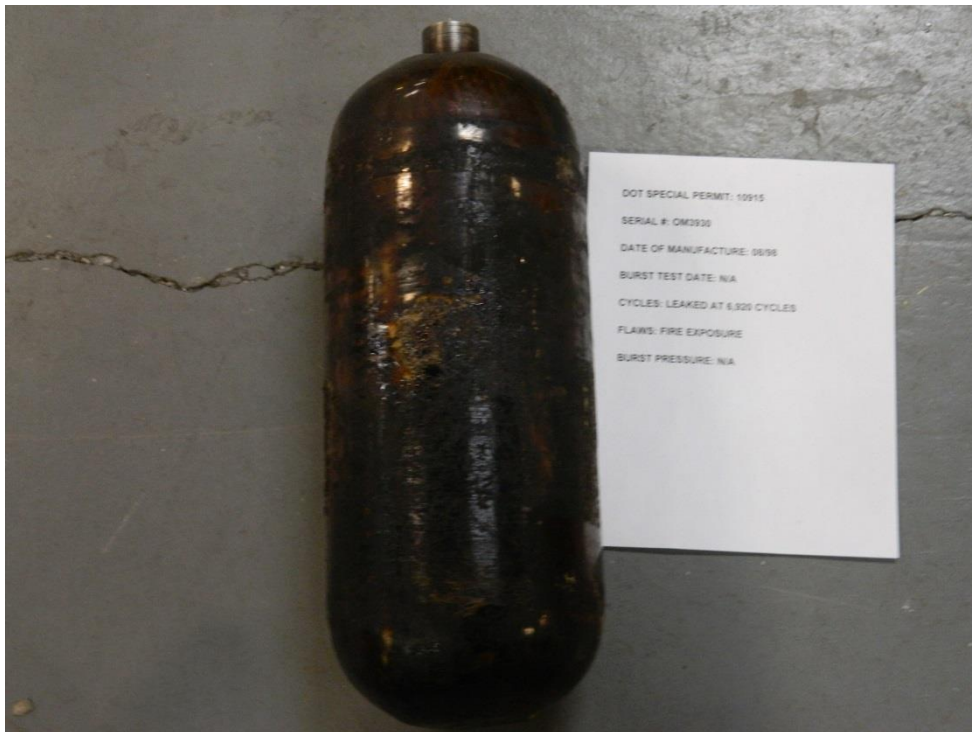


Figure E.48 – End-of-Life burst of ALT639-30041.



DOT SPECIAL PERMIT: 10945  
SERIAL #: ALT604-3764  
DATE OF MANUFACTURE: 09/98  
BURST TEST DATE: N/A  
CYCLES: LEAKED AT 3,917 CYCLES  
FLAWS: FIRE EXPOSURE  
BURST PRESSURE: N/A

**Figure E.49 – End-of-Life burst of ALT604-3764.**



DOT SPECIAL PERMIT: 10915  
SERIAL #: OM3930  
DATE OF MANUFACTURE: 05/98  
BURST TEST DATE: N/A  
CYCLES: LEAKED AT 6,926 CYCLES  
FLAWS: FIRE EXPOSURE  
BURST PRESSURE: N/A

**Figure E.50 – End-of-Life burst of OM3930.**